SUPPORTING INFORMATION

Kinetics of Sulfur-Transfer from Titanocene (Poly)Sulfides to Sulfenyl Chlorides: Rapid Metal-Assisted Concerted Substitution

Pedro H. Helou de Oliveira,[a] Patrick J. Boaler, [a] Guoxiong Hua,[b] Nathan M. West,[c] Robert T. Hembre,[c] Jonathan M. Penney,[d] Malik H. Al-Afyouni,[d] J. Derek Woolins,[e] Andrés García-Domínguez,[a*] and Guy C. Lloyd-Jones[a*]

*E-mail: v1agarc9@ed.ac.uk; guy.lloyd-jones@ed.ac.uk

[a]School of Chemistry, University of Edinburgh, David Brewster Road, Edinburgh, EH9 3FJ, UK; [b]School of Chemistry, University of St Andrews, North Haugh, St Andrews, KY16 9ST; [c]Eastman Chemical Company, Kingsport, Tennessee 37660, USA; [d]Flexsys America L.P., 260 Springside Drive, Akron, OH 44333, USA.[e]Department of Chemistry, Khalifa University, Abu Dhabi, UAE.

TABLE OF CONTENTS

1. General Considerations

Chemicals. Unless otherwise stated, the chemical reactions were assembled under air within a well-ventilated fume hood. Disulfur dichloride (S_2Cl_2, Aldrich, 98%), fluorobenzene (PhF, Aldrich, 98%), dimethyl sulfone (Aldrich, 98%), were used without further purification. For synthetic procedures, *N*-chlorosuccinimide (NCS, Aldrich 98%), sulfur flowers (Fisher, 99%), titanocene dichloride (Cp_2TiCl_2, Fluorochem, 97%), 4-chlorothiophenol (Acros, 97%), 4-bromothiophenol (Acros, 95%), 4-nitrothiophenol (Fluorochem, 90%), 4-fluorothiophenol (Fluorochem, 97%), thiophenol (Acros, 97%), 4-methoxythiophenol (Fluorochem, 97%), 4,4-dithiodimorpholine (TCI, 98%), sulfuryl chloride (SO_2Cl_2, Acros, 98%), phthalimide (Aldrich, 99%) and thioacetic acid (Acros, 96%) were used without further purification. Ammonium sulfide ($(NH_4)_2S$, Fluorochem, 40-48% wt in water) and hydrochloric acid (HCl, Fisher Scientific, 37% wt in water) were used as received and diluted solutions of these components were prepared by addition of degassed (N_2 bubbling for 15 min) deionized water. Sulfenyl chlorides prepared by synthesis were stored at - 40 °C in a glovebox freezer. Unless otherwise stated acetone (Fisher Scientific, reagent grade), dichloromethane (DCM, Aldrich, HPLC grade), *n*-Hexane (Aldrich, HPLC grade), methyl tert-butyl ether (MTBE, Fisher Scientific, 99%) and magnesium sulfate ($MgSO_4$, Merck) were used as received. Anhydrous DCM (Fisher Scientific, HPLC grade, unstabilised) was dispensed from a MBraun® solvent system (SPS-800) equipped with alumina columns under positive pressure of Argon. Synthetic procedures have not been optimized.

Chromatography. Analytical thin-layer chromatography (TLC) was performed on precoated aluminium-backed plates (Silica gel 60 F_{254}; Merck). Visualization by UV light was performed at 254 nm wavelength. Flash column chromatography was performed using Merck Geduran® Si 60 (40-63 µm) silica gel. Silica was initially loaded as a slurry with the eluent. Eluents made of solvent mixtures were prepared by adding the corresponding volume of solvent per volume of the other using a measuring cylinder and shaking the mixture thoroughly before loading into the column. In-house N_2 gas was used to apply pressure. A dry loading technique was used to load crude mixtures into the column, using DCM (to partially dissolve the crude product), followed by careful evaporation in a rotatory evaporator, using Celite® 545 (Aldrich) as the supporting material for sample preparation.

Stock solutions for kinetic experiments. Volumetric glassware was dried overnight in a vacuum oven at 80 °C and allowed to cool down at ambient temperature under air before use. Stock solutions were freshly prepared the same day of the experiment by weighing the chemical reagents directly into volumetric flasks using analytical balances (± 0.01 mg weight precision). The required volume of the corresponding stock solution to prepare samples for kinetic experiments was measured with gas-tight syringes and detachable Sterican® needles.

NMR Spectroscopy. NMR spectra were acquired with a Bruker Avance HD III 400 MHz spectrometer fitted with a 5 mm BBO Prodigy CryoProbe (LN_2) in borosilicate NMR tubes (O.D. ~ 5 mm) with Teflon caps at a probe temperature of 300 K unless otherwise stated. NMR tubes were dried overnight in a vacuum oven at 80 °C and allowed to cool down at ambient temperature under

air before use. ^{1}H, $^{13}C\{^{1}H\}$ and ^{19}F NMR spectra were acquired at 400, 101, and 377 MHz, respectively. In describing NMR parameters in standard pulse-acquire measurments abbreviations are as follows: NS = Number of scans; AQ = acquisition time; D1 = recycling delay. ^{1}H NMR data were processed using MestReNova software (version 14.2.3). Chemical shifts are reported in parts per million (ppm). Integrations were performed after phase correction followed by base-line correction (Whitaker smoother). Chemical characterization (Section S10) was performed by dissolving the sample in ~ 0.6 mL of $CDCl_3$. ^{1}H NMR spectra were referenced using the residual protiated $CHCl_3$ signal (δ = 7.26 ppm), ^{13}C NMR spectra referenced to the centre of the multiplet of the deuterated $CDCl_3$ (δ = 77.16 ppm) and ^{19}F NMR chemical shifts referenced to $BF_3{\cdot}Et_2O$ as an external standard. Abbreviations are as follows: singlet (s), doublet (d), triplet (t), doublet of doublets (dd), triplet of triplets (tt), sextet (hex), doublet of sextets (dhex) and multiplet (m). Spectra for reaction monitoring were acquired in DCM without a deuterium lock and referenced to the solvent peak (DCM, 5.30 ppm) using solvent suppression. Solvent suppression for ^{1}H NMR spectra was performed with the WET pulse sequence using a single scan with 90-degree flip angle. [S1] Stopped-flow NMR experiments were performed using a three-syringe variable ratio instrumentation previously described.[S2] Concentrations at each time point have been calculated by calibrating to an internal standard of known concentration, using fluorobenzene (PhF), 1-fluoronaphthalene or dimethylsulfone (Me_2SO_2) as internal standards.

Stopped-Flow UV. Kinetic experiments were carried out in a well-ventilated fume-hood with a Hi-Tech Scientific SFA-20 accessory equipped with two independent 2.5 mL 'reagent syringes' connected to three-way PTFE valves and coupled through a thermostated umbilical to a Hellma Analytics fused-silica flow cell with an integral mixer (80 μL cell volume, 10 x 2 mm size). The outlet of the reaction cell is connected via the umbilical to a 'trigger-syringe' equipped with a microswitch at the end. The microswitch sends a stabilised 5V signal to the spectrophotometer and PC to time the start of the data collection for reaction monitoring. The average dead-time (i.e., the time taken for the nascent reaction to be transported from the mixer to the cell window) is approximately 10 ms when using dichloromethane as solvent. UV spectra were recorded using a OceanOptics USB4000 and Flame Spectrometers connected *via* the cuvette holder to a DH2000-BAL UV lamp using solarised resistant grade optical fibres. The temperature was controlled using a chiller (Lauda, Alpha RA 8) by flowing a mixture of ethylene glycol and water through both the umbilical and cuvette holder. The actual reaction temperature was measured with a 0.1 °C uncertainty using a thermocouple connected into the UV-cuvette holder. Unless otherwise stated, kinetic measurements described herein were performed at 22 °C (295 K) with DCM as background. Prior to each assay, the temperature was allowed to stabilise, the system washed with anhydrous DCM (ca. 25 mL) and a background UV spectrum recorded. The solutions were then connected to the three-way PTFE valves using tubes equipped with screw-end fittings and their contents loaded into the 'reagent syringes' by 'pulling', slowly withdrawing the syringe plungers to minimize introduction of bubbles. The system was flushed twice with the corresponding reagent solutions (5 mL of each) to ensure

complete purging of DCM while removing any remaining bubbles in the syringe. The system was reloaded, and three consecutive shots (0.1 mL of each stock solution consumed per shot) performed without recording. Then, a series of 6 – 10 consecutive shots were performed, and the evolution of the reaction monitored by UV recording a series of 50 – 500 consecutive spectra over time with a 300 – 530 nm spectral window unless otherwise stated. The UV-vis spectra were analyzed with Kinetic Studio software (version 5.02). UV spectrum shown at t_{UV} = 0 seconds corresponds to the first spectrum recorded after triggering the system. For consecutive reactions, a time offset was applied to account for the dead time as follows: $t_{rxn} = t_{UV} + 0.010$ s. In reactions exhibiting exponential decay of absorbance, pseudo-first order reaction rate constants (k_{obs} (s^{-1})) of individual runs were obtained by non-linear regression of the exponential temporal decay of the absorbance averaged across a 0.6 nm spectral range at the required wavelength. The pseudo-first order reaction rate constants provided in the sections below are average values of all the consecutive runs given in the experiments. Averaging of values and statistical analysis was carried out with the Microsoft Excel data analysis package using the Summary Statistics function.

Kinetic simulations. Kinetic models were fitted to experimental data using standard numerical methods approach.[S3] Fitting of models were performed by minimizing the sum of square residues using Excel Solver.

2. Stopped-Flow UV-Vis Experiments with Exponential Evolution of Absorbance

2.1. Representative Procedure to Extract Bimolecular Rate Constants

The reaction of Cp_2TiS_5 with S_2Cl_2 is used herein to describe the general procedure for the determination of bimolecular rate constants in cases where exponential evolution of absorbance was observed. Unless otherwise stated, kinetic measurements were performed at 22 °C (295 K) in anhydrous DCM using a 10 mm light-path. Solutions of disulfur dichloride (S_2Cl_2) were used in excess concentrations to achieve pseudo-first order kinetics. Stock concentrations of S_2Cl_2 at different concentrations of S_2Cl_2 were attained by dilution of a concentrated stock solution. A typical stack of temporal UV spectra is shown in Figure S1A**,** highlighting characteristic changes dominated by the growth of Cp_2TiCl_2 and decay of Cp_2TiS_5. Two isosbestic points (λ = 380, 425 nm) were observed. Absorbance values at λ = 495 nm were plotted against time and fitted to an exponential-decay function to extract the pseudo-first order decay rate constant, k_{obs} (Figure S1B). For each kinetic assay n-runs were performed to provide an average 'k_{obs}' value (Figure S1C), which were then plotted against their corresponding initial S_2Cl_2 concentration. The resulting plot k_{obs} vs $[S_2Cl_2]_0$ was fitted to a linear model including the origin as a data point (Figure S1D). The linearity suggests first order dependence on S_2Cl_2 concentration with the slope as the bimolecular rate constant value ($k_{rxn} = 3.2 \cdot 10^2\ M^{-1}s^{-1}$).

Three assays were performed at three different initial Cp_2TiS_5 concentrations to eliminate the possibility of a higher order process exhibiting pseudo first-order kinetics through, for example, compensating self/auto-catalysis (Figure S2). Overlay after normalisation for time (x-time displacement) and background (y-axis displacement) shows coherence between the three runs, indicating that the titanocene decays exponentially, and within experimental error, with the same rate constant (k_{obs} = 7.8 ± 0.2 s^{-1}; when $[S_2Cl_2]_0$ = 0.024 M) independent of the initial concentration, $[Cp_2TiS_5]_0$. This eliminates the possibility of any significant contributions by higher order process. Conversion of the observed rate constant into the bimolecular rate constant ($k_{rxn} = k_{obs}/[S_2Cl_2]_0 = 3.25 \pm 0.09 \times 10^2$) gives a value that is identical within experimental error to that determined in Figure S1D. All data are thus consistent with the reaction being first-order in Cp_2TiS_5 and first order in S_2Cl_2, leading to overall bimolecular kinetics: $-\,d[Cp_2TiS_5]/dt = k_{rxn}\,[Cp_2TiS_5]^1[S2Cl2]^1$.

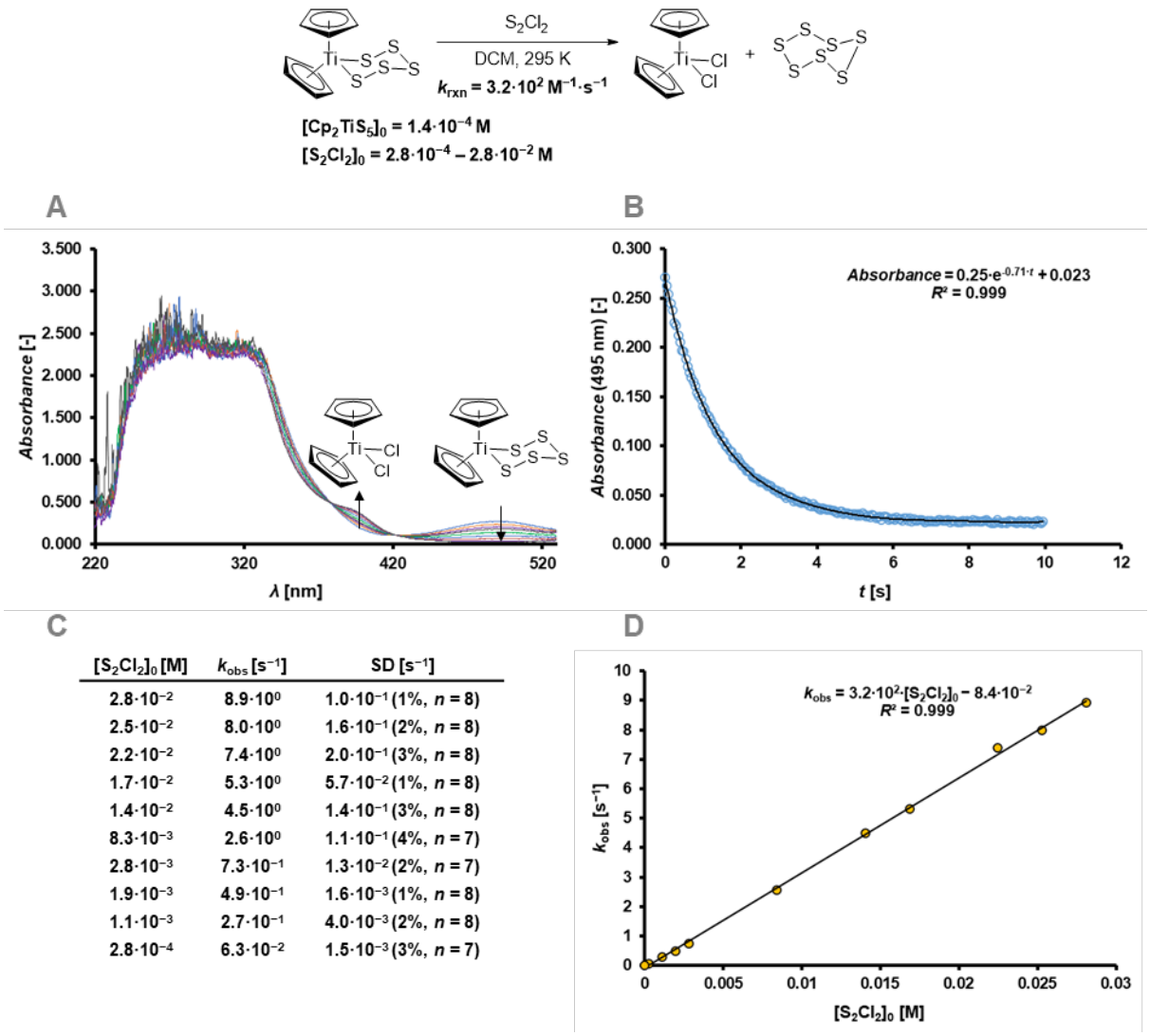

$[S_2Cl_2]_0$ [M]	k_{obs} [s^{-1}]	SD [s^{-1}]
$2.8 \cdot 10^{-2}$	$8.9 \cdot 10^{0}$	$1.0 \cdot 10^{-1}$ (1%, $n = 8$)
$2.5 \cdot 10^{-2}$	$8.0 \cdot 10^{0}$	$1.6 \cdot 10^{-1}$ (2%, $n = 8$)
$2.2 \cdot 10^{-2}$	$7.4 \cdot 10^{0}$	$2.0 \cdot 10^{-1}$ (3%, $n = 8$)
$1.7 \cdot 10^{-2}$	$5.3 \cdot 10^{0}$	$5.7 \cdot 10^{-2}$ (1%, $n = 8$)
$1.4 \cdot 10^{-2}$	$4.5 \cdot 10^{0}$	$1.4 \cdot 10^{-1}$ (3%, $n = 8$)
$8.3 \cdot 10^{-3}$	$2.6 \cdot 10^{0}$	$1.1 \cdot 10^{-1}$ (4%, $n = 7$)
$2.8 \cdot 10^{-3}$	$7.3 \cdot 10^{-1}$	$1.3 \cdot 10^{-2}$ (2%, $n = 7$)
$1.9 \cdot 10^{-3}$	$4.9 \cdot 10^{-1}$	$1.6 \cdot 10^{-3}$ (1%, $n = 8$)
$1.1 \cdot 10^{-3}$	$2.7 \cdot 10^{-1}$	$4.0 \cdot 10^{-3}$ (2%, $n = 8$)
$2.8 \cdot 10^{-4}$	$6.3 \cdot 10^{-2}$	$1.5 \cdot 10^{-3}$ (3%, $n = 7$)

Figure S1. Reaction of Cp_2TiS_5 with S_2Cl_2. A) Stack of UV-spectra for reaction monitoring. B) Exponential decay model (black line) fitted to experimental data (circles) of temporal absorbance at 495 nm. C) Initial concentrations, average pseudo-first order rate constants and standard deviations. D) Linear relationship and fitting for pseudo-first order rate constants at various initial S_2Cl_2 concentrations.

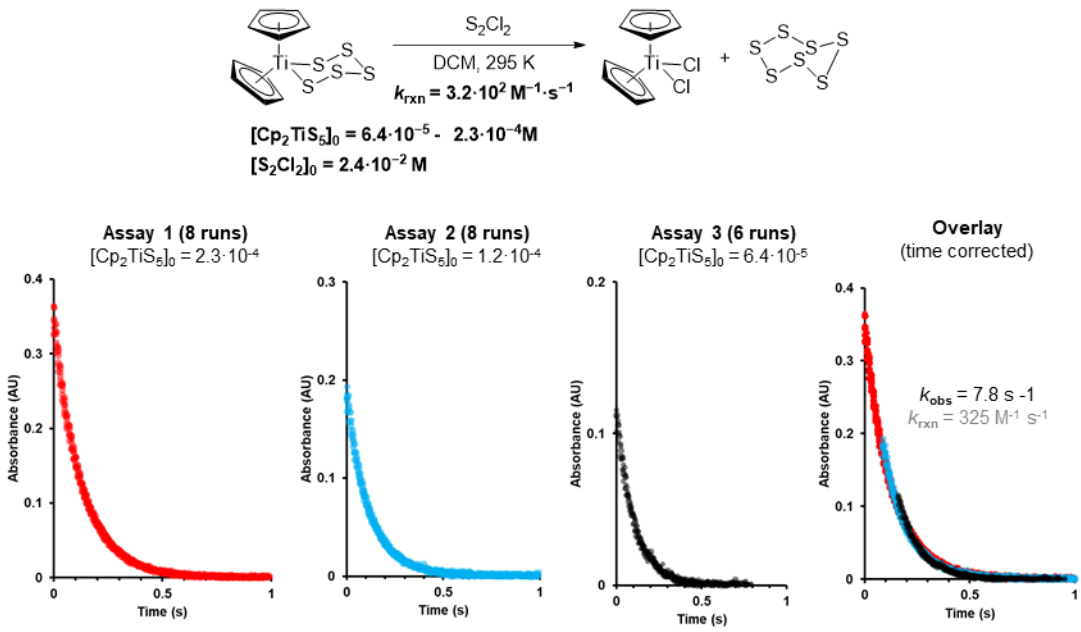

Figure S2. Reaction of Cp_2TiS_5 with S_2Cl_2: assessment of the effect of initial Cp_2TiS_5 concentration on the reaction evolution. The overlay between runs shows a consistent exponential decay in the absorbance, leading to the same pseudo first-order (k_{obs} = 7.8 s^{-1}) and overall second-order (k_{obs} = 325 $M^{-1}s^{-1}$) kinetics. This concentration independent behaviour confirms a simple first-order kinetic dependence on [Cp_2TiS_5], eliminating the possibility of higher order processes that could lead to similar kinetic profiles, but would give k_{obs} that is concentration dependent.

2.2 Reaction of Cp_2TiS_5 with S_2Cl_2 in DCM: Effect of Temperature

The reactions were performed at the required temperature (10.3 °C – 26.3 °C, *vide infra*) in anhydrous DCM using a 10 mm light-path. All runs were performed at the same reagent initial concentrations ($[Cp_2TiS_5]_0 = 1.3 \cdot 10^{-4}$ M, $[S_2Cl_2]_0 = 2.1 \cdot 10^{-2}$ M). The same UV spectroscopic features as those in Section S2.1 were observed. The reaction is relatively insensitive to temperature in the range studied. Bimolecular rate constants were determined by dividing pseudo first order constants by the initial concentration of the electrophile: k_{rxn} ($M^{-1}s^{-1}$) = $k_{obs}/[S_2Cl_2]_0$. Averaged pseudo-first order rate constants (k_{obs} = 6.9 ± 0.1 s^{-1}) and bimolecular rate constants (k_{rxn} = 322 ± 3 $M^{-1} \cdot s^{-1}$) determined at each temperature are summarised within Figure S2. Biomolecular rate constant values, k_{rxn}, were used for Eyring analysis. Cp_2TiS_5 and S_2Cl_2 have two identical reaction sites each, which provide access to four identical transition states and four identical reaction pathways toward the final product. The experimentally measured process rate constant can be expressed as the contribution from four identical microkinetic S-S bond forming events ($k_{rxn} = 4k_{S\text{-}S}$) with activation parameters $\Delta G^{\ddagger}$, $\Delta H^{\ddagger}$ and $\Delta S^{\ddagger}$. The expression used to calculate activation parameters from variable temperature experiments considering statistical contributions is shown in Figure S3.

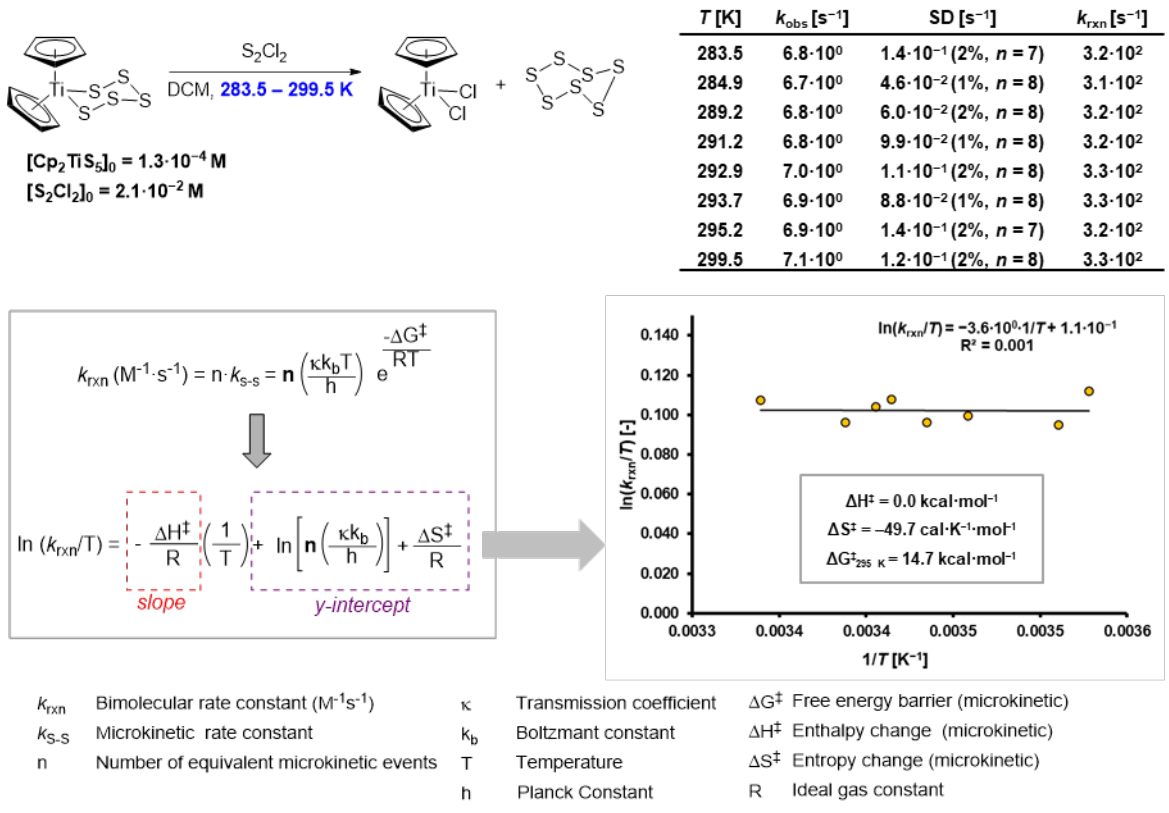

T [K]	k_{obs} [s^{-1}]	SD [s^{-1}]	k_{rxn} [s^{-1}]
283.5	$6.8 \cdot 10^{0}$	$1.4 \cdot 10^{-1}$ (2%, n = 7)	$3.2 \cdot 10^{2}$
284.9	$6.7 \cdot 10^{0}$	$4.6 \cdot 10^{-2}$ (1%, n = 8)	$3.1 \cdot 10^{2}$
289.2	$6.8 \cdot 10^{0}$	$6.0 \cdot 10^{-2}$ (2%, n = 8)	$3.2 \cdot 10^{2}$
291.2	$6.8 \cdot 10^{0}$	$9.9 \cdot 10^{-2}$ (1%, n = 8)	$3.2 \cdot 10^{2}$
292.9	$7.0 \cdot 10^{0}$	$1.1 \cdot 10^{-1}$ (2%, n = 8)	$3.3 \cdot 10^{2}$
293.7	$6.9 \cdot 10^{0}$	$8.8 \cdot 10^{-2}$ (1%, n = 8)	$3.3 \cdot 10^{2}$
295.2	$6.9 \cdot 10^{0}$	$1.4 \cdot 10^{-1}$ (2%, n = 7)	$3.2 \cdot 10^{2}$
299.5	$7.1 \cdot 10^{0}$	$1.2 \cdot 10^{-1}$ (2%, n = 8)	$3.3 \cdot 10^{2}$

k_{rxn}	Bimolecular rate constant ($M^{-1}s^{-1}$)	κ	Transmission coefficient	$\Delta G^{\ddagger}$	Free energy barrier (microkinetic)
$k_{S\text{-}S}$	Microkinetic rate constant	k_b	Boltzmant constant	$\Delta H^{\ddagger}$	Enthalpy change (microkinetic)
n	Number of equivalent microkinetic events	T	Temperature	$\Delta S^{\ddagger}$	Entropy change (microkinetic)
		h	Planck Constant	R	Ideal gas constant

Figure S3. Reaction of Cp_2TiS_5 with S_2Cl_2 in DCM at 283.5 – 299.5 K. Summary of rate constants and Eyring analysis including statistical corrections (n = 4; κ = 1).

2.3 Reaction of Cp_2TiS_5 with S_2Cl_2: Effect of Solvent

The reactions were performed at 22 °C (295 K) in the corresponding solvent (*vide infra*) using a 10 mm light-path. The same UV spectroscopic features as those in Section S2.1 were observed. Average pseudo-first order rate constants (k_{obs}) and bimolecular rate constants (k_{rxn}) determined in each solvent are summarised below (Figure S4). Overall, the results show a strong dependence on the solvent polarity, with more polar solvents leading to faster rates. Graphical analyses against various solvent polarity parameters[S4], are shown in Figure S5.

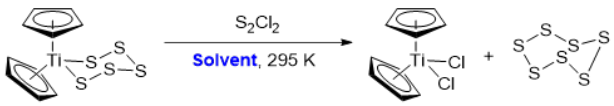

Solvent	$[S_2Cl_2]_0$ [M]	k_{obs} [s^{-1}]	SD [s^{-1}]
$CHCl_3$ ($[Cp_2TiS_5]_0 = 1.4\cdot10^{-4}$ M)	$2.8\cdot10^{-2}$	$1.1\cdot10^{1}$	$1.1\cdot10^{-1}$ (1%, *n* = 8)
	$2.5\cdot10^{-2}$	$1.0\cdot10^{1}$	$1.6\cdot10^{-1}$ (2%, *n* = 8)
	$2.2\cdot10^{-2}$	$8.8\cdot10^{0}$	$7.2\cdot10^{-2}$ (1%, *n* = 8)
	$1.7\cdot10^{-2}$	$6.7\cdot10^{0}$	$1.6\cdot10^{-1}$ (2%, *n* = 8)
	$1.1\cdot10^{-2}$	$4.6\cdot10^{0}$	$8.2\cdot10^{-2}$ (2%, *n* = 8)
	$8.3\cdot10^{-3}$	$3.5\cdot10^{0}$	$8.0\cdot10^{-2}$ (2%, *n* = 8)
	$5.5\cdot10^{-3}$	$2.4\cdot10^{0}$	$2.1\cdot10^{-2}$ (1%, *n* = 8)
	$2.8\cdot10^{-3}$	$1.4\cdot10^{0}$	$1.1\cdot10^{-2}$ (1%, *n* = 7)
DCE ($[Cp_2TiS_5]_0 = 1.3\cdot10^{-4}$ M)	$2.8\cdot10^{-2}$	$2.7\cdot10^{0}$	$3.6\cdot10^{-2}$ (1%, *n* = 8)
	$2.5\cdot10^{-2}$	$2.4\cdot10^{0}$	$4.8\cdot10^{-2}$ (2%, *n* = 8)
	$2.2\cdot10^{-2}$	$2.2\cdot10^{0}$	$3.5\cdot10^{-2}$ (2%, *n* = 8)
	$1.7\cdot10^{-2}$	$1.6\cdot10^{0}$	$2.5\cdot10^{-2}$ (2%, *n* = 8)
	$1.1\cdot10^{-2}$	$1.1\cdot10^{0}$	$1.7\cdot10^{-2}$ (2%, *n* = 8)
	$8.4\cdot10^{-3}$	$8.0\cdot10^{-1}$	$1.1\cdot10^{-2}$ (1%, *n* = 8)
	$5.6\cdot10^{-3}$	$5.2\cdot10^{-1}$	$1.2\cdot10^{-2}$ (2%, *n* = 8)
	$2.8\cdot10^{-3}$	$2.7\cdot10^{-1}$	$2.4\cdot10^{-3}$ (1%, *n* = 7)
$PhCF_3$ ($[Cp_2TiS_5]_0 = 1.6\cdot10^{-4}$ M)	$2.8\cdot10^{-2}$	$9.8\cdot10^{-2}$	$2.1\cdot10^{-3}$ (2%, *n* = 5)
	$2.3\cdot10^{-2}$	$8.3\cdot10^{-2}$	$4.0\cdot10^{-3}$ (5%, *n* = 5)
	$1.7\cdot10^{-2}$	$6.2\cdot10^{-2}$	$5.7\cdot10^{-4}$ (1%, *n* = 5)
	$1.4\cdot10^{-2}$	$5.2\cdot10^{-2}$	$7.9\cdot10^{-4}$ (2%, *n* = 5)
	$1.1\cdot10^{-2}$	$4.1\cdot10^{-2}$	$4.8\cdot10^{-4}$ (1%, *n* = 5)
	$5.6\cdot10^{-3}$	$2.2\cdot10^{-2}$	$3.9\cdot10^{-4}$ (2%, *n* = 5)
PhCl ($[Cp_2TiS_5]_0 = 1.4\cdot10^{-4}$ M)	$5.5\cdot10^{-3}$	$1.1\cdot10^{0}$	$8.9\cdot10^{-2}$ (8%, *n* = 8)
	$4.9\cdot10^{-3}$	$1.1\cdot10^{0}$	$4.5\cdot10^{-2}$ (4%, *n* = 8)
	$3.8\cdot10^{-3}$	$8.1\cdot10^{-1}$	$3.2\cdot10^{-2}$ (4%, *n* = 8)
	$2.7\cdot10^{-3}$	$6.0\cdot10^{-1}$	$1.6\cdot10^{-2}$ (3%, *n* = 8)
	$1.9\cdot10^{-3}$	$4.1\cdot10^{-1}$	$9.7\cdot10^{-3}$ (2%, *n* = 8)
	$5.5\cdot10^{-4}$	$1.4\cdot10^{-1}$	$1.4\cdot10^{-2}$ (10%, *n* = 8)
CCl_4 ($[Cp_2TiS_5]_0 = 2.0\cdot10^{-4}$ M)	$2.8\cdot10^{-2}$	$8.9\cdot10^{0}$	$1.0\cdot10^{-1}$ (1%, *n* = 8)
	$2.5\cdot10^{-2}$	$8.0\cdot10^{0}$	$1.6\cdot10^{-1}$ (2%, *n* = 8)
	$2.2\cdot10^{-2}$	$7.4\cdot10^{0}$	$2.0\cdot10^{-1}$ (3%, *n* = 8)
	$1.7\cdot10^{-2}$	$5.3\cdot10^{0}$	$5.7\cdot10^{-2}$ (1%, *n* = 8)
	$1.4\cdot10^{-2}$	$4.5\cdot10^{0}$	$1.4\cdot10^{-1}$ (3%, *n* = 8)

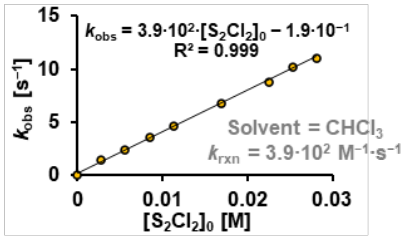

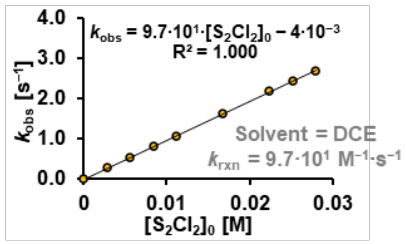

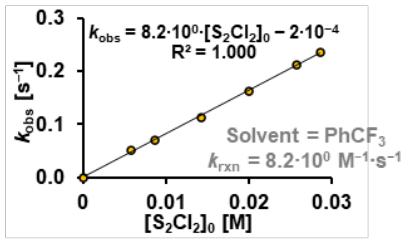

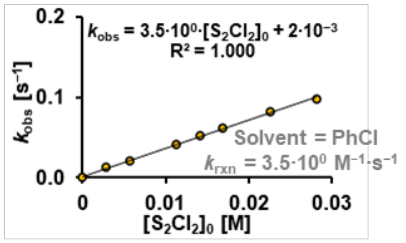

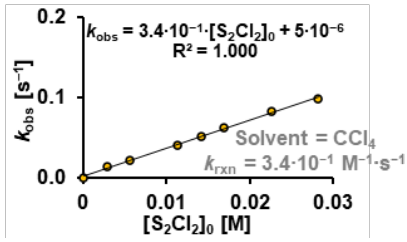

Figure S4. Reaction of Cp_2TiS_5 with S_2Cl_2 in various solvents at 295K. Summary of conditions, pseudo-first order rate constants and linear fitting against $[S_2Cl_2]_0$.

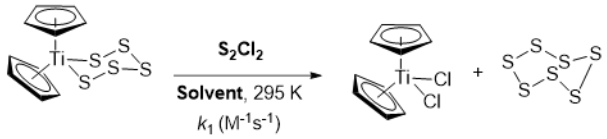

Solvent	k_1 ($M^{-1}s^{-1}$)	ε	ET_{30}	SP	SdP	SA	SB
CS_2	0.18	2.64	32.8	1	0	0	0.0104
CCl_4	0.34	230	32.4	0.768	0	0	0.044
PhCl	3.5	5.74	36.8	0.833	0.537	0	0.113
$PhCF_3$	8.2	9.40	38.5	0.694	0.663	0.014	0.073
DCE	97	10.74	41.3	0.771	0.742	0.03	0.126
DCM	320	9.02	40.7	0.761	0.769	0.04	0.178
$CHCl_3$	390	4.89	39.1	0.783	0.614	0.047	0.071

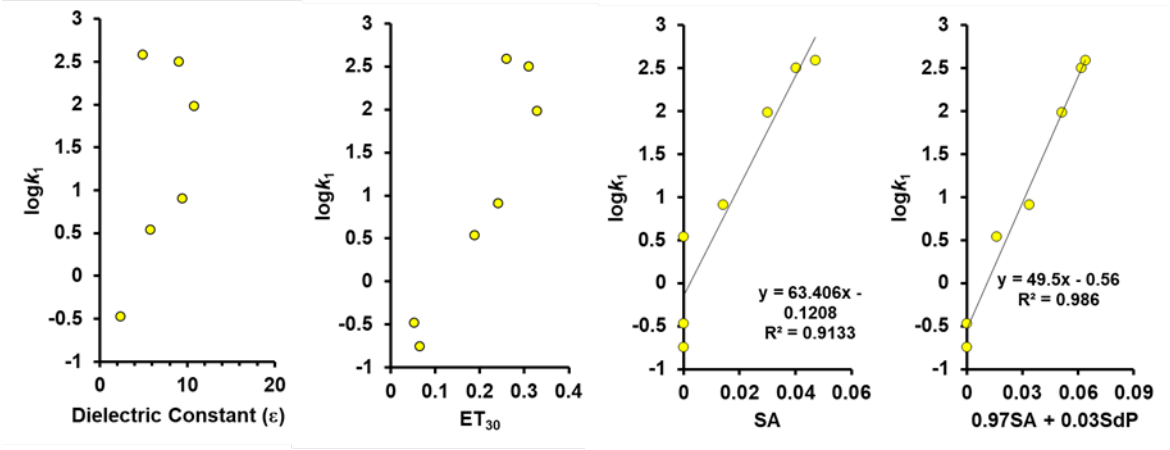

Figure S5. Representation of bimolecular rate constant values against dieletric constant, ET_{30} and Catalán parameters (SA, SdP). Decimal logarithms are used in the plots (i.e., log = $\log_{10}$).

2.4 Reaction of $^{R}Cp_2TiS_5$ with S_2Cl_2

Reactions were performed at 22 °C (295 K) in DCM with a 10 mm light-path. Spectroscopic features similar to those of Cp_2TiS_5 were observed for all complexes. The change of absorbance over time was monitored at λ = 495 nm for all reactions. Average pseudo-first order rate constants (k_{obs}) and bimolecular rate constants (k_{rxn}) determined for each complex are summarised below (Figure S6). Overall, the results show the rate to vary slightly with alkyl substitution on the cyclopentadienyl ring. Graphical analyses against various parameters, are shown in Figure S7. No linear correlations with steric parameters (Taft, Charton, cone-angle)[S5] or Hammett[S6] substituent constants observed.

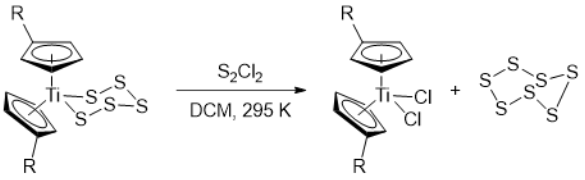

R, c_0 [M]	$[S_2Cl_2]_0$ [M]	k_{obs} [s^{-1}]	SD [s^{-1}]
Et (c_0 = 5.3·10^{-5} M)	5.0·10^{-3}	1.2·10^{0}	4.5·10^{-2} (4%, *n* = 8)
	4.5·10^{-3}	1.1·10^{0}	3.1·10^{-2} (3%, *n* = 8)
	3.5·10^{-3}	8.5·10^{-1}	2.8·10^{-2} (3%, *n* = 8)
	3.0·10^{-3}	7.3·10^{-1}	2.3·10^{-2} (3%, *n* = 8)
	2.5·10^{-3}	5.7·10^{-1}	9.1·10^{-3} (2%, *n* = 8)
	2.0·10^{-3}	4.9·10^{-1}	8.8·10^{-3} (2%, *n* = 8)
	1.5·10^{-3}	3.6·10^{-1}	7.4·10^{-3} (2%, *n* = 8)
	5.0·10^{-4}	1.2·10^{-1}	3.5·10^{-3} (3%, *n* = 8)
n-Pr (c_0 = 5.0·10^{-5} M)	5.0·10^{-3}	1.2·10^{0}	8.6·10^{-2} (7%, *n* = 8)
	4.5·10^{-3}	1.1·10^{0}	3.0·10^{-2} (3%, *n* = 8)
	3.8·10^{-3}	8.9·10^{-1}	8.2·10^{-2} (9%, *n* = 8)
	3.0·10^{-3}	7.6·10^{-1}	1.2·10^{-2} (2%, *n* = 8)
	2.5·10^{-3}	6.3·10^{-1}	1.5·10^{-2} (2%, *n* = 3)
	2.0·10^{-3}	5.5·10^{-1}	1.0·10^{-2} (2%, *n* = 8)
	1.5·10^{-3}	3.9·10^{-1}	6.5·10^{-3} (2%, *n* = 8)
	5.0·10^{-4}	1.4·10^{-1}	9.3·10^{-3} (7%, *n* = 7)
i-Pr (c_0 = 3.8·10^{-5} M)	5.3·10^{-3}	4.7·10^{-1}	8.3·10^{-3} (2%, *n* = 7)
	4.7·10^{-3}	4.4·10^{-1}	2.7·10^{-2} (6%, *n* = 8)
	3.7·10^{-3}	3.3·10^{-1}	2.9·10^{-2} (9%, *n* = 8)
	2.6·10^{-3}	2.4·10^{-1}	9.1·10^{-3} (4%, *n* = 8)
	1.6·10^{-3}	1.5·10^{-1}	4.0·10^{-3} (3%, *n* = 8)
	5.3·10^{-4}	5.6·10^{-2}	7.4·10^{-3} (13%, *n* = 8)
n-Bu (c_0 = 4.7·10^{-5} M)	5.5·10^{-3}	1.1·10^{0}	8.9·10^{-2} (8%, *n* = 8)
	4.9·10^{-3}	1.1·10^{0}	4.5·10^{-2} (4%, *n* = 8)
	3.8·10^{-3}	8.1·10^{-1}	3.2·10^{-2} (4%, *n* = 8)
	2.7·10^{-3}	6.0·10^{-1}	1.6·10^{-2} (3%, *n* = 8)
	1.9·10^{-3}	4.1·10^{-1}	9.7·10^{-3} (2%, *n* = 8)
	5.5·10^{-4}	1.4·10^{-1}	1.4·10^{-2} (10%, *n* = 8)

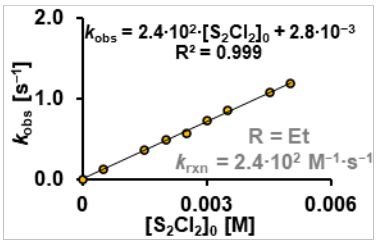

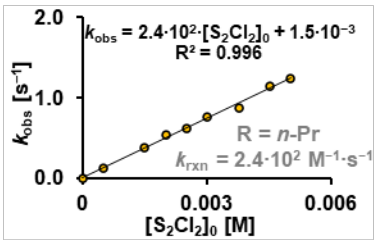

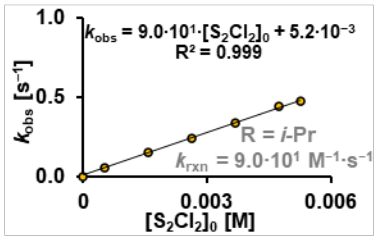

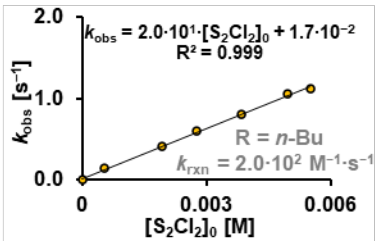

Figure S6. Reaction of $^{R}Cp_2TiS_5$ with S_2Cl_2 in DCM at 295K. Summary of conditions, pseudo-first order rate constants and linear fitting against $[S_2Cl_2]_0$.

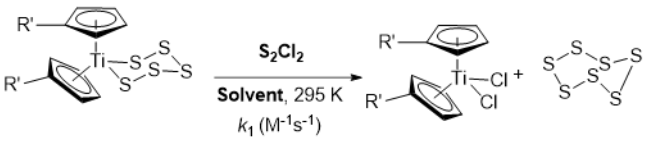

R'	k_1 ($M^{-1}s^{-1}$)	$-E_s$	ν	θ_1 (°)	θ_2 (°)	σ_p	σ_m
H	320	-1.24	0	128	55	0	0
Et	240	0.07	0.56	146	85	-0.15	-0.07
n-Pr	240	0.36	0.68	178	172	-0.13	-0.06
i-Pr	90	0.47	0.76	170	107	-0.15	-0.04
n-Bu	200	0.39	0.68	N/A	N/A	-0.16	-0.08

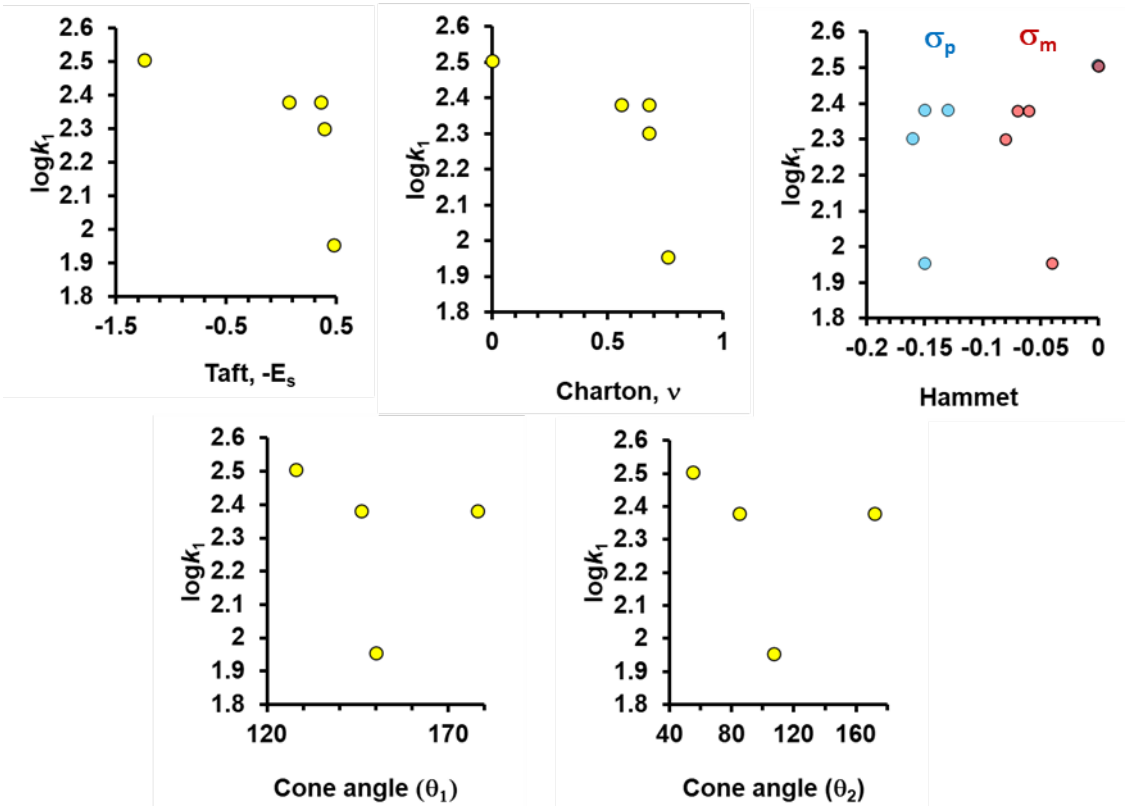

Figure S7. Representation of bimolecular rate constant values against steric and electronic parameters. No linear correlations were observed. Decimal logarithms are used in the plots (i.e., log = $\log_{10}$).

2.5 Reaction of $Cp_2TiS_4(CMe_2)$ with S_2Cl_2

The reactions were performed at 22 °C (295 K) in DCM using a 10 mm light-path. Spectroscopic features similar to those of using unsubstituted Cp_2TiS_5 were observed for all complexes. Change in absorbance at λ = 495 nm was monitored in all conditions. Figure S8 summarises the decay rate constants of this signal (k_{obs}) at various initial reagent concentrations. The linearity suggests first order dependence on S_2Cl_2 concentration with the slope as the bimolecular rate constant value for the overall process ($k_{rxn} = 3.4 \cdot 10^4$ $M^{-1}s^{-1}$).

Experiments at different temperatures (277.0 – 293.5 K) were also carried out at single initial concentrations ($[Cp_2TiS_4(CMe_2)]_0 = 5.2 \cdot 10^{-5}$ M, $[S_2Cl_2]_0 = 1.9 \cdot 10^{-4}$ M (Figure S9). Bimolecular rate constants were determined by dividing pseudo first order constants by the initial concentration of the electrophile: k_{rxn} ($M^{-1}s^{-1}$) = $k_{obs}/[S_2Cl_2]_0$. Biomolecular rate constant values, k_{rxn} were used for Eyring analysis (Figure S9). $Cp_2TiS_4(CMe_2)$ and S_2Cl_2 have two identical reaction sites each, which provide access to four identical transition states and four identical reaction pathways toward the final product. The experimentally measured process rate constant can be express as the result of four identical microkinetic S-S bond forming events ($k_{rxn} = 4k_{S\text{-}S}$) with activation parameters, $\Delta G^{\ddagger}$, $\Delta H^{\ddagger}$ and $\Delta S^{\ddagger}$. The expression used to calculate activation parameters from variable temperature experiments considering statistical contributions is shown in Figure S8.

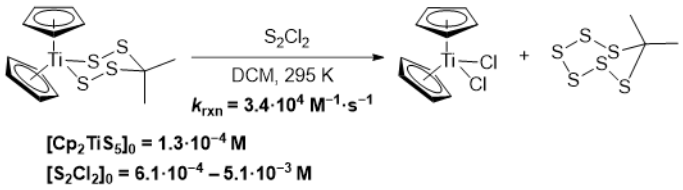

$[S_2Cl_2]_0$ [M]	k_{obs} [s^{-1}]	SD [s^{-1}]
$5.1 \cdot 10^{-3}$	$1.7 \cdot 10^{2}$	$1.8 \cdot 10^{1}$ (11%, n = 8)
$2.0 \cdot 10^{-3}$	$7.5 \cdot 10^{1}$	$6.1 \cdot 10^{0}$ (8%, n = 8)
$1.8 \cdot 10^{-3}$	$6.1 \cdot 10^{1}$	$1.1 \cdot 10^{0}$ (2%, n = 8)
$1.5 \cdot 10^{-3}$	$5.0 \cdot 10^{1}$	$1.4 \cdot 10^{0}$ (3%, n = 8)
$1.3 \cdot 10^{-3}$	$4.2 \cdot 10^{1}$	$6.0 \cdot 10^{-1}$ (1%, n = 8)
$1.0 \cdot 10^{-3}$	$3.2 \cdot 10^{1}$	$5.3 \cdot 10^{-1}$ (2%, n = 8)
$8.1 \cdot 10^{-4}$	$2.5 \cdot 10^{1}$	$1.0 \cdot 10^{0}$ (4%, n = 8)
$6.1 \cdot 10^{-4}$	$2.0 \cdot 10^{1}$	$2.1 \cdot 10^{-1}$ (1%, n = 8)

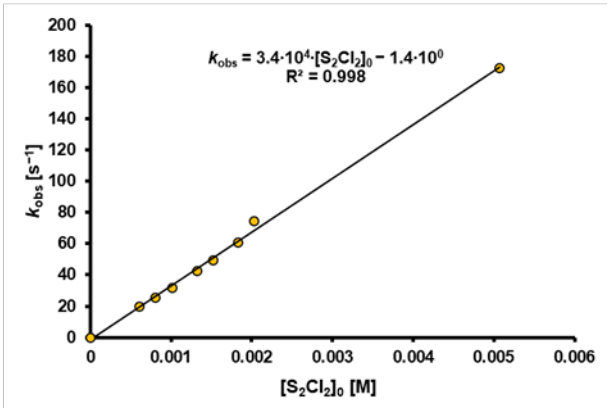

Figure S8. Reaction of $Cp_2TiS_4(CMe_2)$ with S_2Cl_2 in DCM at 295K. Summary of conditions, pseudo-first order rate constants and linear fitting against $[S_2Cl_2]_0$.

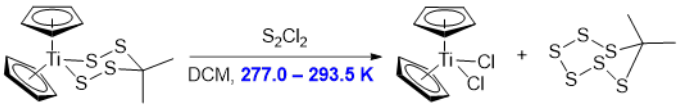

$[Cp_2TiS_5]_0 = 5.2 \cdot 10^{-5}$ M
$[S_2Cl_2]_0 = 1.9 \cdot 10^{-4}$ M

T [K]	k_{obs} [s^{-1}]	SD [s^{-1}]	k_{rxn} [s^{-1}]
277.0	$7.8 \cdot 10^{0}$	$3.1 \cdot 10^{-1}$ (4%, n = 7)	$4.1 \cdot 10^{4}$
281.0	$7.5 \cdot 10^{0}$	$2.3 \cdot 10^{-1}$ (3%, n = 8)	$4.0 \cdot 10^{4}$
284.9	$7.0 \cdot 10^{0}$	$1.6 \cdot 10^{-1}$ (2%, n = 8)	$3.7 \cdot 10^{4}$
289.1	$6.9 \cdot 10^{0}$	$1.8 \cdot 10^{-1}$ (3%, n = 8)	$3.6 \cdot 10^{4}$
291.8	$6.6 \cdot 10^{0}$	$1.0 \cdot 10^{-1}$ (2%, n = 8)	$3.5 \cdot 10^{4}$
293.5	$6.5 \cdot 10^{0}$	$1.5 \cdot 10^{-1}$ (2%, n = 8)	$3.5 \cdot 10^{4}$
295.2[a]	–	–	$3.4 \cdot 10^{4}$

[a] k_{rxn} at T = 295.2 K obtained from experiments varying $[S_2Cl_2]_0$, see Figure S5

$$k_{rxn}\,(M^{-1}\cdot s^{-1}) = n \cdot k_{s\text{-}s} = \mathbf{n}\left(\frac{\kappa k_b T}{h}\right) e^{\frac{-\Delta G^{\ddagger}}{RT}}$$

$$\ln\left(k_{rxn}/T\right) = -\frac{\Delta H^{\ddagger}}{R}\left(\frac{1}{T}\right) + \ln\left[\mathbf{n}\left(\frac{\kappa k_b}{h}\right)\right] + \frac{\Delta S^{\ddagger}}{R}$$

slope; y-intercept

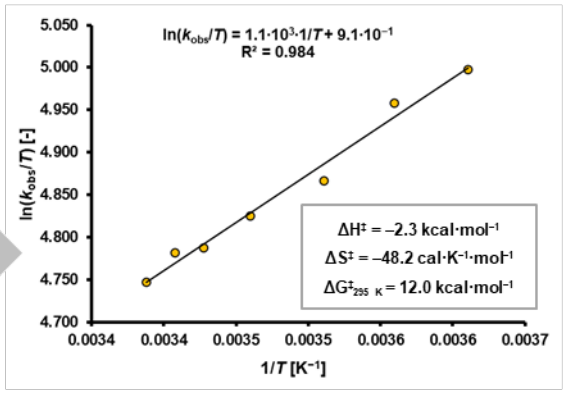

k_{rxn}	Bimolecular rate constant ($M^{-1}s^{-1}$)	κ	Transmission coefficient	$\Delta G^{\ddagger}$	Free energy barrier (microkinetic)
$k_{S\text{-}S}$	Microkinetic rate constant	k_b	Boltzmant constant	$\Delta H^{\ddagger}$	Enthalpy change (microkinetic)
n	Number of equivalent microkinetic events	T	Temperature	$\Delta S^{\ddagger}$	Entropy change (microkinetic)
		h	Planck Constant	R	Ideal gas constant

Figure S9. Reaction of $Cp_2TiS_4(CMe_2)$ with S_2Cl_2 in DCM at different temperatures. Summary of rate constants and Eyring analysis including statistical corrections (n = 4; κ = 1).

2.6 Reaction of $Cp_2Ti(SPh)Cl$ with S_2Cl_2

The reactions were performed at 22 °C (295 K) in DCM using a 10 mm light-path. Temporal evolution of UV spectra is shown in Figure S10. Decay of absorbance at 495 nm is exponential (Figure S10B), indicating first order kinetic dependency in titanocene complex concentration. No change in spectroscopic features were observed (see comparison of Figure S10C and Figure S10D), which indicates that the complex does not disproportionate. Results from exponential decays at 495 nm at various initial concentrations of S_2Cl_2 are shown in Figure S10E. The extracted decay constants (*k*obs) showed linear correlation with $[S_2Cl_2]_0$ (Figure S10E). The observed process rate constant ($k_{rxn} = 1.2 \cdot 10^5\ M^{-1}s^{-1}$) is representative of various simultaneous processes of the form {$Cp_2Ti(SPh)Cl$ + RSCl}, because the initial reaction generates additional reactive sulfur electrophiles (e.g., PhS_3Cl). Comparison of this system against others can only be qualitative.

Results from reaction of $Cp_2Ti(SPh)Cl$ with S_2Cl_2 at various temperatures are shown in Figure S11. The results show that a decrease in temperature of approximately 15 ^oC causes a slight increase in rate ($k_{283K} = 1.2\ k_{297K}$).

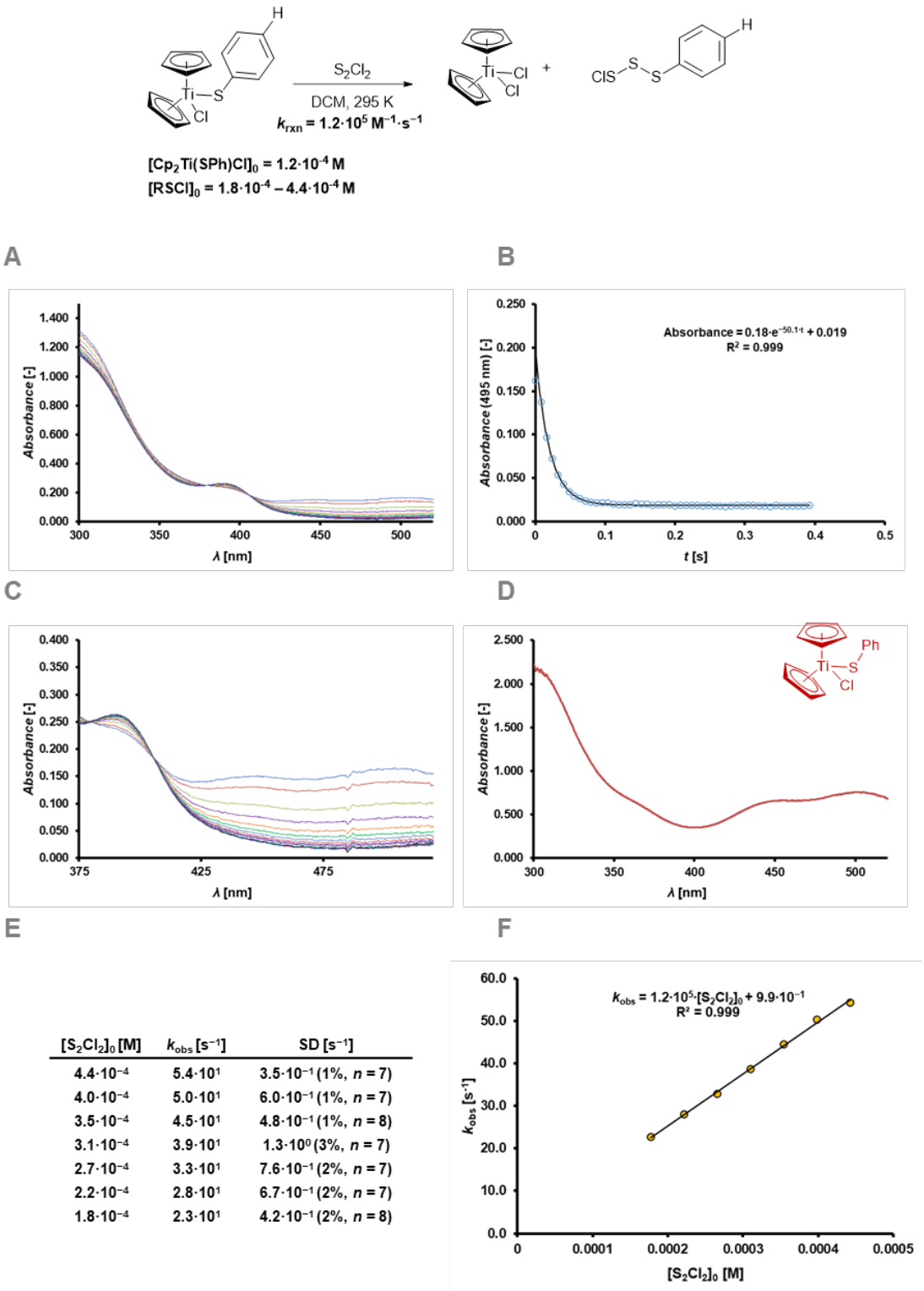

$[S_2Cl_2]_0$ [M]	k_{obs} [s^{-1}]	SD [s^{-1}]
$4.4 \cdot 10^{-4}$	$5.4 \cdot 10^{1}$	$3.5 \cdot 10^{-1}$ (1%, $n = 7$)
$4.0 \cdot 10^{-4}$	$5.0 \cdot 10^{1}$	$6.0 \cdot 10^{-1}$ (1%, $n = 7$)
$3.5 \cdot 10^{-4}$	$4.5 \cdot 10^{1}$	$4.8 \cdot 10^{-1}$ (1%, $n = 8$)
$3.1 \cdot 10^{-4}$	$3.9 \cdot 10^{1}$	$1.3 \cdot 10^{0}$ (3%, $n = 7$)
$2.7 \cdot 10^{-4}$	$3.3 \cdot 10^{1}$	$7.6 \cdot 10^{-1}$ (2%, $n = 7$)
$2.2 \cdot 10^{-4}$	$2.8 \cdot 10^{1}$	$6.7 \cdot 10^{-1}$ (2%, $n = 7$)
$1.8 \cdot 10^{-4}$	$2.3 \cdot 10^{1}$	$4.2 \cdot 10^{-1}$ (2%, $n = 8$)

Figure S10. Reaction of $Cp_2Ti(SPh)Cl$ with S_2Cl_2. A) Stack of UV-spectra for reaction monitoring. B) Exponential decay model (black line) fitted to experimental data (circles) of temporal absorbance at 495 nm. C) Zoomed stacked of spectra. D) UV-spectrum of starting titanocene solution before initiating the reaction. E) Initial concentrations, average pseudo-first order rate constants and standard deviations. F) Linear relationship and fitting for pseudo-first order rate constants at various initial S_2Cl_2 concentrations.

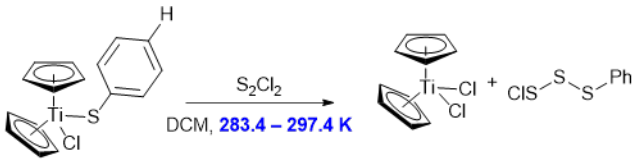

$[Cp_2Ti(SPh)Cl]_0 = 1.3 \cdot 10^{-4}$ M

$[S_2Cl_2]_0 = 3.4 \cdot 10^{-4}$ M

T [K]	k_{obs} [s^{-1}]	SD [s^{-1}]	k_{rxn} [s^{-1}]
283.4	$6.2 \cdot 10^{1}$	$2.5 \cdot 10^{0}$ (4%, n = 8)	$1.8 \cdot 10^{5}$
285.9	$6.0 \cdot 10^{1}$	$1.4 \cdot 10^{0}$ (2%, n = 8)	$1.7 \cdot 10^{5}$
287.8	$5.9 \cdot 10^{1}$	$1.0 \cdot 10^{0}$ (2%, n = 7)	$1.7 \cdot 10^{5}$
289.3	$5.7 \cdot 10^{1}$	$1.5 \cdot 10^{0}$ (3%, n = 8)	$1.6 \cdot 10^{5}$
291.9	$5.6 \cdot 10^{1}$	$1.8 \cdot 10^{0}$ (3%, n = 8)	$1.6 \cdot 10^{5}$
294.2	$5.4 \cdot 10^{1}$	$1.1 \cdot 10^{0}$ (2%, n = 8)	$1.6 \cdot 10^{5}$
297.4	$5.1 \cdot 10^{1}$	$1.8 \cdot 10^{0}$ (3%, n = 8)	$1.5 \cdot 10^{5}$

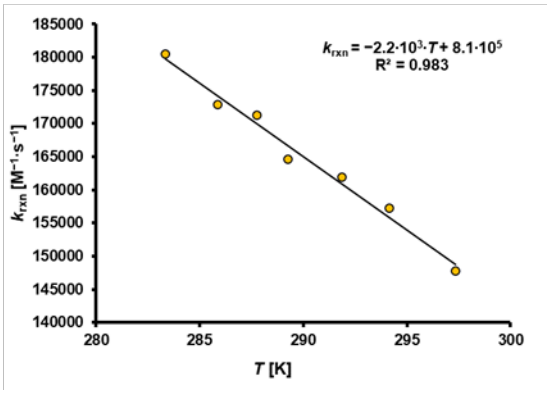

Figure S11. Reaction of $Cp_2Ti(SPh)Cl$ with S_2Cl_2 within 297 – 283 K. Summary of results and analysis of bimolecular process rate constants at variable temperature.

2.7 Reactions of $Cp_2Ti(SAr)_2$ with S_2Cl_2

The reactions were performed at 22 °C (295 K) in DCM using a 10 mm light-path. Comparison of the temporal evolution of UV spectra (Figure S12C) with that of the starting complex in DCM (blue line in Figure S12D) shows complete disappearance of main characteristic spectroscopic features of $Cp_2Ti(SAr)_2$. The spectra observed after initiation matched with those of the mono-thiophenolate complex (e.g. $Cp_2TiCl(SPh)$; red line in Figure S12D), suggesting the first step of the reaction is mostly complete within the deadtime (<10 ms). Decay of absorbance at 495 nm, corresponding to $Cp_2Ti(SPh)Cl$ is exponential (Figure S12B) and correlates linearly with $[S_2Cl_2]_0$ (Figure S12E,F). The observed process rate constant, $k_{rxn} = 1.2 \cdot 10^5\ M^{-1}s^{-1}$ is in agreement with that obtained by monitoring of the monothiophenolate complex alone. Neither of the constants (k_{obs}, k_{rxn}) represent the process $\{Cp_2Ti(SAr)_2 + S_2Cl_2\}$ in isolation, because of the generation of reactive ArS_3Cl as products**.** Comparisons of these values with others in this work must thus be qualitative.

The procedure was repeated with other complexes to provide a qualitative comparison of electronic effects. Results are shown below in Figure S13, and show the general trend that the more electron rich the thiophenolate ligand is, the faster the nucleophilic substitution process.

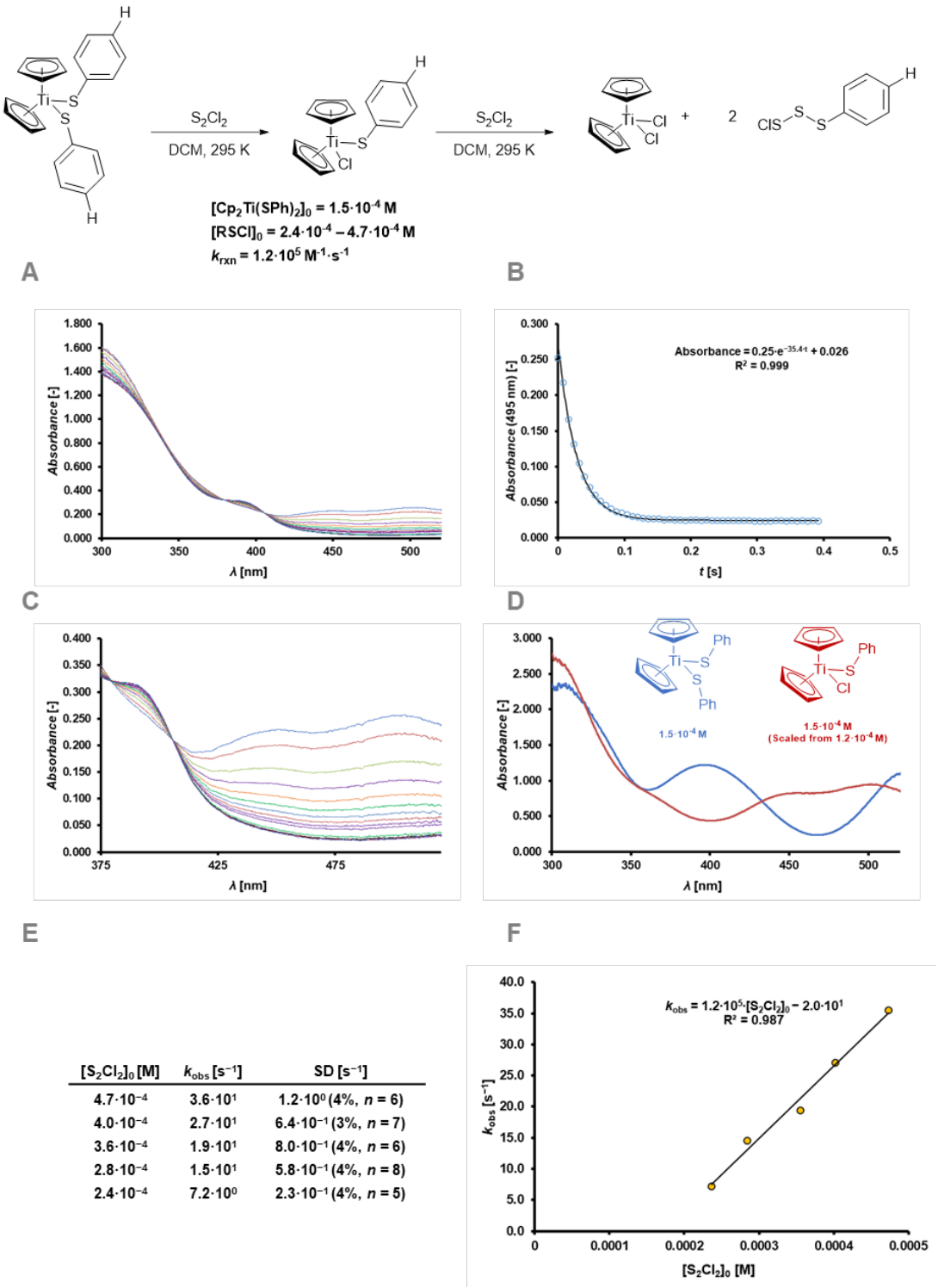

$[S_2Cl_2]_0$ [M]	k_{obs} [s^{-1}]	SD [s^{-1}]
$4.7 \cdot 10^{-4}$	$3.6 \cdot 10^{1}$	$1.2 \cdot 10^{0}$ (4%, $n = 6$)
$4.0 \cdot 10^{-4}$	$2.7 \cdot 10^{1}$	$6.4 \cdot 10^{-1}$ (3%, $n = 7$)
$3.6 \cdot 10^{-4}$	$1.9 \cdot 10^{1}$	$8.0 \cdot 10^{-1}$ (4%, $n = 6$)
$2.8 \cdot 10^{-4}$	$1.5 \cdot 10^{1}$	$5.8 \cdot 10^{-1}$ (4%, $n = 8$)
$2.4 \cdot 10^{-4}$	$7.2 \cdot 10^{0}$	$2.3 \cdot 10^{-1}$ (4%, $n = 5$)

Figure S12. Reaction of $Cp_2Ti(SPh)_2$ with S_2Cl_2. A) Stack of UV-spectra. B) Exponential decay model (black line) fitted to experimental data (circles) of temporal absorbance at 495 nm. C) Zoomed stack of spectra. D) Overlay of UV-spectrum of starting titanocene bis(thiophenolate) solution before initiating the reaction (blue line) and independent sample of monothiophenolate intermediate (red line). E) Initial concentrations, average pseudo-first order rate constants and standard deviations. F) Linear relationship and fitting for pseudo-first order rate constants at various initial S_2Cl_2 concentrations. A non-zero intercept was observed.

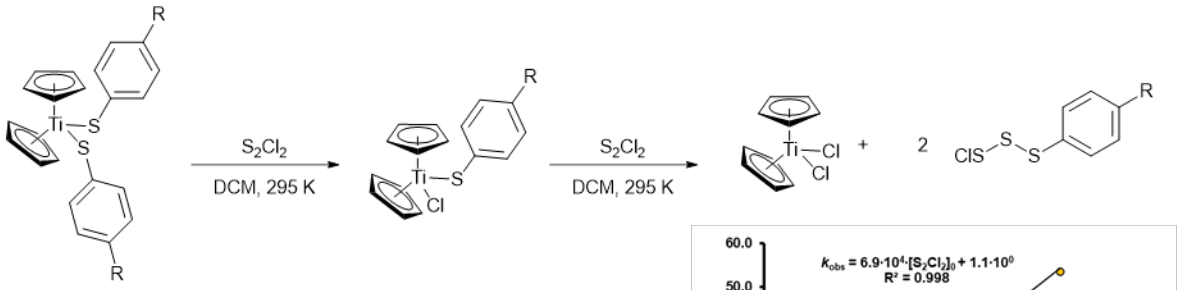

Substituent	$[S_2Cl_2]_0$ [M]	k_{obs} [s^{-1}]	SD [s^{-1}]
R = F	$7.7\cdot10^{-4}$	$5.3\cdot10^{1}$	$2.1\cdot10^{0}$ (4%, *n* = 7)
($[Cp_2Ti(SAr)_2]_0 = 6.2\cdot10^{-5}$ M)	$5.1\cdot10^{-4}$	$3.8\cdot10^{1}$	$2.4\cdot10^{0}$ (6%, *n* = 8)
	$3.8\cdot10^{-4}$	$2.8\cdot10^{1}$	$9.4\cdot10^{-1}$ (3%, *n* = 6)
	$2.6\cdot10^{-4}$	$1.9\cdot10^{1}$	$2.4\cdot10^{-1}$ (1%, *n* = 8)
	$1.9\cdot10^{-4}$	$1.5\cdot10^{1}$	$4.7\cdot10^{-1}$ (3%, *n* = 7)
	$1.3\cdot10^{-4}$	$9.2\cdot10^{0}$	$2.8\cdot10^{-1}$ (3%, *n* = 8)
R = Cl	$7.6\cdot10^{-4}$	$3.2\cdot10^{1}$	$5.8\cdot10^{-1}$ (2%, *n* = 8)
($[Cp_2Ti(SAr)_2]_0 = 1.2\cdot10^{-4}$ M)	$6.3\cdot10^{-4}$	$2.7\cdot10^{1}$	$3.8\cdot10^{-1}$ (1%, *n* = 8)
	$5.0\cdot10^{-4}$	$2.2\cdot10^{1}$	$2.1\cdot10^{-1}$ (1%, *n* = 7)
	$3.8\cdot10^{-4}$	$1.7\cdot10^{1}$	$2.7\cdot10^{-1}$ (2%, *n* = 8)
	$2.5\cdot10^{-4}$	$1.1\cdot10^{1}$	$3.3\cdot10^{-1}$ (3%, *n* = 6)
	$2.0\cdot10^{-4}$	$7.4\cdot10^{0}$	$2.3\cdot10^{-1}$ (3%, *n* = 8)
R = OMe	$2.4\cdot10^{-4}$	$9.5\cdot10^{1}$	$3.1\cdot10^{0}$ (3%, *n* = 6)
($[Cp_2Ti(SAr)_2]_0 = 7.3\cdot10^{-5}$ M)	$2.0\cdot10^{-4}$	$8.1\cdot10^{1}$	$2.9\cdot10^{0}$ (4%, *n* = 8)
	$1.8\cdot10^{-4}$	$6.6\cdot10^{1}$	$3.5\cdot10^{0}$ (5%, *n* = 6)
	$1.5\cdot10^{-4}$	$5.6\cdot10^{1}$	$3.4\cdot10^{0}$ (6%, *n* = 8)
	$1.4\cdot10^{-4}$	$4.4\cdot10^{1}$	$1.8\cdot10^{0}$ (4%, *n* = 8)
	$1.3\cdot10^{-4}$	$4.2\cdot10^{1}$	$2.0\cdot10^{0}$ (5%, *n* = 8)
	$9.5\cdot10^{-5}$	$1.7\cdot10^{1}$	$1.6\cdot10^{0}$ (10%, *n* = 6)

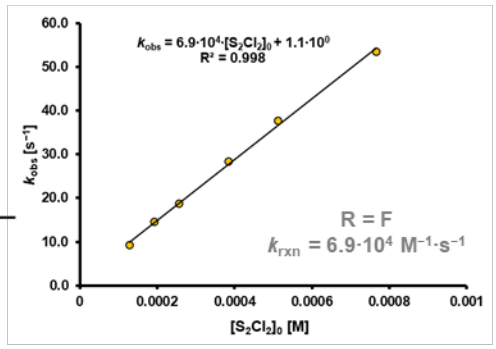

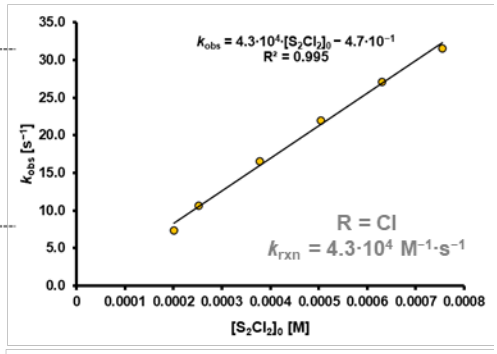

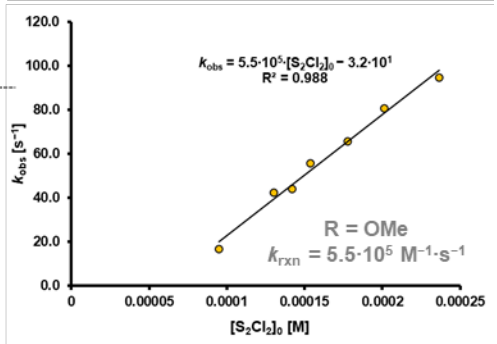

Figure S13. Reaction of bisthiophenolate derivatives $Cp_2Ti(R\text{-}C_6H_4S)_2$ with S_2Cl_2 in DCM at 295 K. Summary of initial conditions and analysis against initial concentration of S_2Cl_2. A non-zero intercept was observed

3. Stopped-Flow UV-Vis of sequential reactions

3.1 Representative procedure to extract bimolecular rate constants

The reaction of Cp_2TiS_5 with *N*-morpholinosulfenyl chloride has been used to describe the representative procedure for the detection and determination of bimolecular rate constants in sequential reactions monitored via *in-situ* stopped-flow UV. Kinetic measurements were performed at 22 °C (295 K) in anhydrous DCM using a 10 mm light-path. Solutions of the sulfur electrophile (RSCl) were used in excess concentrations to achieve pseudo-first order kinetic conditions. Different concentrations of the sulfenyl chloride were achieved by dilution of a concentrated stock solution. A typical stack of temporal UV spectra is shown in Figure S14. The lack of isosbestic points and evolution of absorbance at 495 nm (Figure S15 – S27) are indicative of a consecutive process.

A consecutive bimolecular reaction model was used to fit the temporal evolution of absorbance assuming individual absorbance of all species involved were additive (eq. S1). Measurement of relative rate constants of consecutive steps (k_{rel}, eq. S2) was first required as a constraint to provide a unique solution. Relative reaction rate constants were extracted via NMR reaction monitoring or titrations (see Section S4.2). Numerical modelling was performed using a system of differential equations (eq. S3 - S6) to extract the temporal concentrations that input into eq. S1. Absorbance evolution of runs at the same initial electrophile concentration were averaged. Fitting was performed simultaneously to all reaction conditions (i.e. $[RSCl]_0$ variations) for a given sulfur electrophile. Results of fittings are shown in Figure S15 – S27.

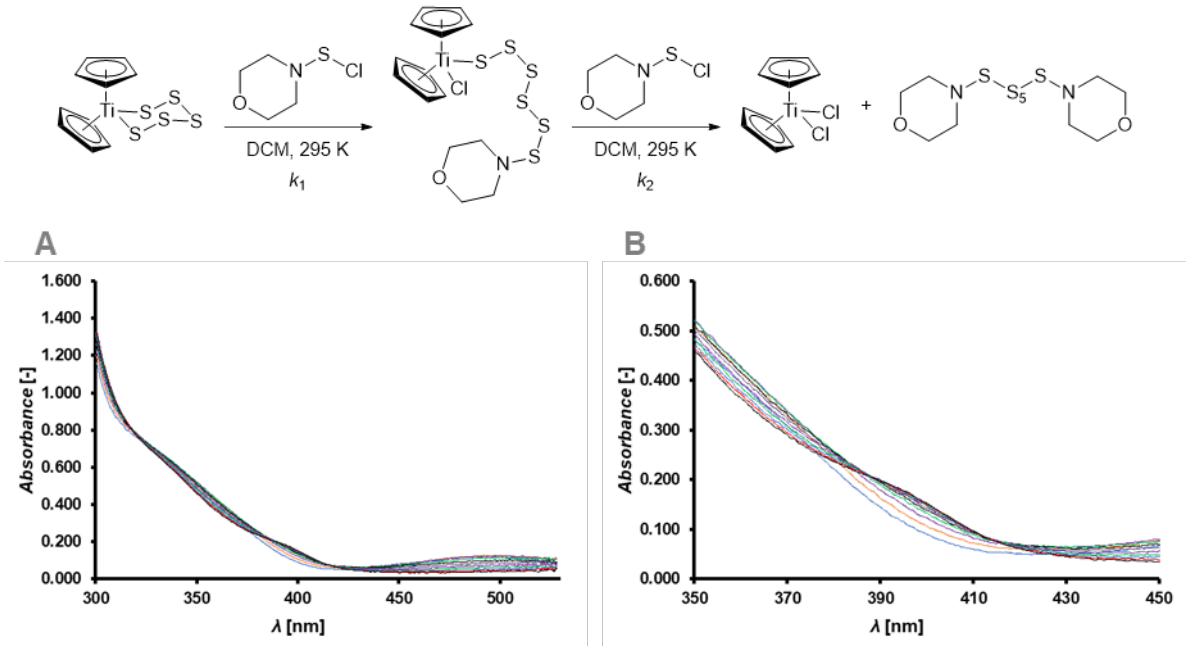

Figure S14. Reaction of Cp_2TiS_5 with (*N*-Morpholino)sulfenyl chloride in DCM at 295K. A) Temporal evolution of UV spectra. B) Spectra evolution within the wavelength range 350 – 450 nm showing the lack of isosbestic points.

$$\mathbf{A} \xrightarrow[k_1]{\mathbf{E}} \mathbf{B} \xrightarrow[k_2]{\mathbf{E}} \mathbf{C + P}$$

$$Abs = \varepsilon_A[A] + \varepsilon_B[B] + \varepsilon_C[C] + \varepsilon_E[E] + \varepsilon_P[P] + X \quad \textbf{(eq. S1)}$$

$$k_{rel} = k_2 / k_1 \quad \textbf{(eq. S2)}$$

$$\frac{d[A]}{dt} = -k_1[A][E] \quad \textbf{(eq. S3)}$$

$$\frac{d[B]}{dt} = k_1[A][E] - k_1 k_{rel}[B][E] \quad \textbf{(eq. S4)}$$

$$\frac{d[C]}{dt} = \frac{d[P]}{dt} = k_1 k_{rel}[B][E] \quad \textbf{(eq. S5)}$$

$$\frac{d[E]}{dt} = -k_1[A][E] - k_1 k_{rel}[B][E] \quad \textbf{(eq. S6)}$$

3.2 Reaction of Cp_2TiS_5 with *N*-morpholinosulfenyl chloride

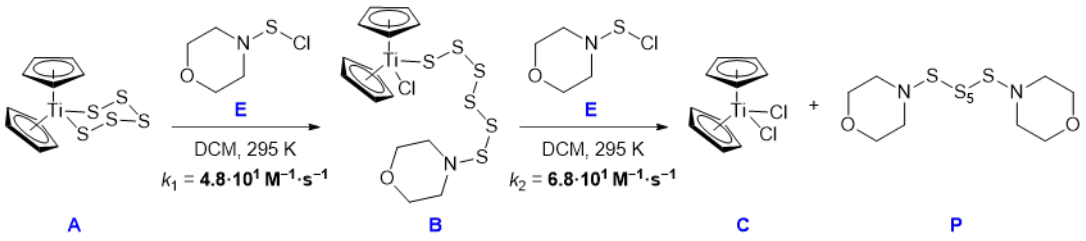

$k_{rel} = k_2/k_1 = 1.4$

$[Cp_2TiS_5]_0 = 5.3 \cdot 10^{-5}$ M

$[E]_0 = 4.9 \cdot 10^{-4} - 4.9 \cdot 10^{-3}$ M

ε_A(495 nm): 2240 $M^{-1} \cdot cm^{-1}$

ε_B(495 nm): 3382 $M^{-1} \cdot cm^{-1}$ (Fitted)

ε_C(495 nm): 160 $M^{-1} \cdot cm^{-1}$

ε_E(495 nm): 0 $M^{-1} \cdot cm^{-1}$

ε_P(495 nm): 118 $M^{-1} \cdot cm^{-1}$ (Fitted)

Fitted Model*:

$Abs = [A] \cdot \varepsilon_A + [B] \cdot \varepsilon_B + [C] \cdot \varepsilon_C + [E] \cdot \varepsilon_E + [P] \cdot \varepsilon_P + x$

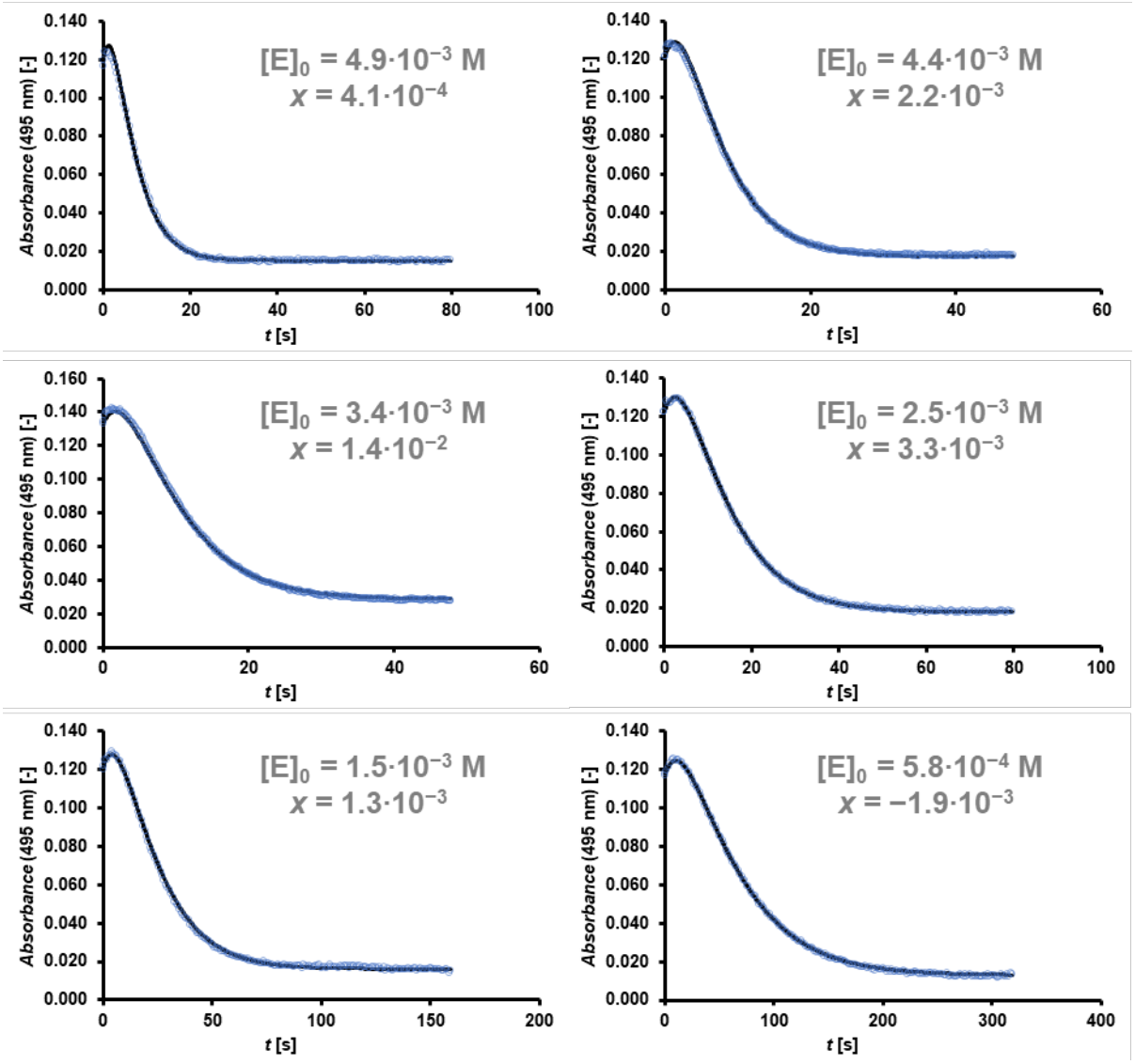

Figure S15. Reaction of Cp_2TiS_5 with (*N*-Morpholino)sulfenyl chloride in DCM at 295K. Summary of conditions and fitting results.

3.3 Reaction of Cp_2TiS_5 with AcSSCl

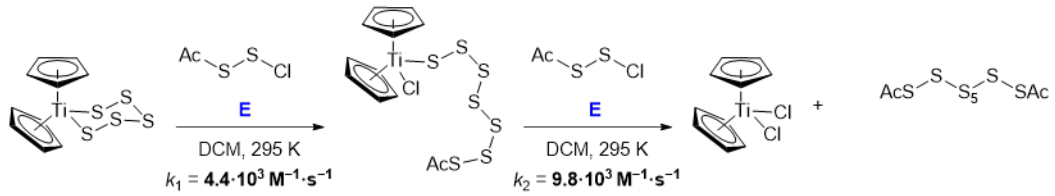

$k_{rel} = k_2/k_1 = 2.2$

ε_A(495 nm): 2240 $M^{-1}\cdot cm^{-1}$

ε_B(495 nm): 3131 $M^{-1}\cdot cm^{-1}$ (Fitted)

ε_C(495 nm): 160 $M^{-1}\cdot cm^{-1}$

ε_E(495 nm): 0 $M^{-1}\cdot cm^{-1}$

ε_P(495 nm): 26 $M^{-1}\cdot cm^{-1}$ (Fitted)

$[Cp_2TiS_5]_0 = 5.2\cdot10^{-5}$ M

$[E]_0 = 8.0\cdot10^{-4} - 3.0\cdot10^{-3}$ M

Fitted Model*:

Abs = $[A]\cdot\varepsilon_A + [B]\cdot\varepsilon_B + [C]\cdot\varepsilon_C + [E]\cdot\varepsilon_E + [P]\cdot\varepsilon_P + x$

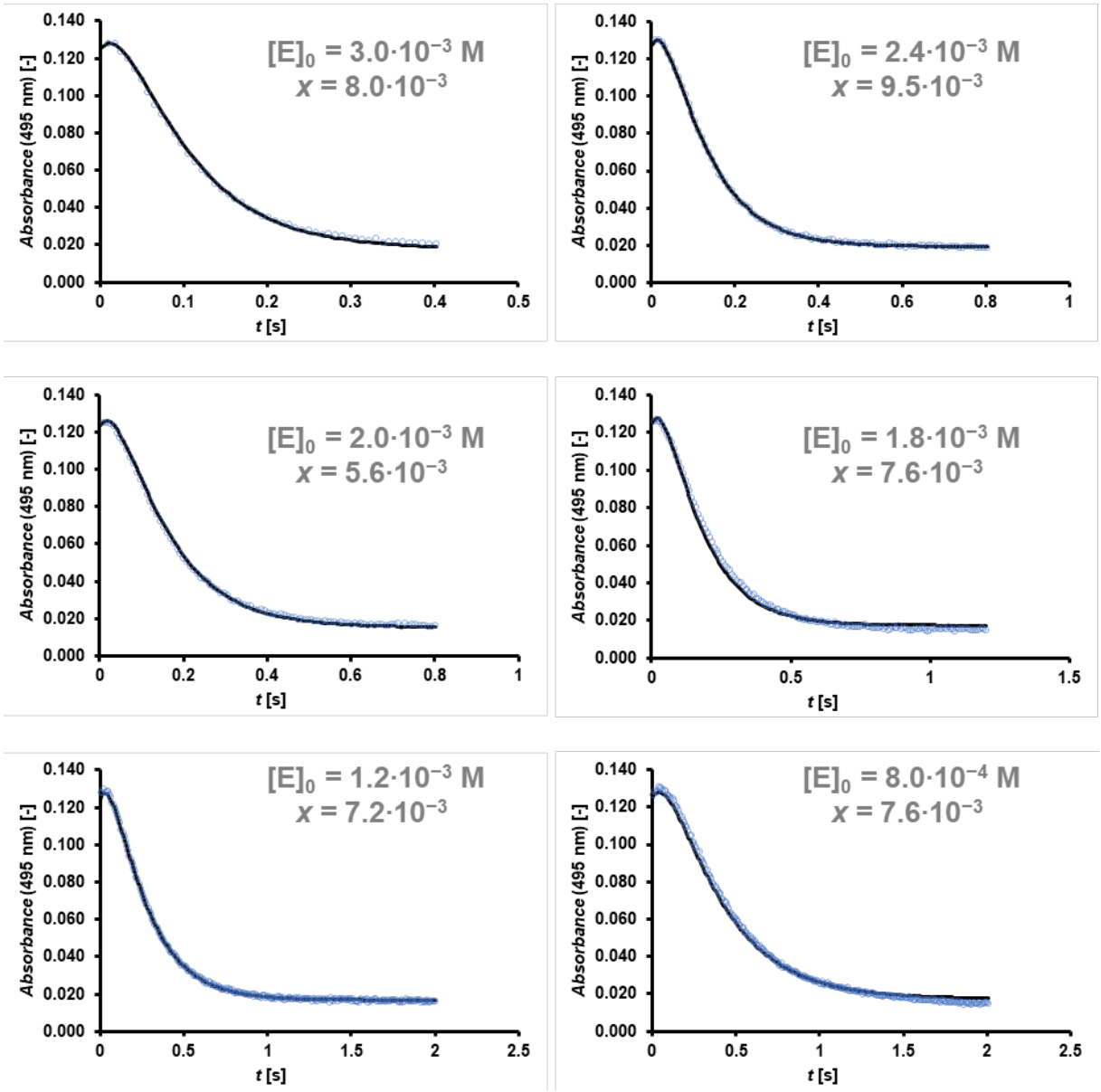

Figure S16. Reaction of Cp_2TiS_5 with (acetylthio)sulfenyl chloride in DCM at 295K. Summary of conditions and fitting results.

3.4 Reaction of Cp_2TiS_5 with *N*-phthalimidosulfenyl chloride

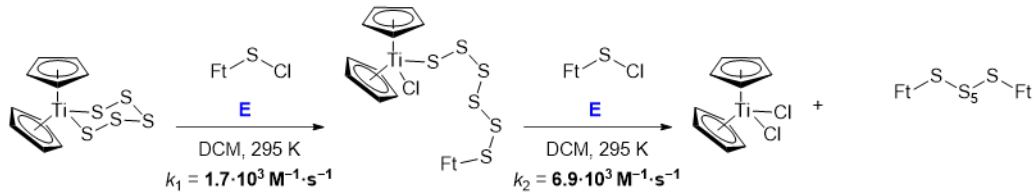

$k_{rel} = k_2/k_1 = 4.0$

ε_A(495 nm): 448 $M^{-1}\cdot cm^{-1}$

ε_B(495 nm): 520 $M^{-1}\cdot cm^{-1}$ (Fitted)

ε_C(495 nm): 32 $M^{-1}\cdot cm^{-1}$

ε_E(495 nm): 1 $M^{-1}\cdot cm^{-1}$

ε_P(495 nm): 0 $M^{-1}\cdot cm^{-1}$ (Fitted)

$[Cp_2TiS_5]_0 = 6.5\cdot10^{-5}$ M

$[E]_0 = 1.0\cdot10^{-3} - 3.1\cdot10^{-3}$ M

Fitted Model*:

Abs = $[A]\cdot\varepsilon_A + [B]\cdot\varepsilon_B + [C]\cdot\varepsilon_C + [E]\cdot\varepsilon_E + [P]\cdot\varepsilon_P + x$

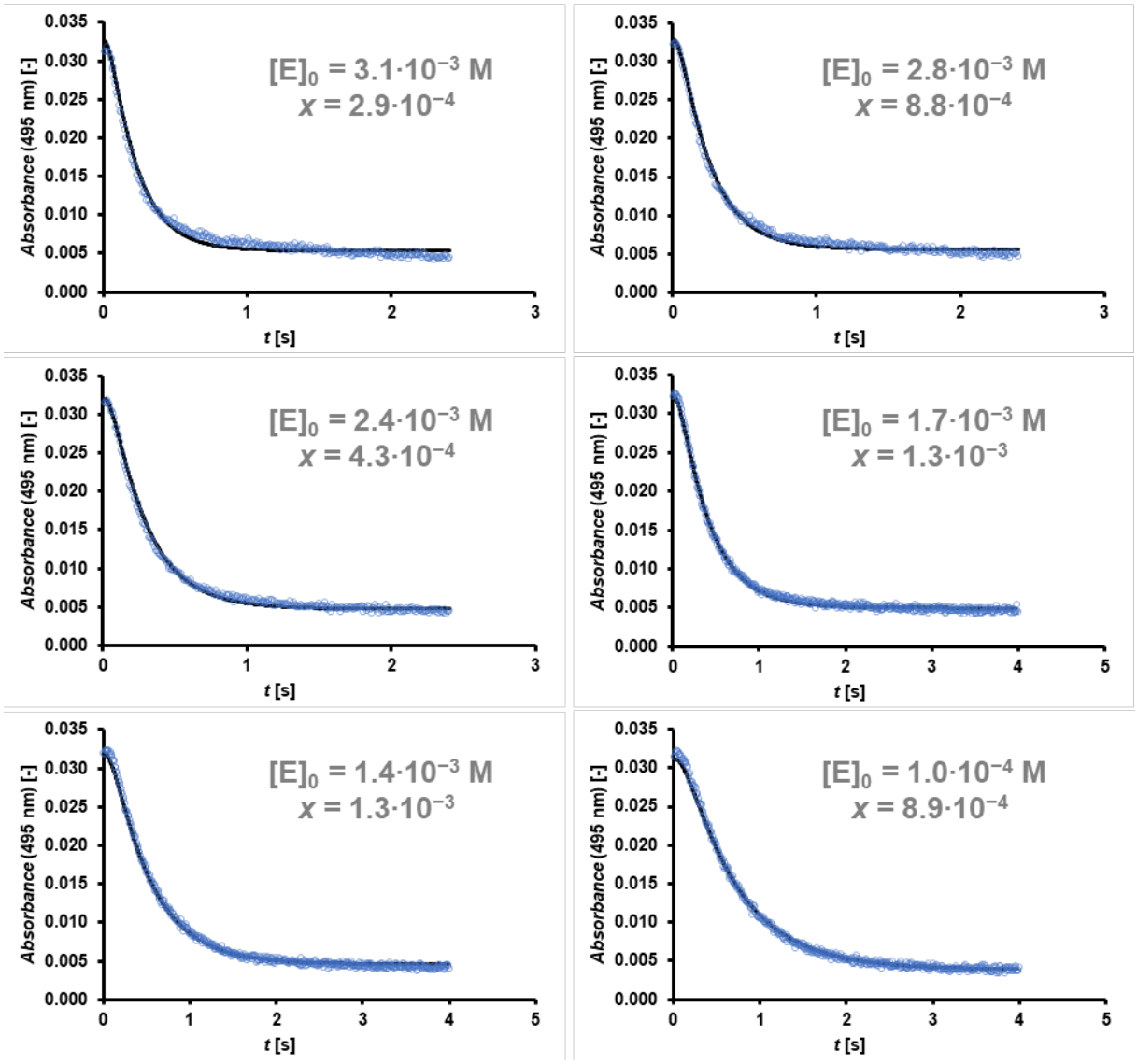

Figure S17. Reaction of Cp_2TiS_5 with (*N*-phthalimido)sulfenyl chloride (FtSCl) in DCM at 295K. Summary of conditions and fitting results.

3.5 Reaction of Cp_2TiS_5 with 4-nitrophenylsulfenyl chloride

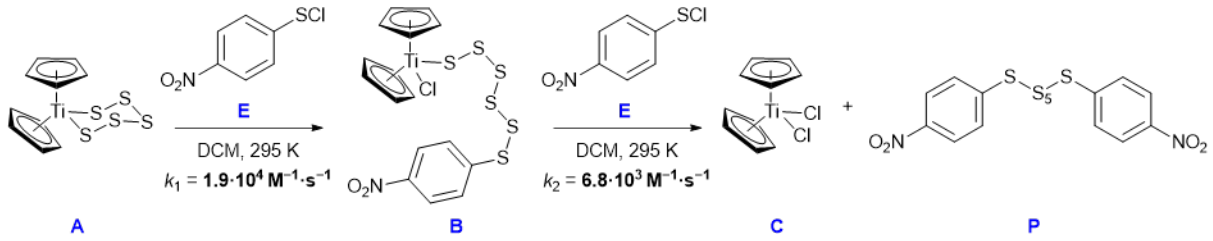

A B C P

$k_{rel} = k_2/k_1 = 0.36$

ε_A(495 nm): 2240 $M^{-1}\cdot cm^{-1}$

ε_B(495 nm): 2991 $M^{-1}\cdot cm^{-1}$ (Fitted)

ε_C(495 nm): 160 $M^{-1}\cdot cm^{-1}$

ε_E(495 nm): 5 $M^{-1}\cdot cm^{-1}$

ε_P(495 nm): 79 $M^{-1}\cdot cm^{-1}$ (Fitted)

$[Cp_2TiS_5]_0 = 9.0\cdot10^{-5}$ M

$[E]_0 = 2.5\cdot10^{-4} - 2.5\cdot10^{-3}$ M

Fitted Model*:

Abs = $[A]\cdot\varepsilon_A + [B]\cdot\varepsilon_B + [C]\cdot\varepsilon_C + [E]\cdot\varepsilon_E + [P]\cdot\varepsilon_P + x$

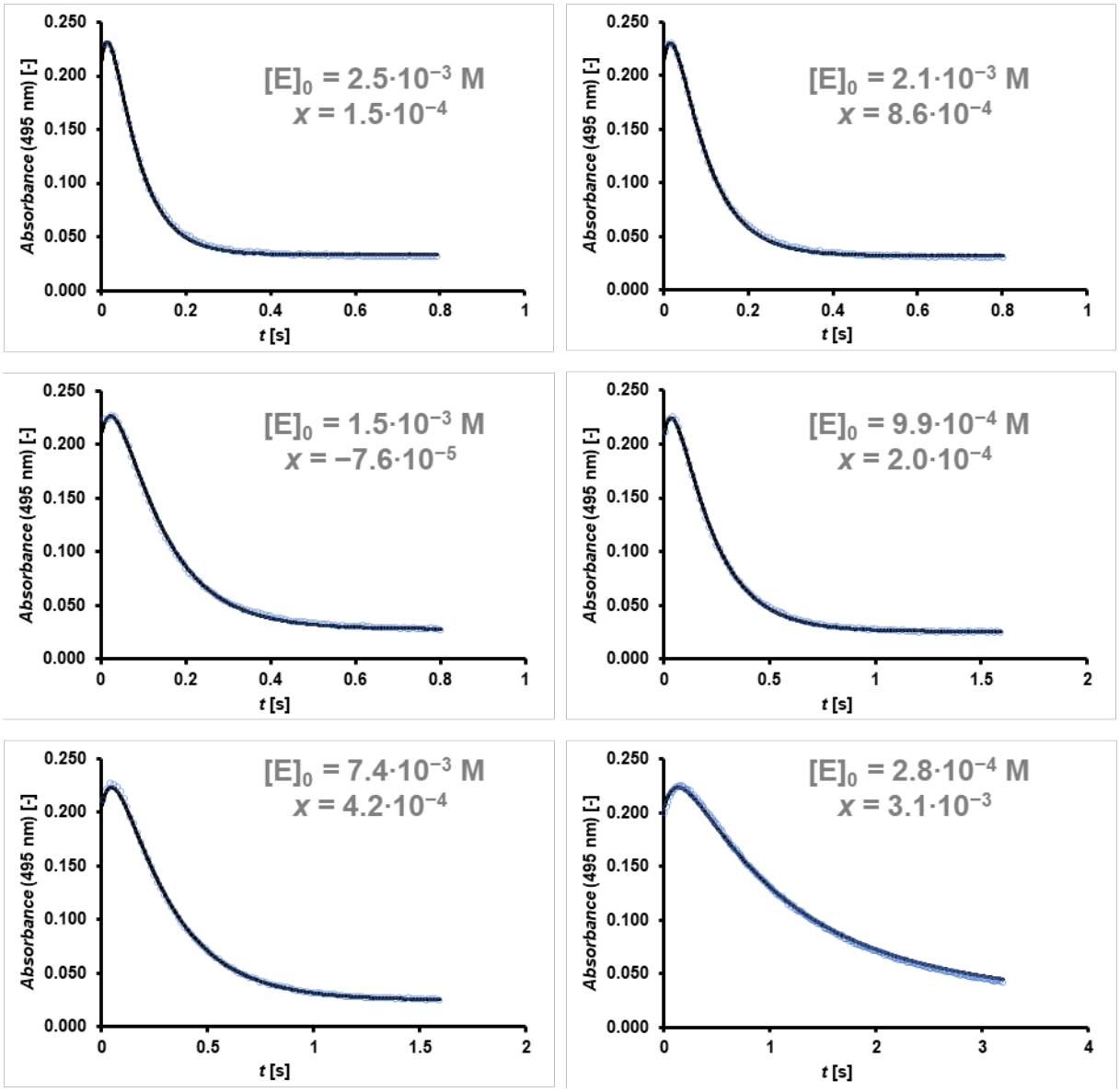

Figure S18. Reaction of Cp_2TiS_5 with (4-nitrophenyl)sulfenyl chloride in DCM at 295K. Summary of conditions and fitting results.

3.6 Reaction of Cp_2TiS_5 with 4-chlorophenylsulfenyl chloride

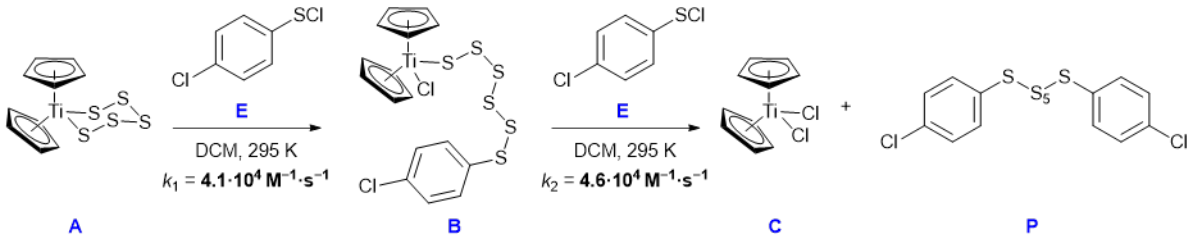

$k_{rel} = k_2/k_1$ =1.12

ε_A(495 nm): 2240 $M^{-1}\cdot cm^{-1}$

ε_B(495 nm): 2903 $M^{-1}\cdot cm^{-1}$ (Fitted)

ε_C(495 nm): 160 $M^{-1}\cdot cm^{-1}$

ε_E(495 nm): 5 $M^{-1}\cdot cm^{-1}$

ε_P(495 nm): 115 $M^{-1}\cdot cm^{-1}$ (Fitted)

$[Cp_2TiS_5]_0 = 9.0\cdot10^{-5}$ M

$[E]_0 = 5.2\cdot10^{-4} - 2.1\cdot10^{-3}$ M

Fitted Model*:

Abs = $[A]\cdot\varepsilon_A + [B]\cdot\varepsilon_B + [C]\cdot\varepsilon_C + [E]\cdot\varepsilon_E + [P]\cdot\varepsilon_P + x$

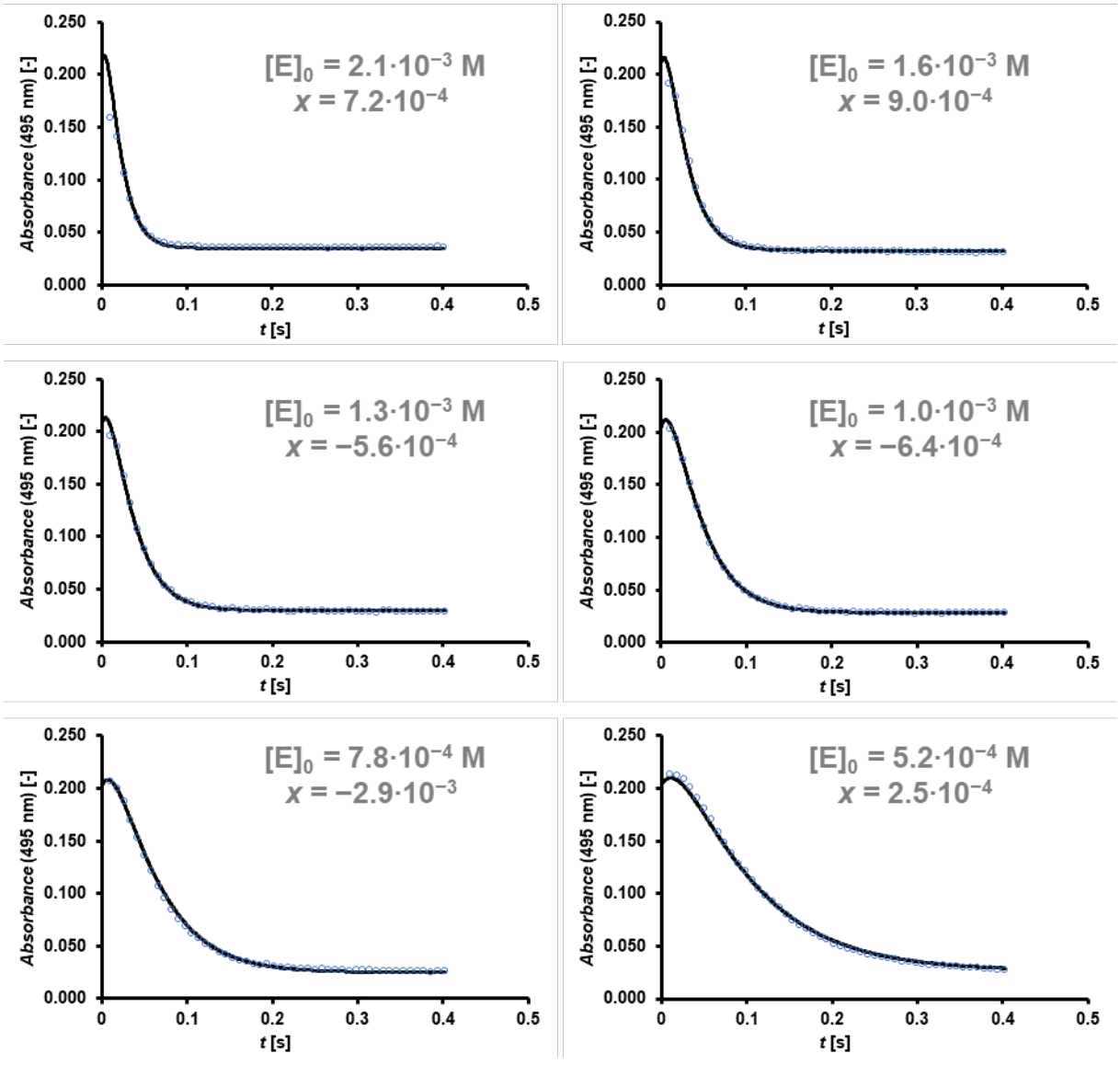

Figure S19. Reaction of Cp_2TiS_5 with (4-chlorophenyl)sulfenyl chloride in DCM at 295K. Summary of conditions and fitting results.

3.7 Reaction of Cp_2TiS_5 with 4-fluorophenylsulfenyl chloride

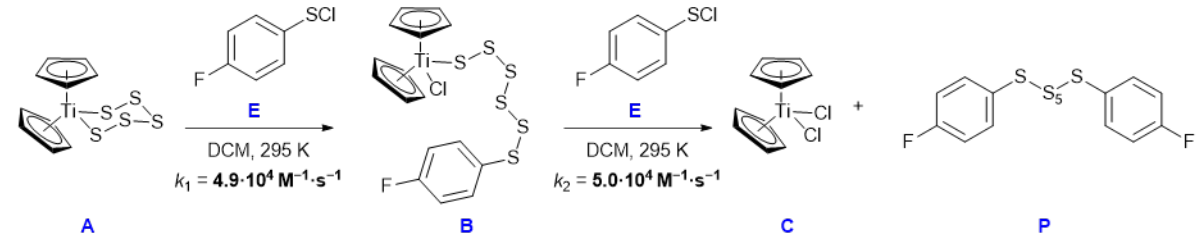

$k_{rel} = k_2/k_1$ =1.02

ε_A(495 nm): 448 $M^{-1}\cdot cm^{-1}$

ε_B(495 nm): 821 $M^{-1}\cdot cm^{-1}$ (Fitted)

ε_C(495 nm): 32 $M^{-1}\cdot cm^{-1}$

ε_E(495 nm): 1.6 $M^{-1}\cdot cm^{-1}$

ε_P(495 nm): 13 $M^{-1}\cdot cm^{-1}$ (Fitted)

$[Cp_2TiS_5]_0 = 6.5\cdot10^{-5}$ M

$[E]_0 = 4.8\cdot10^{-4} - 2.9\cdot10^{-3}$ M

Fitted Model*:

Abs = $[A]\cdot\varepsilon_A + [B]\cdot\varepsilon_B + [C]\cdot\varepsilon_C + [E]\cdot\varepsilon_E + [P]\cdot\varepsilon_P + x$

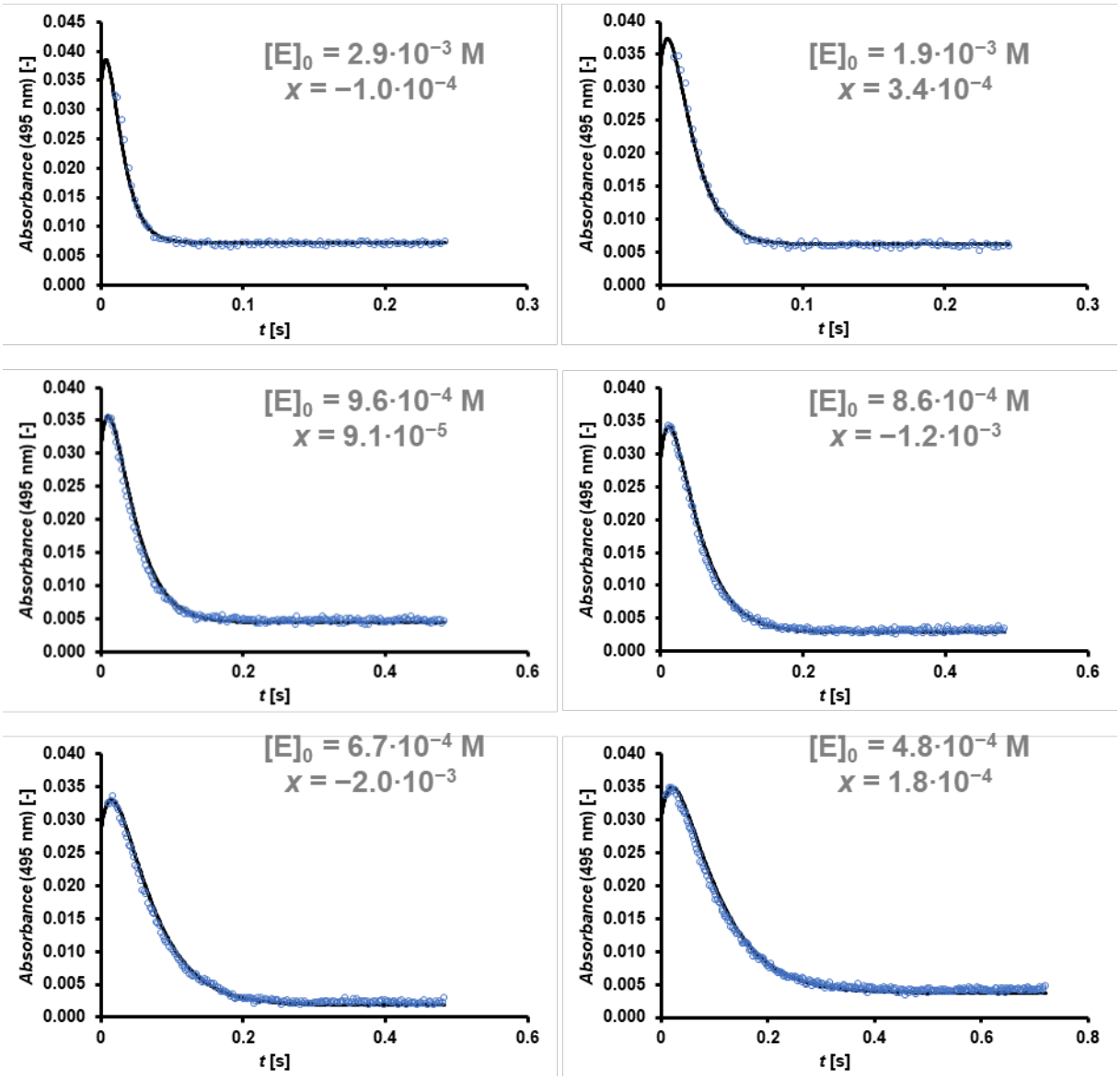

Figure S20. Reaction of Cp_2TiS_5 with (4-fluorophenyl)sulfenyl chloride in DCM at 295K. Summary of conditions and fitting results.

3.8 Reaction of Cp_2TiS_5 with 4-methoxyphenylsulfenyl chloride

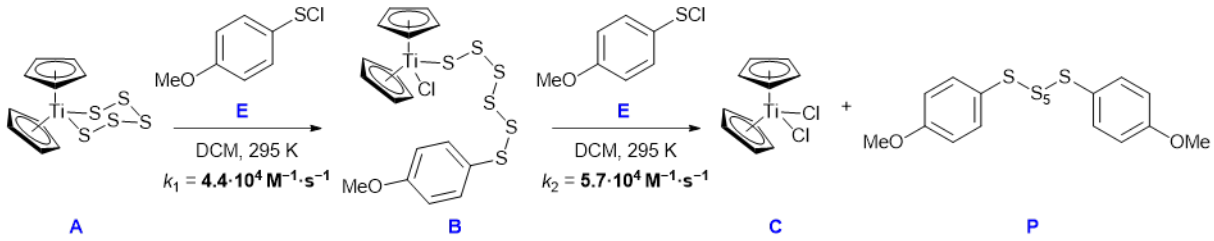

A B C P

$k_{rel} = k_2/k_1$ =1.30

ε_A(495 nm): 2240 $M^{-1}\cdot cm^{-1}$

ε_B(495 nm): 4394 $M^{-1}\cdot cm^{-1}$ (Fitted)

ε_C(495 nm): 160 $M^{-1}\cdot cm^{-1}$

ε_E(495 nm): 20 $M^{-1}\cdot cm^{-1}$

ε_P(495 nm): 51 $M^{-1}\cdot cm^{-1}$ (Fitted)

$[Cp_2TiS_5]_0 = 9.8\cdot10^{-5}$ M

$[E]_0 = 5.6\cdot10^{-4} - 1.7\cdot10^{-3}$ M

Fitted Model*:

Abs = $[A]\cdot\varepsilon_A + [B]\cdot\varepsilon_B + [C]\cdot\varepsilon_C + [E]\cdot\varepsilon_E + [P]\cdot\varepsilon_P + x$

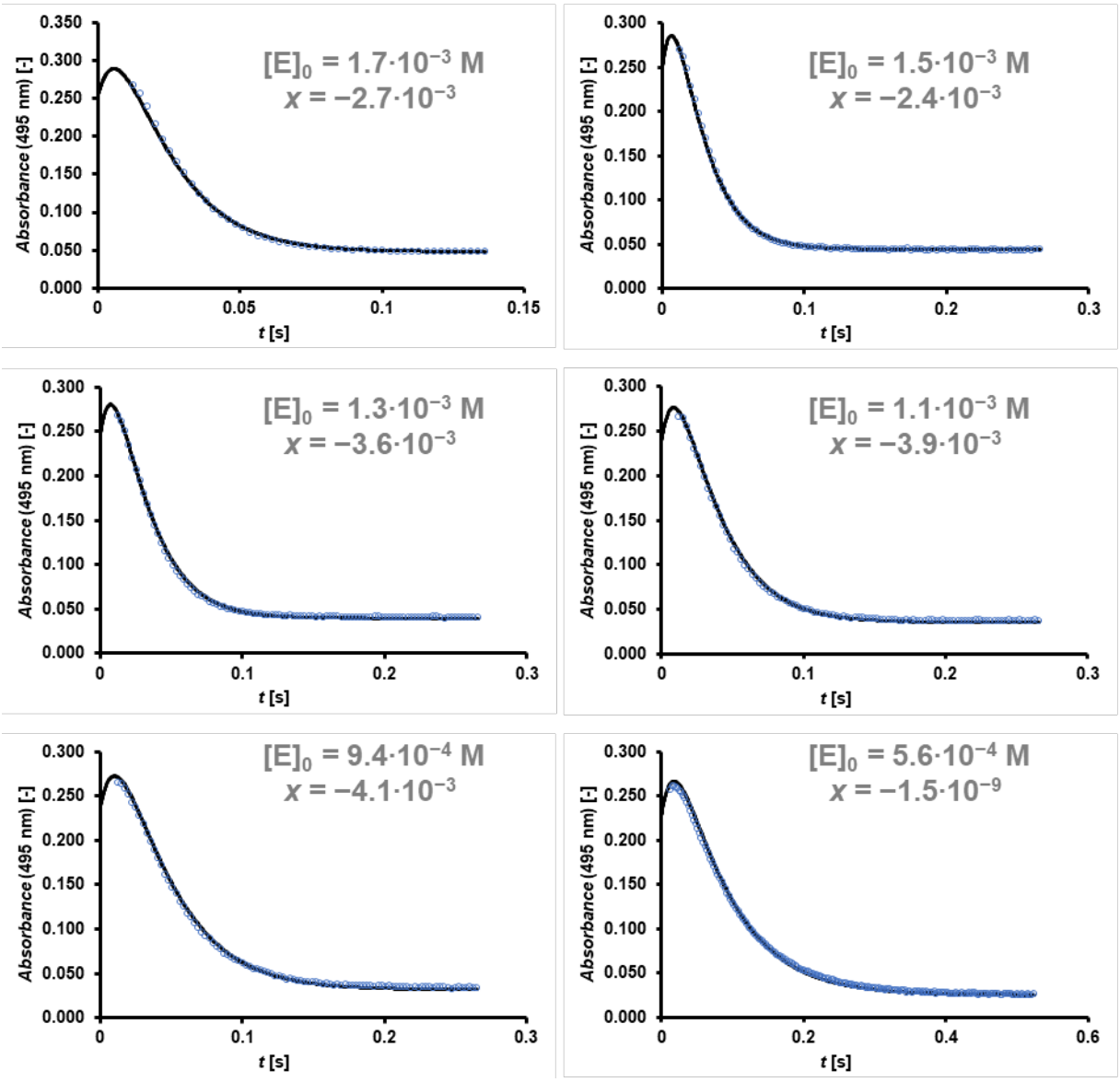

Figure S21. Reaction of Cp_2TiS_5 with (4-methoxyphenyl)sulfenyl chloride in DCM at 295K. Summary of conditions and fitting results.

3.9 Reaction of Cp_2TiS_5 with 4-bromophenylsulfenyl chloride

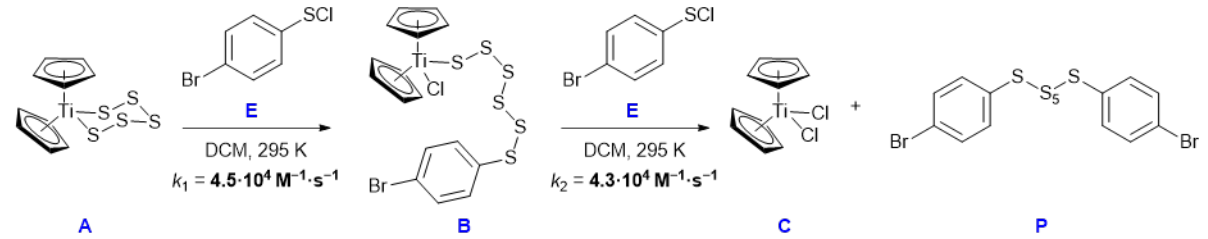

$k_{rel} = k_2/k_1$ =0.96

$[Cp_2TiS_5]_0$ = 9.0·10⁻⁵ M

$[E]_0$ = 5.8·10⁻⁴ – 2.0·10⁻³ M

ε_A(495 nm): 2240 M⁻¹·cm⁻¹

ε_B(495 nm): 2642 M⁻¹·cm⁻¹ (Fitted)

ε_C(495 nm): 160 M⁻¹·cm⁻¹

ε_E(495 nm): 8.6 M⁻¹·cm⁻¹

ε_P(495 nm): 81 M⁻¹·cm⁻¹ (Fitted)

Fitted Model*:

Abs = [A]·ε_A + [B]·ε_B + [C]·ε_C + [E]·ε_E + [P]·ε_P + x

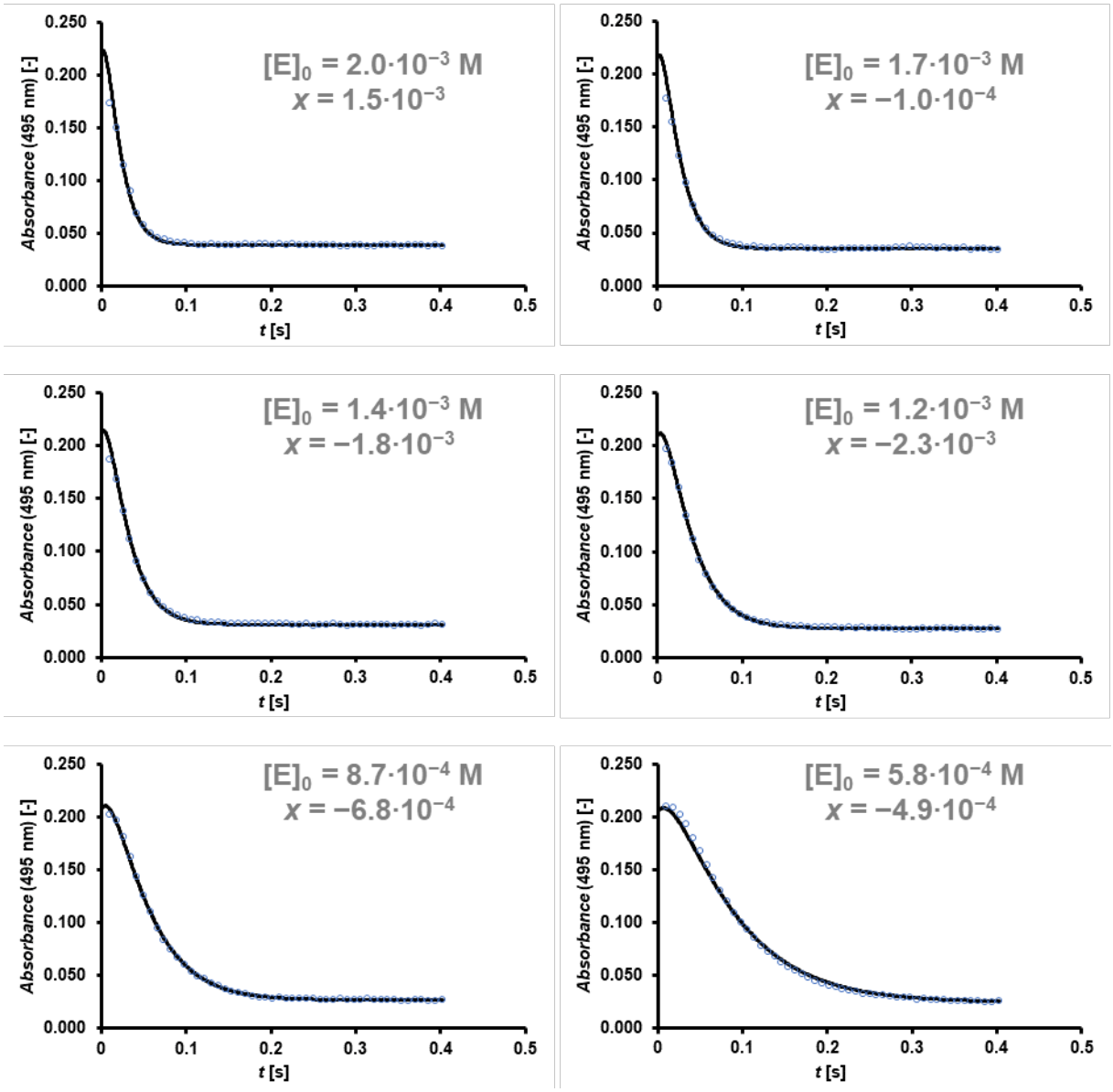

Figure S22. Reaction of Cp_2TiS_5 with (4-bromophenyl)sulfenyl chloride in DCM at 295K. Summary of conditions and fitting results.

3.10 Reaction of Cp_2TiS_5 with phenylsulfenyl chloride

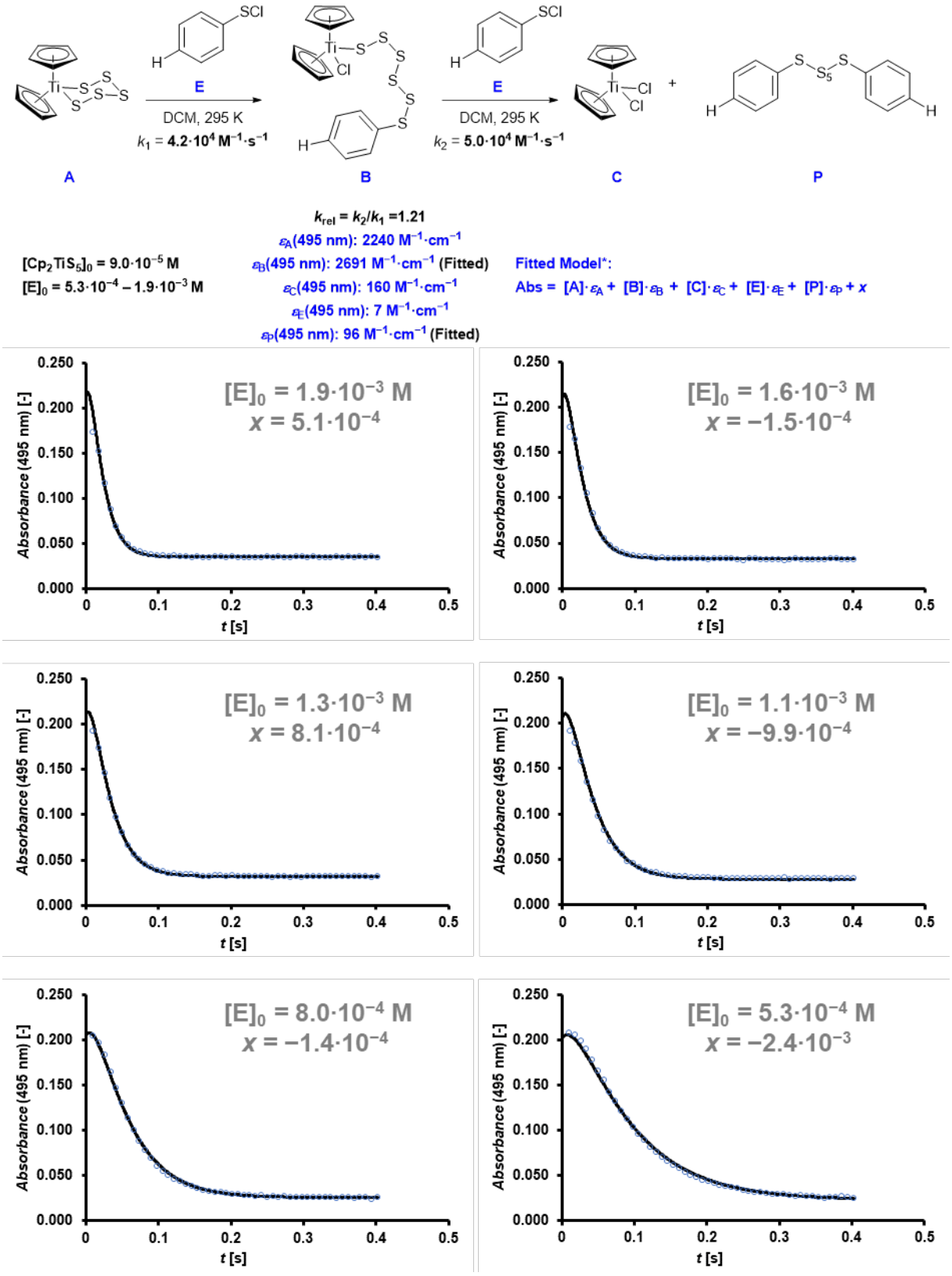

Figure S23. Reaction of Cp_2TiS_5 with phenylsulfenyl chloride in DCM at 295K. Summary of conditions and fitting results.

3.11 Reaction of $Cp_2Ti(SPh)_2$ with *N*-morpholinosulfenyl chloride

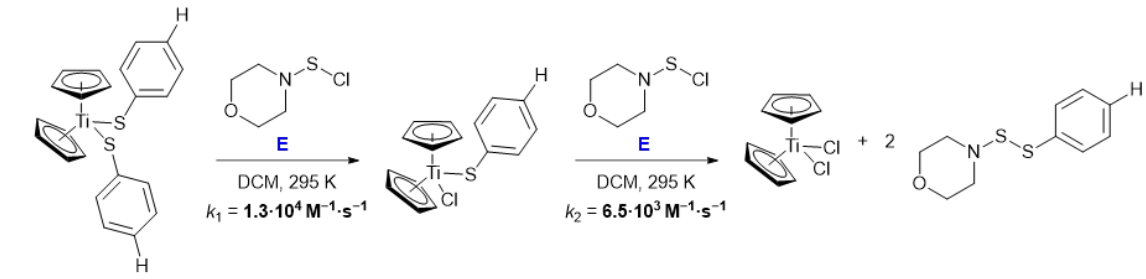

A B C P

$k_{rel} = k_2/k_1$ =0.49

ε_A(495 nm): 1905 $M^{-1}\cdot cm^{-1}$

ε_B(495 nm): 3019 $M^{-1}\cdot cm^{-1}$ (Fitted)

ε_C(495 nm): 160 $M^{-1}\cdot cm^{-1}$

ε_E(495 nm): 0 $M^{-1}\cdot cm^{-1}$

ε_P(495 nm): 0 $M^{-1}\cdot cm^{-1}$ (Fitted)

$[Cp_2Ti(SAr)_2]_0 = 6.7\cdot10^{-5}$ M

$[E]_0 = 9.4\cdot10^{-4} - 4.1\cdot10^{-3}$ M

Fitted Model*:

$Abs = [A]\cdot\varepsilon_A + [B]\cdot\varepsilon_B + [C]\cdot\varepsilon_C + [E]\cdot\varepsilon_E + [P]\cdot\varepsilon_P + x$

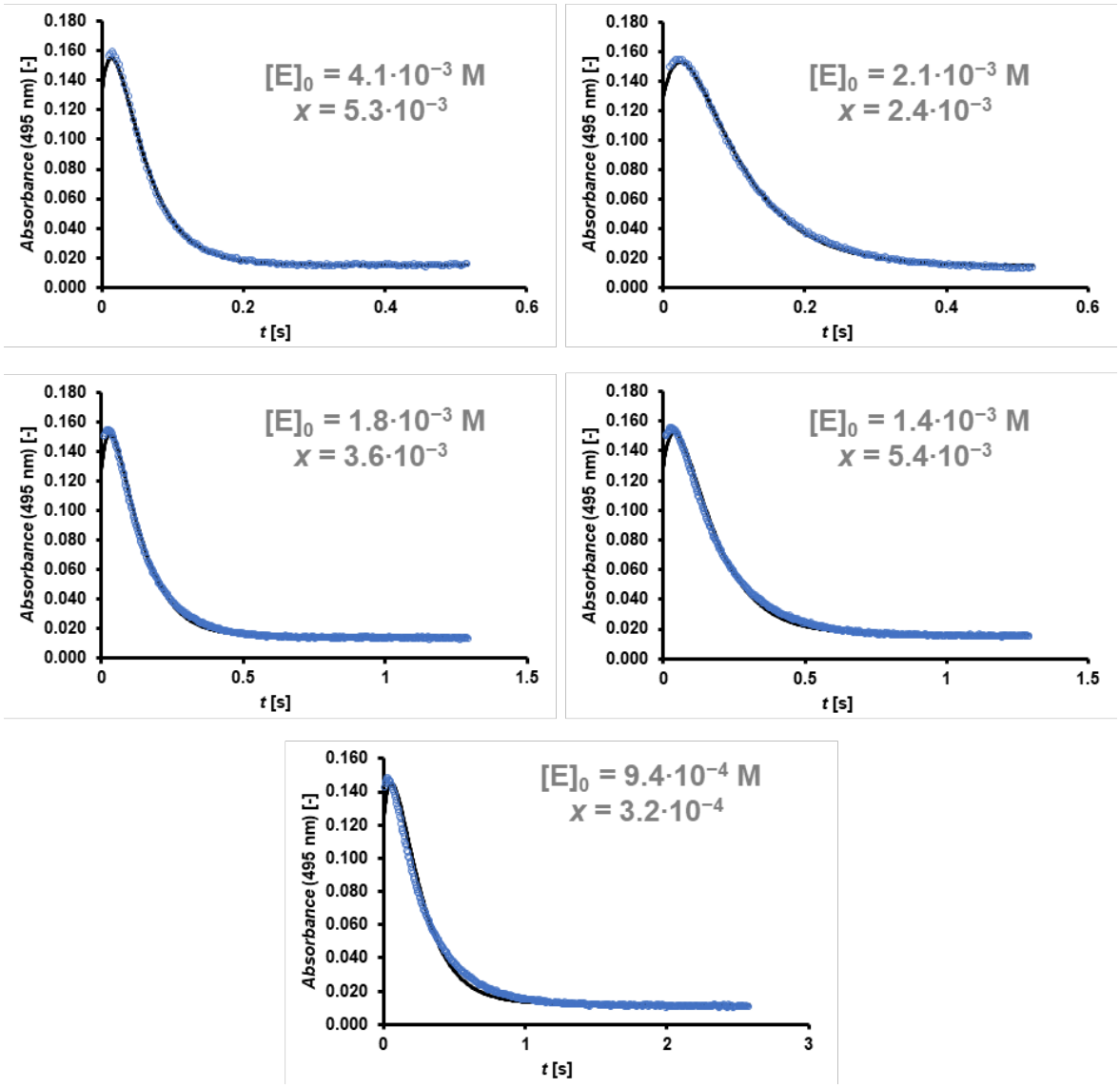

Figure S24. Reaction of bisthiophenolate $Cp_2Ti(SPh)_2$ with (*N*-morpholino)sulfenyl chloride in DCM at 295K. Summary of conditions and fitting results.

3.12 Reaction of $Cp_2Ti(4\text{-}F\text{-}C_6H_4S)_2$ with *N*-morpholinosulfenyl chloride

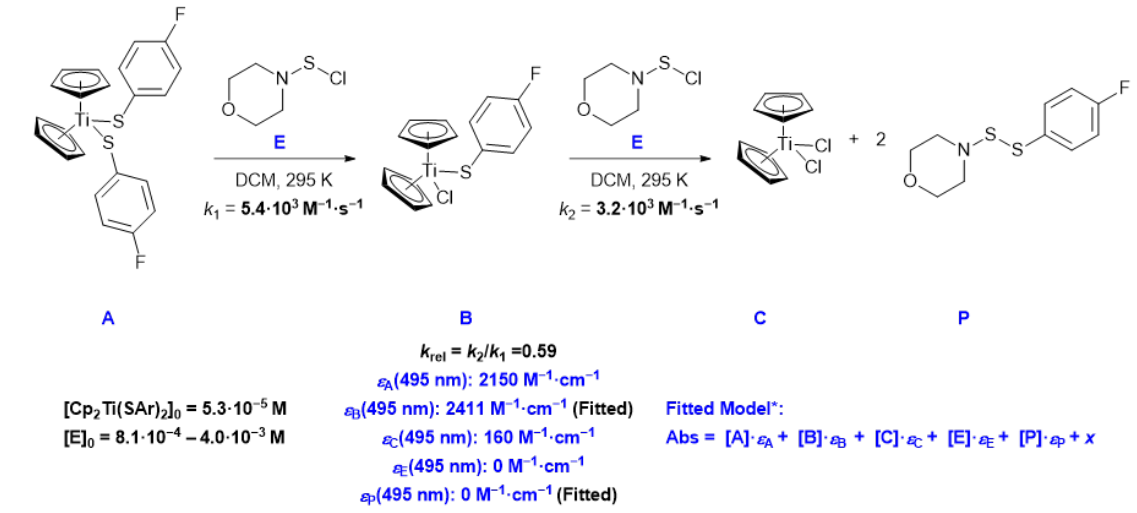

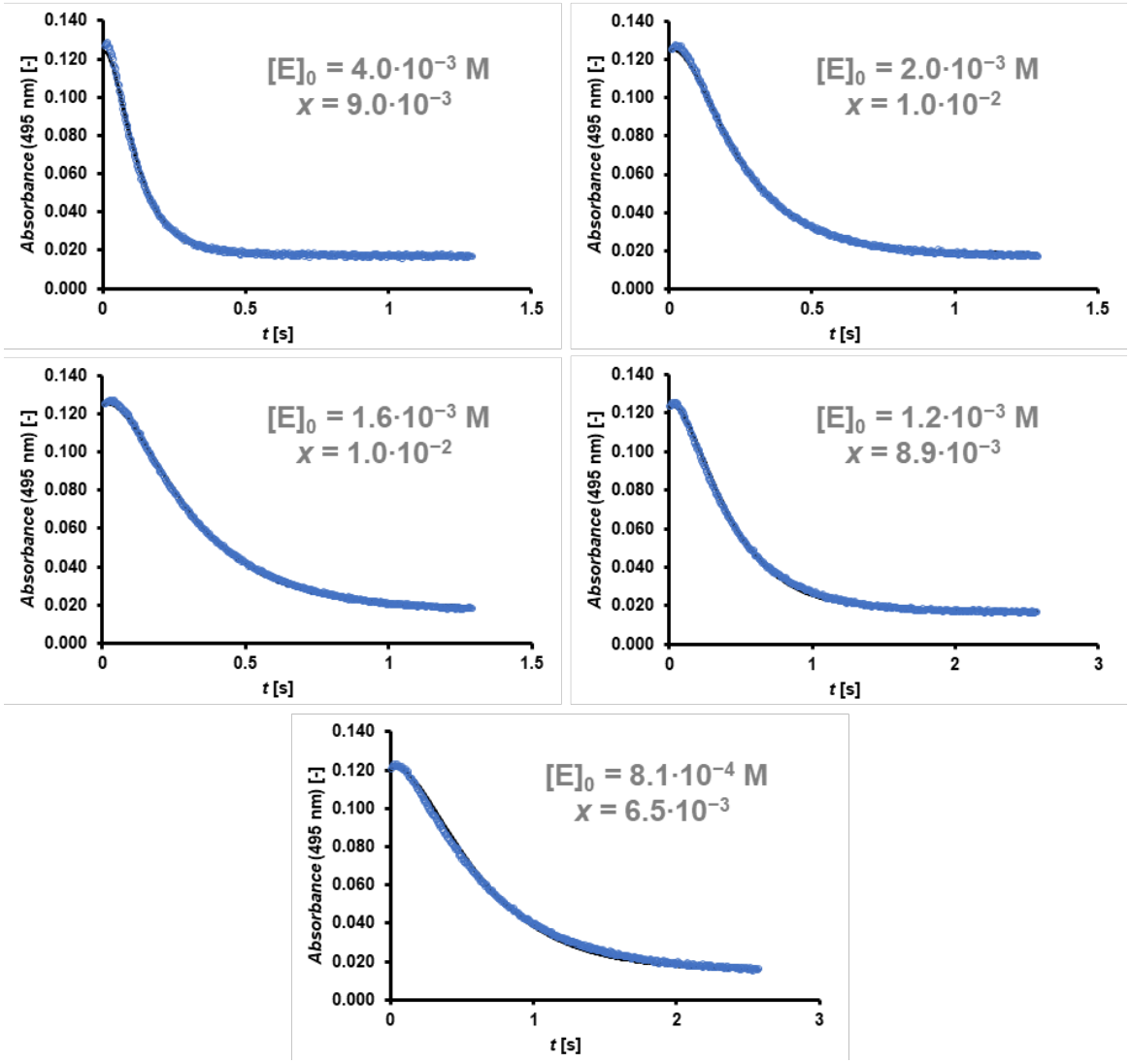

Figure S25. Reaction of bisthiophenolate $Cp_2Ti(4\text{-}F\text{-}C_6H_4S)_2$ with (*N*-morpholino)sulfenyl chloride in DCM at 295K. Summary of conditions and fitting results.

3.13 Reaction of $Cp_2Ti(4\text{-}Cl\text{-}C_6H_4S)_2$ with *N*-morpholinosulfenyl chloride

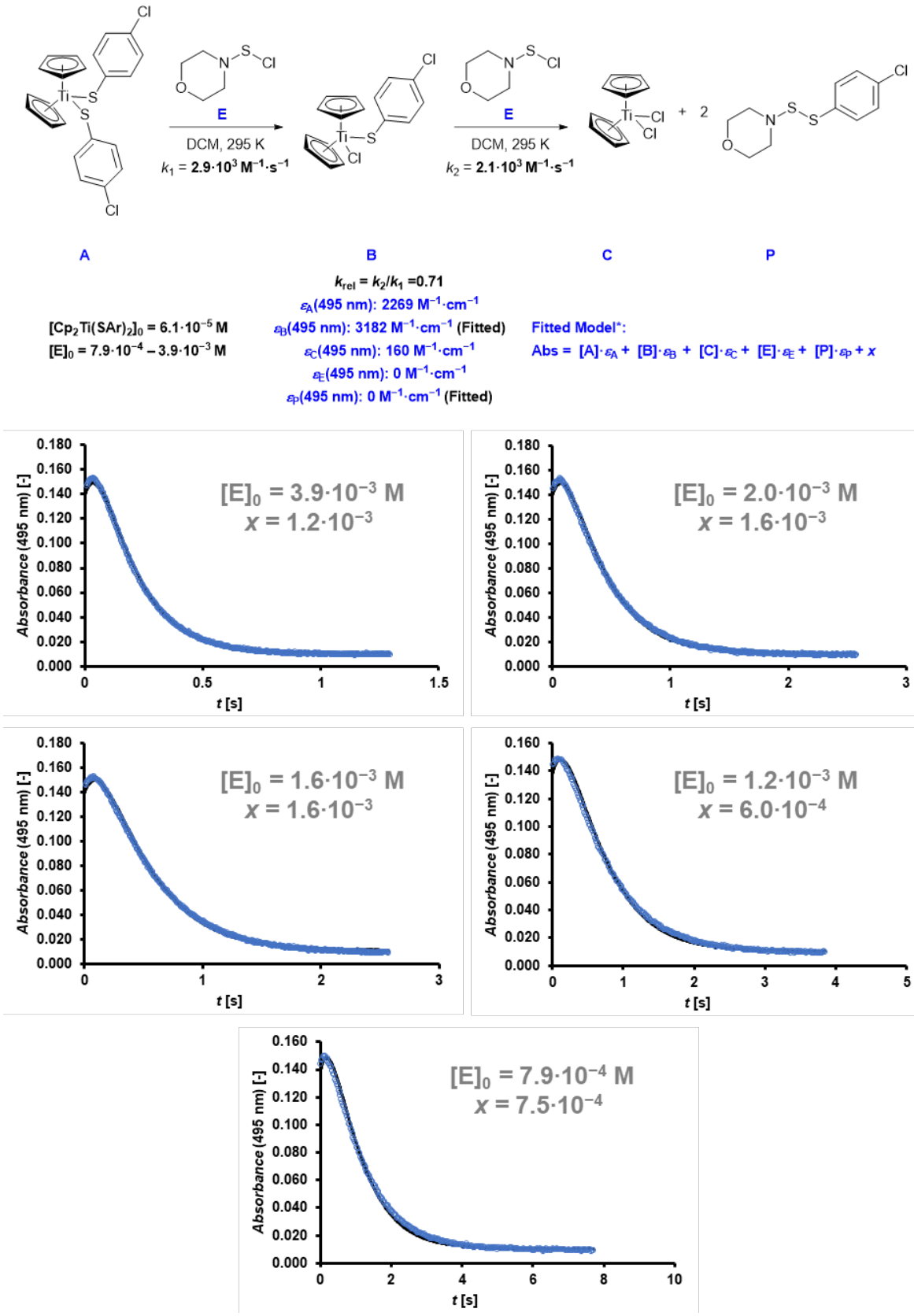

Figure S26. Reaction of bisthiophenolate $Cp_2Ti(4\text{-}Cl\text{-}C_6H_4S)_2$ with (*N*-morpholino)sulfenyl chloride in DCM at 295K. Summary of conditions and fitting results.

3.14 Reaction of $Cp_2Ti(4\text{-}MeO\text{-}C_6H_4S)_2$ with *N*-morpholinosulfenyl chloride

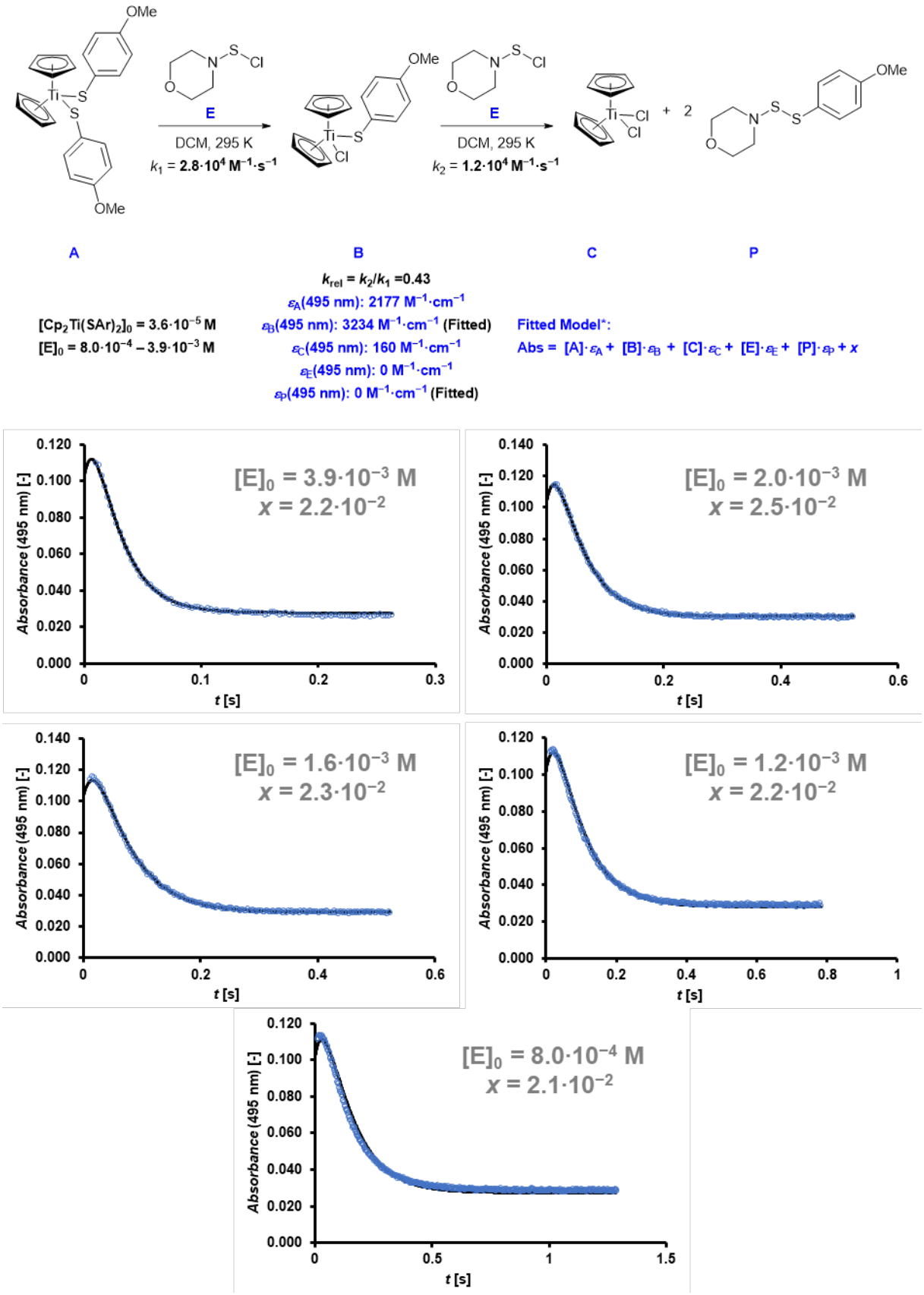

Figure S27. Reaction of bisthiophenolate $Cp_2Ti(4\text{-}MeO\text{-}C_6H_4S)_2$ with (*N*-morpholino)sulfenyl chloride in DCM at 295K. Summary of conditions and fitting results.

3.15 Hammett correlations with 4-substituted phenyl systems

Linear free-energy correlations were performed using Hammett constant values tabulated by Hansh, Leo and Taft,[S6a] except for fluorine, where the value σ_p = 0.15[S6b] was used because it is better parametrized for reactions in non-aqueous systems. No clear correlation between 4-subsituted phenyl electrophiles was attained when using Cp_2TiS_5 as the reference (Figure S28). For titanocene bisthiophenolates, the more electron-rich derivatives led to higher reaction rates (Figure S29). Within the data-set examined herein curvature was observed when using standard Hammett values. Linear correlation was achieved when using Yukawa-Tsuno 'standard' parameters σ^0,[S7] which account for resonance effects in stabilizing positive charge.

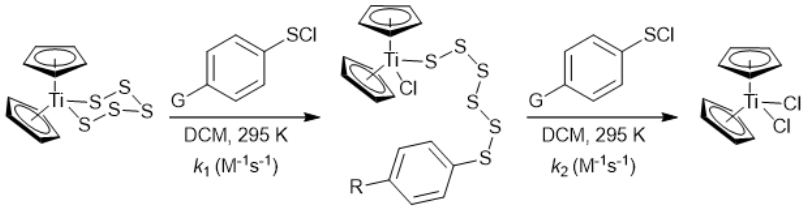

G	k_1 ($M^{-1}s^{-1}$)	k_2 ($M^{-1}s^{-1}$)	σ_p
OMe	$4.4 \cdot 10^4$	$5.7 \cdot 10^4$	- 0.27
H	$4.2 \cdot 10^4$	$5.0 \cdot 10^4$	0
F	$4.9 \cdot 10^4$	$5.0 \cdot 10^4$	0.15
Cl	$4.1 \cdot 10^4$	$4.6 \cdot 10^4$	0.23
Br	$4.5 \cdot 10^4$	$4.3 \cdot 10^4$	0.21
NO_2	$1.9 \cdot 10^4$	$6.8 \cdot 10^3$	0.78

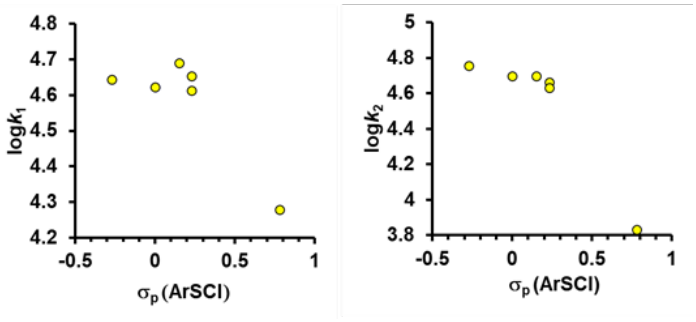

Figure S28. Hammett plots for the reaction of Cp_2TiS_5 with phenylsulfenyl chloride derivatives.

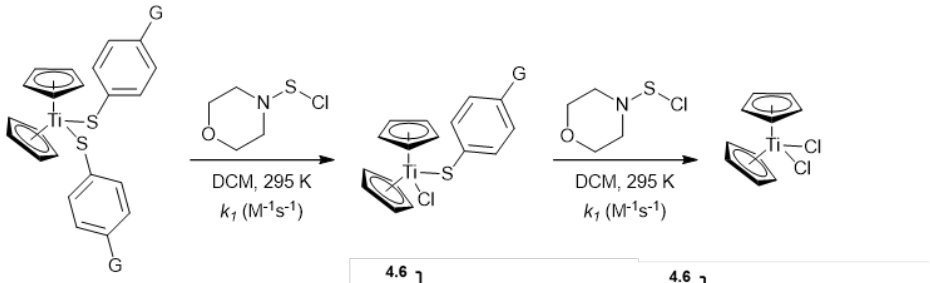

G	k_1 ($M^{-1}s^{-1}$)	k_2 ($M^{-1}s^{-1}$)	σ_p	σ^0
OMe	$4.4 \cdot 10^4$	$5.7 \cdot 10^4$	- 0.27	- 0.1
H	$4.2 \cdot 10^4$	$5.0 \cdot 10^4$	0	0
F	$4.9 \cdot 10^4$	$5.0 \cdot 10^4$	0.15	0.2
Cl	$4.1 \cdot 10^4$	$4.6 \cdot 10^4$	0.23	0.28

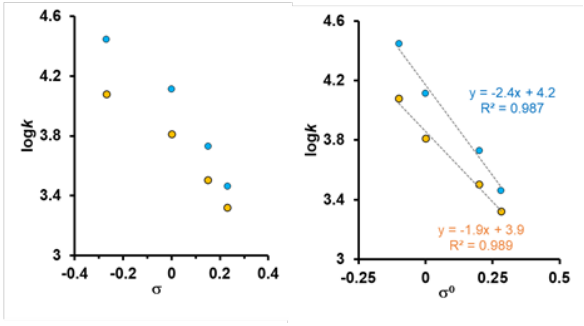

Figure S29. LFER plots for the reaction of $Cp_2Ti(SAr)X$ (X = Cl, SAr) with *N*-morpholinosulfenyl chloride.

4. Stopped-Flow NMR experiments

4.1. ^{1}H NMR Monitoring of Cp_2TiS_5 with *N*-morpholinosulfenyl chloride

Reactions were set-up using a variable-ratio three-syringe stopped-flow NMR instrumentation described in our previous work[S2] using three stock solutions in DCM: Stock solution A: Cp_2TiS_5, 1-fluoronapthalene (internal standard); Solution B: *N*-morpholinosulfenyl chloride, 1-fluoronapthalene (internal standard). Soluction C: 1-fluoronapthalene (internal standard).The system was thermostatically equilibrated before each experiment to match the spectrometer probe temperature. Stock solutions were then loaded into the corresponding syringe. Each reaction profile was obtained interleaving data of 10-15 identical reactions (syringe ratio A:B:C = 0.5:0.5:0; total volume = 600 μL, flow rate = 1 mL/s) using different delays between reaction initiation and application of the first 90-degree pulse. The system was flushed with syringe C after each individual run. Monitoring was performed via ^{1}H NMR{^{13}C} (zg 90, AQ = 4.5 s) using WET pulse sequence for solvent suppression. Experimental temporal concentration data was fitted to a two consecutive bimolecular reaction model using the set of differential equations below (eq. S7 – eq. S10) to provide absolute values of bimolecular rate constants for each single step (k_1, k_2). Fitting results and Eyring analyses are shown in Figure S30. A stack of NMR of the reaction at 275K is shown in Figure S31.

$$\underset{\mathbf{A}}{\mathbf{Cp_2TiS_5}} \xrightarrow[k_1]{\mathbf{RSCl}} \underset{\mathbf{B}}{\mathbf{Cp_2TiCl(S_6R)}} \xrightarrow[k_2]{\mathbf{RSCl}} \underset{\mathbf{C}}{\mathbf{Cp_2TiCl_2}} + \underset{\mathbf{P}}{\mathbf{R_2S_7}}$$

$$\frac{d[A]}{dt} = -k_1[A][RSCl] \qquad \textbf{(eq. S7)}$$

$$\frac{d[B]}{dt} = k_1[A][RSCl] - k_2[B][RSCl] \qquad \textbf{(eq. S8)}$$

$$\frac{d[C]}{dt} = \frac{d[P]}{dt} = k_2[B][RSCl] \qquad \textbf{(eq. S9)}$$

$$\frac{d[RSCl]}{dt} = -k_1[A][RSCl] - k_2[B][RSCl] \qquad \textbf{(eq. S10)}$$

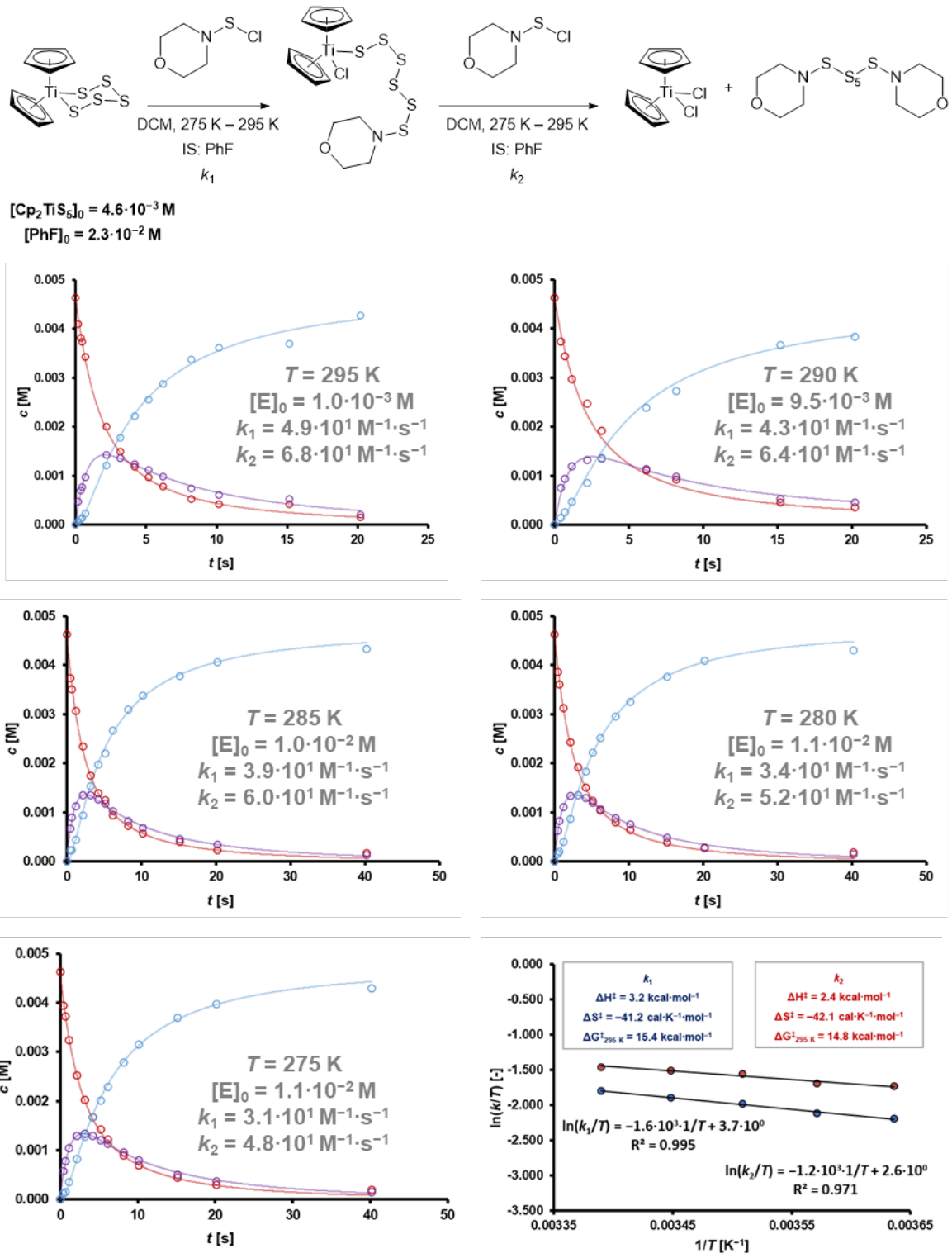

Figure S30. Reaction of Cp_2TiS_5 with *N*-morpholinosulfenyl chloride: SF-NMR reaction monitoring at various temperatures and Eyring analyses considering statistical contributions using equation in Section S2.2 (with n = 2 for k_1 and n = 1 for k_2 with $\kappa = 1$).

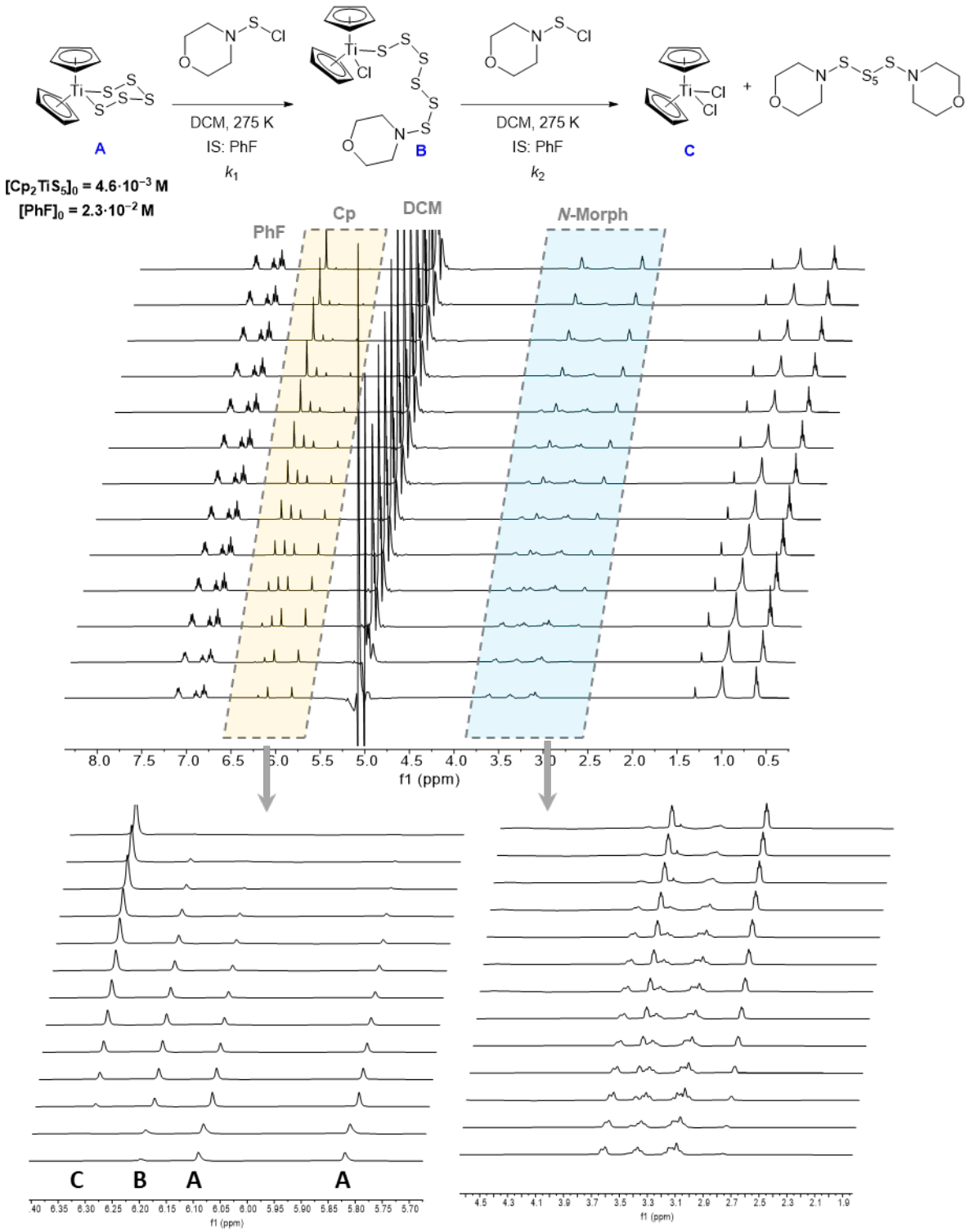

Figure S31. Stack of ^{1}H-NMR spectra from SF-NMR reaction monitoring of Cp_2TiS_5 with *N*-morpholinosulfenyl chloride at 275 K.

4.2 SF-NMR titrations

4.2.1 Reaction of Cp_2TiS_5 with 4-substituted phenylsulfenyl chlorides

A) 4-Fluorophenylsulfenyl chloride as titrant.

Dimethylsulfone (Me_2SO_2) was used as an internal standard. A stock solution of 'solvent' was prepared by dissolving a known amount of Me_2SO_2 in anhydrous DCM to keep the concentration of internal standard constant in all runs. Titrations were performed using substoichoimetric amounts of sulfur electrophile with a variable-ratio three-syringe stopped-flow NMR instrumentation using three stock solutions: stock solution A: starting titanocene (Cp_2TiS_5) in 'solvent', solution B: sulfur electrophile (RSCl, 4-fluorophenylsulfenyl chloride) in 'solvent', stock solution C: 'solvent'. The system was thermostatically equilibrated to 22 °C (295 K) before each experiment, to match the spectrometer probe temperature. Stock solutions were then loaded into the corresponding syringe. Each titration assay was then performed by keeping the volume injected from syringe A constant and varying the volume ratio of syringes B and C (total volume = 600 μL, flow rate = 1 mL/s). The system was flushed with DCM after each individual run and allowed to reach magnetic equilibrium for at least one minute before the next run. Measurements were performed *via* ^{1}H NMR{^{13}C} (zg 90, NS = 1, AQ = 4.5 s) using WET pulse sequence for solvent suppression. A stack of NMR spectra is shown in Figure S32. The molar fraction of starting titanocene (*f*Cp_2TiS) was calculated from the integrals of the Cp signals (zoomed region in Figure S32). The equivalents of electrophile used (defined as the molar ratio of initial concentrations, $[RSCl]_0/[Cp_2TiS_5]_0$) was plotted against the remaining fraction of starting titanocene, *f*Cp_2TiS_5.[S3] Experimental results were fitted to a consecutive bimolecular competition model using equation described in Figure S33. This procedure provides the relative reaction rate constants between the consecutive steps ($k_{rel} = k_2/k_1 = 1.02$), not their absolute values.

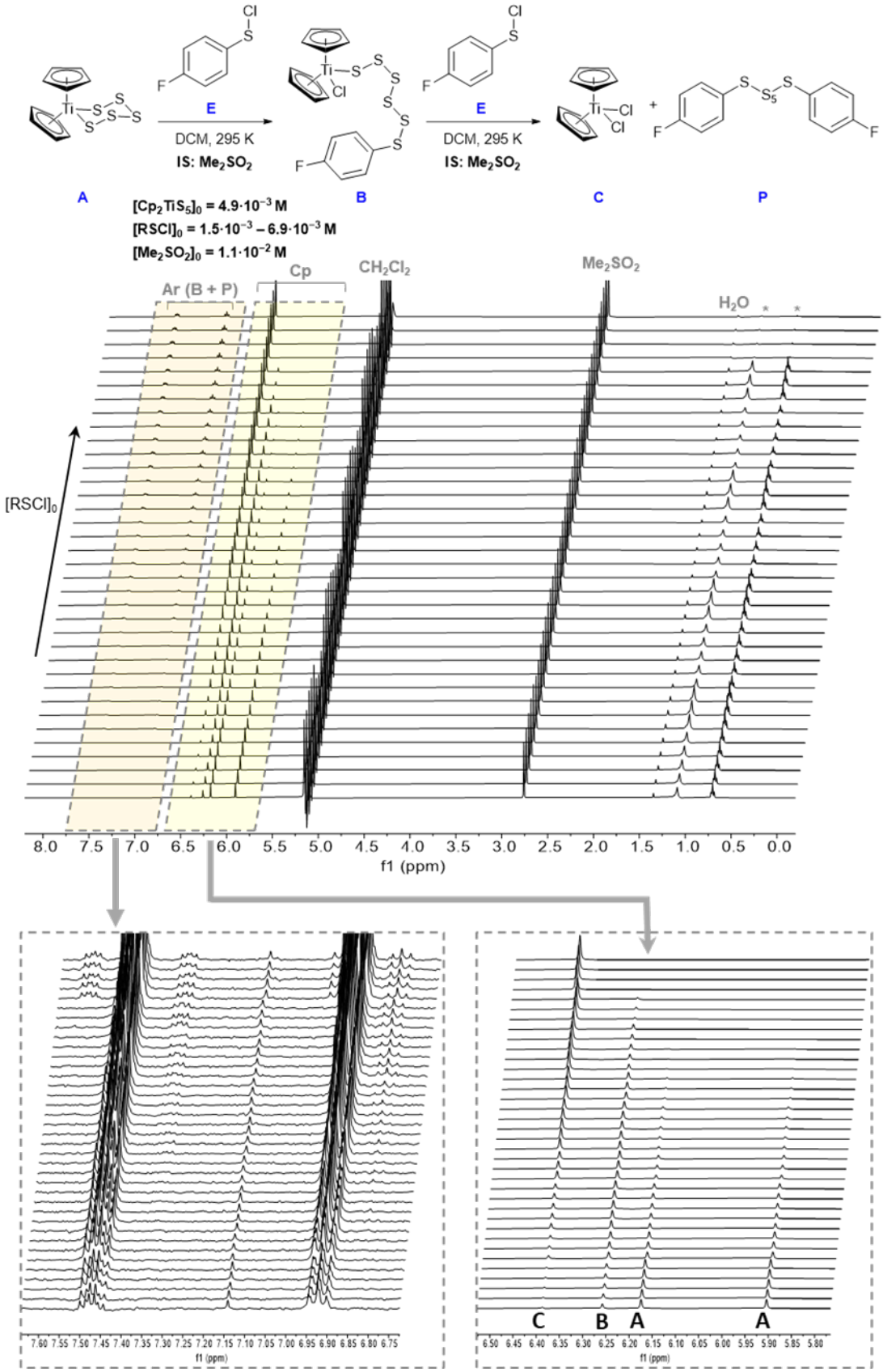

Figure S32. SF-NMR titration of Cp_2TiS_5 with 4-F-C_6H_4SCl: labelled Stack of NMR after addition of titrant with zoom-in on diagnostic titanocene peaks.

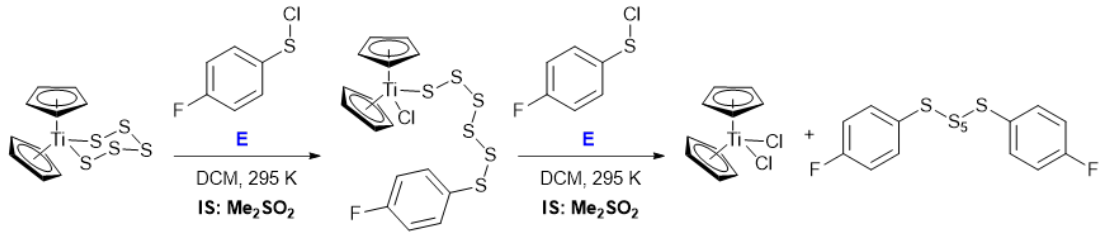

$[Cp_2TiS_5]_0 = 4.9 \cdot 10^{-3}$ M
$[RSCl]_0 = 1.5 \cdot 10^{-3} - 6.9 \cdot 10^{-3}$ M
$[Me_2SO_2]_0 = 1.1 \cdot 10^{-2}$ M

$[RSCl]_0$ [M]	$[RSCl]_0/[Cp_2TiS_5]_0$ [–]	fCp_2TiS_5 [–]
$6.9 \cdot 10^{-3}$	1.41	0.15
$6.9 \cdot 10^{-3}$	1.40	0.15
$6.7 \cdot 10^{-3}$	1.39	0.15
$6.1 \cdot 10^{-3}$	1.23	0.22
$5.8 \cdot 10^{-3}$	1.22	0.22
$5.9 \cdot 10^{-3}$	1.22	0.22
$6.0 \cdot 10^{-3}$	1.21	0.23
$5.9 \cdot 10^{-3}$	1.21	0.23
$4.8 \cdot 10^{-3}$	1.01	0.31
$4.9 \cdot 10^{-3}$	1.01	0.32
$4.9 \cdot 10^{-3}$	1.01	0.32
$3.8 \cdot 10^{-3}$	0.79	0.43
$3.8 \cdot 10^{-3}$	0.79	0.43
$3.7 \cdot 10^{-3}$	0.78	0.44
$3.9 \cdot 10^{-3}$	0.78	0.44
$3.8 \cdot 10^{-3}$	0.78	0.44
$2.7 \cdot 10^{-3}$	0.57	0.57
$2.8 \cdot 10^{-3}$	0.57	0.57
$2.7 \cdot 10^{-3}$	0.56	0.58
$1.6 \cdot 10^{-3}$	0.32	0.74
$1.6 \cdot 10^{-3}$	0.32	0.74
$1.6 \cdot 10^{-3}$	0.32	0.74
$1.5 \cdot 10^{-3}$	0.31	0.74
$1.5 \cdot 10^{-3}$	0.31	0.75

$$\frac{[RSCl]_0}{[Cp_2TiS_5]_0} = -\left(\left(\frac{k_{rel}^{-1} \cdot fCp_2TiS_5^{\,k_{rel}^{-1}}}{k_{rel}^{-1} - 1}\right) + \left(\frac{k_{rel}^{-1} - 2}{k_{rel}^{-1} - 1}\right) \cdot fCp_2TiS_5 - 2\right)$$

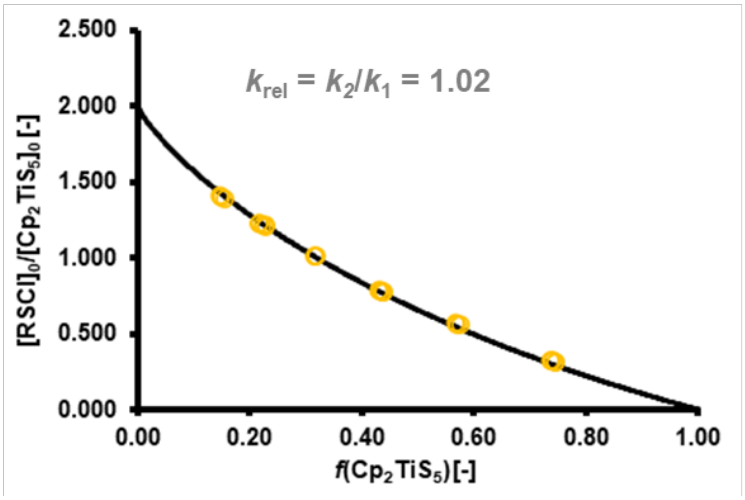

Figure S33. SF-NMR titration of Cp_2TiS_5 with 4-F-C_6H_4SCl: summary of initial conditions and graphical analysis of results.

B) 4-Nitrophenylsulfenyl chloride as titrant.

Dimethylsulfone (Me_2SO_2) was used as an internal standard. A stock solution of 'solvent' was prepared by dissolving a known amount of Me_2SO_2 in anhydrous DCM to keep the concentration of internal standard constant in all runs. Titrations were performed using substoichoimetric amounts of sulfur electrophile with a variable-ratio three-syringe stopped-flow NMR instrumentation using three stock solutions: stock solution A: starting titanocene (Cp_2TiS_5) in 'solvent', solution B: sulfur electrophile (RSCl, 4-nitrophenylsulfenyl chloride) in 'solvent', stock solution C: 'solvent'. The system was thermostatically equilibrated to 22 °C (295 K) before each experiment, to match the spectrometer probe temperature. Stock solutions were then loaded into the corresponding syringe. Each titration assay was then performed by keeping the volume injected from syringe A constant and varying the volume ratio of syringes B and C (total volume = 600 μL, flow rate = 1 mL/s). The system was flushed with DCM after each individual run and allowed to reach magnetic equilibrium for at least one minute before the next run. Measurements were performed *via* ^{1}H NMR{^{13}C} (zg 90, NS = 1, AQ = 4.5 s) using WET pulse sequence for solvent suppression. A stack of NMR spectra is shown in Figure S34. The molar fraction of starting titanocene (*f*Cp_2TiS) was calculated from the integrals of the Cp signals (zoomed region in Figure S34). The equivalents of electrophile used (defined as the molar ratio of initial concentrations, $[RSCl]_0/[Cp_2TiS_5]_0$) was plotted against the remaining fraction of starting titanocene, *f*Cp_2TiS_5.[S3] Experimental results were fitted to a consecutive bimolecular competition model using equation described in Figure S35. This procedure provides the relative reaction rate constants between the consecutive steps ($k_{rel} = k_2/k_1 = 0.36$), not their absolute values.

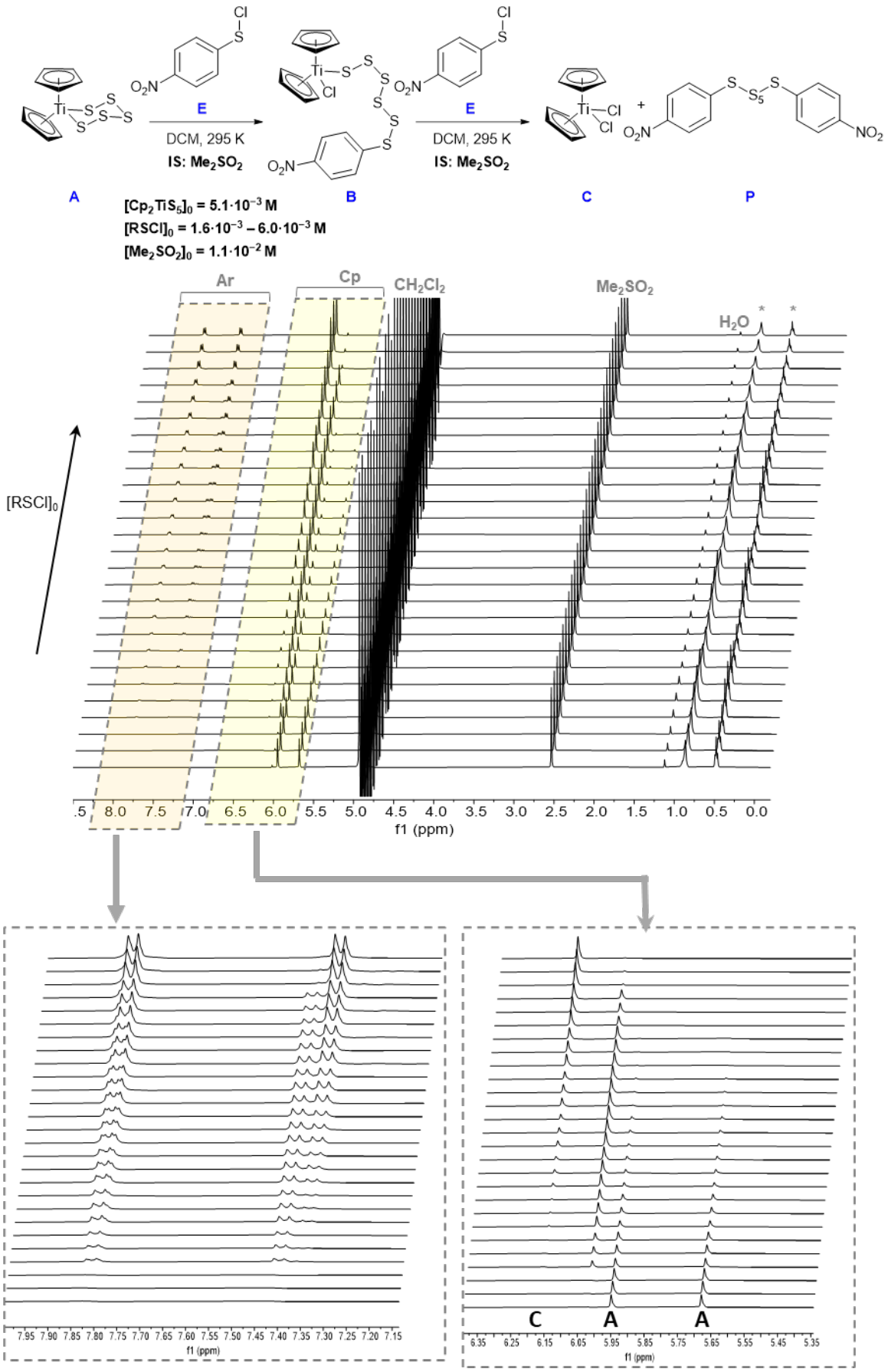

Figure S34. SF-NMR titration of Cp_2TiS_5 with 4-NO_2-C_6H_4SCl: labelled Stack of NMR after addition of titrant with zoom-in on diagnostic titanocene peaks.

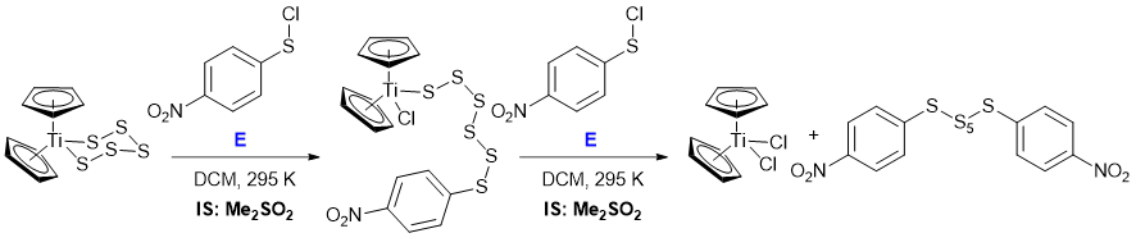

$[Cp_2TiS_5]_0 = 5.1 \cdot 10^{-3}$ M
$[RSCl]_0 = 1.6 \cdot 10^{-3} - 6.0 \cdot 10^{-3}$ M
$[Me_2SO_2]_0 = 1.1 \cdot 10^{-2}$ M

$[RSCl]_0$ [M]	$[RSCl]_0/[Cp_2TiS_5]_0$ [–]	fCp_2TiS_5 [–]
$6.0 \cdot 10^{-3}$	1.18	0.13
$6.0 \cdot 10^{-3}$	1.18	0.13
$5.9 \cdot 10^{-3}$	1.17	0.13
$4.9 \cdot 10^{-3}$	0.96	0.24
$4.8 \cdot 10^{-3}$	0.94	0.25
$4.8 \cdot 10^{-3}$	0.94	0.25
$4.2 \cdot 10^{-3}$	0.83	0.32
$4.1 \cdot 10^{-3}$	0.82	0.32
$4.0 \cdot 10^{-3}$	0.80	0.34
$2.8 \cdot 10^{-3}$	0.56	0.50
$2.9 \cdot 10^{-3}$	0.57	0.50
$2.9 \cdot 10^{-3}$	0.57	0.50
$1.7 \cdot 10^{-3}$	0.34	0.68
$1.7 \cdot 10^{-3}$	0.34	0.69
$1.6 \cdot 10^{-3}$	0.31	0.71

$$\frac{[RSCl]_0}{[Cp_2TiS_5]_0} = -\left(\left(\frac{k_{rel}^{-1} \cdot fCp_2TiS_5^{k_{rel}^{-1}}}{k_{rel}^{-1} - 1}\right) + \left(\frac{k_{rel}^{-1} - 2}{k_{rel}^{-1} - 1}\right) \cdot fCp_2TiS_5 - 2\right)$$

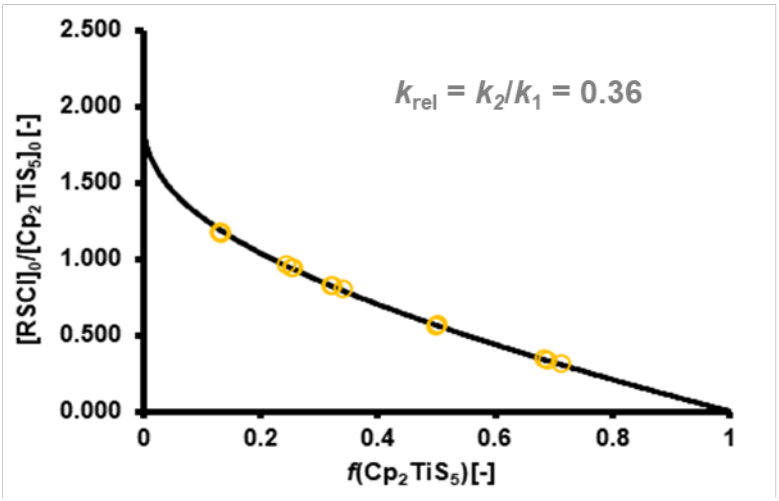

Figure S35. SF-NMR titration of Cp_2TiS_5 with 4-NO_2-C_6H_4SCl: summary of initial conditions and graphical analysis of results.

C) 4-Chlorophenylsulfenyl chloride as titrant.

Dimethylsulfone (Me_2SO_2) was used as an internal standard. A stock solution of 'solvent' was prepared by dissolving a known amount of Me_2SO_2 in anhydrous DCM to keep the concentration of internal standard constant in all runs. Titrations were performed using substoichoimetric amounts of sulfur electrophile with a variable-ratio three-syringe stopped-flow NMR instrumentation using three stock solutions: stock solution A: starting titanocene (Cp_2TiS_5) in 'solvent', solution B: sulfur electrophile (RSCl, 4-chlorophenylsulfenyl chloride) in 'solvent', stock solution C: 'solvent'. The system was thermostatically equilibrated to 22 °C (295 K) before each experiment, to match the spectrometer probe temperature. Stock solutions were then loaded into the corresponding syringe. Each titration assay was then performed by keeping the volume injected from syringe A constant and varying the volume ratio of syringes B and C (total volume = 600 μL, flow rate = 1 mL/s). The system was flushed with DCM after each individual run and allowed to reach magnetic equilibrium for at least one minute before the next run. Measurements were performed *via* ^{1}H NMR{^{13}C} (zg 90, NS = 1, AQ = 4.5 s) using WET pulse sequence for solvent suppression. A stack of NMR spectra is shown in Figure S36. The molar fraction of starting titanocene (*f*Cp_2TiS) was calculated from the integrals of the Cp signals (zoomed region in Figure S36). The equivalents of electrophile used (defined as the molar ratio of initial concentrations, $[RSCl]_0/[Cp_2TiS_5]_0$) was plotted against the remaining fraction of starting titanocene, *f*Cp_2TiS_5.[S3] Experimental results were fitted to a consecutive bimolecular competition model using equation described in Figure S37. This procedure provides the relative reaction rate constants between the consecutive steps ($k_{rel} = k_2/k_1 = 1.12$), not their absolute values.

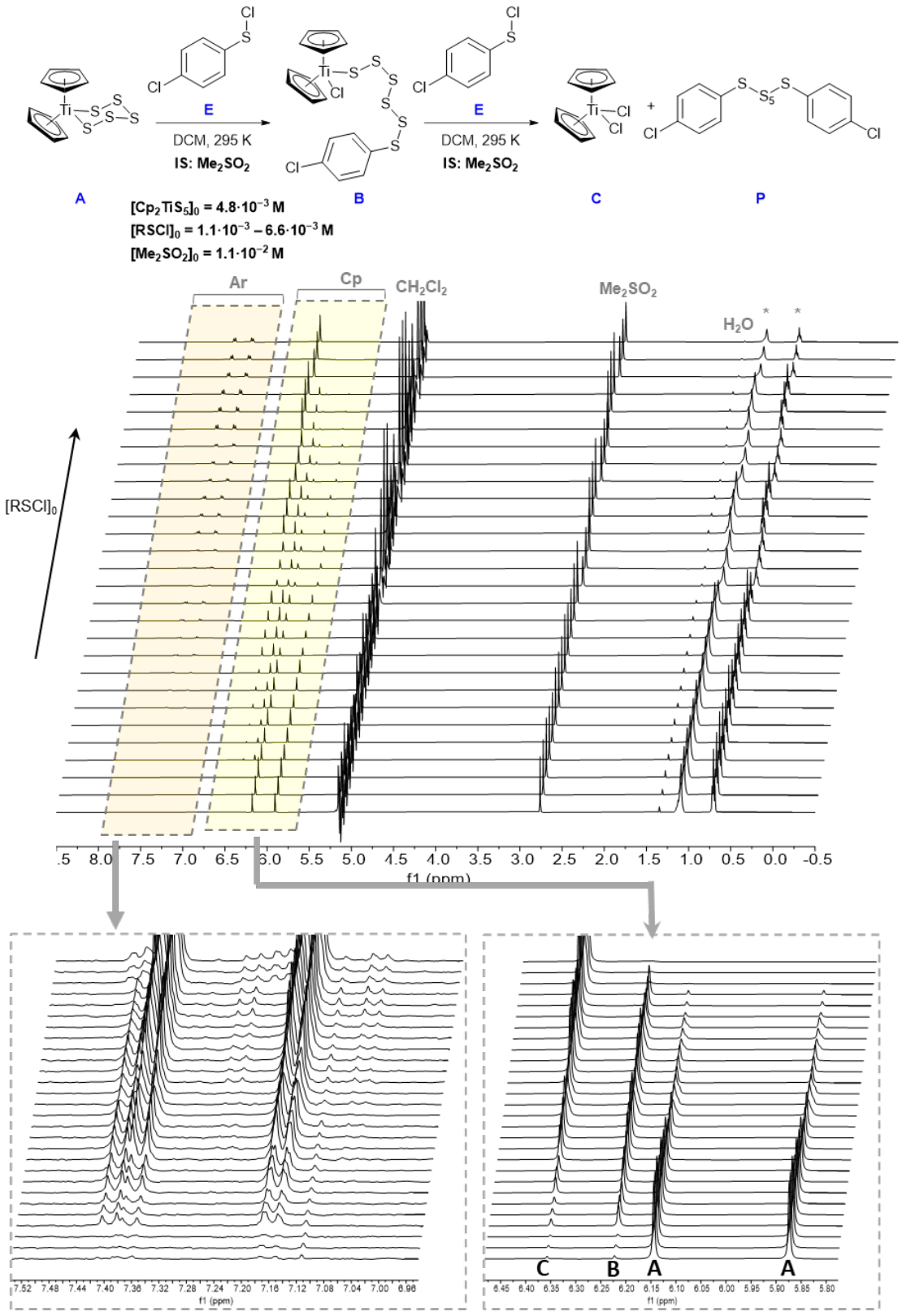

Figure S36. SF-NMR titration of Cp_2TiS_5 with 4-Cl-C_6H_4SCl: labelled Stack of NMR after addition of titrant with zoom-in on diagnostic titanocene peaks.

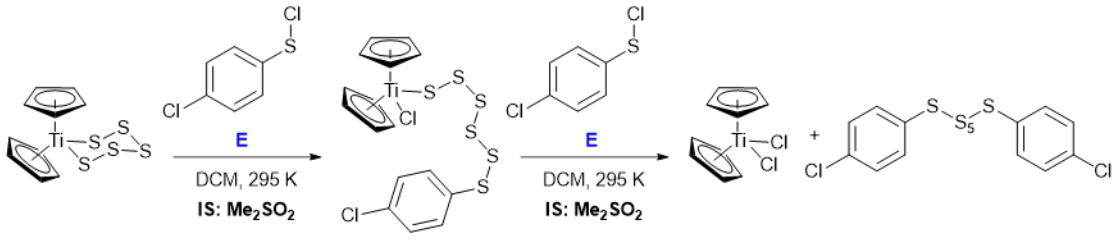

$[Cp_2TiS_5]_0 = 4.8 \cdot 10^{-3}$ M
$[RSCl]_0 = 1.1 \cdot 10^{-3} - 6.6 \cdot 10^{-3}$ M
$[Me_2SO_2]_0 = 1.1 \cdot 10^{-2}$ M

$[RSCl]_0$ [M]	$[RSCl]_0/[Cp_2TiS_5]_0$ [–]	fCp_2TiS_5 [–]
$6.6 \cdot 10^{-3}$	1.38	0.17
$6.6 \cdot 10^{-3}$	1.37	0.18
$6.5 \cdot 10^{-3}$	1.36	0.18
$6.2 \cdot 10^{-3}$	1.29	0.19
$6.2 \cdot 10^{-3}$	1.28	0.20
$6.2 \cdot 10^{-3}$	1.28	0.20
$4.4 \cdot 10^{-3}$	0.93	0.37
$4.4 \cdot 10^{-3}$	0.91	0.39
$4.1 \cdot 10^{-3}$	0.87	0.39
$4.4 \cdot 10^{-3}$	0.90	0.39
$4.4 \cdot 10^{-3}$	0.90	0.39
$4.1 \cdot 10^{-3}$	0.82	0.42
$4.0 \cdot 10^{-3}$	0.82	0.42
$2.1 \cdot 10^{-3}$	0.43	0.67
$2.1 \cdot 10^{-3}$	0.43	0.67
$2.0 \cdot 10^{-3}$	0.41	0.68
$1.1 \cdot 10^{-3}$	0.23	0.81
$1.0 \cdot 10^{-3}$	0.22	0.82
$1.1 \cdot 10^{-3}$	0.22	0.83

$$\frac{[RSCl]_0}{[Cp_2TiS_5]_0} = -\left(\left(\frac{{k_{rel}}^{-1} \cdot fCp_2TiS_5{}^{{k_{rel}}^{-1}}}{{k_{rel}}^{-1} - 1}\right) + \left(\frac{{k_{rel}}^{-1} - 2}{{k_{rel}}^{-1} - 1}\right) \cdot fCp_2TiS_5 - 2\right)$$

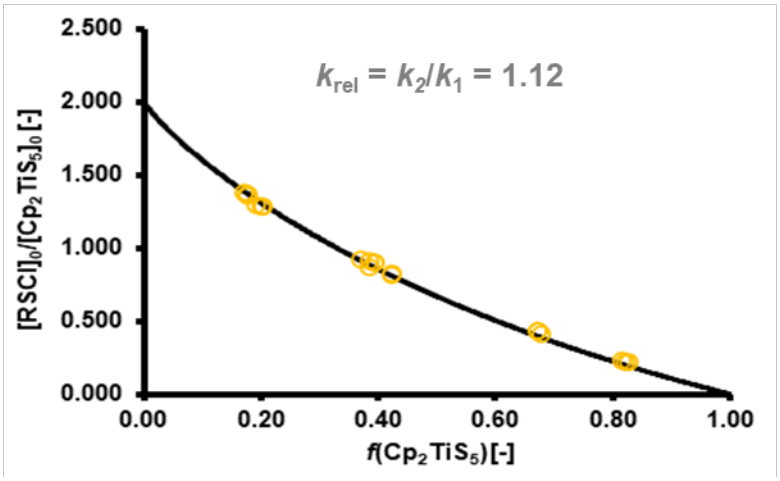

Figure S37. SF-NMR titration of Cp_2TiS_5 with 4-Cl-C_6H_4SCl: summary of initial conditions and graphical analysis of results.

D) 4-Methoxyphenylsulfenyl chloride as titrant.

Dimethylsulfone (Me_2SO_2) was used as an internal standard. A stock solution of 'solvent' was prepared by dissolving a known amount of Me_2SO_2 in anhydrous DCM to keep the concentration of internal standard constant in all runs. Titrations were performed using substoichoimetric amounts of sulfur electrophile with a variable-ratio three-syringe stopped-flow NMR instrumentation using three stock solutions: stock solution A: starting titanocene (Cp_2TiS_5) in 'solvent', solution B: sulfur electrophile (RSCl, 4-methoxyphenylsulfenyl chloride) in 'solvent', stock solution C: 'solvent'. The system was thermostatically equilibrated to 22 °C (295 K) before each experiment, to match the spectrometer probe temperature. Stock solutions were then loaded into the corresponding syringe. Each titration assay was then performed by keeping the volume injected from syringe A constant and varying the volume ratio of syringes B and C (total volume = 600 μL, flow rate = 1 mL/s). The system was flushed with DCM after each individual run and allowed to reach magnetic equilibrium for at least one minute before the next run. Measurements were performed *via* ^{1}H NMR{^{13}C} (zg 90, NS = 1, AQ = 4.5 s) using WET pulse sequence for solvent suppression. A stack of NMR spectra is shown in Figure S38. The molar fraction of starting titanocene (*f*Cp_2TiS) was calculated from the integrals of the Cp signals (zoomed region in Figure S38). The equivalents of electrophile used (defined as the molar ratio of initial concentrations, $[RSCl]_0/[Cp_2TiS_5]_0$) was plotted against the remaining fraction of starting titanocene, *f*Cp_2TiS_5.[S3] Experimental results were fitted to a consecutive bimolecular competition model using equation described in Figure S39. This procedure provides the relative reaction rate constants between the consecutive steps ($k_{rel} = k_2/k_1 = 1.30$), not their absolute values.

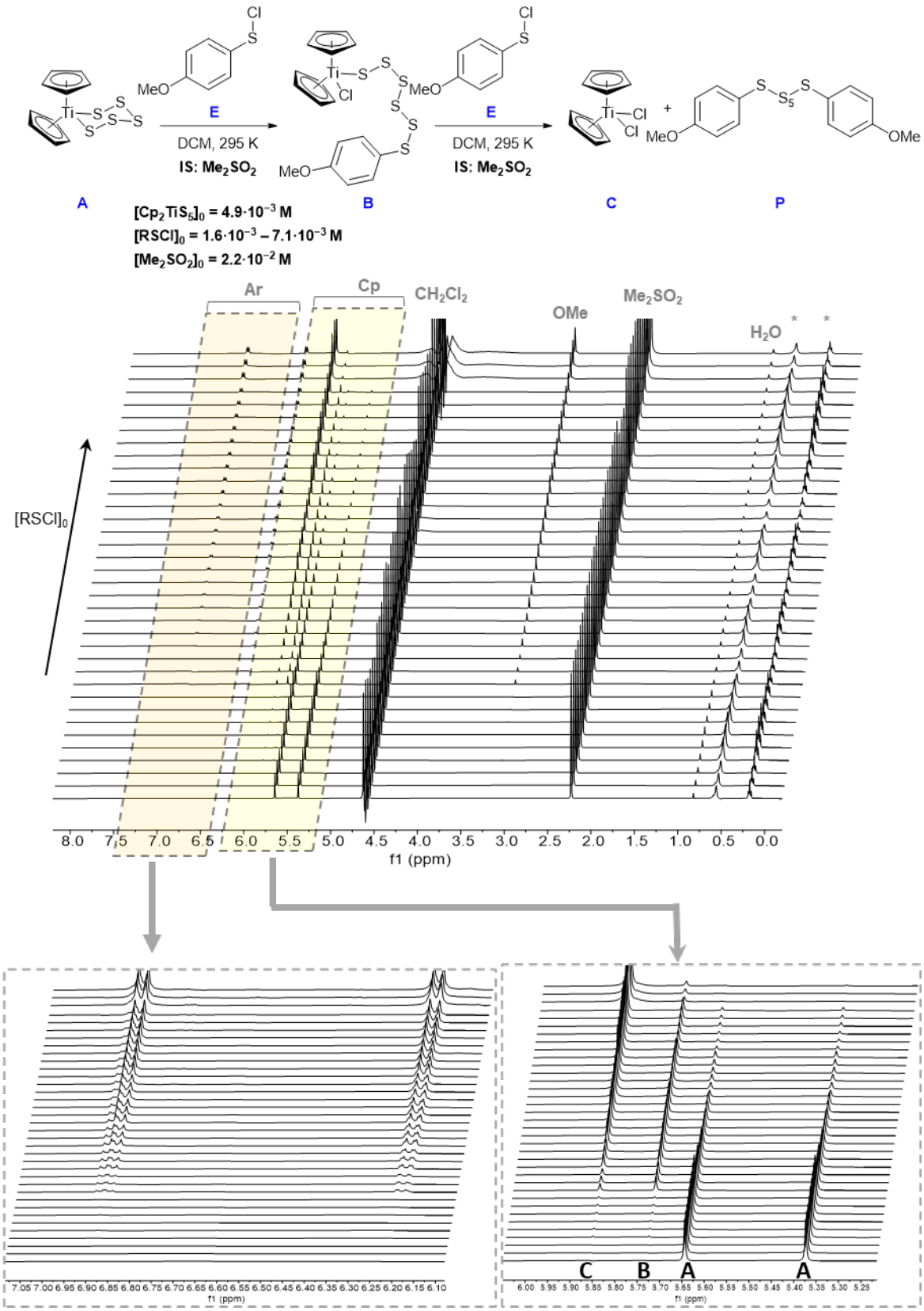

Figure S38. SF-NMR titration of Cp_2TiS_5 with 4-MeO-C_6H_4SCl: labelled Stack of NMR after addition of titrant with zoom-in on diagnostic titanocene peaks.

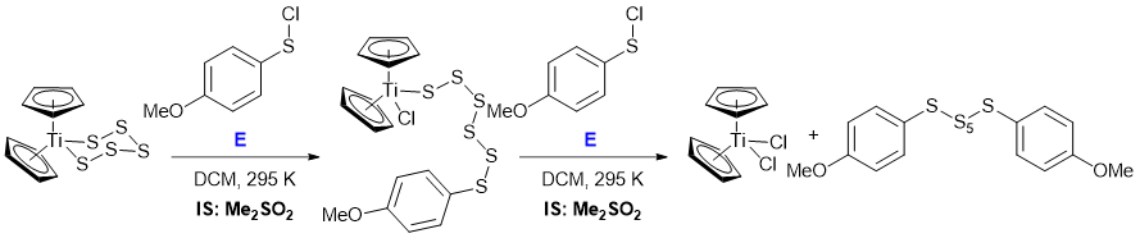

$[Cp_2TiS_5]_0 = 4.9 \cdot 10^{-3}$ M

$[RSCl]_0 = 1.6 \cdot 10^{-3} - 7.1 \cdot 10^{-3}$ M

$[Me_2SO_2]_0 = 2.2 \cdot 10^{-2}$ M

$[RSCl]_0$ [M]	$[RSCl]_0/[Cp_2TiS_5]_0$ [–]	fCp_2TiS_5 [–]
$7.1 \cdot 10^{-3}$	1.59	0.11
$7.2 \cdot 10^{-3}$	1.59	0.11
$7.2 \cdot 10^{-3}$	1.43	0.16
$7.2 \cdot 10^{-3}$	1.43	0.16
$7.1 \cdot 10^{-3}$	1.41	0.17
$6.5 \cdot 10^{-3}$	1.33	0.20
$6.6 \cdot 10^{-3}$	1.32	0.20
$6.4 \cdot 10^{-3}$	1.30	0.21
$5.2 \cdot 10^{-3}$	1.08	0.31
$5.2 \cdot 10^{-3}$	1.08	0.31
$5.1 \cdot 10^{-3}$	1.06	0.33
$4.2 \cdot 10^{-3}$	0.88	0.41
$4.1 \cdot 10^{-3}$	0.87	0.42
$4.1 \cdot 10^{-3}$	0.84	0.43
$2.9 \cdot 10^{-3}$	0.59	0.58
$1.9 \cdot 20^{-3}$	0.58	0.58
$2.9 \cdot 10^{-3}$	0.58	0.59
$1.7 \cdot 10^{-3}$	0.34	0.74
$1.7 \cdot 10^{-3}$	0.34	0.75
$1.6 \cdot 10^{-3}$	0.32	0.76

$$\frac{[RSCl]_0}{[Cp_2TiS_5]_0} = -\left(\left(\frac{k_{rel}^{-1} \cdot fCp_2TiS_5^{\,k_{rel}^{-1}}}{k_{rel}^{-1} - 1}\right) + \left(\frac{k_{rel}^{-1} - 2}{k_{rel}^{-1} - 1}\right) \cdot fCp_2TiS_5 - 2\right)$$

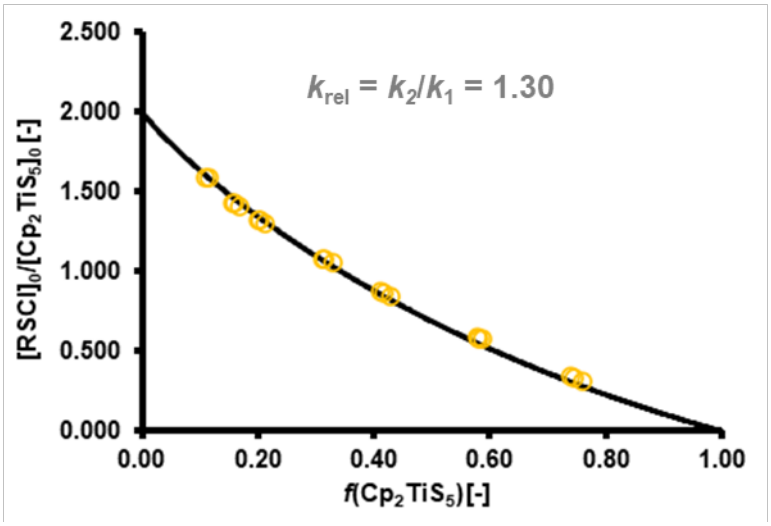

Figure S39. SF-NMR titration of Cp_2TiS_5 with 4-MeO-C_6H_4SCl: summary of initial conditions and graphical analysis of results.

E) 4-Bromophenylsulfenyl chloride as titrant.

Dimethylsulfone (Me_2SO_2) was used as an internal standard. A stock solution of 'solvent' was prepared by dissolving a known amount of Me_2SO_2 in anhydrous DCM to keep the concentration of internal standard constant in all runs. Titrations were performed using substoichoimetric amounts of sulfur electrophile with a variable-ratio three-syringe stopped-flow NMR instrumentation using three stock solutions: stock solution A: starting titanocene (Cp_2TiS_5) in 'solvent', solution B: sulfur electrophile (RSCl, 4-bromophenylsulfenyl chloride) in 'solvent', stock solution C: 'solvent'. The system was thermostatically equilibrated to 22 °C (295 K) before each experiment, to match the spectrometer probe temperature. Stock solutions were then loaded into the corresponding syringe. Each titration assay was then performed by keeping the volume injected from syringe A constant and varying the volume ratio of syringes B and C (total volume = 600 μL, flow rate = 1 mL/s). The system was flushed with DCM after each individual run and allowed to reach magnetic equilibrium for at least one minute before the next run. Measurements were performed *via* ^{1}H NMR{^{13}C} (zg 90, NS = 1, AQ = 4.5 s) using WET pulse sequence for solvent suppression. A stack of NMR spectra is shown in Figure S40. The molar fraction of starting titanocene (*f*Cp_2TiS) was calculated from the integrals of the Cp signals (zoomed region in Figure S40). The equivalents of electrophile used (defined as the molar ratio of initial concentrations, $[RSCl]_0/[Cp_2TiS_5]_0$) was plotted against the remaining fraction of starting titanocene, *f*Cp_2TiS_5.[S3] Experimental results were fitted to a consecutive bimolecular competition model using equation described in Figure S41. This procedure provides the relative reaction rate constants between the consecutive steps ($k_{rel} = k_2/k_1 = 0.96$), not their absolute values.

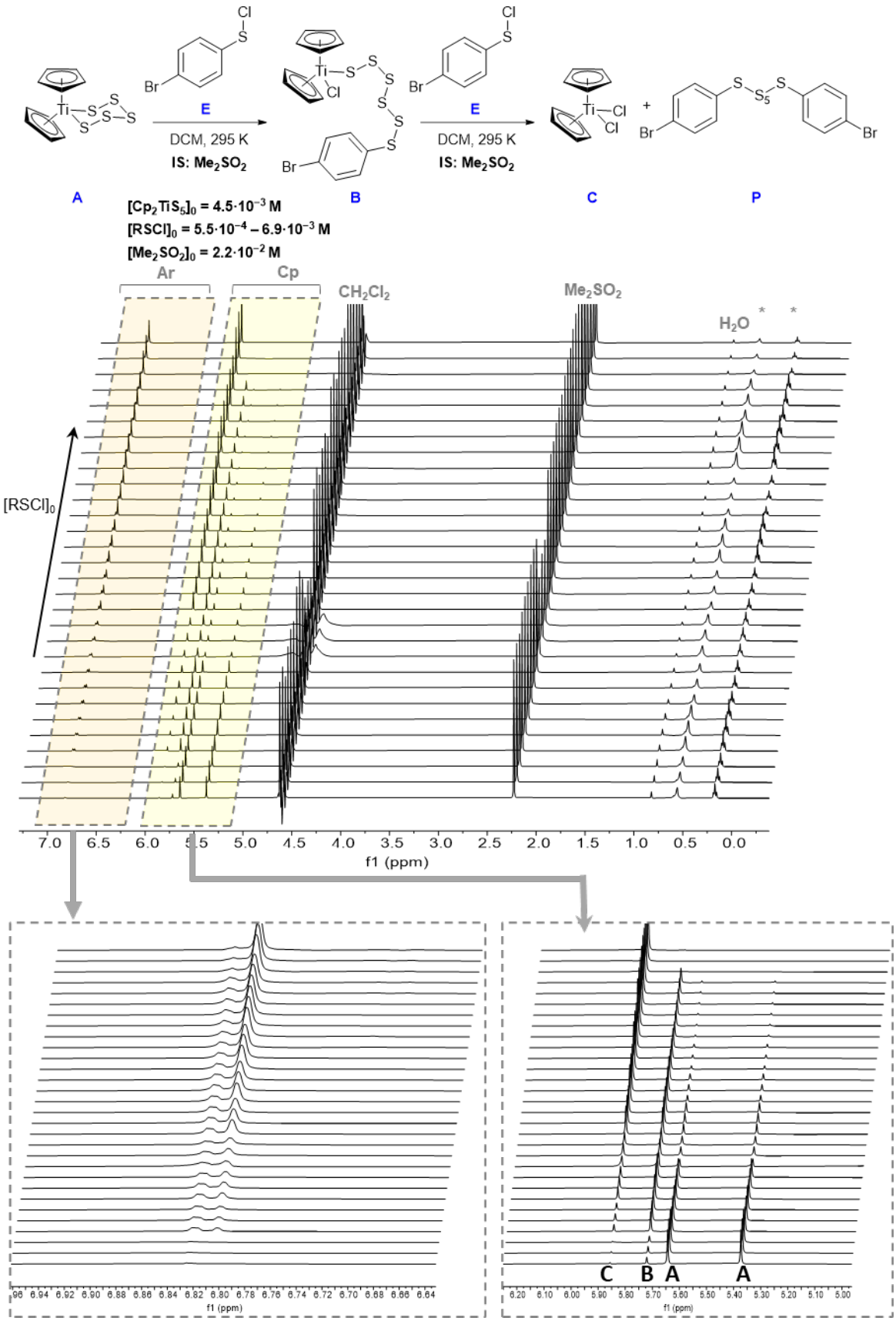

Figure S40. SF-NMR titration of Cp_2TiS_5 with 4-Br-C_6H_4SCl: labelled Stack of NMR after addition of titrant with zoom-in on diagnostic titanocene peaks.

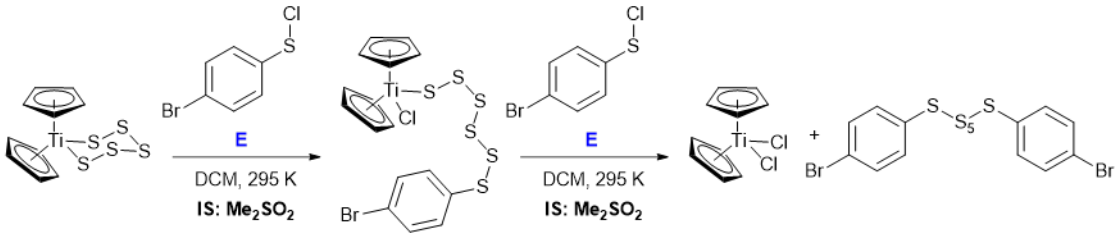

A B C P

$[Cp_2TiS_5]_0 = 4.5 \cdot 10^{-3}$ M

$[RSCl]_0 = 5.5 \cdot 10^{-4} - 6.9 \cdot 10^{-3}$ M

$[Me_2SO_2]_0 = 2.2 \cdot 10^{-2}$ M

$[RSCl]_0$ [M]	$[RSCl]_0/[Cp_2TiS_5]_0$ [–]	fCp_2TiS_5 [–]
$6.9 \cdot 10^{-3}$	1.53	0.10
$5.9 \cdot 10^{-3}$	1.33	0.17
$5.8 \cdot 10^{-3}$	1.32	0.17
$5.9 \cdot 10^{-3}$	1.32	0.17
$4.9 \cdot 10^{-3}$	1.10	0.27
$4.9 \cdot 10^{-3}$	1.10	0.27
$4.9 \cdot 10^{-3}$	1.09	0.27
$4.1 \cdot 10^{-3}$	0.90	0.38
$3.7 \cdot 10^{-3}$	0.88	0.38
$3.7 \cdot 10^{-3}$	0.88	0.38
$2.9 \cdot 10^{-3}$	0.64	0.52
$2.9 \cdot 10^{-3}$	0.64	0.52
$2.9 \cdot 10^{-3}$	0.64	0.52
$2.1 \cdot 10^{-3}$	0.45	0.64
$2.0 \cdot 10^{-3}$	0.45	0.64
$2.1 \cdot 10^{-3}$	0.45	0.64
$6.3 \cdot 10^{-3}$	0.14	0.89
$6.0 \cdot 10^{-3}$	0.13	0.89
$5.5 \cdot 10^{-3}$	0.12	0.90

$$\frac{[RSCl]_0}{[Cp_2TiS_5]_0} = -\left(\left(\frac{k_{rel}^{-1} \cdot fCp_2TiS_5^{\,k_{rel}^{-1}}}{k_{rel}^{-1} - 1}\right) + \left(\frac{k_{rel}^{-1} - 2}{k_{rel}^{-1} - 1}\right) \cdot fCp_2TiS_5 - 2\right)$$

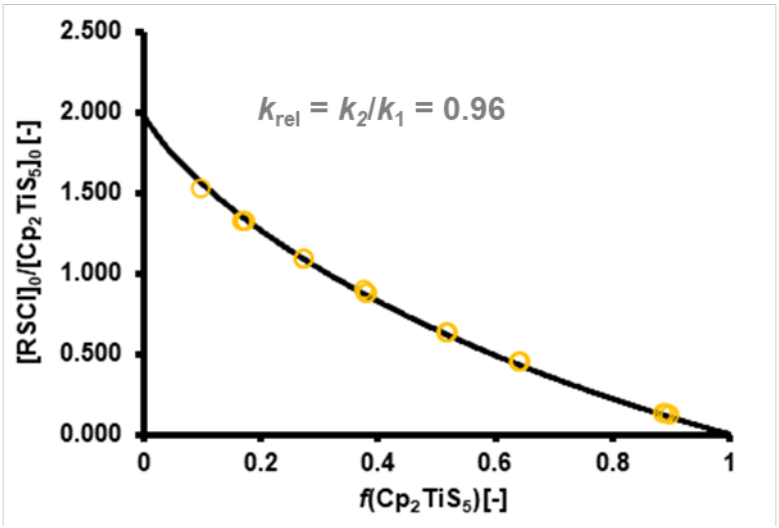

Figure S41. SF-NMR titration of Cp_2TiS_5 with 4-Br-C_6H_4SCl: summary of initial conditions and graphical analysis of results.

F) Phenylsulfenyl chloride as titrant.

Dimethylsulfone (Me_2SO_2) was used as an internal standard. A stock solution of 'solvent' was prepared by dissolving a known amount of Me_2SO_2 in anhydrous DCM to keep the concentration of internal standard constant in all runs. Titrations were performed using substoichoimetric amounts of sulfur electrophile with a variable-ratio three-syringe stopped-flow NMR instrumentation using three stock solutions: stock solution A: starting titanocene (Cp_2TiS_5) in 'solvent', solution B: sulfur electrophile (RSCl, phenylsulfenyl chloride) in 'solvent', stock solution C: 'solvent'. The system was thermostatically equilibrated to 22 °C (295 K) before each experiment, to match the spectrometer probe temperature. Stock solutions were then loaded into the corresponding syringe. Each titration assay was then performed by keeping the volume injected from syringe A constant and varying the volume ratio of syringes B and C (total volume = 600 μL, flow rate = 1 mL/s). The system was flushed with DCM after each individual run and allowed to reach magnetic equilibrium for at least one minute before the next run. Measurements were performed *via* ^{1}H NMR{^{13}C} (zg 90, NS = 1, AQ = 4.5 s) using WET pulse sequence for solvent suppression. A stack of NMR spectra is shown in Figure S42. The molar fraction of starting titanocene (*f*Cp_2TiS) was calculated from the integrals of the Cp signals (zoomed region in Figure S42). The equivalents of electrophile used (defined as the molar ratio of initial concentrations, $[RSCl]_0/[Cp_2TiS_5]_0$) was plotted against the remaining fraction of starting titanocene, *f*Cp_2TiS_5.[S3] Experimental results were fitted to a consecutive bimolecular competition model using equation described in Figure S43. This procedure provides the relative reaction rate constants between the consecutive steps ($k_{rel} = k_2/k_1 = 1.21$), not their absolute values.

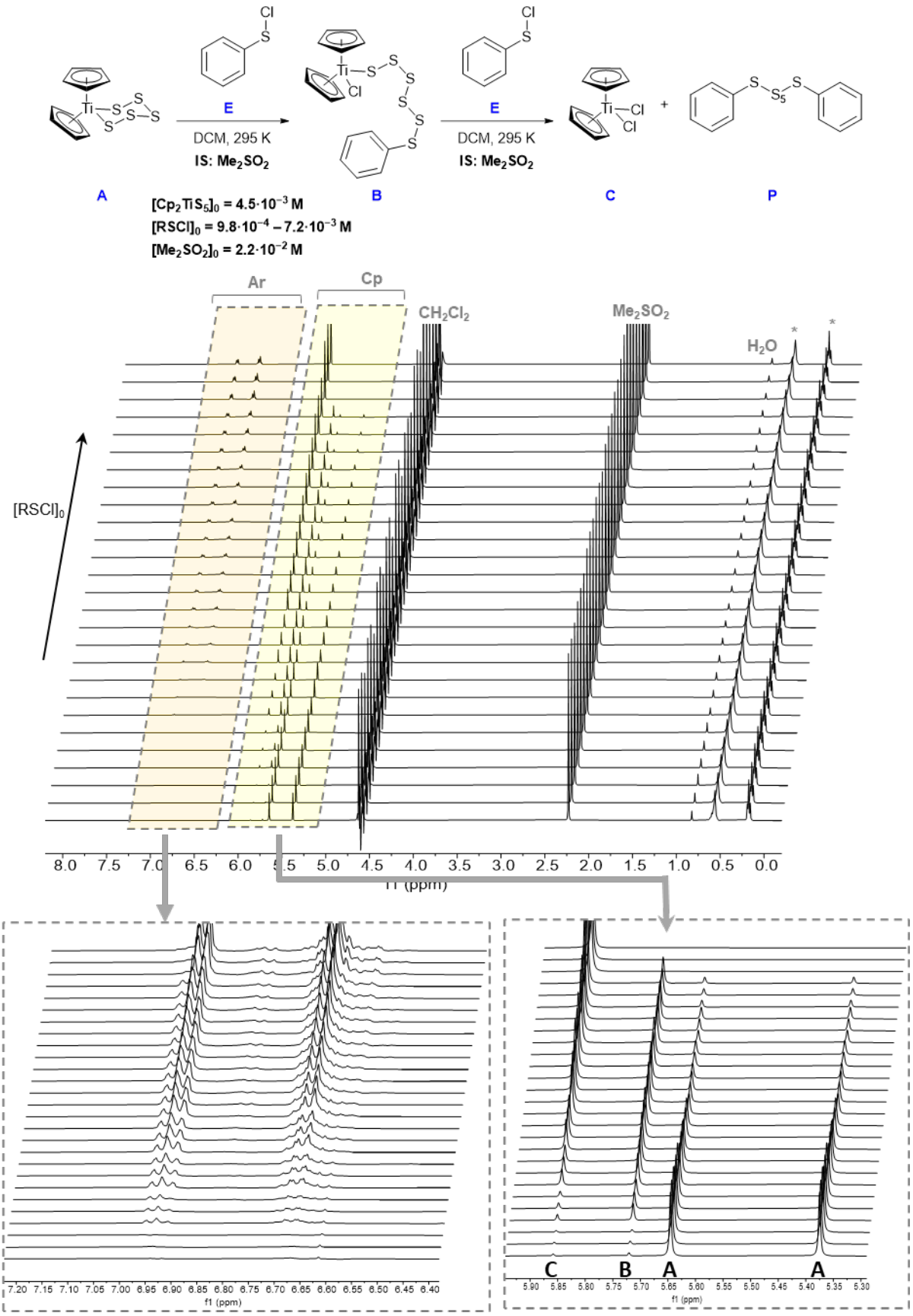

Figure S42. SF-NMR titration of Cp_2TiS_5 with PhSCl: labelled Stack of NMR after addition of titrant with zoom-in on diagnostic titanocene peaks.

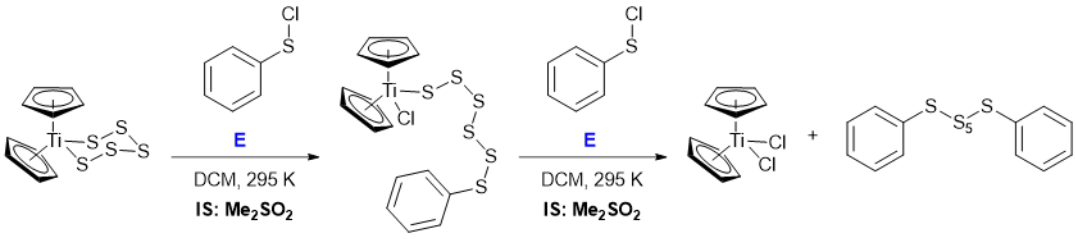

$[Cp_2TiS_5]_0 = 4.5 \cdot 10^{-3}$ M
$[RSCl]_0 = 9.8 \cdot 10^{-4} - 7.2 \cdot 10^{-3}$ M
$[Me_2SO_2]_0 = 2.2 \cdot 10^{-2}$ M

$[RSCl]_0$ [M]	$[RSCl]_0/[Cp_2TiS_5]_0$ [–]	fCp_2TiS_5 [–]
$7.2 \cdot 10^{-3}$	1.59	0.10
$7.1 \cdot 10^{-3}$	1.58	0.11
$7.0 \cdot 10^{-3}$	1.57	0.11
$6.2 \cdot 10^{-3}$	1.37	0.18
$6.1 \cdot 10^{-3}$	1.36	0.19
$6.2 \cdot 10^{-3}$	1.36	0.19
$5.5 \cdot 10^{-3}$	1.26	0.22
$5.3 \cdot 10^{-3}$	1.24	0.23
$5.3 \cdot 10^{-3}$	1.23	0.24
$4.9 \cdot 10^{-3}$	1.09	0.30
$4.8 \cdot 10^{-3}$	1.08	0.30
$4.6 \cdot 10^{-3}$	1.06	0.32
$3.5 \cdot 10^{-3}$	0.78	0.45
$3.4 \cdot 10^{-3}$	0.77	0.46
$3.3 \cdot 10^{-3}$	0.76	0.47
$2.3 \cdot 10^{-3}$	0.50	0.61
$2.2 \cdot 10^{-3}$	0.50	0.63
$2.1 \cdot 10^{-3}$	0.48	0.63
$1.0 \cdot 10^{-3}$	0.22	0.82
$9.7 \cdot 10^{-4}$	0.22	0.83
$9.8 \cdot 10^{-4}$	0.21	0.83

$$\frac{[RSCl]_0}{[Cp_2TiS_5]_0} = -\left(\left(\frac{k_{rel}^{-1} \cdot fCp_2TiS_5^{\,k_{rel}^{-1}}}{k_{rel}^{-1} - 1}\right) + \left(\frac{k_{rel}^{-1} - 2}{k_{rel}^{-1} - 1}\right) \cdot fCp_2TiS_5 - 2\right)$$

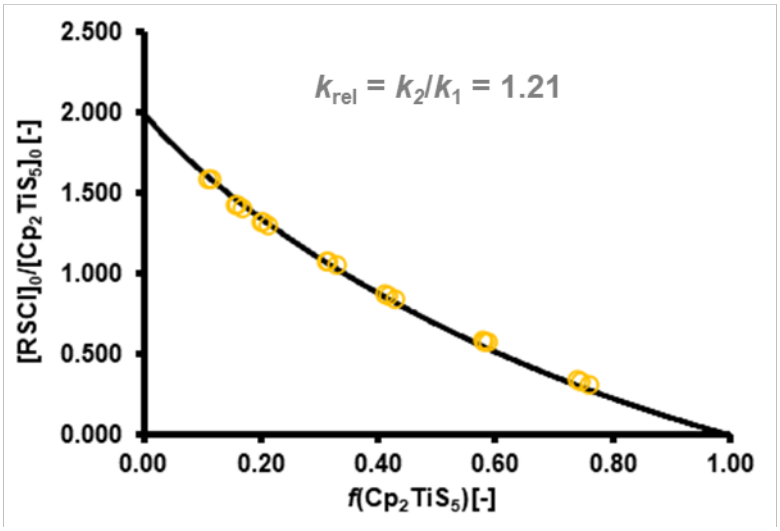

Figure S43. SF-NMR titration of Cp_2TiS_5 with PhSCl: summary of initial conditions and graphical analysis of results.

4.2.2. Reaction of Cp_2TiS_5 with other sulfenyl chlorides

A) Acetylthiosulfenyl chloride as titrant.

Fluorobenzene (PhF) was used as an internal standard. A stock solution of 'solvent' was prepared by dissolving a known amount of PhF in anhydrous DCM to keep the concentration of internal standard constant in all runs. Titrations were performed using substoichoimetric amounts of sulfur electrophile with a variable-ratio three-syringe stopped-flow NMR instrumentation using three stock solutions; stock solution A: starting titanocene (Cp_2TiS_5) in 'solvent', solution B: sulfur electrophile (RSCl, acetylthiosulfenyl chloride) in 'solvent', stock solution C: 'solvent'. The system was thermostatically equilibrated to 22 ^{o}C (295 K) before each experiment, to match the spectrometer probe temperature. Stock solutions were then loaded into the corresponding syringe. Each titration assay was then performed by keeping the volume injected from syringe A constant and varying the volume ratio of syringes B and C (total volume = 600 μL, flow rate = 1 mL/s). The system was flushed with DCM after each individual run and allowed to reach magnetic equilibrium for at least one minute before the next run. Measurements were performed *via* ^{1}H NMR{^{13}C} (zg 90, NS = 1, AQ = 4.5 s) using WET pulse sequence for solvent suppression. A stack of NMR spectra is shown in Figure S44. The molar fraction of starting titanocene (*f*Cp_2TiS) was calculated from the integrals of the Cp signals (zoomed region in Figure S44). The equivalents of electrophile used (defined as the molar ratio of initial concentrations, $[RSCl]_0/[Cp_2TiS_5]_0$) was plotted against the remaining fraction of starting titanocene, *f*Cp_2TiS_5.[S3] Experimental results were fitted to a consecutive bimolecular competition model using equation described in Figure S45. This procedure provides the relative reaction rate constants between the consecutive steps ($k_{rel} = k_2/k_1 = 2.21$), not their absolute values.

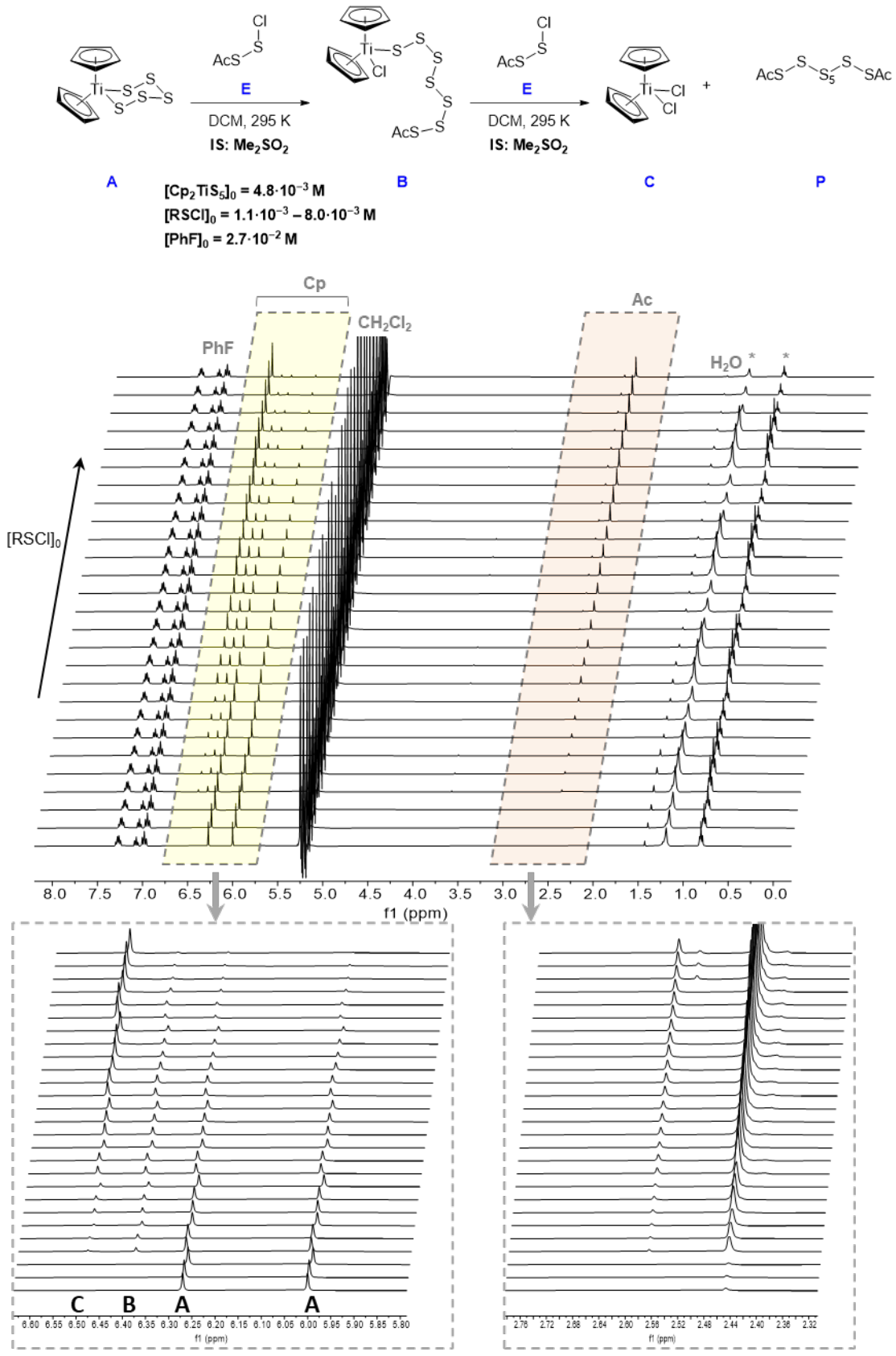

Figure S44. SF-NMR titration of Cp_2TiS_5 with AcSSCl: labelled Stack of NMR after addition of titrant with zoom-in on diagnostic titanocene peaks.

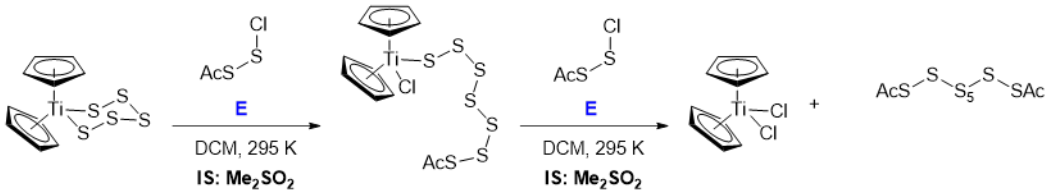

$[Cp_2TiS_5]_0 = 4.8 \cdot 10^{-3}$ M
$[RSCl]_0 = 1.1 \cdot 10^{-3} - 8.0 \cdot 10^{-3}$ M
$[PhF]_0 = 2.7 \cdot 10^{-2}$ M

$[RSCl]_0$ [M]	$[RSCl]_0/[Cp_2TiS_5]_0$ [–]	fCp_2TiS_5 [–]
$7.9 \cdot 10^{-3}$	1.68	0.12
$8.0 \cdot 10^{-3}$	1.67	0.13
$7.2 \cdot 10^{-3}$	1.50	0.18
$7.1 \cdot 10^{-3}$	1.49	0.18
$7.1 \cdot 10^{-3}$	1.48	0.18
$6.2 \cdot 10^{-3}$	1.30	0.26
$6.2 \cdot 10^{-3}$	1.29	0.26
$6.1 \cdot 10^{-3}$	1.29	0.27
$4.7 \cdot 10^{-3}$	0.99	0.39
$4.7 \cdot 10^{-3}$	0.99	0.39
$4.7 \cdot 10^{-3}$	0.97	0.40
$4.0 \cdot 10^{-3}$	0.83	0.47
$4.0 \cdot 10^{-3}$	0.83	0.47
$4.0 \cdot 10^{-3}$	0.82	0.48
$3.3 \cdot 10^{-3}$	0.69	0.54
$3.2 \cdot 10^{-3}$	0.67	0.55
$3.0 \cdot 10^{-3}$	0.63	0.58
$1.8 \cdot 10^{-3}$	0.38	0.73
$1.8 \cdot 10^{-3}$	0.38	0.74
$1.8 \cdot 10^{-3}$	0.37	0.74
$1.2 \cdot 10^{-3}$	0.25	0.81
$1.1 \cdot 10^{-3}$	0.24	0.82
$1.1 \cdot 10^{-3}$	0.22	0.83

$$\frac{[RSCl]_0}{[Cp_2TiS_5]_0} = -\left(\left(\frac{{k_{rel}}^{-1} \cdot f{Cp_2TiS_5}^{{k_{rel}}^{-1}}}{{k_{rel}}^{-1} - 1}\right) + \left(\frac{{k_{rel}}^{-1} - 2}{{k_{rel}}^{-1} - 1}\right) \cdot fCp_2TiS_5 - 2\right)$$

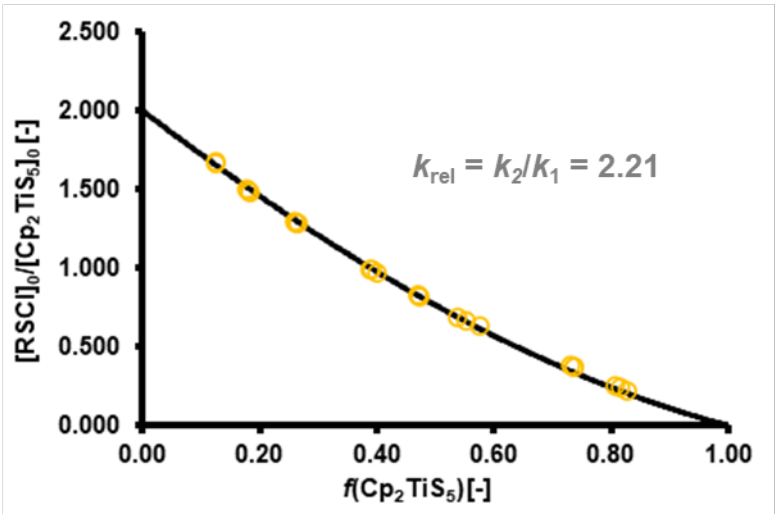

Figure S45. SF-NMR titration of Cp_2TiS_5 with AcSSCl: summary of initial conditions and graphical analysis of results.

B) *N*-Phthalamidosulfenyl chloride as titrant.

Dimethylsulfone (Me_2SO_2) was used as an internal standard. A stock solution of 'solvent' was prepared by dissolving a known amount of Me_2SO_2 in anhydrous DCM to keep the concentration of internal standard constant in all runs. Titrations were performed using substoichoimetric amounts of sulfur electrophile with a variable-ratio three-syringe stopped-flow NMR instrumentation using three stock solutions; stock solution A: starting titanocene (Cp_2TiS_5) in 'solvent', solution B: sulfur electrophile (RSCl, *N*-phthalamidosulfenyl chloride) in 'solvent', stock solution C: 'solvent'. The system was thermostatically equilibrated to 22 °C (295 K) before each experiment, to match the spectrometer probe temperature. Stock solutions were then loaded into the corresponding syringe. Each titration assay was then performed by keeping the volume injected from syringe A constant and varying the volume ratio of syringes B and C (total volume = 600 μL, flow rate = 1 mL/s). The system was flushed with DCM after each individual run and allowed to reach magnetic equilibrium for at least one minute before the next run. Measurements were performed *via* ^{1}H NMR{^{13}C} (zg 90, NS = 1, AQ = 4.5 s) using WET pulse sequence for solvent suppression. A stack of NMR spectra is shown in Figure S46. The molar fraction of starting titanocene (*f*Cp_2TiS) was calculated from the integrals of the Cp signals (zoomed region in Figure S46). The equivalents of electrophile used (defined as the molar ratio of initial concentrations, $[RSCl]_0/[Cp_2TiS_5]_0$) was plotted against the remaining fraction of starting titanocene, *f*Cp_2TiS_5.[S3] Experimental results were fitted to a consecutive bimolecular competition model using equation described in Figure S47. This procedure provides the relative reaction rate constants between the consecutive steps ($k_{rel} = k_2/k_1 = 3.97$), not their absolute values.

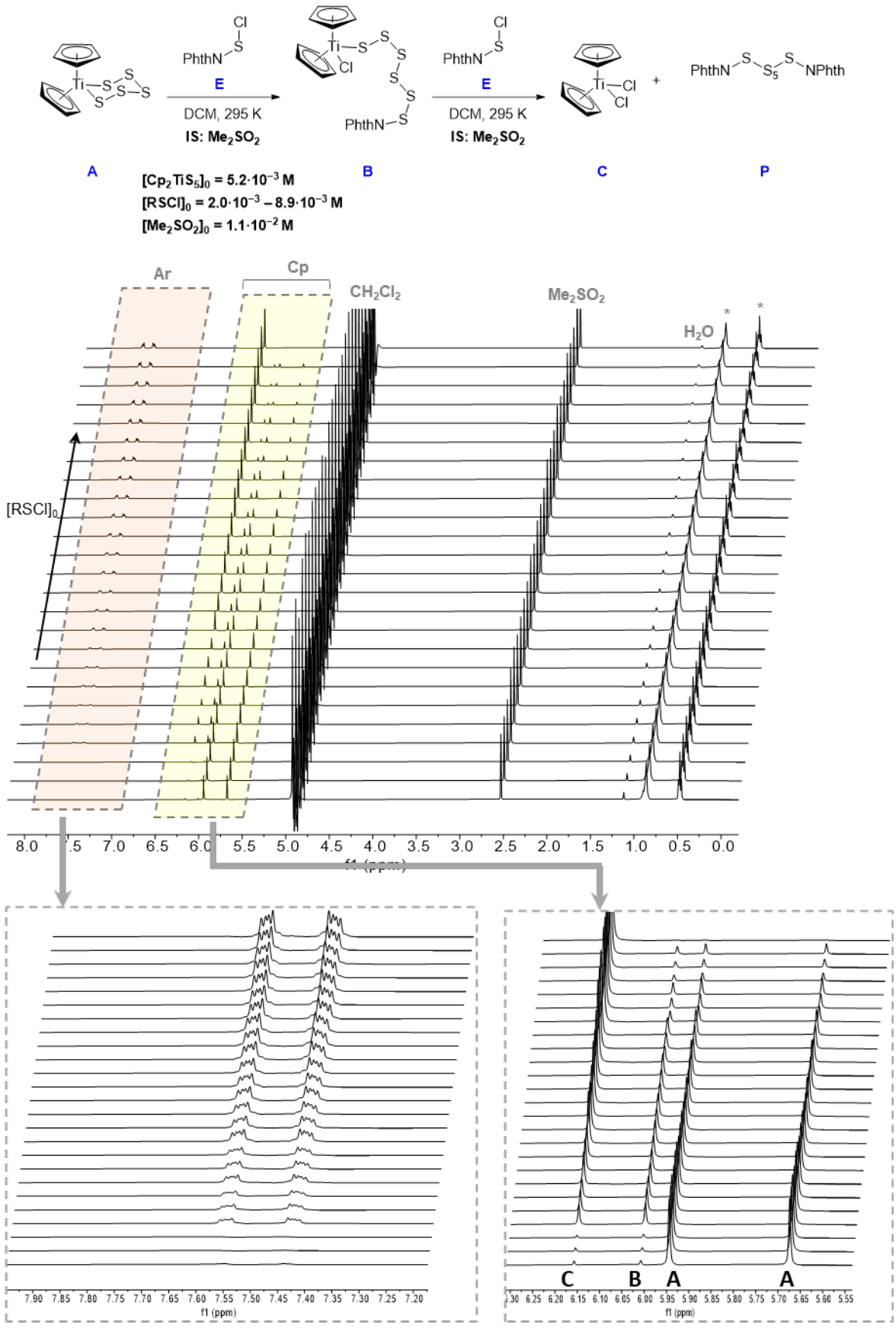

Figure S46. SF-NMR titration of Cp_2TiS_5 with PhthNSCl: labelled Stack of NMR after addition of titrant with zoom-in on diagnostic titanocene peaks.

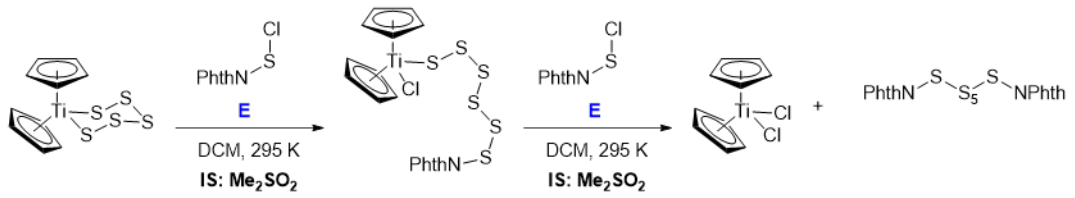

$[Cp_2TiS_5]_0 = 5.2 \cdot 10^{-3}$ M
$[RSCl]_0 = 2.0 \cdot 10^{-3} - 8.9 \cdot 10^{-3}$ M
$[Me_2SO_2]_0 = 1.1 \cdot 10^{-2}$ M

$[RSCl]_0$ [M]	$[RSCl]_0/[Cp_2TiS_5]_0$ [–]	fCp_2TiS_5 [–]
$8.9 \cdot 10^{-3}$	1.70	0.13
$8.8 \cdot 10^{-3}$	1.70	0.13
$8.5 \cdot 10^{-3}$	1.67	0.14
$7.8 \cdot 10^{-3}$	1.50	0.21
$7.6 \cdot 10^{-3}$	1.48	0.22
$7.4 \cdot 10^{-3}$	1.47	0.22
$6.5 \cdot 10^{-3}$	1.25	0.32
$6.4 \cdot 10^{-3}$	1.25	0.32
$6.2 \cdot 10^{-3}$	1.22	0.33
$5.1 \cdot 10^{-3}$	0.98	0.44
$5.0 \cdot 10^{-3}$	0.97	0.45
$4.8 \cdot 10^{-3}$	0.96	0.45
$4.3 \cdot 10^{-3}$	0.83	0.51
$4.2 \cdot 10^{-3}$	0.83	0.51
$4.2 \cdot 10^{-3}$	0.83	0.51
$3.0 \cdot 10^{-3}$	0.57	0.64
$2.9 \cdot 10^{-3}$	0.57	0.64
$2.9 \cdot 10^{-3}$	0.56	0.65
$2.0 \cdot 10^{-3}$	0.40	0.73
$2.0 \cdot 10^{-3}$	0.39	0.73
$2.0 \cdot 10^{-3}$	0.38	0.74

$$\frac{[RSCl]_0}{[Cp_2TiS_5]_0} = -\left(\left(\frac{k_{rel}^{-1} \cdot fCp_2TiS_5^{\,k_{rel}^{-1}}}{k_{rel}^{-1} - 1}\right) + \left(\frac{k_{rel}^{-1} - 2}{k_{rel}^{-1} - 1}\right) \cdot fCp_2TiS_5 - 2\right)$$

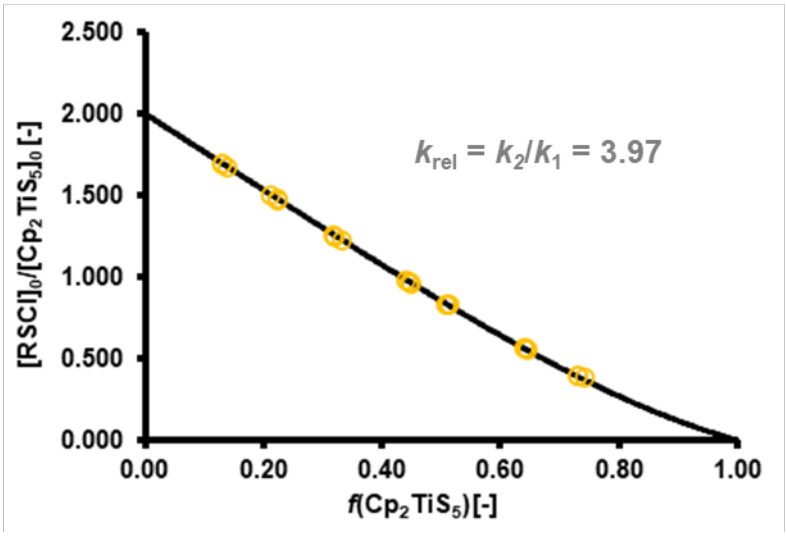

Figure S47. SF-NMR titration of Cp_2TiS_5 with PhthNSCl: summary of initial conditions and graphical analysis of results.

4.2.3 Reaction of $Cp_2Ti(SAr)_2$ with *N*-morpholinosulfenyl chloride

A) Titration of $Cp_2Ti(SPh)_2$.

4-(trimethylsilyl)fluorobenzene (*p*-TMSPhF) was used as an internal standard. A stock solution of 'solvent' was prepared by dissolving a known amount of internal standard in anhydrous DCM to keep the concentration of internal standard constant in all runs. Titrations were performed using substoichoimetric amounts of sulfur electrophile with a variable-ratio three-syringe stopped-flow NMR instrumentation using three stock solutions; stock solution A: starting titanocene ($Cp_2Ti(SPh)_2$) in 'solvent', solution B: sulfur electrophile (*N*-morpholinosulfenyl chloride) in 'solvent', stock solution C: 'solvent'. The system was thermostatically equilibrated to 22 °C (295 K) before each experiment, to match the spectrometer probe temperature. Stock solutions were then loaded into the corresponding syringe. Each titration assay was then performed by keeping the volume injected from syringe A constant and varying the volume ratio of syringes B and C (total volume = 600 μL, flow rate = 1 mL/s). The system was flushed with DCM after each individual run and allowed to reach magnetic equilibrium for at least one minute before the next run. Measurements were performed *via* ^1H NMR{^{13}C} (zg 90, NS = 1, AQ = 4.5 s) using WET pulse sequence for solvent suppression. A stack of NMR spectra is shown in Figure S48. The molar fraction of starting titanocene ($f Cp_2Ti(SAr)_2$) was calculated from the integrals of the Cp signals (zoomed region in Figure S48). The equivalents of electrophile used (defined as the molar ratio of initial concentrations, $[RSCl]_0/[Cp_2TiS_5]_0$) was plotted against the remaining fraction of starting titanocene, $f Cp_2Ti(SAr)_2$.[S3] Experimental results were fitted to a consecutive bimolecular competition model using equation described in Figure S49. This procedure provides the relative reaction rate constants between the consecutive steps ($k_{rel} = k_2/k_1 = 0.49$), not their absolute values.

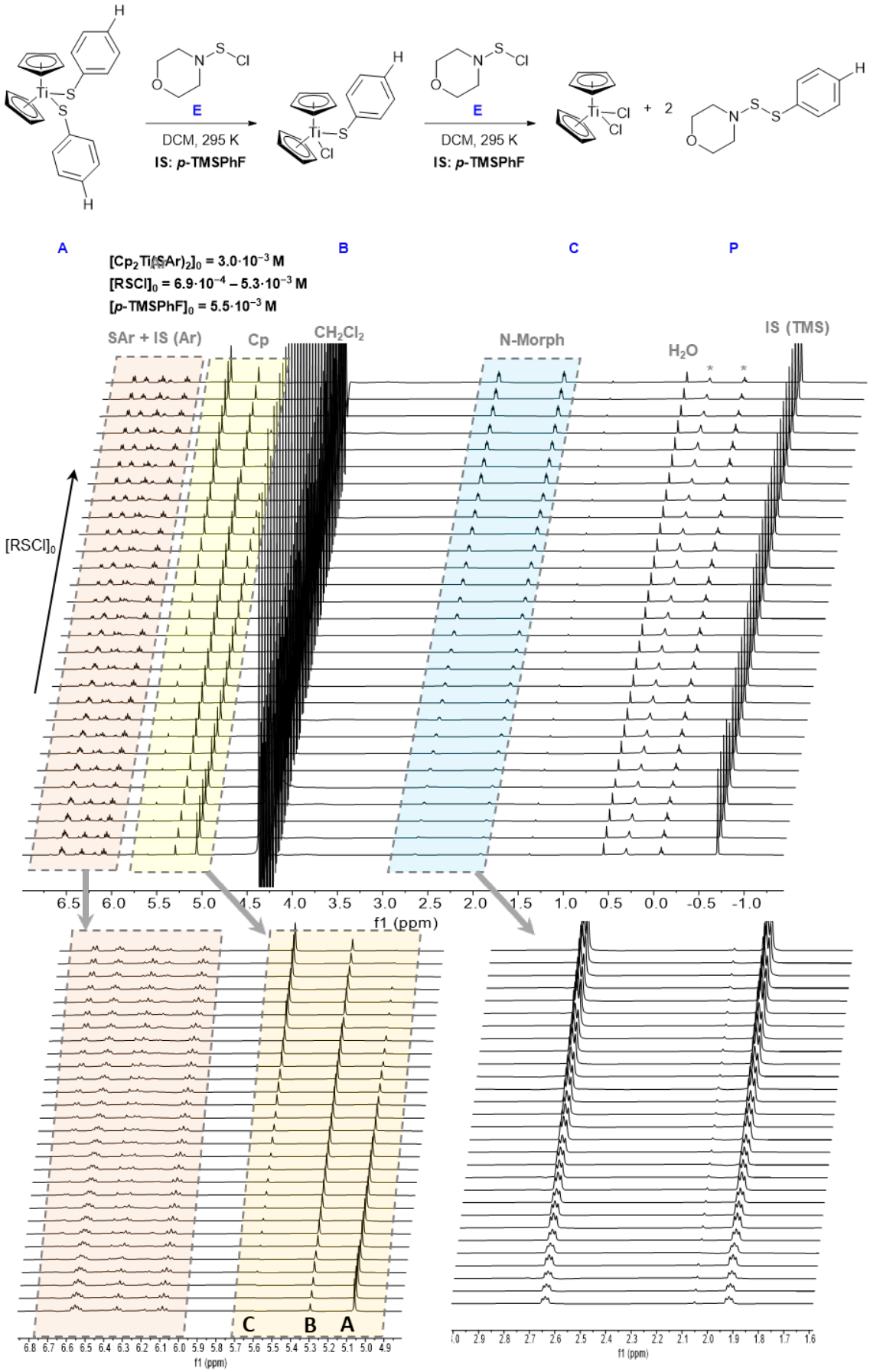

Figure S48. SF-NMR titration of $Cp_2Ti(SPh)_2$ with *N*-Morpholinosulfenyl chloride: labelled stack of NMR after addition of titrant with zoom-in on diagnostic titanocene peaks.

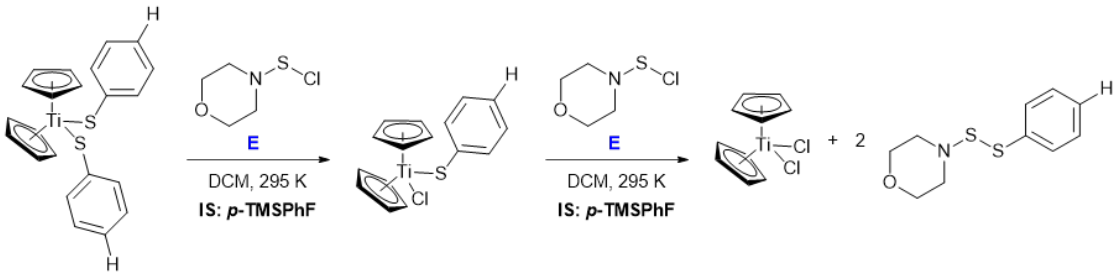

A $[Cp_2Ti(SAr)_2]_0 = 3.0 \cdot 10^{-3}$ M
$[RSCl]_0 = 6.9 \cdot 10^{-4} - 5.3 \cdot 10^{-3}$ M
$[p\text{-TMSPhF}]_0 = 5.5 \cdot 10^{-3}$ M
B C P

$[RSCl]_0$ [M]	$[RSCl]_0/[Cp_2Ti(SAr)_2]_0$ [–]	$fCp_2Ti(SAr)_2$ [–]
$5.3 \cdot 10^{-3}$	1.69	0.02
$5.1 \cdot 10^{-3}$	1.67	0.02
$5.2 \cdot 10^{-3}$	1.68	0.02
$5.3 \cdot 10^{-3}$	1.65	0.03
$4.4 \cdot 10^{-3}$	1.48	0.06
$4.3 \cdot 10^{-3}$	1.48	0.06
$4.3 \cdot 10^{-3}$	1.48	0.06
$3.7 \cdot 10^{-3}$	1.27	0.13
$3.7 \cdot 10^{-3}$	1.26	0.14
$3.7 \cdot 10^{-3}$	1.25	0.14
$3.0 \cdot 10^{-3}$	1.04	0.23
$3.1 \cdot 10^{-3}$	1.05	0.23
$3.1 \cdot 10^{-3}$	1.05	0.23
$2.5 \cdot 10^{-3}$	0.84	0.34
$2.4 \cdot 10^{-3}$	0.83	0.35
$2.4 \cdot 10^{-3}$	0.81	0.36
$1.8 \cdot 10^{-3}$	0.62	0.48
$1.9 \cdot 10^{-3}$	0.62	0.48
$1.8 \cdot 10^{-3}$	0.62	0.49
$1.8 \cdot 10^{-3}$	0.60	0.50
$1.5 \cdot 10^{-3}$	0.51	0.56
$1.5 \cdot 10^{-3}$	0.50	0.57
$1.5 \cdot 10^{-3}$	0.50	0.57
$1.2 \cdot 10^{-3}$	0.39	0.65
$1.1 \cdot 10^{-3}$	0.39	0.65
$1.2 \cdot 10^{-3}$	0.38	0.66
$7.5 \cdot 10^{-4}$	0.25	0.77
$7.1 \cdot 10^{-4}$	0.24	0.78
$6.9 \cdot 10^{-4}$	0.23	0.79

$$\frac{[RSCl]_0}{[Cp_2TiS_5]_0} = -\left(\left(\frac{k_{rel}^{-1} \cdot fCp_2TiS_5^{\,k_{rel}^{-1}}}{k_{rel}^{-1} - 1}\right) + \left(\frac{k_{rel}^{-1} - 2}{k_{rel}^{-1} - 1}\right) \cdot fCp_2TiS_5 - 2\right)$$

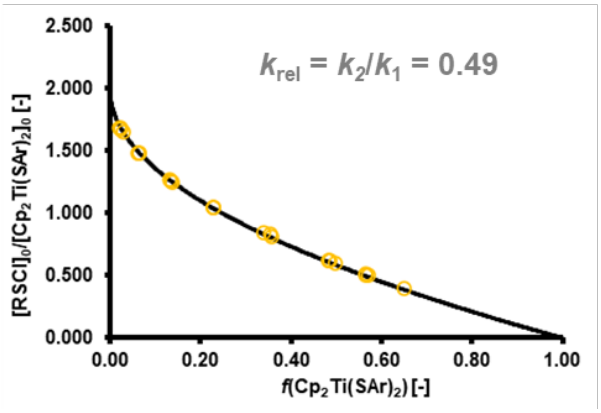

Figure S49. SF-NMR titration of $Cp_2Ti(SPh)_2$ with *N*-Morpholinosulfenyl chloride: summary of initial conditions and graphical analysis of results.

B) Titration of $Cp_2Ti(4\text{-}F\text{-}C_6H_4S)_2$

4-(trimethylsilyl)fluorobenzene (*p*-TMSPhF) was used as an internal standard. A stock solution of 'solvent' was prepared by dissolving a known amount of internal standard in anhydrous DCM to keep the concentration of internal standard constant in all runs. Titrations were performed using substoichoimetric amounts of sulfur electrophile with a variable-ratio three-syringe stopped-flow NMR instrumentation using three stock solutions; stock solution A: starting titanocene ($Cp_2Ti(4\text{-}F\text{-}C_6H_4S)_2$) in 'solvent', solution B: sulfur electrophile (*N*-morpholinosulfenyl chloride) in 'solvent', stock solution C: 'solvent'. The system was thermostatically equilibrated to 22 °C (295 K) before each experiment, to match the spectrometer probe temperature. Stock solutions were then loaded into the corresponding syringe. Each titration assay was then performed by keeping the volume injected from syringe A constant and varying the volume ratio of syringes B and C (total volume = 600 μL, flow rate = 1 mL/s). The system was flushed with DCM after each individual run and allowed to reach magnetic equilibrium for at least one minute before the next run. Measurements were performed *via* ^1H NMR{^{13}C} (zg 90, NS = 1, AQ = 4.5 s) using WET pulse sequence for solvent suppression. A stack of NMR spectra is shown in Figure S50. The molar fraction of starting titanocene ($f Cp_2Ti(SAr)_2$) was calculated from the integrals of the Cp signals (zoomed region in Figure S50). The equivalents of electrophile used (defined as the molar ratio of initial concentrations, $[RSCl]_0/[Cp_2TiS_5]_0$) was plotted against the remaining fraction of starting titanocene, $f Cp_2Ti(SAr)_2$.[S3] Experimental results were fitted to a consecutive bimolecular competition model using equation described in Figure S51. This procedure provides the relative reaction rate constants between the consecutive steps ($k_{rel} = k_2/k_1 = 0.59$), not their absolute values.

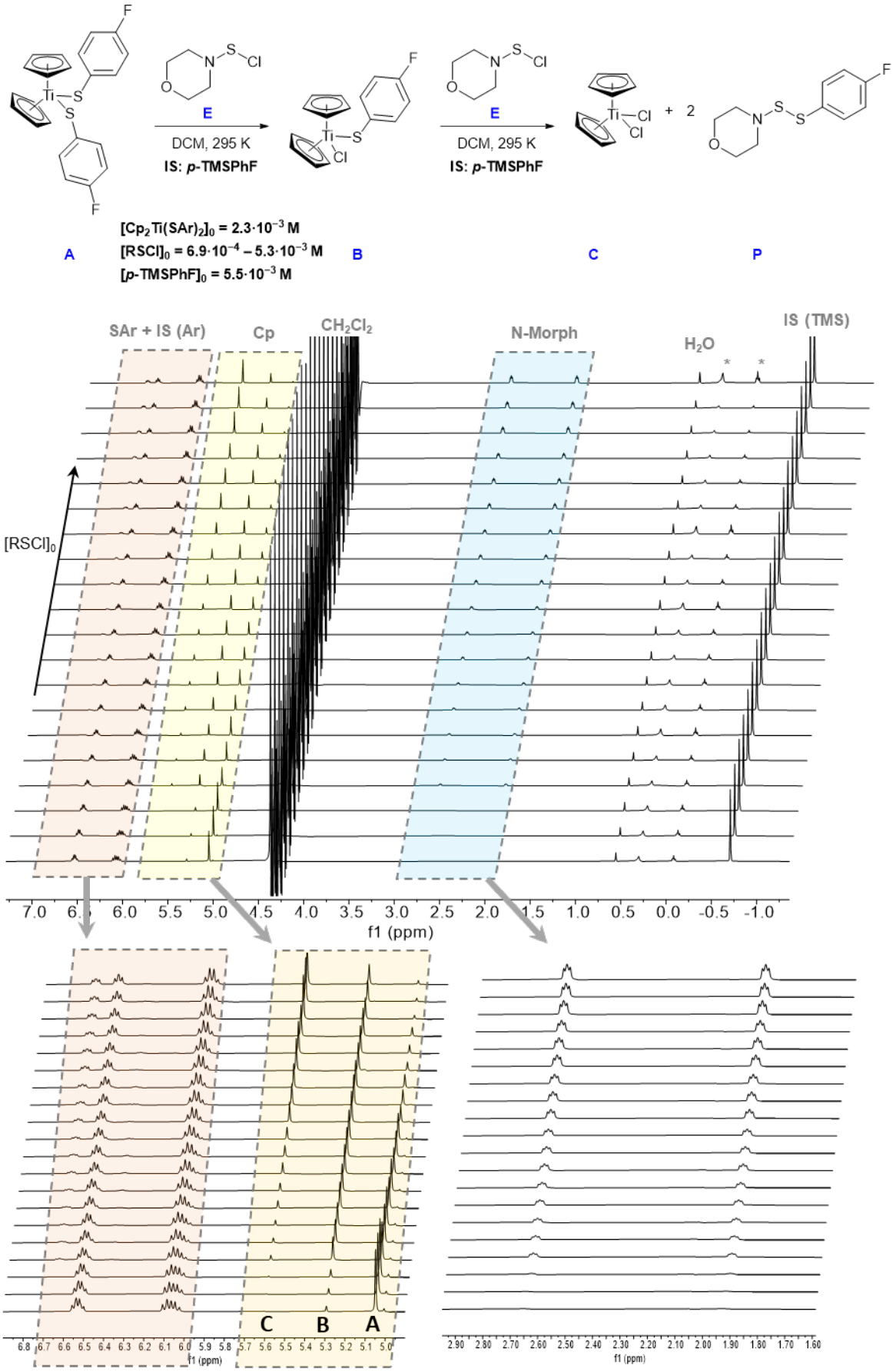

Figure S50. SF-NMR titration of $Cp_2Ti(4\text{-}F\text{-}C_6H_4S)_2$with *N*-Morpholinosulfenyl chloride: labelled stack of NMR after addition of titrant with zoom-in on diagnostic titanocene peaks.

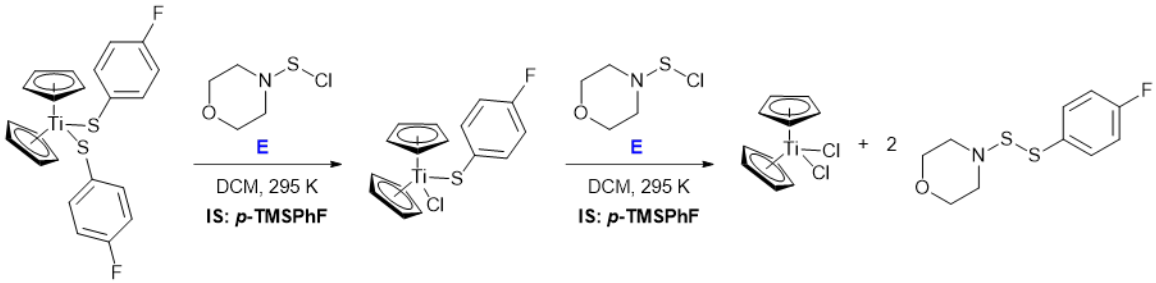

A

$[Cp_2Ti(SAr)_2]_0 = 2.3 \cdot 10^{-3}$ M
$[RSCl]_0 = 6.9 \cdot 10^{-4} - 5.3 \cdot 10^{-3}$ M
$[p\text{-TMSPhF}]_0 = 5.5 \cdot 10^{-3}$ M

B

C

P

$[RSCl]_0$ [M]	$[RSCl]_0/[Cp_2Ti(SAr)_2]_0$ [–]	$fCp_2Ti(SAr)_2$ [–]
$3.6 \cdot 10^{-3}$	1.58	0.05
$3.6 \cdot 10^{-3}$	1.58	0.05
$4.0 \cdot 10^{-3}$	1.57	0.06
$3.0 \cdot 10^{-3}$	1.34	0.12
$3.1 \cdot 10^{-3}$	1.34	0.12
$3.0 \cdot 10^{-3}$	1.32	0.13
$2.5 \cdot 10^{-3}$	1.12	0.22
$2.5 \cdot 10^{-3}$	1.09	0.23
$2.4 \cdot 10^{-3}$	1.05	0.24
$1.8 \cdot 10^{-3}$	0.79	0.38
$1.8 \cdot 10^{-3}$	0.79	0.38
$1.8 \cdot 10^{-3}$	0.78	0.39
$1.4 \cdot 10^{-3}$	0.64	0.47
$1.4 \cdot 10^{-3}$	0.64	0.47
$1.1 \cdot 10^{-3}$	0.51	0.57
$1.1 \cdot 10^{-3}$	0.50	0.57
$1.1 \cdot 10^{-3}$	0.50	0.57
$3.4 \cdot 10^{-4}$	0.15	0.87
$2.6 \cdot 10^{-4}$	0.12	0.90
$2.4 \cdot 10^{-4}$	0.10	0.91

$$\frac{[RSCl]_0}{[Cp_2TiS_5]_0} = -\left(\left(\frac{k_{rel}^{-1} \cdot fCp_2TiS_5^{k_{rel}^{-1}}}{k_{rel}^{-1} - 1}\right) + \left(\frac{k_{rel}^{-1} - 2}{k_{rel}^{-1} - 1}\right) \cdot fCp_2TiS_5 - 2\right)$$

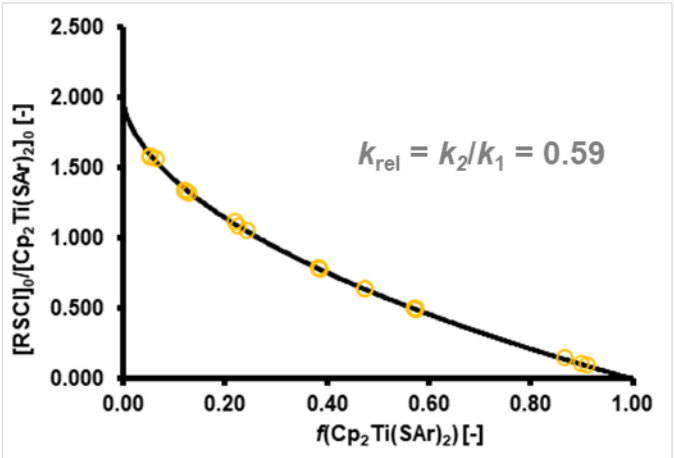

Figure S51. SF-NMR titration of $Cp_2Ti(4\text{-}F\text{-}C_6H_4S)_2$with *N*-Morpholinosulfenyl chloride: summary of initial conditions and graphical analysis of results.

C) Titration of $Cp_2Ti(4\text{-}Cl\text{-}C_6H_4S)_2$

4-(trimethylsilyl)fluorobenzene (*p*-TMSPhF) was used as an internal standard. A stock solution of 'solvent' was prepared by dissolving a known amount of internal standard in anhydrous DCM to keep the concentration of internal standard constant in all runs. Titrations were performed using substoichoimetric amounts of sulfur electrophile with a variable-ratio three-syringe stopped-flow NMR instrumentation using three stock solutions; stock solution A: starting titanocene ($Cp_2Ti(4\text{-}Cl\text{-}C_6H_4S)_2$) in 'solvent', solution B: sulfur electrophile (*N*-morpholinosulfenyl chloride) in 'solvent', stock solution C: 'solvent'. The system was thermostatically equilibrated to 22 °C (295 K) before each experiment, to match the spectrometer probe temperature. Stock solutions were then loaded into the corresponding syringe. Each titration assay was then performed by keeping the volume injected from syringe A constant and varying the volume ratio of syringes B and C (total volume = 600 μL, flow rate = 1 mL/s). The system was flushed with DCM after each individual run and allowed to reach magnetic equilibrium for at least one minute before the next run. Measurements were performed *via* ^1H NMR{^{13}C} (zg 90, NS = 1, AQ = 4.5 s) using WET pulse sequence for solvent suppression. A stack of NMR spectra is shown in Figure S52. The molar fraction of starting titanocene ($fCp_2Ti(SAr)_2$) was calculated from the integrals of the Cp signals (zoomed region in Figure S52). The equivalents of electrophile used (defined as the molar ratio of initial concentrations, $[RSCl]_0/[Cp_2TiS_5]_0$) was plotted against the remaining fraction of starting titanocene, $fCp_2Ti(SAr)_2$.[S3] Experimental results were fitted to a consecutive bimolecular competition model using equation described in Figure S53. This procedure provides the relative reaction rate constants between the consecutive steps ($k_{rel} = k_2/k_1 = 0.71$), not their absolute values.

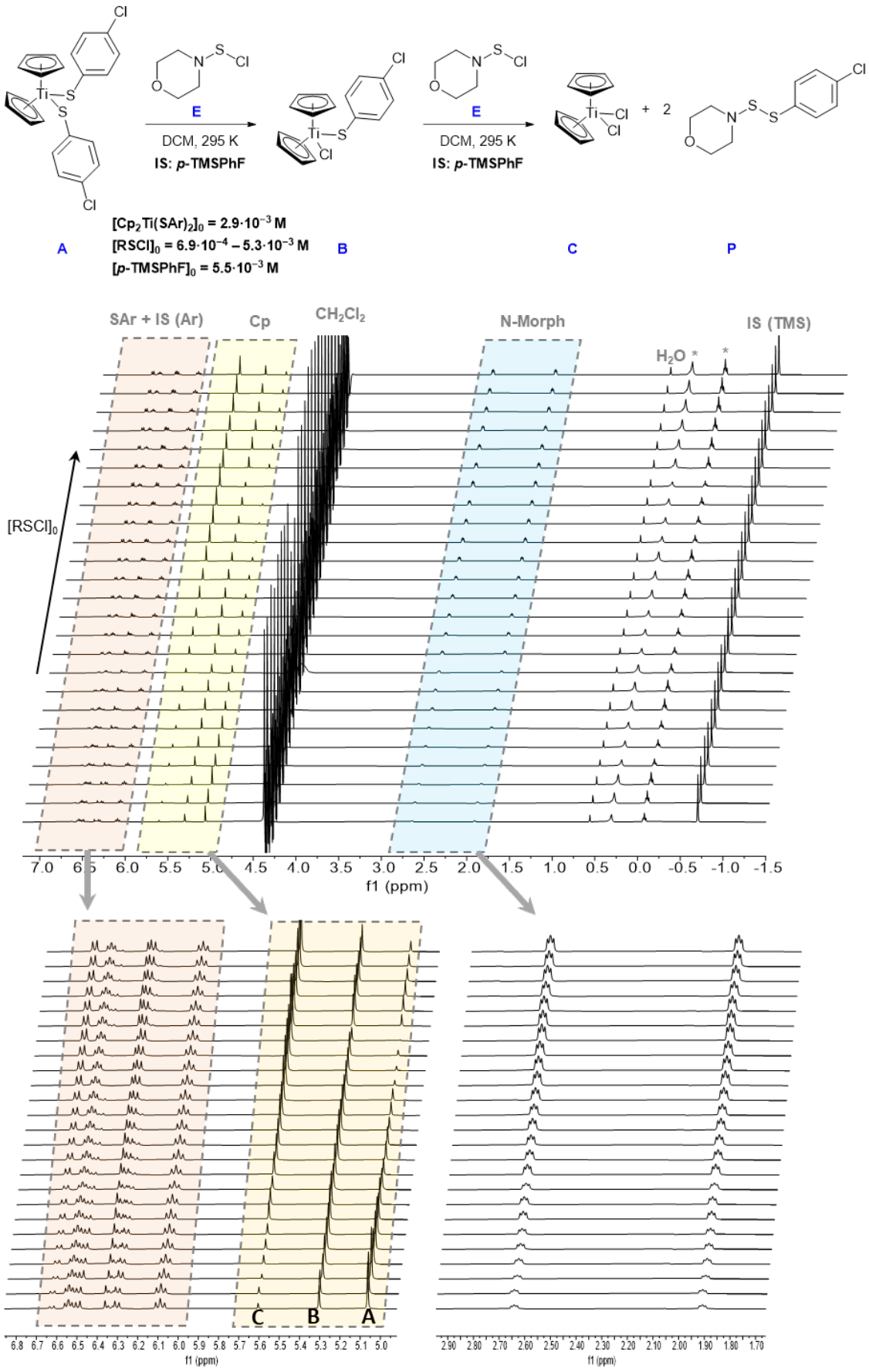

Figure S52. SF-NMR titration of $Cp_2Ti(4\text{-}Cl\text{-}C_6H_4S)_2$with *N*-Morpholinosulfenyl chloride: labelled stack of NMR after addition of titrant with zoom-in on diagnostic titanocene peaks.

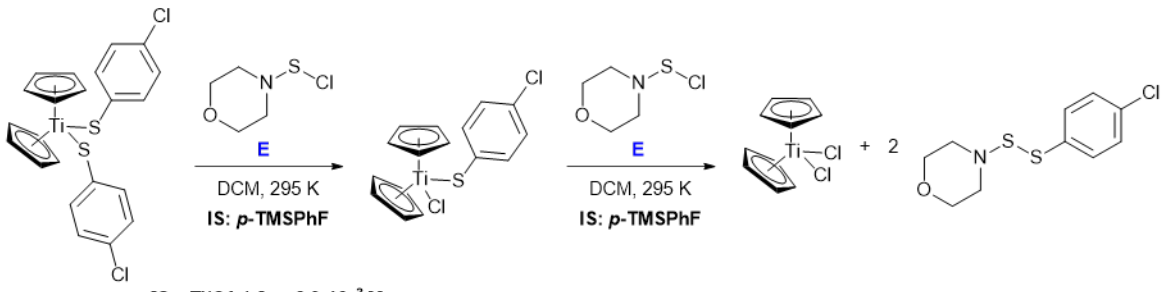

A: $[Cp_2Ti(SAr)_2]_0 = 2.9 \cdot 10^{-3}$ M; $[RSCl]_0 = 6.9 \cdot 10^{-4} - 5.3 \cdot 10^{-3}$ M; $[p\text{-TMSPhF}]_0 = 5.5 \cdot 10^{-3}$ M

B

C

P

$[RSCl]_0$ [M]	$[RSCl]_0/[Cp_2Ti(SAr)_2]_0$ [–]	$fCp_2Ti(SAr)_2$ [–]
$5.2 \cdot 10^{-3}$	1.80	0.01
$4.4 \cdot 10^{-3}$	1.59	0.05
$4.4 \cdot 10^{-3}$	1.56	0.06
$4.4 \cdot 10^{-3}$	1.57	0.07
$5.0 \cdot 10^{-3}$	1.52	0.10
$4.9 \cdot 10^{-3}$	1.45	0.11
$4.8 \cdot 10^{-3}$	1.46	0.12
$4.9 \cdot 10^{-3}$	1.45	0.12
$4.0 \cdot 10^{-3}$	1.39	0.14
$4.7 \cdot 10^{-3}$	1.37	0.14
$4.6 \cdot 10^{-3}$	1.34	0.15
$3.7 \cdot 10^{-3}$	1.29	0.16
$3.5 \cdot 10^{-3}$	1.26	0.17
$3.1 \cdot 10^{-3}$	1.10	0.22
$3.1 \cdot 10^{-3}$	1.10	0.23
$2.8 \cdot 10^{-3}$	1.10	0.23
$2.5 \cdot 10^{-3}$	0.90	0.32
$2.4 \cdot 10^{-3}$	0.89	0.34
$2.5 \cdot 10^{-3}$	0.88	0.34
$1.9 \cdot 10^{-3}$	0.68	0.46
$1.9 \cdot 10^{-3}$	0.66	0.47
$1.8 \cdot 10^{-3}$	0.64	0.48
$1.3 \cdot 10^{-3}$	0.51	0.58
$1.2 \cdot 10^{-3}$	0.46	0.61
$1.2 \cdot 10^{-3}$	0.43	0.63

$$\frac{[RSCl]_0}{[Cp_2TiS_5]_0} = -\left(\left(\frac{{k_{rel}}^{-1} \cdot f{Cp_2TiS_5}^{{k_{rel}}^{-1}}}{{k_{rel}}^{-1} - 1}\right) + \left(\frac{{k_{rel}}^{-1} - 2}{{k_{rel}}^{-1} - 1}\right) \cdot fCp_2TiS_5 - 2\right)$$

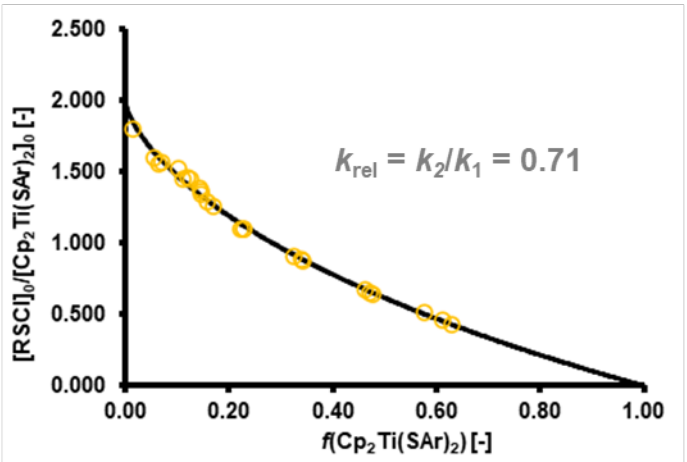

Figure S53. SF-NMR titration of $Cp_2Ti(4\text{-Cl-}C_6H_4S)_2$with *N*-Morpholinosulfenyl chloride: summary of initial conditions and graphical analysis of results.

D) Titration of $Cp_2Ti(4\text{-}MeO\text{-}C_6H_4S)_2$

4-(trimethylsilyl)fluorobenzene (*p*-TMSPhF) was used as an internal standard. A stock solution of 'solvent' was prepared by dissolving a known amount of internal standard in anhydrous DCM to keep the concentration of internal standard constant in all runs. Titrations were performed using substoichoimetric amounts of sulfur electrophile with a variable-ratio three-syringe stopped-flow NMR instrumentation using three stock solutions; stock solution A: starting titanocene ($Cp_2Ti(4\text{-}MeO\text{-}C_6H_4S)_2$) in 'solvent', solution B: sulfur electrophile (*N*-morpholinosulfenyl chloride) in 'solvent', stock solution C: 'solvent'. The system was thermostatically equilibrated to 22 °C (295 K) before each experiment, to match the spectrometer probe temperature. Stock solutions were then loaded into the corresponding syringe. Each titration assay was then performed by keeping the volume injected from syringe A constant and varying the volume ratio of syringes B and C (total volume = 600 μL, flow rate = 1 mL/s). The system was flushed with DCM after each individual run and allowed to reach magnetic equilibrium for at least one minute before the next run. Measurements were performed *via* ^1H NMR{^{13}C} (zg 90, NS = 1, AQ = 4.5 s) using WET pulse sequence for solvent suppression. A stack of NMR spectra is shown in Figure S54. The molar fraction of starting titanocene ($fCp_2Ti(SAr)_2$) was calculated from the integrals of the Cp signals (zoomed region in Figure S54). The equivalents of electrophile used (defined as the molar ratio of initial concentrations, $[RSCl]_0/[Cp_2TiS_5]_0$) was plotted against the remaining fraction of starting titanocene, $fCp_2Ti(SAr)_2$.[S3] Experimental results were fitted to a consecutive bimolecular competition model using equation described in Figure S55. This procedure provides the relative reaction rate constants between the consecutive steps ($k_{rel} = k_2/k_1 = 0.43$), not their absolute values.

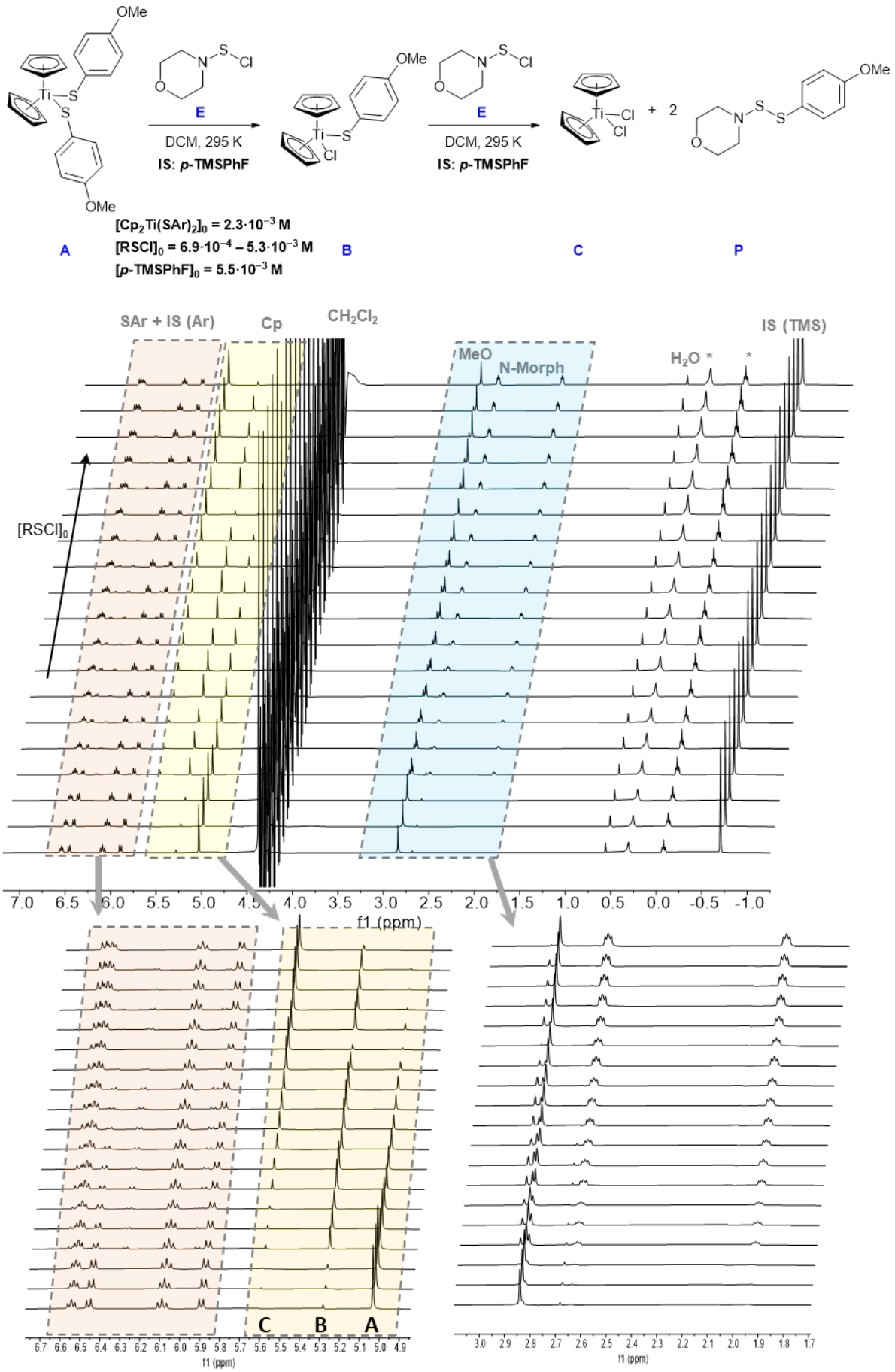

Figure S54. SF-NMR titration of $Cp_2Ti(4\text{-}MeO\text{-}C_6H_4S)_2$with *N*-Morpholinosulfenyl chloride: labelled stack of NMR after addition of titrant with zoom-in on diagnostic titanocene peaks.

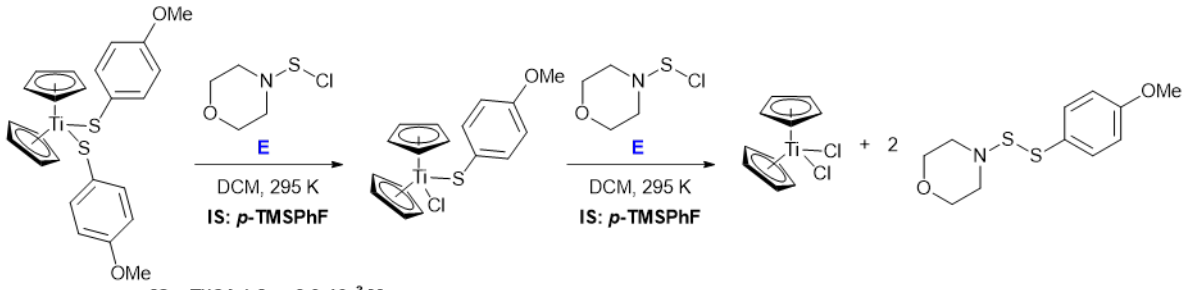

A $[Cp_2Ti(SAr)_2]_0 = 2.3 \cdot 10^{-3}$ M
$[RSCl]_0 = 6.9 \cdot 10^{-4} - 5.3 \cdot 10^{-3}$ M
$[p\text{-TMSPhF}]_0 = 5.5 \cdot 10^{-3}$ M

B C P

$[RSCl]_0$ [M]	$[RSCl]_0/[Cp_2Ti(SAr)_2]_0$ [–]	$fCp_2Ti(SAr)_2$ [–]
$3.7 \cdot 10^{-3}$	1.64	0.02
$3.7 \cdot 10^{-3}$	1.64	0.02
$3.7 \cdot 10^{-3}$	1.60	0.03
$3.1 \cdot 10^{-3}$	1.34	0.10
$2.4 \cdot 10^{-3}$	1.06	0.22
$2.4 \cdot 10^{-3}$	1.09	0.22
$2.4 \cdot 10^{-3}$	1.06	0.22
$1.9 \cdot 10^{-3}$	0.82	0.35
$1.8 \cdot 10^{-3}$	0.79	0.36
$1.2 \cdot 10^{-3}$	0.50	0.57
$1.1 \cdot 10^{-3}$	0.49	0.57
$1.1 \cdot 10^{-3}$	0.48	0.58
$2.6 \cdot 10^{-3}$	0.11	0.91
$2.3 \cdot 10^{-3}$	0.09	0.92
$2.3 \cdot 10^{-3}$	0.09	0.92

$$\frac{[RSCl]_0}{[Cp_2TiS_5]_0} = -\left(\left(\frac{k_{rel}^{-1} \cdot fCp_2TiS_5^{k_{rel}^{-1}}}{k_{rel}^{-1} - 1}\right) + \left(\frac{k_{rel}^{-1} - 2}{k_{rel}^{-1} - 1}\right) \cdot fCp_2TiS_5 - 2\right)$$

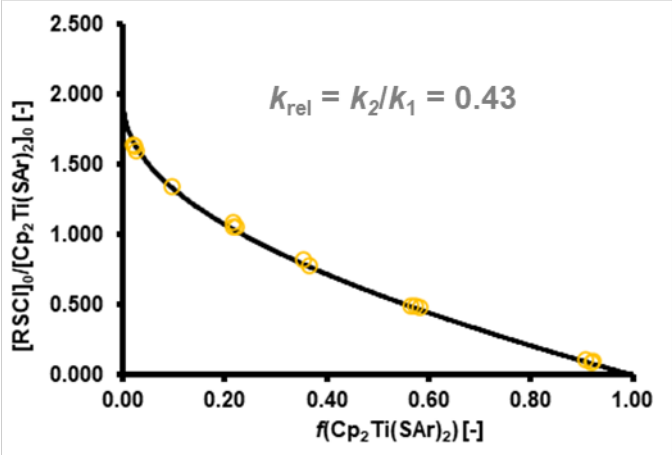

Figure S55. SF-NMR titration of $Cp_2Ti(4\text{-MeO-}C_6H_4S)_2$with *N*-Morpholinosulfenyl chloride: summary of initial conditions and graphical analysis of results.

5. ^{1}H NMR monitoring in standard NMR tubes

5.1 Reaction of Cp_2TiS_5 with S_2Cl_2 in CS_2

Fluorobenzene was weighed directly into a 10 mL volumetric flask. Then titanocene pentasulfide (Cp_2TiS_5) was added as a solid and CS_2 added to the mark. The resulting suspension was thoroughly shaken and transferred to a glass syringe connected to a 0.2 μM PTFE filter syringe. The resulting red-coloured filtrate was used as a titanocene pentasulfide stock solution. The concentration of Cp_2TiS_5 in the stock solution was calculated via ^{1}H NMR. Solutions of the electrophile (S_2Cl_2) were prepared by weighing the reagent into a volumetric flask and dissolved up to the mark using CS_2. Each reaction was set up for ^{1}H NMR monitoring as follows: 0.8 mL of titanocene stock was transferred into a standard borosilicate 5 mm O.D. NMR tube followed by 0.9 mL of CS_2. The tube was capped, shaken and introduced into the NMR spectrometer with temperature set up at 300 K. After shimming, a single scan ^{1}H NMR spectra (zg 30, AQ = 4.0 s) was recorded without a deuterium lock. The tube was ejected, the cap opened and 0.1 mL of electrophile stock solution added. The tube was capped and shaken thoroughly horizontally for approximately 15 seconds. The tube was introduced in the spectrometer and a series of single scan spectra recorded periodically with a fixed delay between them. The data was fitted to a second order reaction model using a numerical approach to directly extract the bimolecular rate constant. A representative temporal stack of NMR spectra and concentration-time plots including both experimental and fitted data are shown below in Figure S56. Signals indicating the presence of an intermediate were not observed. Syringes with disposable Sterican® needles were employed through this work. The use of mycrosyringes with built-in metallic needles for addition of S_2Cl_2 stock solution led to accelerated reaction profiles (Figure S56, run B vs run D), suggesting extraction of active catalysts. We have not performed further experiments to confirm the identity of the active catalysts, the role of the solvent or the electrophile (S_2Cl_2) in its extraction, or the effect of catalysis in the reaction outcome.

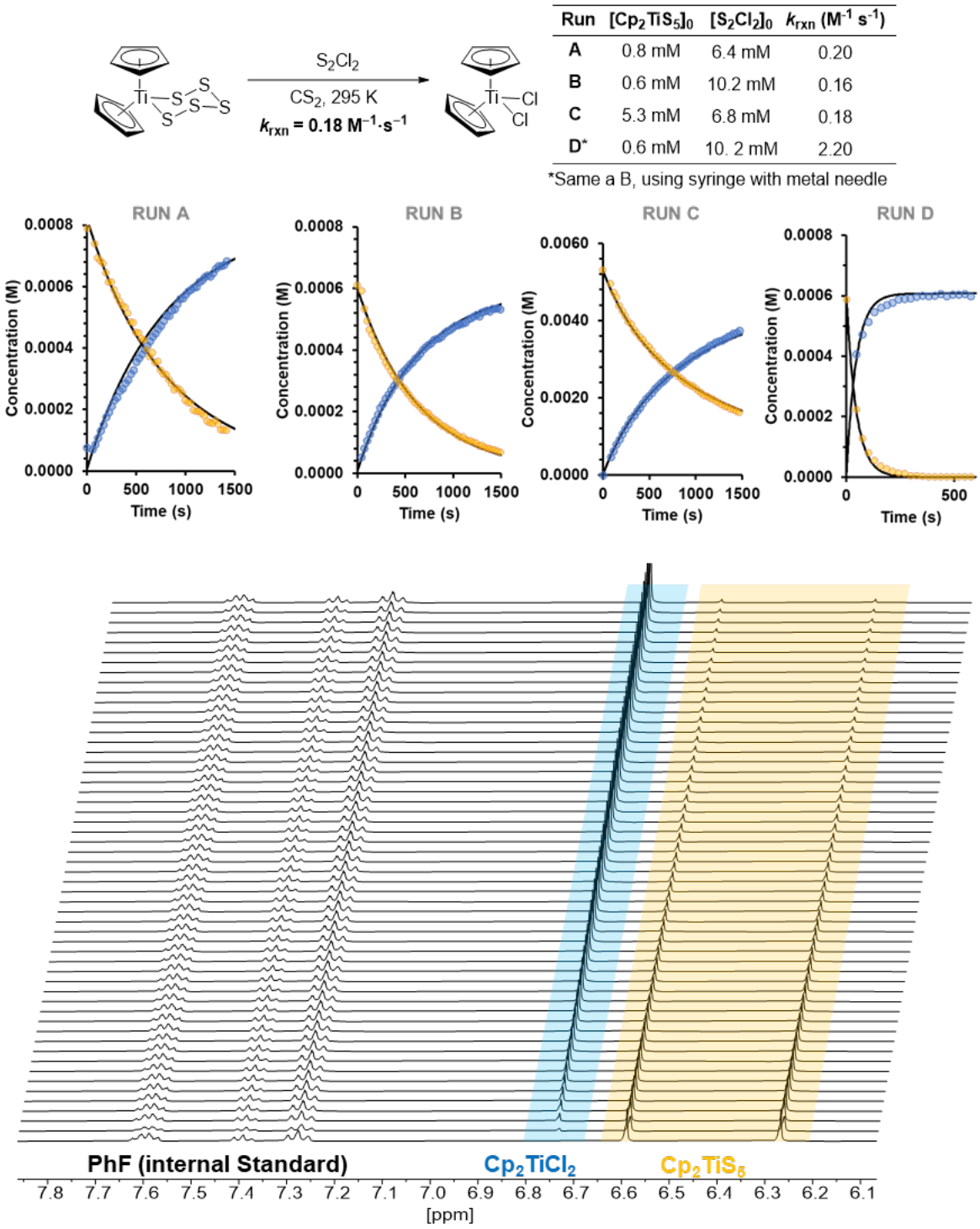

Run	$[Cp_2TiS_5]_0$	$[S_2Cl_2]_0$	k_{rxn} (M^{-1} s^{-1})
A	0.8 mM	6.4 mM	0.20
B	0.6 mM	10.2 mM	0.16
C	5.3 mM	6.8 mM	0.18
D*	0.6 mM	10. 2 mM	2.20

*Same a B, using syringe with metal needle

Figure S56. ^{1}H NMR reaction monitoring of the reaction of Cp_2TiS_5 with S_2Cl_2 in CS_2 at 300K: initial reaction conditions, temporal concentration profiles of titanocene derivatives and zoomed-in representative stack of temporal NMR spectra (run B).

5.2 Reaction of Cp_2TiS_5 with S_2Cl_2 in CCl_4

Same procedure than section S5.1 was followed using CCl_4 as solvent. Stack of NMR spectra and concentration-time plots including both experimental and fitted data are shown below in Figure S57. Rate constant data is consistent with that obtained via stopped-flow UV experiments.

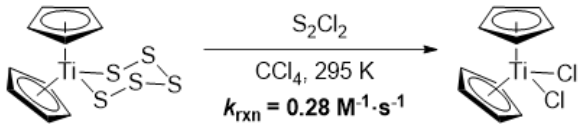

Run	$[Cp_2TiS_5]_0$	$[S_2Cl_2]_0$	k_{rxn} (M^{-1} s^{-1})
A	1.8 mM	35.0 mM	0.26
B	1.8 mM	17.3 mM	0.28
C	0.9 mM	17.3 mM	0.28

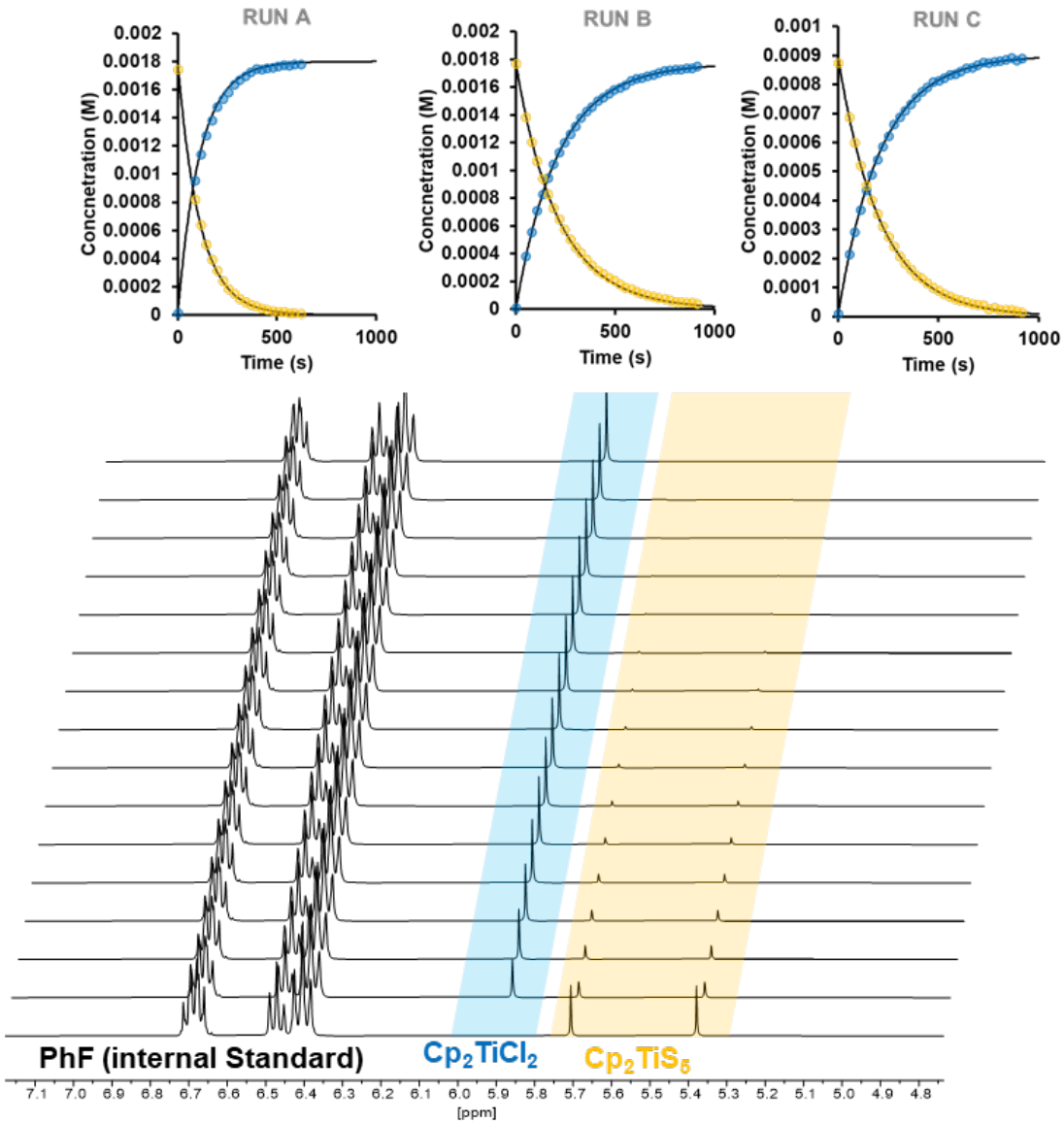

Figure S57. ^{1}H NMR reaction monitoring of the reaction of Cp_2TiS_5 with S_2Cl_2 in CCl_4 (300 K): initial reaction conditions, temporal concentration profiles of titanocene derivatives and zoomed-in selected stack of temporal NMR spectra (run B).

6. Summary of empirical rate constants k_1 and k_2

Table S1. Summary of experimental process rate constants for the reaction of titanocene (poly)sulfides with sulfur(II) electrophiles in DCM at 22 °C.

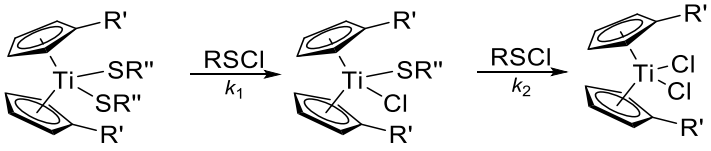

Entry	Titanocene	RSCl[a]	k_1 ($M^{-1}s^{-1}$)	k_2 ($M^{-1}s^{-1}$)
1	Cp_2TiS_5	S_2Cl_2	$3.2\cdot10^2$	-[b]
2	$^{Et}Cp_2TiS_5$	S_2Cl_2	$2.4\cdot10^2$	-[b]
3	$^{n\text{-}Pr}Cp_2TiS_5$	S_2Cl_2	$2.4\cdot10^2$	-[b]
4	$^{n\text{-}Bu}Cp_2TiS_5$	S_2Cl_2	$2.0\cdot10^2$	-[b]
5	$^{i\text{-}Pr}Cp_2TiS_5$	S_2Cl_2	$9.0\cdot10^1$	-[b]
6	$Cp_2TiS_4(CMe_2)$	S_2Cl_2	$3.4\cdot10^4$	-[b]
7[c]	$Cp_2Ti(4\text{-}MeO\text{-}C_6H_4S)_2$	S_2Cl_2	-[b]	$5.5\cdot10^5$
8[c]	$Cp_2Ti(SPh)_2$	S_2Cl_2	-[b]	$1.2\cdot10^5$
9[c]	$Cp_2Ti(4\text{-}F\text{-}C_6H_4S)_2$	S_2Cl_2	-[b]	$6.9\cdot10^4$
10[c]	$Cp_2Ti(4\text{-}Cl\text{-}C_6H_4S)_2$	S_2Cl_2	-[b]	$4.3\cdot10^4$
11	Cp_2TiS_5	MorphNSCl	$4.8\cdot10^1$	$6.8\cdot10^1$
12	Cp_2TiS_5	PhthNSCl	$1.7\cdot10^3$	$6.9\cdot10^3$
13	Cp_2TiS_5	AcSSCl	$4.4\cdot10^3$	$9.8\cdot10^3$
14	Cp_2TiS_5	$4\text{-}MeO\text{-}C_6H_4SCl$	$4.4\cdot10^4$	$5.7\cdot10^4$
15	Cp_2TiS_5	PhSCl	$4.2\cdot10^4$	$5.0\cdot10^4$
16	Cp_2TiS_5	$4\text{-}F\text{-}C_6H_4SCl$	$4.9\cdot10^4$	$5.0\cdot10^4$
17	Cp_2TiS_5	$4\text{-}Cl\text{-}C_6H_4SCl$	$4.1\cdot10^4$	$4.6\cdot10^4$
18	Cp_2TiS_5	$4\text{-}Br\text{-}C_6H_4SCl$	$4.5\cdot10^4$	$4.3\cdot10^4$
19	Cp_2TiS_5	$4\text{-}NO_2\text{-}C_6H_4SCl$	$1.9\cdot10^4$	$6.8\cdot10^3$
20	$Cp_2Ti(4\text{-}MeO\text{-}C_6H_4S)_2$	MorphNSCl	$2.8\cdot10^4$	$1.2\cdot10^4$
21	$Cp_2Ti(SPh)_2$	MorphNSCl	$1.3\cdot10^4$	$6.5\cdot10^3$
22	$Cp_2Ti(4\text{-}F\text{-}C_6H_4S)_2$	MorphNSCl	$5.4\cdot10^3$	$3.2\cdot10^3$
23	$Cp_2Ti(4\text{-}Cl\text{-}C_6H_4S)_2$	MorphNSCl	$2.9\cdot10^3$	$2.1\cdot10^3$

[a] MorphN = *N*-morpholino; PhthN = *N*-phthalimido; Ac = acetyl
[b] Too fast to measure (process/intermediate not detected)
[c] Bimolecular constants are the result of simultaneous processes with other RSCl.

7. Relative reactivity of Cp_2TiS_5 and $Cp_2TiS_4CMe_2$ towards S_2Cl_2

The results from this section demonstrate that, as expected, manual titrations to establish relative rates provide erroneous results for very rapid processes due to inefficient mixing. This aspect is illustrated by the competition of Cp_2TiS_5 and $Cp_2TiS_4(CMe_2)$ for S_2Cl_2 in DCM.

A) Manual titration by ^{1}H NMR. A borosilicate glass 5 mm O.D. NMR tube was loaded with 0.5 mL of a DCM solution of Cp_2TiS_5 and $Cp_2TiS_4(CMe_2)$ in a 1:1 molar ratio. An initial ^{1}H NMR (zg30, NS = 1; AQ = 4s; without deuterium lock) was recorded before titration at 300K. Then a substoichoimetric amount of S_2Cl_2 (dissolved in DCM) was manually added via syringe, shaken thoroughly and another ^{1}H NMR recorded after shimming at 300K. The latter procedure was repeated until ca. 90% total titanacycle conversion. Data of molar fraction of each titanacycle was plotted against total conversion, and modelled to a first order parallel competition model to extract the relative rate constant value, k_{rel} (Figure S58A). The analysis incorrectly suggests that both substrates are consumed at comparable rates, with $Cp_2TiS_4CMe_2$ being slightly more reactive (the value for k_{rel} = 3.0 is incorrect, see section B).

B) Stopped-Flow reaction by UV. A stopped-flow UV reaction was set up by mixing a stock solution containing a mixture of Cp_2TiS_5 and $Cp_2TiS_4CMe_2$ in various molar ratios in DCM with a stock solution of S_2Cl_2 (1.88 mM) in DCM. Monitoring of absorbance at 495 nm was modelled to a competitive absorbance decay to extract the relative rate constant value. The procedure yields a relative rate constant value of k_{rel} = 110 (Figure S58B), that is consistent with absolute values in independent experiments (Table S1, entries 1 and 6, k_{rel} = 110,)

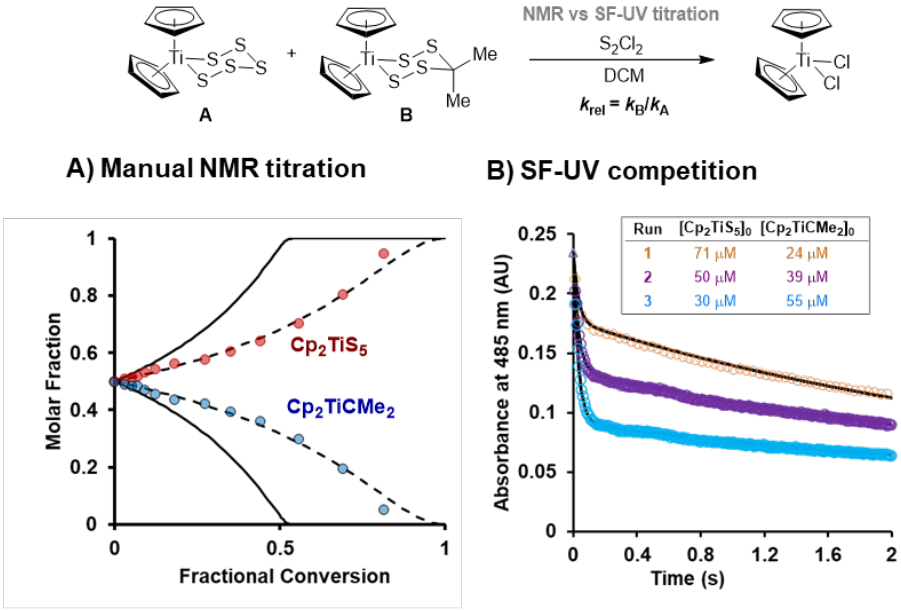

Figure S58. Comparison of relative rate constant data obtained by competition of Cp_2TiS_5 and $Cp_2TiS_4(CMe_2)$ against S_2Cl_2. A) Via manual ^{1}H-NMR titration. B) Via SF-UV reaction. Circles represent experimental data. Modelled data is represented in black lines (bold: k_{rel} = 110; dashed: k_{rel} = 3.0).

8. Stability tests with titanocene (poly)sulfides

A) Test 1: Visual inspection. Two vials were loaded with 5 mL of a solution of monothiophenolate $Cp_2Ti(SPh)Cl$ (0.2 mM in DCM). One of these vials was wrapped in alumunium foil (vial 1, Figure S59). Both vials were left to stand on a bench under standard laboratory light conditions (light distance ca 1.5 m from vial). Visible discolouration of the vial exposed to light (vial 2, Figure S59): after one hour the initial intense red colour faded, which then led to a yellowish solution after an additional hour (Figure S59).

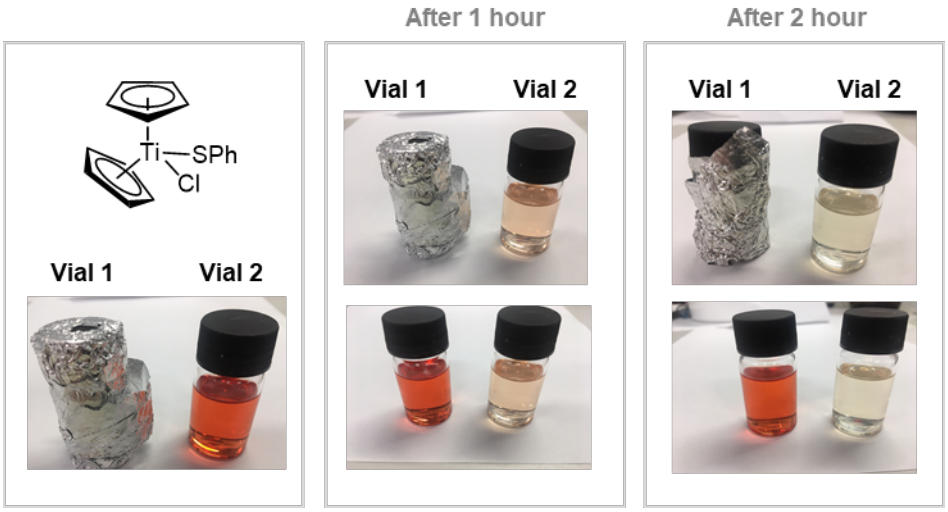

Figure S59. Qualitative test on stability of $Cp_2Ti(SPh)Cl$ to light in DCM solution.

B) Test 2: NMR quantification. A 'solvent' stock solution was prepared by dissolving 20 μL of 1-fluoronaphthalene (internal standard) in 10 mL of DCM. Three vials were charged with solid samples of a mixture 1:1 of Cp_2TiS_5: $Cp_2TiS_4(CMe_2)$ (sample A), $Cp_2Ti(SPh)_2$ (sample B) and $Cp_2Ti(SPh)Cl$ (sample C) under air. 'Solvent' stock (1.5 mL) was added to each vial to dissolve the titanocene complexes, and a ^1H NMR spectrum recorded (t = 0 seconds NMR, before exposure to light). Two NMR samples were prepared from each vial using 0.6 mL of titanocene solution per NMR sample (total NMR samples = 6). From each pair of samples, one NMR tube was wrapped in aluminium foil and the other was not. The pair of NMR samples were laid horizontally on a bench under laboratory light conditions (light distance ca. 1.5 m from NMR tubes). Each sample was measured at different time points, with results of analysis shown in Figure S60. The results showed that titanacycles Cp_2TiS_5 and $Cp_2TiS_4(CMe_2)$ are stable to light exposure (Figure S60, Sample A), while thiophenolate complexes are not (Figure S60, Samples B and C). Further control experiments showed that the content of samples kept in the dark was unchanged after 24h, thus indicating their instability be the result of light-induced degradation. Degraded samples by light of either titanocene thiophenolate complexes were stored in a drawer and re-analyzed after 24h. ^1H NMR spectra of these samples showed no change in concentration, thus eliminating the possibility of a light initiated chain decomposition processes.

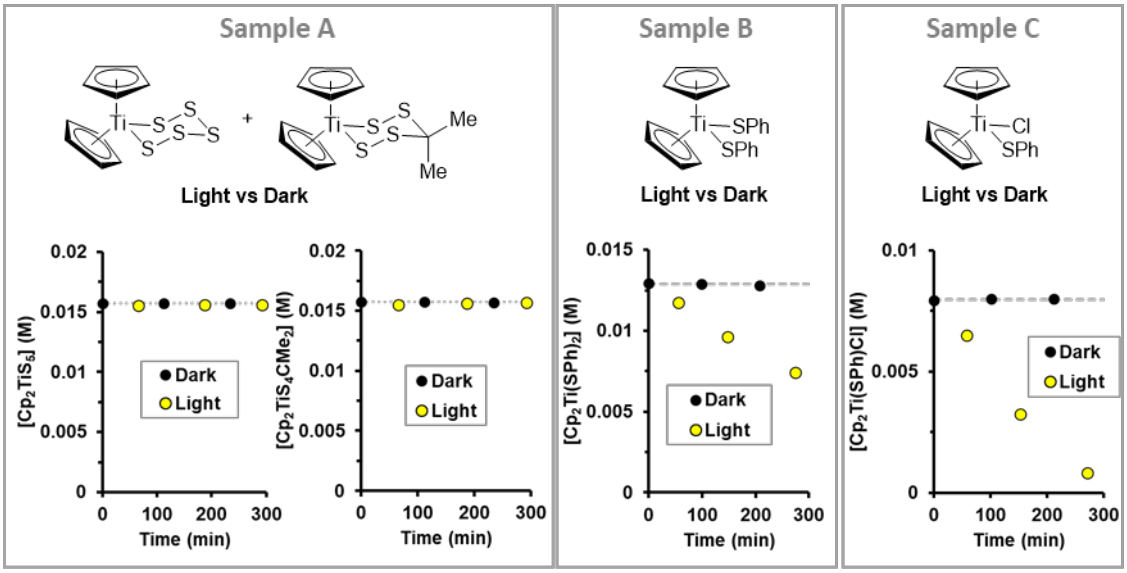

Figure S60. Stability tests of samples of titanocene complexes dissolved in DCM to laboratory light in NMR tubes containing 1-fluoronaphthalene as an internal standard.

C) Test 3: Thermal stability of solid samples. A solid sample (ca. 10 mg) of powdered $Cp_2Ti(SPh)_2$ was taken out of the glovebox and stored in a 7 mL vial under air in a drawer in the dark. NMR analysis of the sample after three weeks showed no decomposition. Same test using a sample of $Cp_2TiCl(SPh)$ showed no change after two weeks.

9. Rate law equation derivation for other scenarios

9.1 Predissociation of Ti-S bond

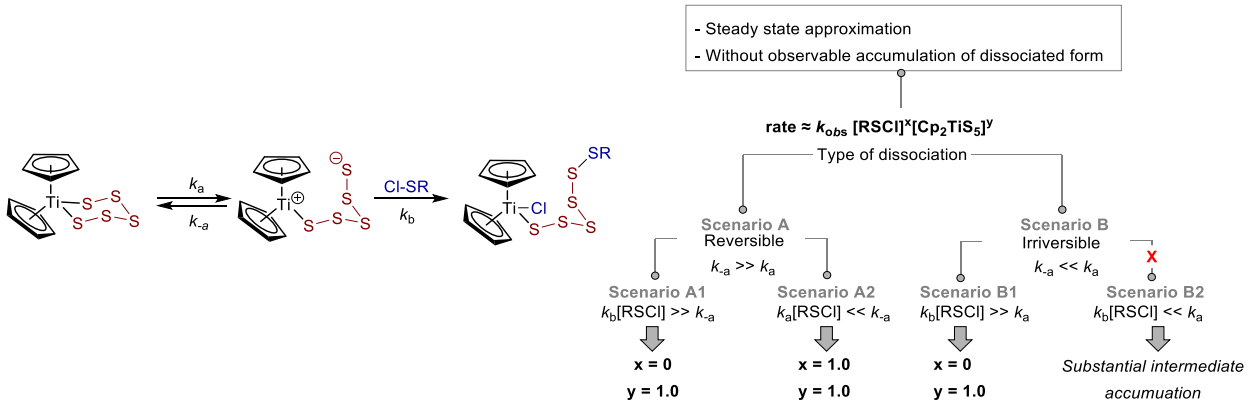

Figure S61. Titanacycle opening via Ti-S bond dissociation: reaction scheme and possible rate law scenarios consistent with negligible accumulation of intermediate/s.

At steady state, the concentration of open form can be expressed as a function of non-dissociated complex eq S11. Considering the rate of product formation is proportional to the electrophile and the concentration of the intermediate (eq. S12), the process rate can then be expressed as a function of the observed closed titanacycle (eq S12, right).

$$[Int] \approx \frac{k_a[Cp_2TiS_5]}{k_b[RSCl] + k_{-a}} \qquad \textbf{(eq S11)}$$

$$rate = k_b[RSCl][Int] \approx \frac{k_a k_b[Cp_2TiS_5][RSCl]}{k_b[RSCl] + k_{-a}} \qquad \textbf{(eq S12)}$$

Several scenarios can be attained depending on parametric conditions:

- **Scenario A1**: Reversible opening & rapid nucleophilic substitution (k_b >> k_{-a} >> k_a)

$$k_b[RSCl] + k_{-a} \approx k_b[RSCl]; and\ rate \approx k_a[Cp_2TiS_5] \qquad \textbf{(eq S13)}$$

- **Scenario A2**: Reversible opening (k_{-a} >> k_a) & slow nucleophilic substitution

$$k_b[RSCl] + k_{-a} \approx k_{-a}; and\ rate \approx \frac{k_b k_a[Cp_2TiS_5][RSCl]}{k_{-a}} \qquad \textbf{(eq S14)}$$

- **Scenario B1**: Phenomenologically slow irreversible ring opening (k_b >> k_a, k_{-a}; k_{-a} ≈ 0)

$$k_b[RSCl] + k_{-a} \approx k_b[RSCl]; and\ rate \approx k_a[Cp_2TiS_5] \qquad \textbf{(eq S15)}$$

If the observed titanocene signal was time averaged, considering the mass balance (eq S16) a kinetically equivalent rate law expression to S12 can be obtained as a function of total titanocene pentasulfide concentration [Ti] (eq S17).

$$[Ti] = [Cp_2TiS_5] + [Int] = [Cp_2TiS_5]\left(1 + \frac{k_a}{k_b[RSCl] + k_{-a}}\right) \qquad \textbf{(eq S16)}$$

$$[Cp_2TiS_5] \approx \frac{(k_b[RSCl] + k_{-a})[Ti]}{k_b[RSCl] + k_{-a} + k_a}; then\ rate \approx \frac{k_b k_a[Ti][RSCl]}{k_b[RSCl] + k_{-a} + k_a} \qquad \textbf{(eq S17)}$$

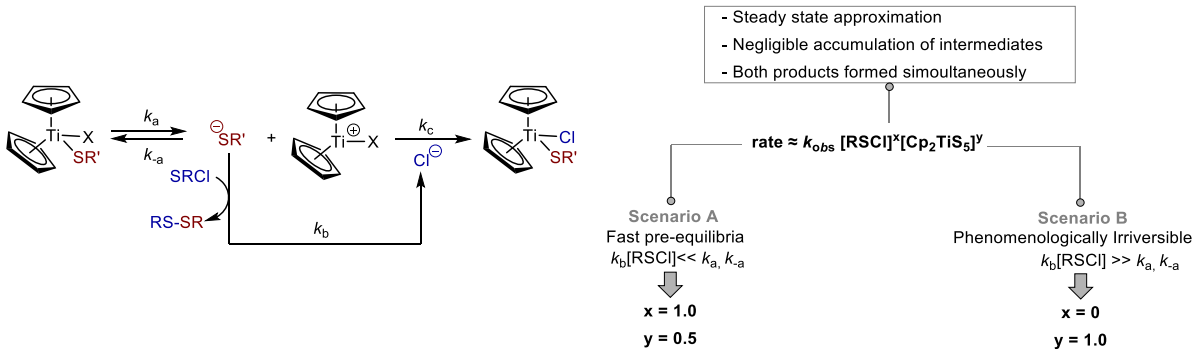

Figure S62. Thiolate pre-dissociation: reaction scheme and possible rate law scenarios consistent with negligible accumulation of intermediate/s.

The reaction orders can differ when using non-cyclic derivatives (i.e. titanocene thiolates). Considering negligible accumulation of intermediates and that both products form simultaneously, the process rate can then be expressed as shown in eq S18. Considering a fast and reversible Ti-S dissociation pre-equilibria (k_a, k_{-a} >> k_b; scenario A) the concentration of thiolate intermediate can be expressed as a function of the dissociation constant and initial titanocene sulfide (eq S19). This leads to a rate equation with fractional order in titanocene pentasulfide (eq S20). On the other hand, if nucleophilic substitution becomes the dominant process (k_a, k_{-a} << k_b), or the dissociation is slow and irreversible, the rate law can be approximated to that of the first process using steady state approximation (eq S21).

$$rate = k_c[Cl^-][Cp_2Ti^+] = k_b[RS'^-][RSCl] \quad \textbf{(eq S18)}$$

- **Scenario A**: fast dissociation pre-equilibria

$$K_d = \frac{[RS'^-][Cp_2Ti^+]}{[Cp_2Ti(X)SR']} = \frac{[RS'^-]^2}{[Cp_2Ti(X)SR']}; then\ [RS'^-] \approx K_d{}^{0.5}[Cp_2Ti(X)SR']^{0.5} \quad \textbf{(eq S19)}$$

$$rate \approx k_b K_d{}^{0.5}[Cp_2Ti(X)SR']^{0.5}[RSCl] \quad \textbf{(eq S20)}$$

- **Scenario B:** fast nucleophilic substitution and/or slow irreversible dissociation

$$[RS'^-] \approx \frac{k_a[Cp_2Ti(X)SR']}{k_b[RSCl]}; then\ rate \approx k_a[Cp_2Ti(X)SR'] \quad \textbf{(eq S21)}$$

While the scenarios represent heterolytic bond dissociation, any of the scenarios above are also applicable to homolytic bond dissociations. These derivations show the impact of the titanocene complex structure (cyclic vs non-cyclic) on the reaction kinetics. The overall bimolecular kinetics, arising from a first-order dependency on titanocene, and a first-order dependency on RSCl, is consistent across of all titanocene derivatives studied in this work, and eliminates scenarios involving thiolate pre-dissociation or ring opening.

9.2 Radical chain reaction

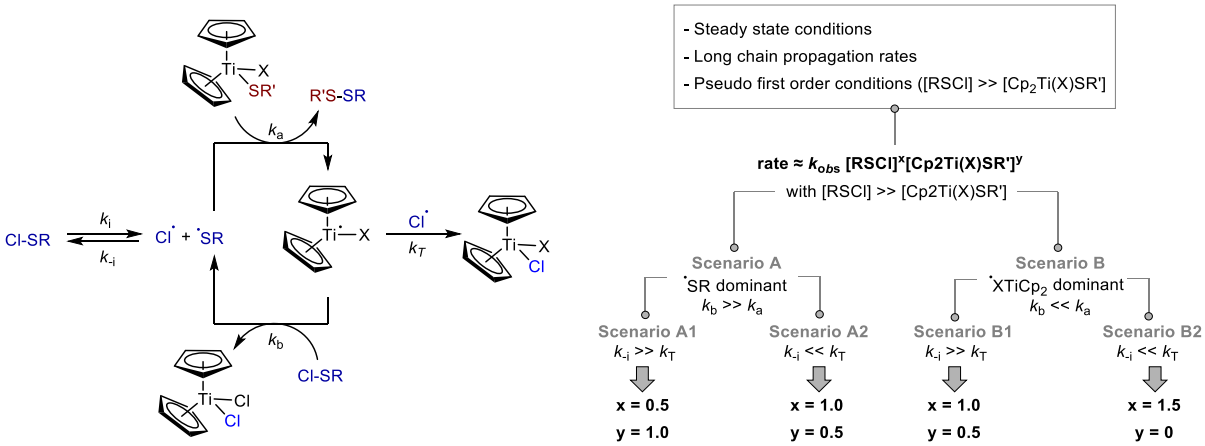

Figure S63. Radical chain mechanism: reaction scheme and possible rate law scenarios with long chain propagation rates.

Considering a process with long chain propagation under steady state conditions, the rates of chain propagation can be approximated as equal (eq S22), which allow estimation of the titanocene chain carrier steady-state concentration (eq S23). Termination and initiation can also be approximated equal, and expressed in terms of chlorine, thiyl radicals as well as both reactants (eq S24). Considering the radical balance (eq S25, left), chlorine concentration can also be expressed as a function of thiyl radical and both reactants (eq S25, right). Combining eq S25 with eq S24 provides equation S26, which provides the steady state concentration of thiyl radicals as a function of the reactants concentration and all individual rate constants associated with each elementary step (eq S26, right)

$$k_b[RSCl][Cp_2Ti(X)^{\cdot}] \approx k_a[Cp_2Ti(X)SR'][RS^{\cdot}] \quad \textbf{(eq S22)}$$

$$[Cp_2Ti(X)^{\cdot}] \approx \frac{k_a[Cp_2Ti(X)SR']}{k_b[RSCl]}[RS^{\cdot}] = \alpha[RS^{\cdot}] \quad \textbf{(eq S23)}$$

$$k_i[RSCl] \approx [Cl^{\cdot}](k_{-i}[RS^{\cdot}] + k_T[Cp_2Ti(X)^{\cdot}]) = [Cl^{\cdot}][RS^{\cdot}](k_{-i} + k_T\alpha) \quad \textbf{(eq S24)}$$

$$[Cl^{\cdot}] \approx ([RS^{\cdot}] + [Cp_2Ti(X)^{\cdot}]) = [RS^{\cdot}](1 + \alpha) \quad \textbf{(eq S25)}$$

$$k_i[RSCl] \approx [RS^{\cdot}]^2(1 + \alpha)(k_{-i} + k_T\alpha); then\ [RS^{\cdot}] \approx \frac{{k_i}^{0.5}[RSCl]^{0.5}}{\sqrt{(1+\alpha)(k_{-i} + k_T\alpha)}} \quad \textbf{(eq S26)}$$

The rate of propagation can thus be expressed as follows (eq S27):

$$rate \approx k_a[Cp_2Ti(X)SR'][RS^{\cdot}] = \frac{{k_i}^{0.5}k_a[RSCl]^{0.5}[Cp_2Ti(X)SR']}{\sqrt{(1+\alpha)(k_{-i} + k_T\alpha)}};\ \alpha \approx \frac{k_a[Cp_2Ti(X)SR']}{k_b[RSCl]} \quad \textbf{(eq S27)}$$

Under excess of electrophile ([RSCl] > [$Cp_2Ti(X)SR'$]), several scenarios can be attained depending on the dominant chain carrier and predominant termination event:

- **Scenario A1**: [RS·] dominant (k_b >> k_a) & recombination dominant (k_{-i} >> k_T)

$$\alpha = \frac{k_a[Cp_2Ti(X)SR']}{k_b[RSCl]} \ll 1, and \sqrt{(1+\alpha)(k_{-i}+k_T\alpha)} \approx \sqrt{k_{-i}} \quad \textbf{(eq S28)}$$

$$rate \approx \frac{{k_i}^{0.5}k_a[RSCl]^{0.5}[Cp_2Ti(X)SR']}{{k_{-i}}^{0.5}} = {K_i}^{0.5}k_a[RSCl]^{0.5}[Cp_2Ti(X)SR'] \quad \textbf{(eq S29)}$$

- **Scenario A2**: [RS·] dominant (k_b >> k_a) & Ti(III) quenching dominant (k_{-i} << k_T)

$$\alpha = \frac{k_a[Cp_2Ti(X)SR']}{k_b[RSCl]} \ll 1, and \sqrt{(1+\alpha)(k_{-i}+k_T\alpha)} \approx \sqrt{\alpha k_T} \quad \textbf{(eq S30)}$$

$$rate \approx \frac{{k_i}^{0.5}k_a[RSCl]^{0.5}[Cp_2Ti(X)SR']}{\frac{{k_T}^{0.5}{k_a}^{0.5}[Cp_2Ti(X)SR']^{0.5}}{{k_b}^{0.5}[RSCl]^{0.5}}} = \left(\frac{k_ik_ak_b}{k_T}\right)^{0.5}[RSCl][Cp_2Ti(X)SR']^{0.5} \quad \textbf{(eq S31)}$$

- **Scenario B1**: [$Cp_2Ti(X)$·] dominant (k_b << k_a) & recombination dominant (k_{-i} >> k_T)

$$\alpha = \frac{k_a[Cp_2Ti(X)SR']}{k_b[RSCl]} \gg 1, and \sqrt{(1+\alpha)(k_{-i}+k_T\alpha)} \approx \sqrt{\alpha k_{-i}} \quad \textbf{(eq S32)}$$

$$rate \approx \frac{{k_i}^{0.5}k_1[RSCl]^{0.5}[Cp_2Ti(X)SR']}{\frac{{k_{-i}}^{0.5}{k_1}^{0.5}[Cp_2Ti(X)SR']^{0.5}}{{k_2}^{0.5}[RSCl]^{0.5}}} = {K_1}^{0.5}{k_1}^{0.5}{k_2}^{0.5}[RSCl][Cp_2Ti(X)SR']^{0.5} \quad \textbf{(eq S33)}$$

- **Scenario B2**: [$Cp_2Ti(X)$·] dominant (k_b << k_a); Ti(III) quenching dominant (k_{-i} << k_T)

$$\alpha = \frac{k_a[Cp_2Ti(X)SR']}{k_b[RSCl]} \gg 1, and \sqrt{(1+\alpha)(k_{-i}+k_T\alpha)} \approx \sqrt{\alpha^2 k_T} \quad \textbf{(eq S34)}$$

$$rate \approx \frac{{k_i}^{0.5}k_a[RSCl]^{0.5}[Cp_2Ti(X)SR']}{\frac{{k_T}^{0.5}k_a[Cp_2Ti(X)SR']}{k_b[RSCl]}} = \frac{{k_i}^{0.5}}{{k_T}^{0.5}}k_b[RSCl]^{1.5} \quad \textbf{(eq S35)}$$

The overall bimolecular kinetics, arising from a first-order dependency on titanocene, and a firstorder dependency on RSCl, is consistent across of all titanocene derivatives studied in this work, and eliminates scenarios involving (long chain) radical processes.

10. Synthesis and spectroscopic data

10.1 Synthetic procedures and characterization data

A) Titanocene Pentasulfide (Cp_2TiS_5)

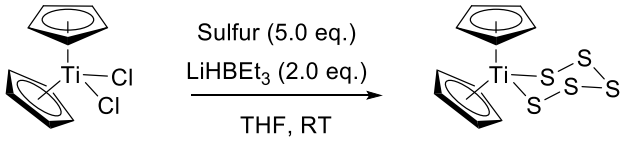

An oven-dried 250 mL three-necked round bottom flask was loaded with a magnetic stirrer and elemental sulfur (481.1 mg, 15 mmol of monoatomic sulfur). The atmosphere in the flask was exchanged with N_2 using three vacuum-N_2 cycles with a Schlenk line. Then 6 mL of a $LiHBEt_3$ solution (1.0 M in THF, 6 mmol, 635.7 mg) was added dropwise with a syringe to the solid sulfur under stirring (**caution!** H_2 gas generation), and the effervescent mixture stirred for 20 minutes at room temperature. A THF solution of Cp_2TiCl_2 (750 mg, 3 mmol, dissolved in 75 mL of dry and degassed THF) was added dropwise over 20 minutes. The resulting mixture was stirred for 14 h at room temperature. THF was removed under reduced pressure and 100 mL of DCM added to the resulting crude. The mixture was filtered in air through a celite plug and the filtrate evaporated under reduced pressure in a rotatory evaporator resulting in a deep black-red solid. The solid was subjected to column chromatography on silica gel using hexane/DCM 1:1 v/v as eluent to isolate Cp_2TiS_5 (0.88 g, 2.62 mmol, 87%) in pure form. Characterization data is consistent with that reported in literature.[S8] ^1H NMR (400 MHz, $CDCl_3$) δ 6.07 (s, 5H, CpH), 6.35 (s, 5H, CpH) ppm; $^{13}C\{^1H\}$ NMR (101 MHz, $CDCl_3$) δ 112.17, 113.16 ppm.

B) Titanocene 4-(2-propylidene)tetrasulfide, ($Cp_2TiS_4CMe_2$)

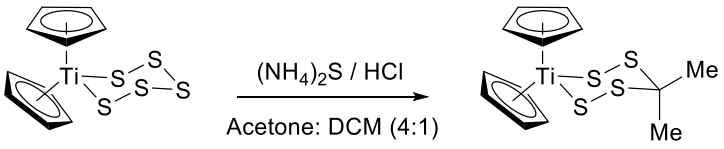

Titanocene pentasulfide Cp_2TiS_5 (1.01 g, 3.0 mmol) was suspended in a solvent mixture of acetone and dichloromethane (v/v = 4/1; 60 mL) under air and stirred for 15 minutes. In parallel, an aqueous 1.0 M HCl solution (6.8 mL, 6.8 mmol) was added dropwise to a stirred aqueous 20%wt $(NH_4)_2S$ solution (4.5 mL, 13.5 mmol) over a 10-minute period. The resulting aqueous sulfide solution was added dropwise to the titanocene pentasulfide suspension over 5 minutes, and the resulting suspension stirred for 35 minutes. Aqueous 1.0 M HCl was added to the suspension (6.0 mL, 6.0 mmol) and the mixture stirred for 30 minutes. Then, another sample of aqueous 1.0 M HCl (6.0 mL, 6.0 mmol) was added followed by a sample of aqueous 20% wt $(NH_4)_2S$ solution (4.0 mL, 3.0 M, 12.0 mmol). The resulting reaction mixture was stirred for 50 minutes before adding deionized water (50 mL) and dichloromethane (50 mL). The mixture was transferred to a separatory funnel, vigorously shaken and the phases separated. The aqueous phase was extracted with

dichloromethane (3 x 50 mL) and the combined of organic phases dried over anhydrous magnesium sulfate, filtered, and concentrated under reduced pressure (rotatory evaporator, 40 °C bath). The resulting crude material was used as a starting material (instead of Cp_2TiS_5) and the same procedure as above was repeated without the use of DCM as co-solvent. The resulting crude material was again subjected to the same recycling procedure. The final crude material resulting after these two recycling steps was subjected to column chromatography (*n*-hexane/MTBE, *v*/*v* = 4/1) and the purple moving band was collected. The red band was determined to be unreacted Cp_2TiS_5 by comparison using TLC with the same eluent system. Evaporation of the purple band provided a purple oil that was triturated with cyclohexane. The solvent was decanted and the solid dried under high vacuum (oil pump, 0.4 Torr, 1h) to deliver $Cp_2TiS_4CMe_2$ (236 mg 0.68 mmol, 23% yield) as a violet free-flowing crystalline solid. Characterization data is consistent with that reported in literature.[S9] ^{1}H NMR (400 MHz, $CDCl_3$) δ 1.01 (s, 3H, CH_3), 1.79 (s, 3H, CH_3), 6.26 (s, 5H, CpH), 6.36 (s, 5H, CpH) ppm; $^{13}C\{^1H\}$ NMR (101 MHz, $CDCl_3$) δ 24.53, 29.98, 55.65, 112.89, 114.13 ppm.

C) Bis(alkylcyclopentadienyl)titanium(IV) pentasulfide ($^{R'}Cp_2TiS_5$)

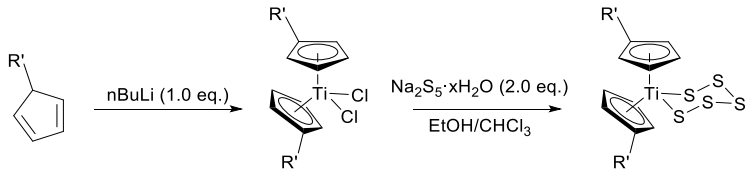

Alkylated $^{R'}Cp_2TiS_5$ derivatives were prepared from substituted cyclopentadienes[S10] using the following general procedure, except for $^{Et}Cp_2TiS_5$, which was prepared from commercially available $^{Et}Cp_2TiCl_2$.

Step 1: n-BuLi (2.5 M in hexane, 10.0 mmol) was added dropwise (addition time: 1h) under positive pressure of N_2 to a solution of alkylated cyclopentadiene, $^{R'}Cp$ (10.0 mmol) in dry degassed THF (100 mL) at -78°C (dry ice/acetone bath). The mixture was warmed up to room temperature and stirred for additional 16 h. The resulting mixture was cooled to -78°C (acetone-dry ice bath) and 5 mL of $TiCl_4$ (1M in THF) was added dropwise over the course of 1 h. The reaction mixture was then warmed up to room temperature and stirred for 3 h. The solvent was removed under reduced pressure and 50 mL of dry $CHCl_3$ added. The resulting red mixture was directly used in step 2 without additional purification or precautions.

Step 2: A mixture of Na_2S xH_2O (10.0 mmol) and sulfur flowers (40.0 mmol) in degassed ethanol (100 mL) was refluxed for 1 h under positive pressure of N_2. After cooling to room temperature, the resulting red-orange sodium polysulfide solution was opened to air and added at once into the chloroform solution of $(RCp)_2TiCl_2$ obtained in step 1. The resulting dark mixture was stirred at room temperature for 1 h and filtered using a glass frit and suction. The filtrate was transferred to a round bottomed flask and the solvent removed under reduced pressured. The crude was extracted with 3x 50 mL DCM. The organic extracts were then combined and transferred to a separatory funnel,

washed with 3x30 mL of dionized water and dried with 1x50 mL brine. The organic layer was dried over $MgSO_4$ and filtered. The solvent was removed under reduced pressure and the resulting crude product subjected to column chromatography on silica gel using hexane/DCM (1/1 v/v) as eluent to give the respective substituted titanocene pentasulfide compound $(RCp)_2TiS_5$ in pure form. Characterization data is shown below:

- **$^{Et}Cp_2TiS_5$** (1.79 g, 4.55 mmol, 91% yield, dark red solid). ^{1}H NMR (600 MHz, $CDCl_3$) δ 1.05 (t, 3H, CH_3, *J* = 7.5 Hz), 1.20 (t, 3H, CH_3, *J* = 7.5 Hz), 2.36 (q, 2H, $CpCH_2$, *J* = 7.5 Hz), 2.63 (q, 2H, $CpCH_2$, *J* = 7.5 Hz), 5.91 (t, 2H, CpH, *J* = 2.6 Hz), 6.14 (t, 2H, CpH, *J* = 2.6 Hz), 6.20 (t, 2H, CpH, *J* = 2.6 Hz) ppm. $^{13}C\{^1H\}$ NMR (151 MHz, $CDCl_3$) δ 14.47, 15.34, 23.73, 23.89, 109.78, 110.80, 114.20, 115.08, 134.18, 134.28 ppm; IR (film) / ν cm^{-1}: 2963, 2926, 2869, 1674, 1491, 1395,1372, 891;HR-MS (ESI+): calcd. for $C_{14}H_{18}S_5TiNa$ $[M+Na]^+$ 416.9389, found: 416.9378.
- **$^{n\text{-}Pr}Cp_2TiS_5$** (0.86 g, 2.03 mmol, 40% yield, dark red solid). ^{1}H NMR (400 MHz, $CDCl_3$) δ 0.89 (t, 3H, CH_3, *J* = 7.4 Hz), 0.95 (t, 3H, CH_3, *J* = 7.4 Hz), 1.45 (m, 2H, CH_2), 1.62 (m, 2H, CH_2), 2.20 – 2.29 (m, 2H, CH_2), 2.49 – 2.57 (m, 2H, CH_2), 5.92 (t, 2H, CpH, *J* = 2.6 Hz), 6.11 (t, 2H, CpH, *J* = 2.6 Hz), 6.13 (t, 2H, CpH, *J* = 2.6 Hz), 6.18 (t, 2H, CpH, *J* = 2.6 Hz) ppm. $^{13}C\{^1H\}$ NMR (101 MHz, $CDCl_3$) δ 13.88, 13.91, 24.49, 24.70, 32.89, 32.98, 110.59, 110.95, 114.20, 115.55, 132.33, 132.57 ppm.
- ; $^{13}C\{^1H\}$ DEPTq NMR (101 MHz, $CDCl_3$) δ 14.02, 14.06, 24.63, 24.86, 33.01, 33.10, 110.67, 111.07, 114.34, 115.68, 132.49, 132.68 ppm; IR (film) / ν cm^{-1} 2955, 2922, 2853, 1658, 1631, 1376, 1260, 822;HR-MS (ESI+): calcd. for $C_{16}H_{22}S_5TiNa$ $[M+Na]^+$ 445.9702, found 445.9710.
- **$^{i\text{-}Pr}Cp_2TiS_5$** (0.96 g, 2.28 mmol, 46% yield, dark red solid). Characterization data is consistent with that reported in literature.[S11] ^{1}H NMR (400 MHz, $CDCl_3$) δ 1.05 (d, 6H, CH_3, *J* = 6.9 Hz), 1.22 (d, 6H, CH_3, *J* = 6.9 Hz), 2.72 (hept, 1H, CpCH, *J* = 6.9 Hz), 3.02 (hept, 1H, CpCH, *J* = 6.9 Hz), 5.87 (t, 2H, CpH, *J* = 2.6 Hz), 6.14 (t, 2H, CpH), 6.19 (t, 2H, CpH, *J* = 2.6 Hz), 6.22 (t, 2H, CpH, *J* = 2.6 Hz) ppm; $^{13}C\{^1H\}$ NMR (101 MHz, $CDCl_3$) δ 23.58, 23.67, 28.83, 29.27, 108.06, 111.05, 113.13, 114.19, 139.76, 140.03 ppm.
- **$^{n\text{-}Bu}Cp_2TiS_5$** (0.79 g, 1.75 mmol, 35% yield, dark red solid). ^{1}H NMR (400 MHz, $CDCl_3$) δ 0.90 (m, 6H, CH_3), 1.22–1.46 (m, 6H, CH_2), 1.50–1.62 (m, CH_2, 2H), 2.19–2.32 (m, 2H, $CpCH_2$), 2.47–2.62 (m, 2H, $CpCH_2$), 5.91 (t, 2H, CpH, *J* = 2.6 Hz), 6.11 (t, 2H, CpH, *J* = 2.6 Hz), 6.13 (t, 2H, CpH, *J* = 2.6 Hz), 6.17 (t, 2H, CpH, *J* = 2.6 Hz) ppm; $^{13}C\{^1H\}$ DEPTq NMR (101 MHz, $CDCl_3$) δ 14.00, 14.02, 22.53, 30.69, 30.72, 33.50, 33.71, 110.56, 111.08, 114.32, 115.60, 132.80, 132.86 ppm; IR (film) / ν cm^{-1}: 2953, 2924, 2857, 1488, 1462, 1376, 1242, 930, 824; HR-MS (ESI+): calcd. for $C_{18}H_{26}S_5TiNa$ $[M+Na]^+$ 473.0010, found 473.0005.

D) Titanocene bis(4-substituted-thiophenolate) derivatives, $Cp_2Ti(4\text{-}G\text{-}C_6H_4S)_2$

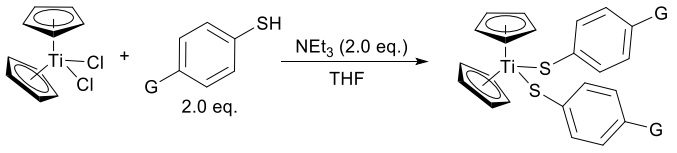

These titanocene derivatives were prepared from commercially available titanocene chloride (Cp_2TiCl_2) and the corresponding 4-substituted thiophenols (ArSH) following a general procedure: Solid Cp_2TiCl_2 (1.0 g, 4.0 mmol) was added to a one-necked round bottom flask containing a magnetic stirring bar and 20 mL of dry and degassed THF. The flask was capped with a septum and flushed with N_2. The resulting dark-red suspension was stirred from 10 minutes at room temperature. Then NEt_3 (1.12 mL, 8.0 mmol) was added and the mixture stirred for 5 minutes at room temperature followed by addition of the corresponding 4-substituted thiophenol (ArSH, 8.0 mmol) at once using a syringe. After addition of the ArSH, the mixture immediately changed to a dark purple colour and was wrapped in aluminium foil to prevent exposure to light. After stirring for 4h at room temperature, the suspension was exposed to air and filtered through a glass frit under suction. The solid was washed with 2x100 mL of Et_2O. The filtrate was evaporated under reduced pressure on a rotavap in the dark. The resulting residue was dry-loaded using Celite® in a glass-column packed with silica gel (21 cm length; 6 cm diameter) to isolate the purple band by flash chromatography. Characterization data is shown below:

- **$Cp_2Ti(4\text{-}MeO\text{-}C_6H_4S)_2$** (1.28 g, 2.82 mmol, 70% yield, purple solid, using DCM as an eluent for chromatography). Characterization data is consistent with that reported in the literature.[S12, S13] ^{1}H NMR (400 MHz, $CDCl_3$) δ 3.84 (s, 6H, OCH_3), 6.03 (s, 10H, CpH), 6.80–6.95 (m, 4H), 7.43–7.54 (m, 4H) ppm; $^{13}C\{^1H\}$ NMR (101 MHz, $CDCl_3$) δ 55.47, 112.71, 113.95, 113.32, 139.68, 157.70 ppm.
- **$Cp_2Ti(SPh)_2$** (1.02 g, 2.59 mmol, 64% yield, purple solid, using DCM as an eluent for chromatography). Characterization data is consistent with that reported in the literature.[S12] ^{1}H NMR (400 MHz, $CDCl_3$) δ 6.03 (s, 10H, CpH), 7.11–7.18 (m, 2H), 7.27–7.34 (m, 4H), 7.53–7.63 (m, 4H) ppm; $^{13}C\{^1H\}$ NMR (101 MHz, $CDCl_3$) δ 112.84, 125.55, 128.35, 132.39, 148.62 ppm.
- **$Cp_2Ti(4\text{-}F\text{-}C_6H_4S)_2$** (1.08 g, 2.51 mmol, 63% yield, purple solid, using DCM as an eluent for chromatography). ^{1}H NMR (400 MHz, $CDCl_3$) δ 6.02 (s, 10H, CpH), 6.93–7.07 (m, 4H), 7.41–7.54 (m, 4H) ppm; $^{13}C\{^1H\}$ NMR (101 MHz, $CDCl_3$) δ 112.87, 115.26, 115.47, 133.63, 133.71, 143.47, 143.50, 159.85, 162.29 ppm; ^{19}F NMR (377 MHz, $CDCl_3$) δ -117.24 (tt, 1F, J = 8.8, 5.5 Hz) ppm; IR (film) / ν cm^{-1}: 2922, 2853, 1482, 1446, 1393, 1154, 1085, 821; HR-MS (ESI+): calcd. for $C_{22}H_{18}F_2S_2TiNa$ $[M+Na]^+$ 455.01897, found 445.0197.
- **$Cp_2Ti(4\text{-}Cl\text{-}C_6H_4S)_2$** (1.33 g, 2.85 mmol, 71% yield, black-violet solid, using toluene as an eluent for chromatography). Characterization data is consistent with that reported in the

literature.[S12, S13] ^{1}H NMR (400 MHz, $CDCl_3$) δ 6.02 (s, 10H, CpH), 7.22–7.28 (m, 4H), 7.42–7.48 (m, 4H) ppm; $^{13}C\{^{1}H\}$ NMR (101 MHz, $CDCl_3$) δ 112.96, 128.48, 131.38, 133.50, 146.99 ppm.

E) Titanocene monothiophenolate chloride, $Cp_2Ti(PhS)Cl$

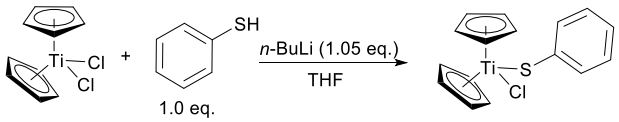

Note: No precautions were taken in this procedure to avoid exposure of the mixtures to light, and we observed decolouration of exposed solutions and fractions.

A two-necked 250 mL round-bottomed flask was charged with a magnetic stirring bar, evacuated and back-filled with N_2. Dry and degassed THF (100 mL) was added followed by thiophenol (1.10 g, 10.0 mmol) using a syringe, and the colorless solution cooled to 0 °C (ice-water bath) under stirring. Then, 4.1 mL of n-BuLi (2.5M in hexanes, 10.5 mmol) were added dropwise for 10 minutes. After addition, the bath was removed and the mixture stirred for 1h allowing to reach room temperature. A mixture titanocene dichloride (2.49 g, 10.0 mmol) in THF (50 mL) was prepared under N_2 in a separate flask containing a stirring bar. Then, the lithium thiophenolate solution was added dropwise at room temperature (addition time: 20 min) under a positive pressure of N_2 and the mixture stirred for 1h. The solvent was then evaporated under reduced pressure on the rotavap. The crude product was then dry loaded using Celite® to a glass column packed with silica gel (21 cm length; 6 cm diameter) and the red band eluted using DCM. Evaporation of the eluent led to $Cp_2Ti(PhS)Cl$ (0.120 g, 3.4 mmol, 3.4% yield) as a red solid. Characterization data is consistent with that reported in literature.[S12] ^{1}H NMR (400 MHz, $CDCl_3$) δ 6.27 (s, 10H, CpH), 7.16–7.24 (m, 1H), 7.31–7.44 (m, 4H), ppm; $^{13}C\{^{1}H\}$ NMR (101 MHz, $CDCl_3$) δ 116.02, 126.31, 128.36, 132.40, 149.15 ppm.

10.2 NMR Spectra

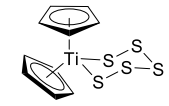

^{1}H NMR

(400 MHz, $CDCl_3$)

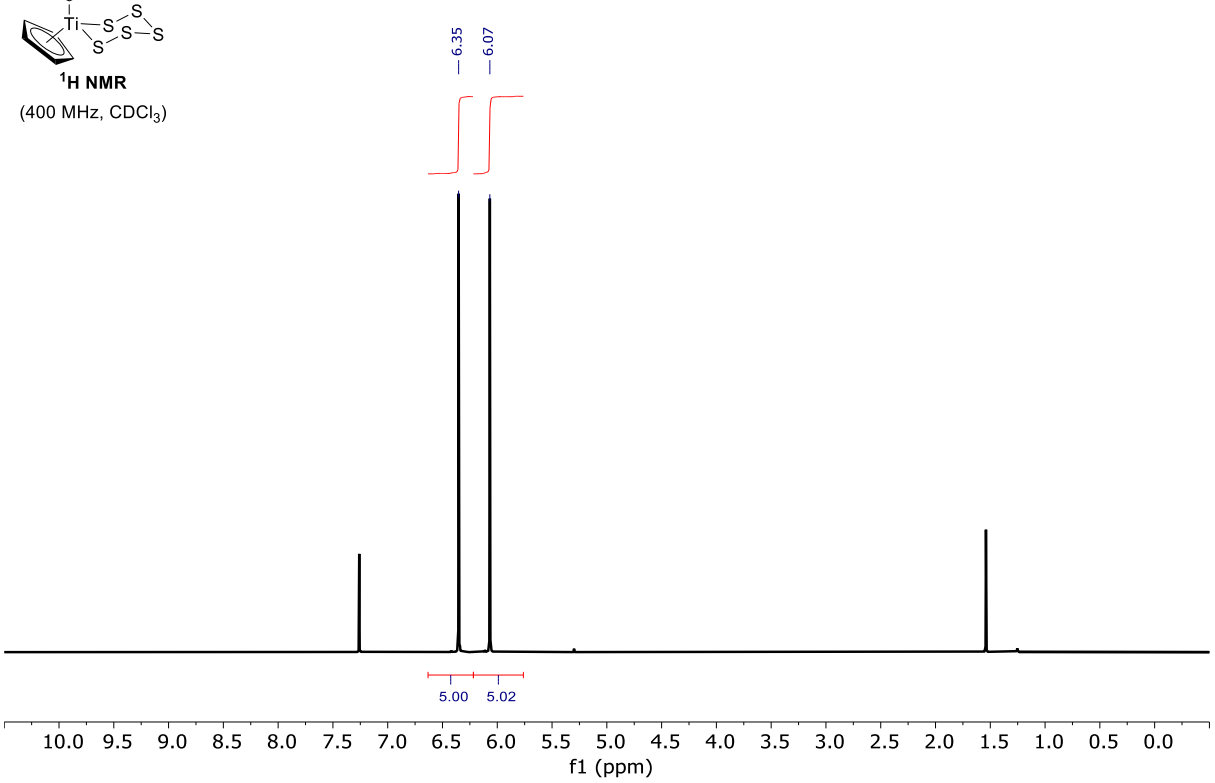

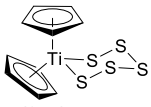

^{13}C{^{1}H} NMR

(101 MHz, $CDCl_3$)

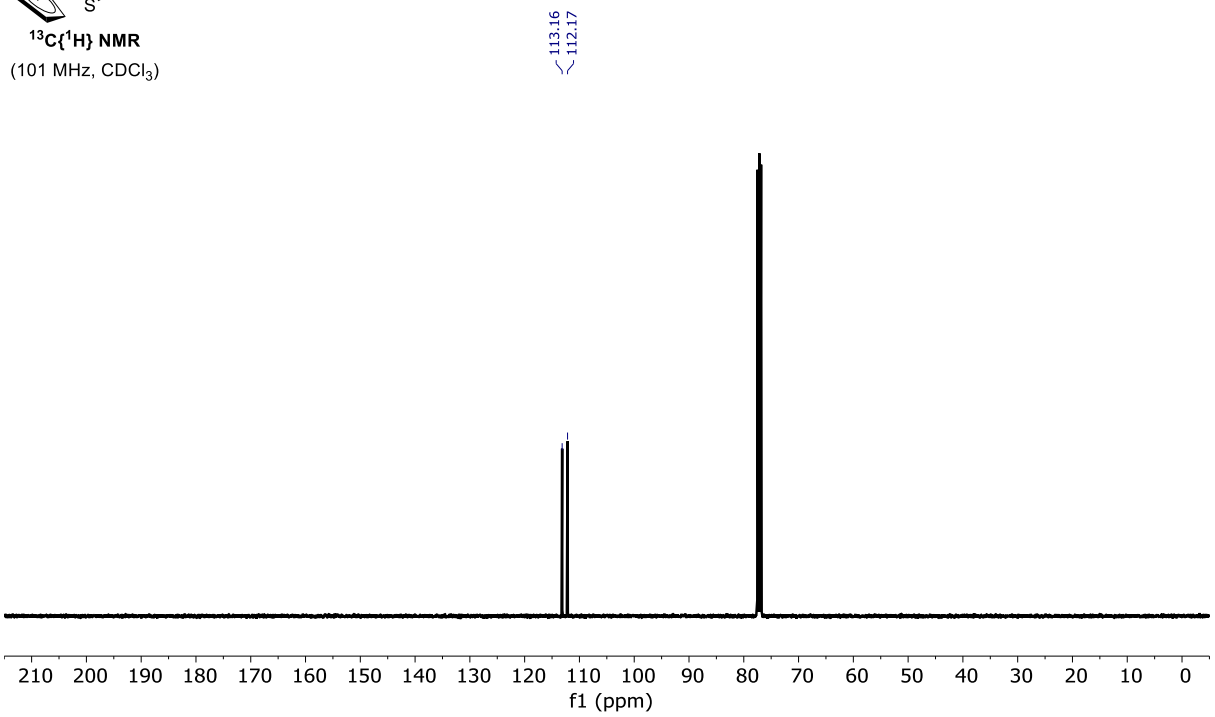

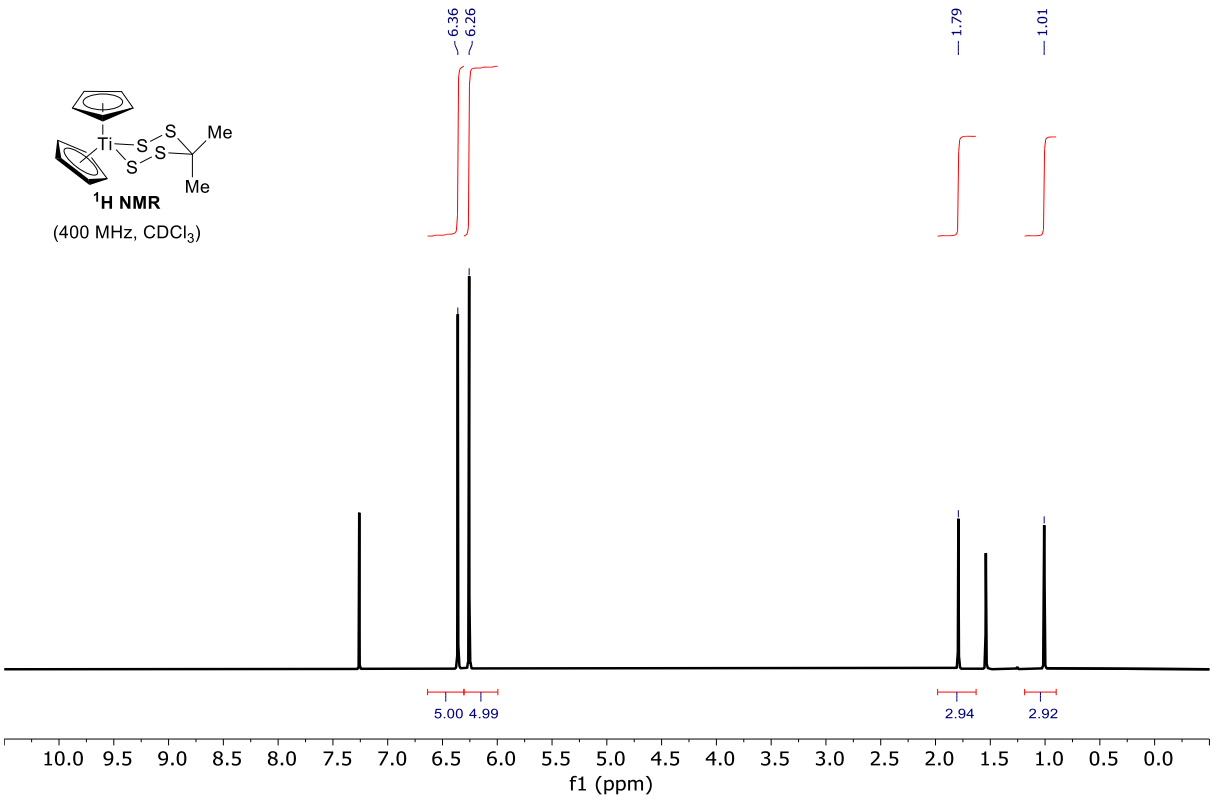

^{1}H NMR

(400 MHz, $CDCl_3$)

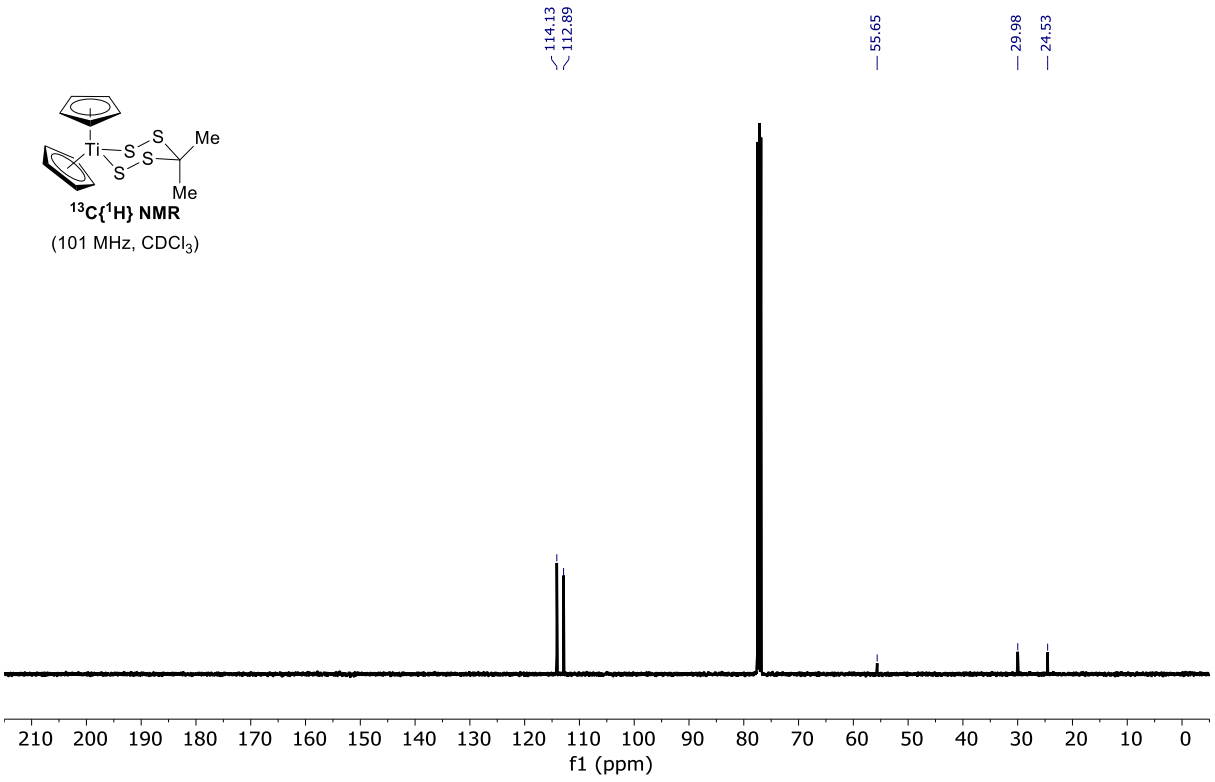

^{13}C{^{1}H} NMR

(101 MHz, $CDCl_3$)

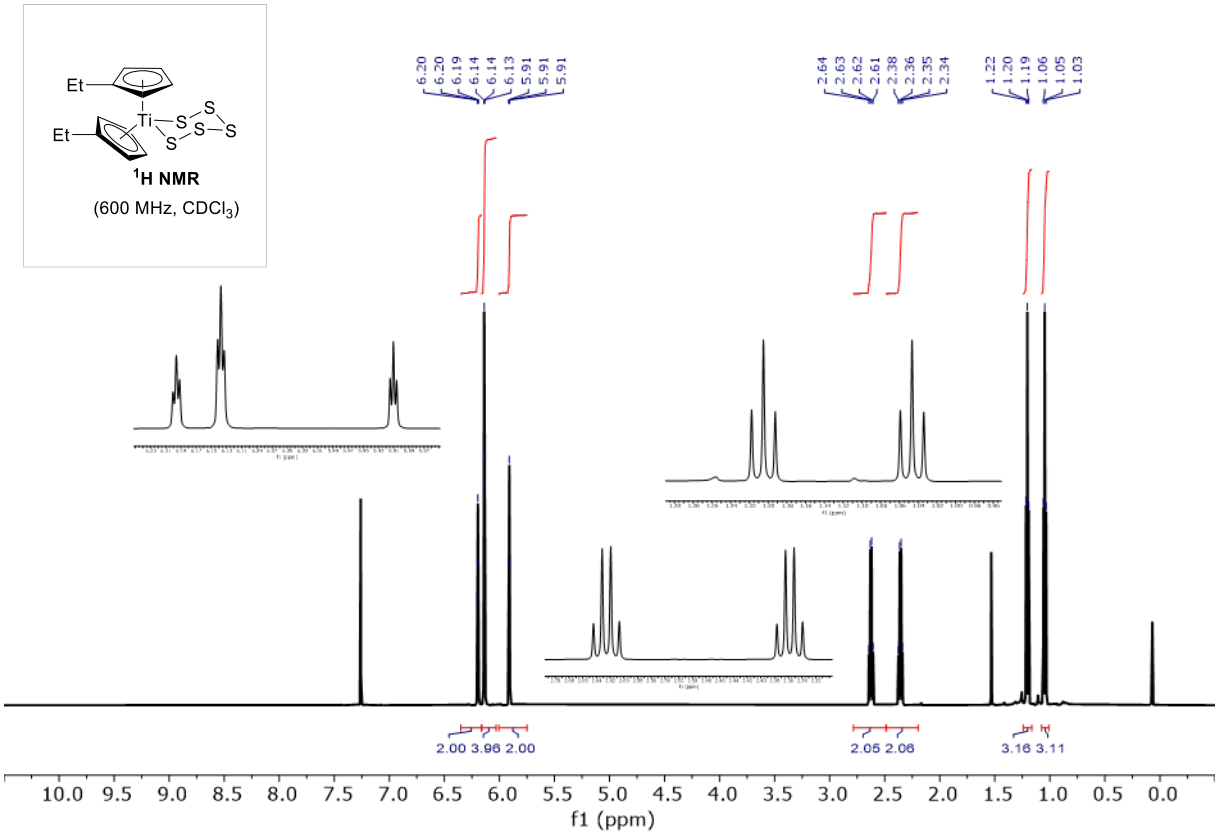
Et
Et
Ti
S
S
S
S
S
^{1}H NMR
(600 MHz, $CDCl_3$)
6.20
6.20
6.19
6.14
6.14
6.13
5.91
5.91
5.91
2.64
2.63
2.62
2.61
2.38
2.36
2.35
2.34
1.22
1.20
1.19
1.06
1.05
1.03
2.00 3.96 2.00
2.05 2.06
3.16 3.11
10.0 9.5 9.0 8.5 8.0 7.5 7.0 6.5 6.0 5.5 5.0 4.5 4.0 3.5 3.0 2.5 2.0 1.5 1.0 0.5 0.0
f1 (ppm)

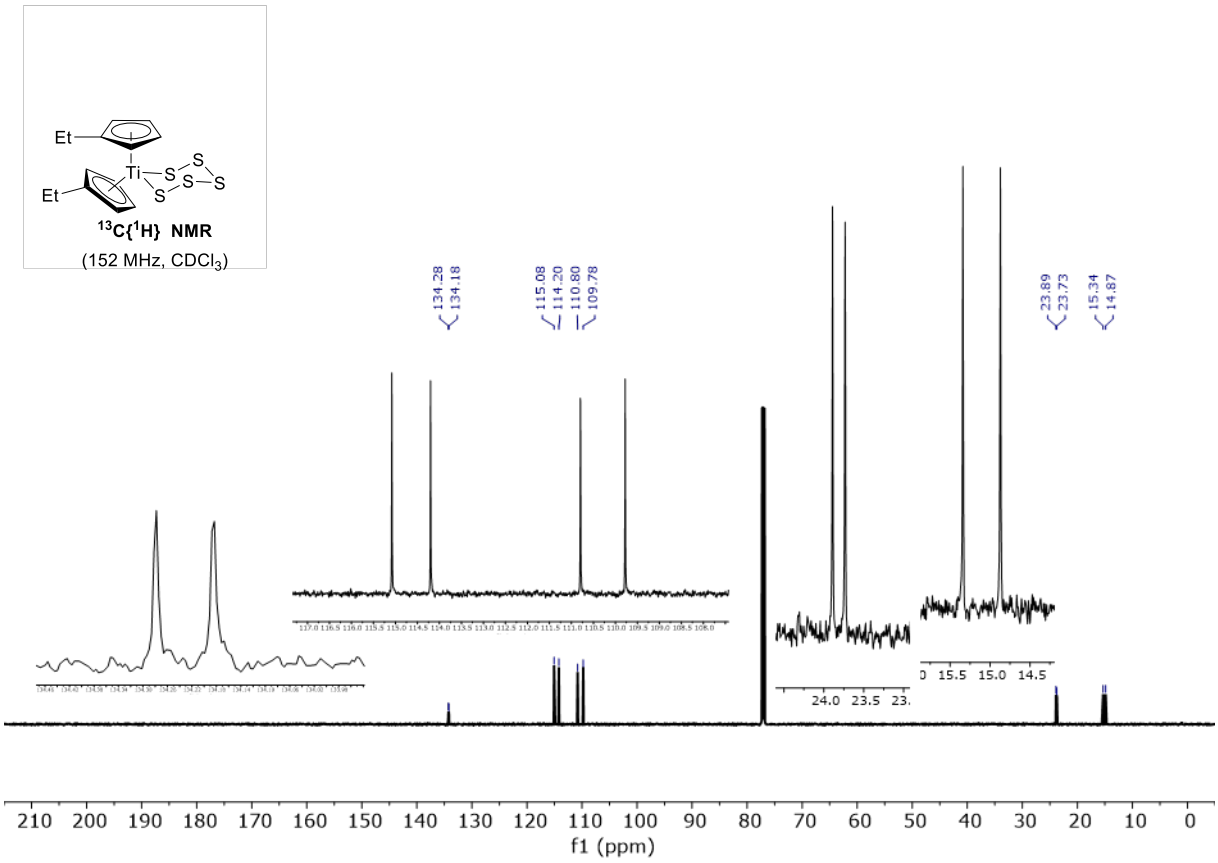
Et
Et
Ti
S
S
S
S
S
^{13}C{^{1}H} NMR
(152 MHz, $CDCl_3$)
134.28
134.18
115.08
114.20
110.80
109.78
23.89
23.73
15.34
14.87
24.0 23.5 23.
15.5 15.0 14.5
210 200 190 180 170 160 150 140 130 120 110 100 90 80 70 60 50 40 30 20 10 0
f1 (ppm)

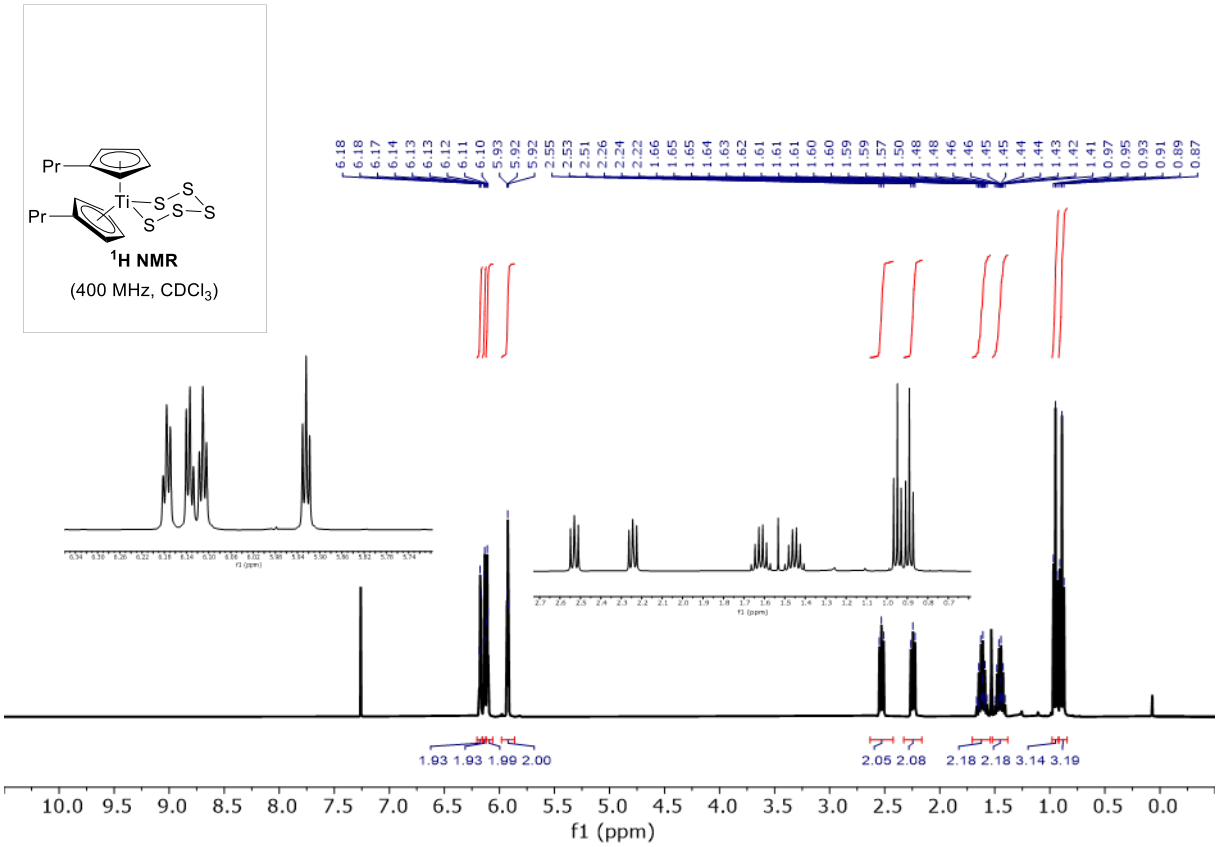
Pr
Ti
S
Pr
^{1}H NMR
(400 MHz, $CDCl_3$)
1.93 1.93 1.99 2.00
2.05 2.08
2.18 2.18 3.14 3.19
f1 (ppm)

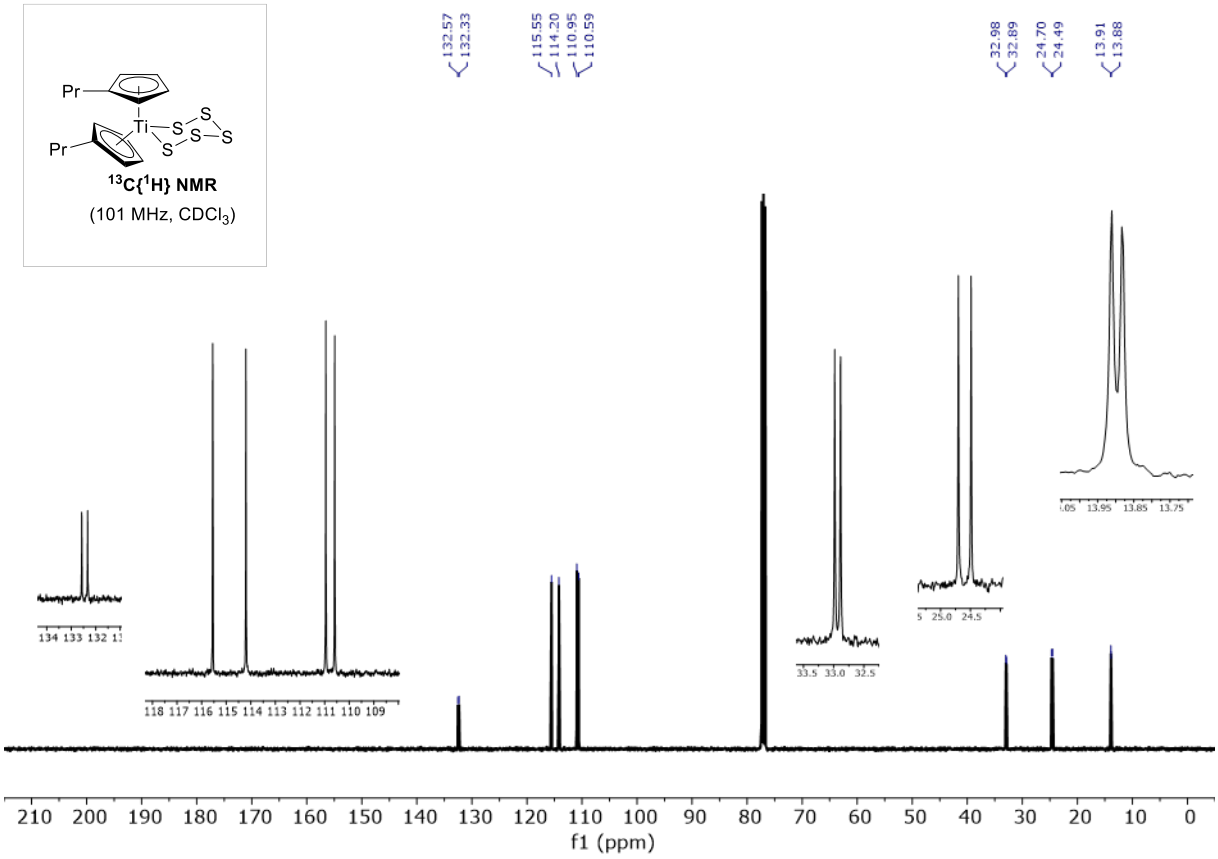
Pr
Ti
S
Pr
^{13}C{^{1}H} NMR
(101 MHz, $CDCl_3$)
132.57
132.33
115.55
114.20
110.95
110.59
32.98
32.89
24.70
24.49
13.91
13.88
f1 (ppm)

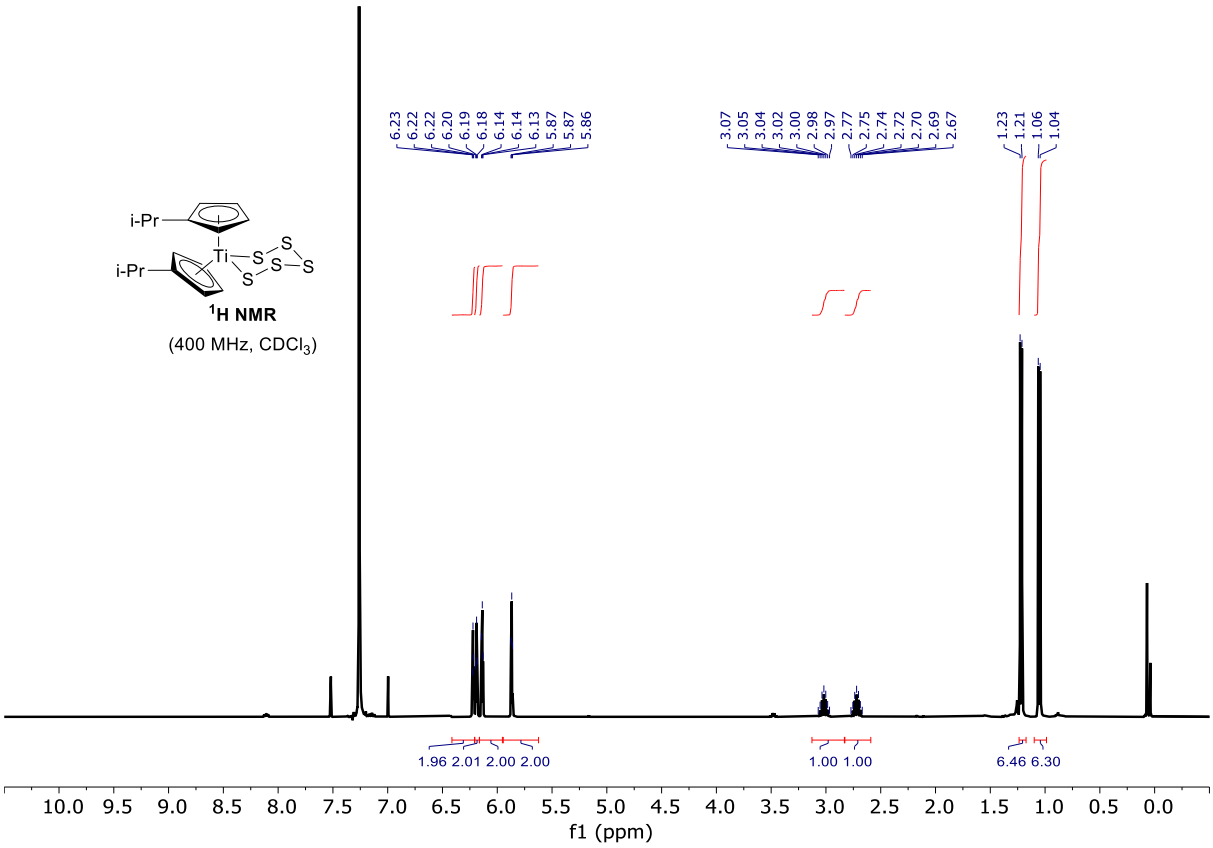
i-Pr
i-Pr
Ti
S
S
S
S
S
^{1}H NMR
(400 MHz, $CDCl_3$)
6.23
6.22
6.22
6.20
6.19
6.18
6.14
6.14
6.13
5.87
5.87
5.86
3.07
3.05
3.04
3.02
3.00
2.98
2.97
2.77
2.75
2.74
2.72
2.70
2.69
2.67
1.23
1.21
1.06
1.04
1.96 2.01 2.00 2.00
1.00 1.00
6.46 6.30
10.0 9.5 9.0 8.5 8.0 7.5 7.0 6.5 6.0 5.5 5.0 4.5 4.0 3.5 3.0 2.5 2.0 1.5 1.0 0.5 0.0
f1 (ppm)

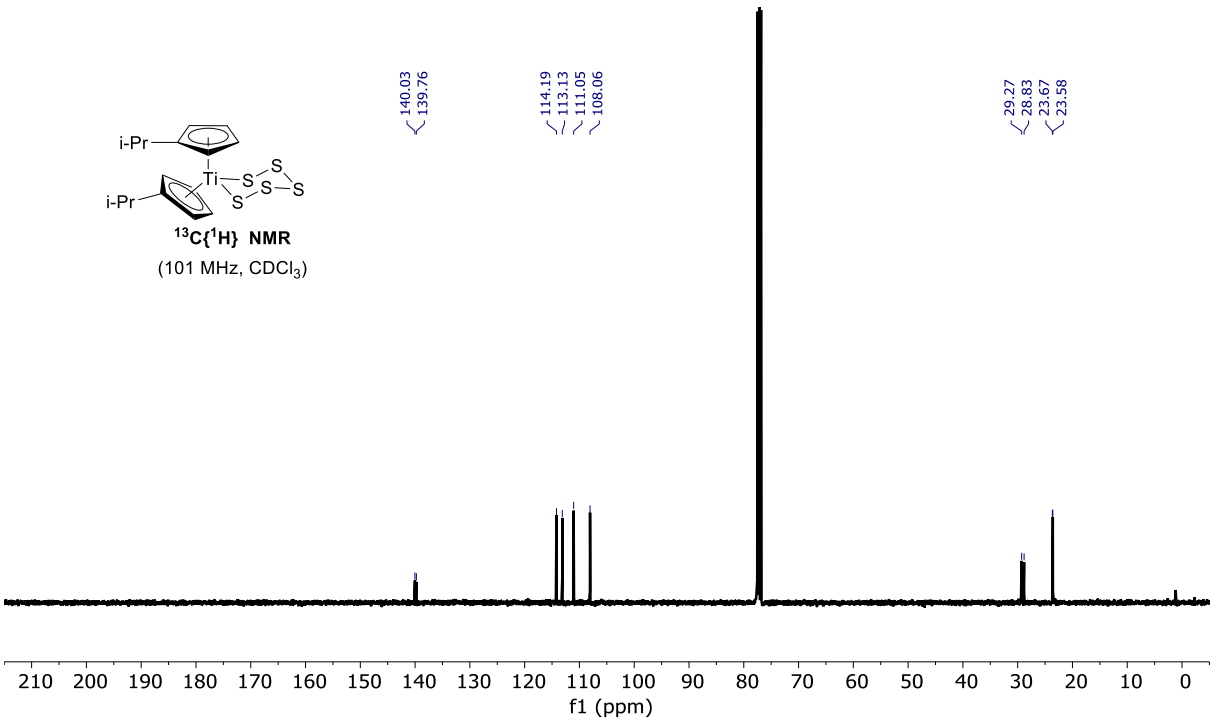
i-Pr
i-Pr
Ti
S
S
S
S
S
^{13}C{^{1}H} NMR
(101 MHz, $CDCl_3$)
140.03
139.76
114.19
113.13
111.05
108.06
29.27
28.83
23.67
23.58
210 200 190 180 170 160 150 140 130 120 110 100 90 80 70 60 50 40 30 20 10 0
f1 (ppm)

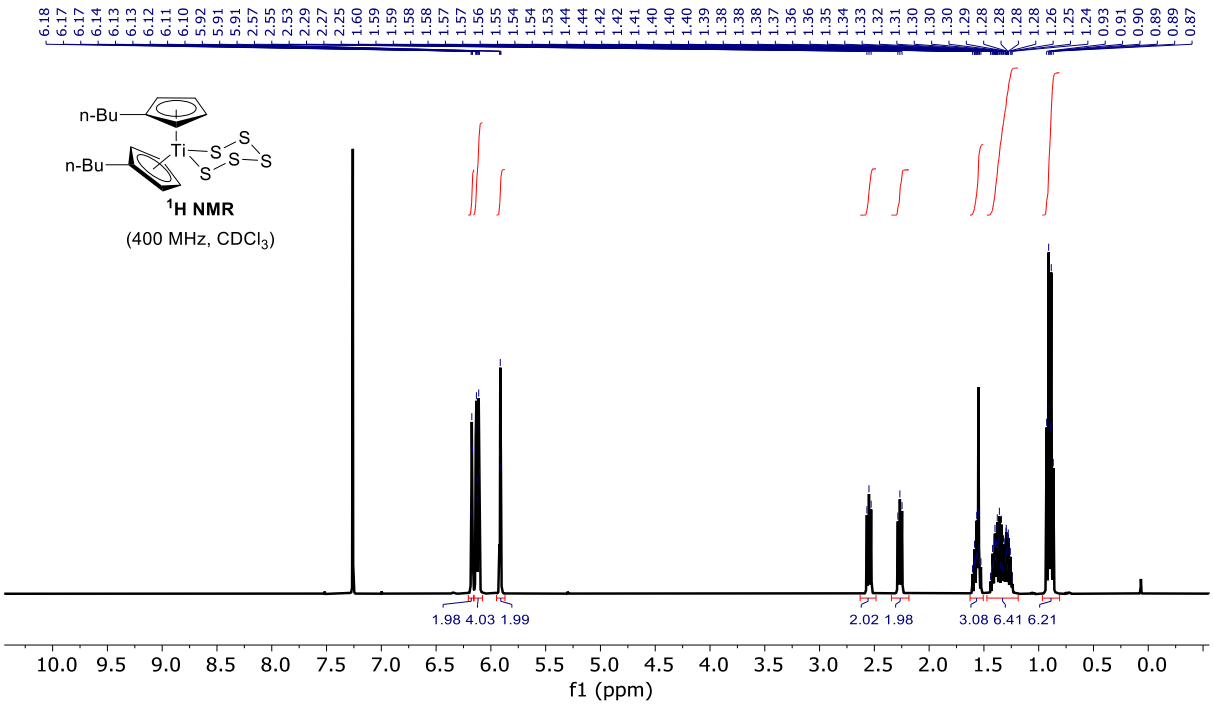
n-Bu
n-Bu
Ti
S
S
S
S
S
^{1}H NMR
(400 MHz, CDCl$_3$)
1.98 4.03 1.99
2.02 1.98
3.08 6.41 6.21
f1 (ppm)

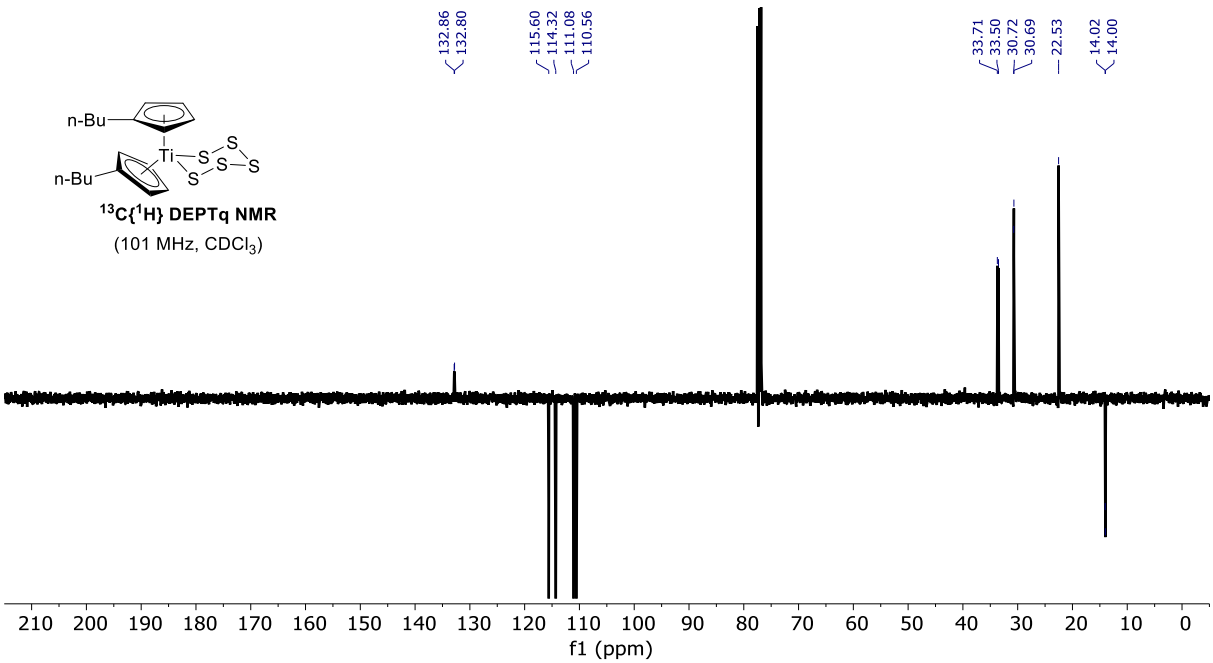
n-Bu
n-Bu
Ti
S
S
S
S
S
^{13}C{^{1}H} DEPTq NMR
(101 MHz, CDCl$_3$)
132.86
132.80
115.60
114.32
111.08
110.56
33.71
33.50
30.72
30.69
22.53
14.02
14.00
f1 (ppm)

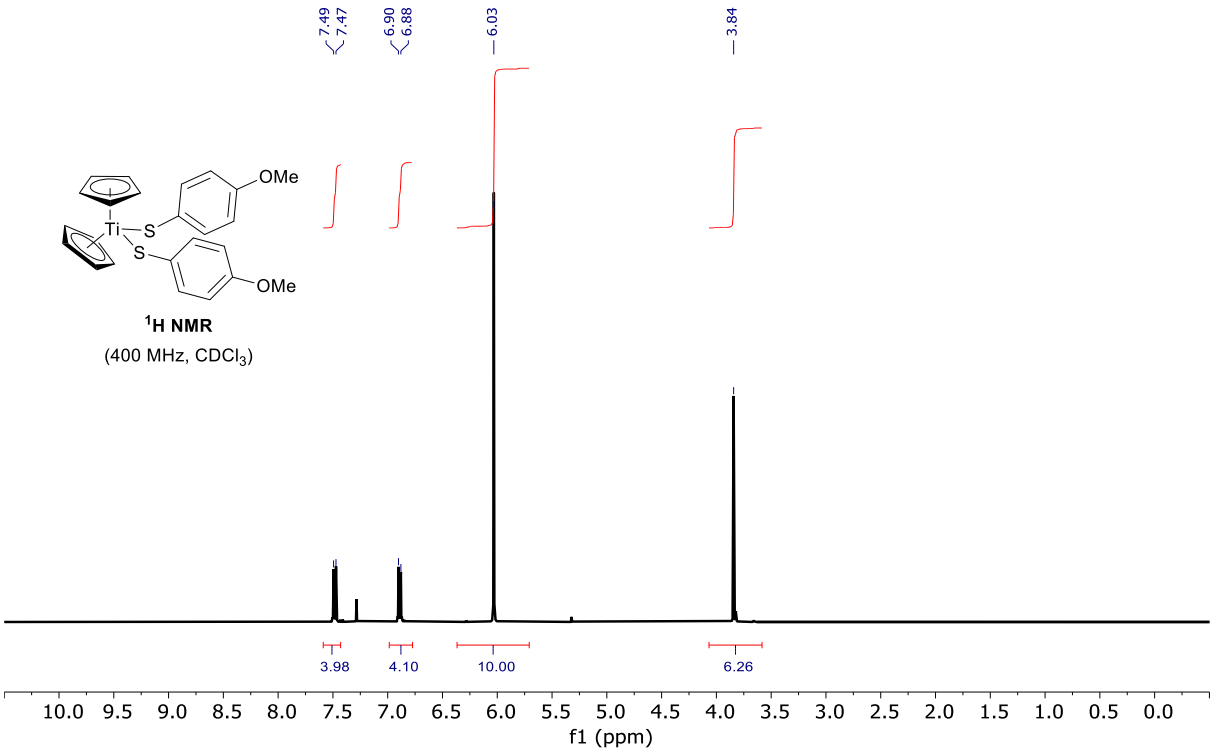

^{1}H NMR

(400 MHz, $CDCl_3$)

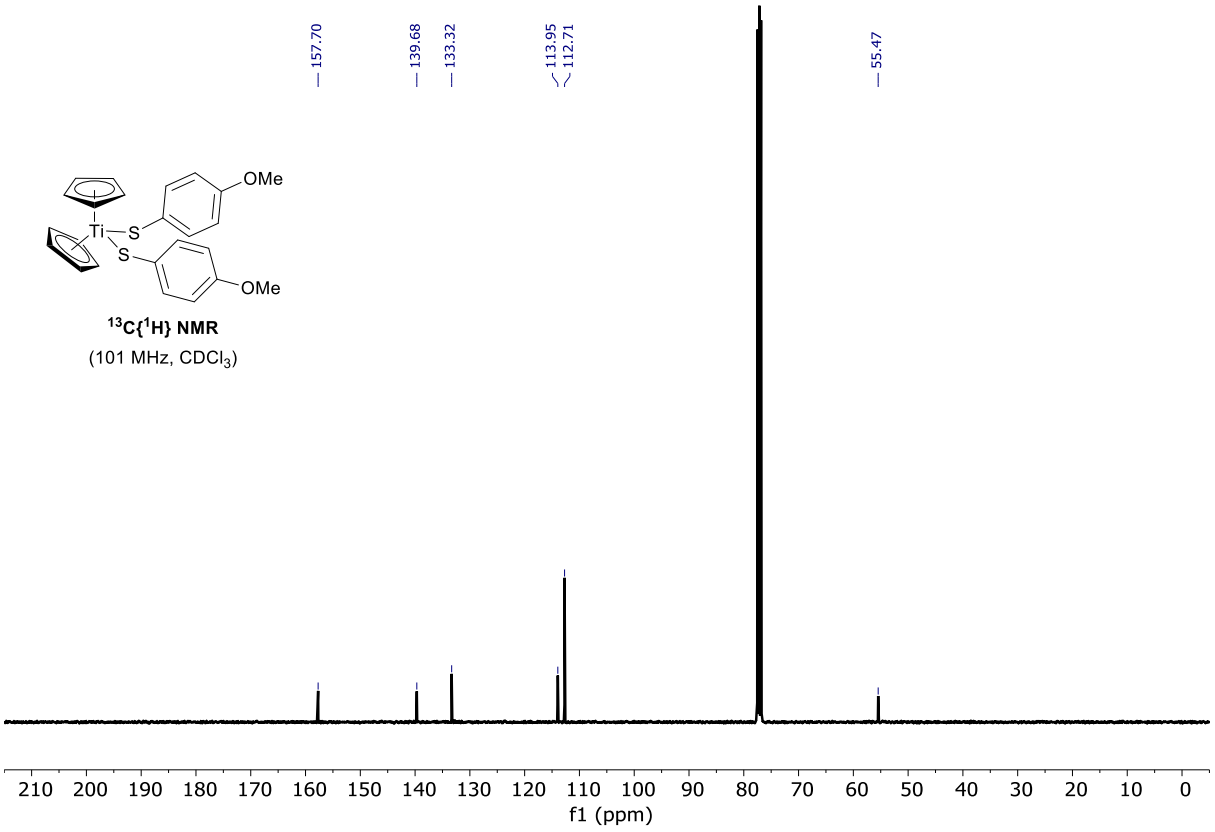

^{13}C{^{1}H} NMR

(101 MHz, $CDCl_3$)

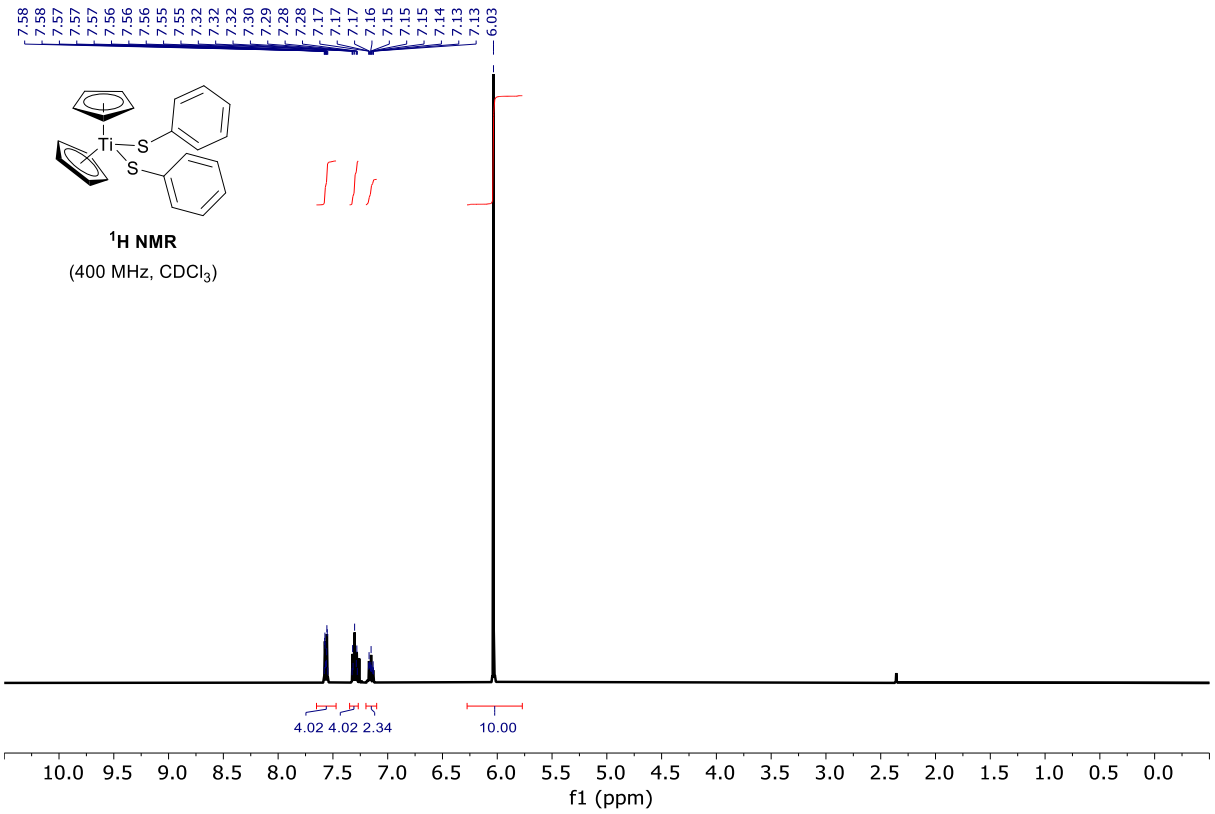

^{1}H NMR

(400 MHz, $CDCl_3$)

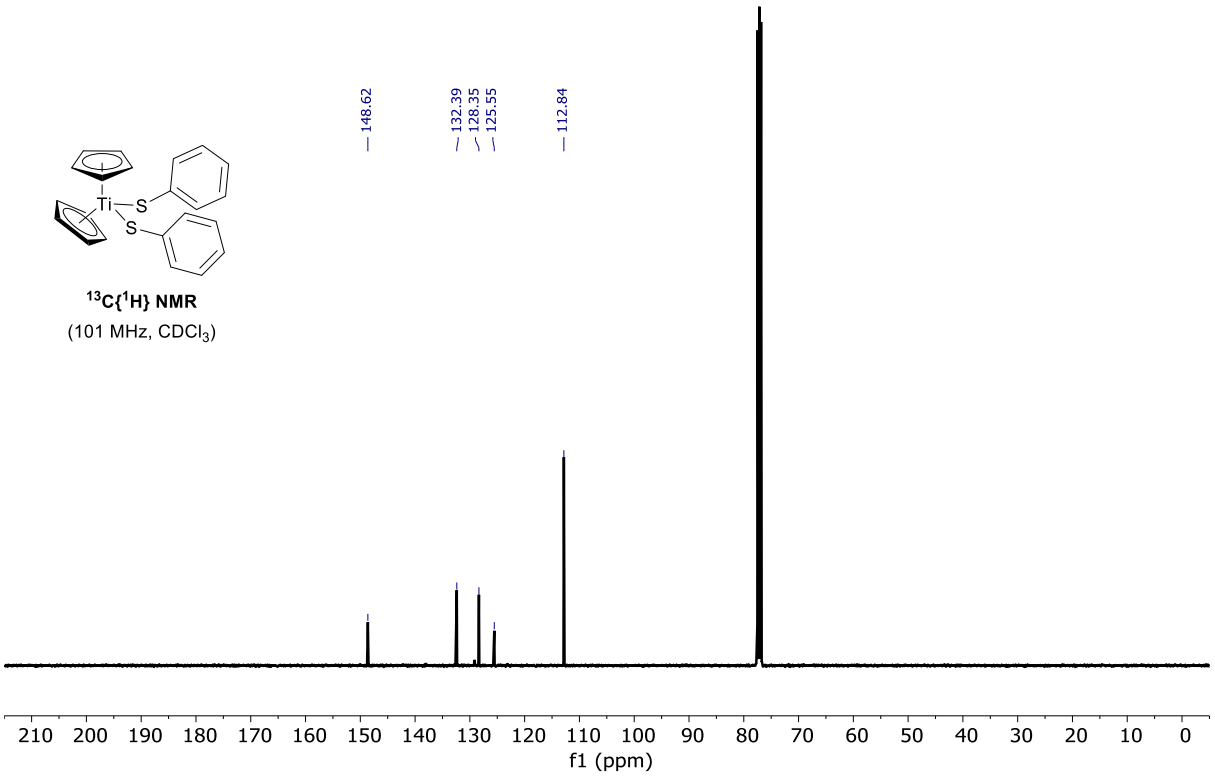

^{13}C{^{1}H} NMR

(101 MHz, $CDCl_3$)

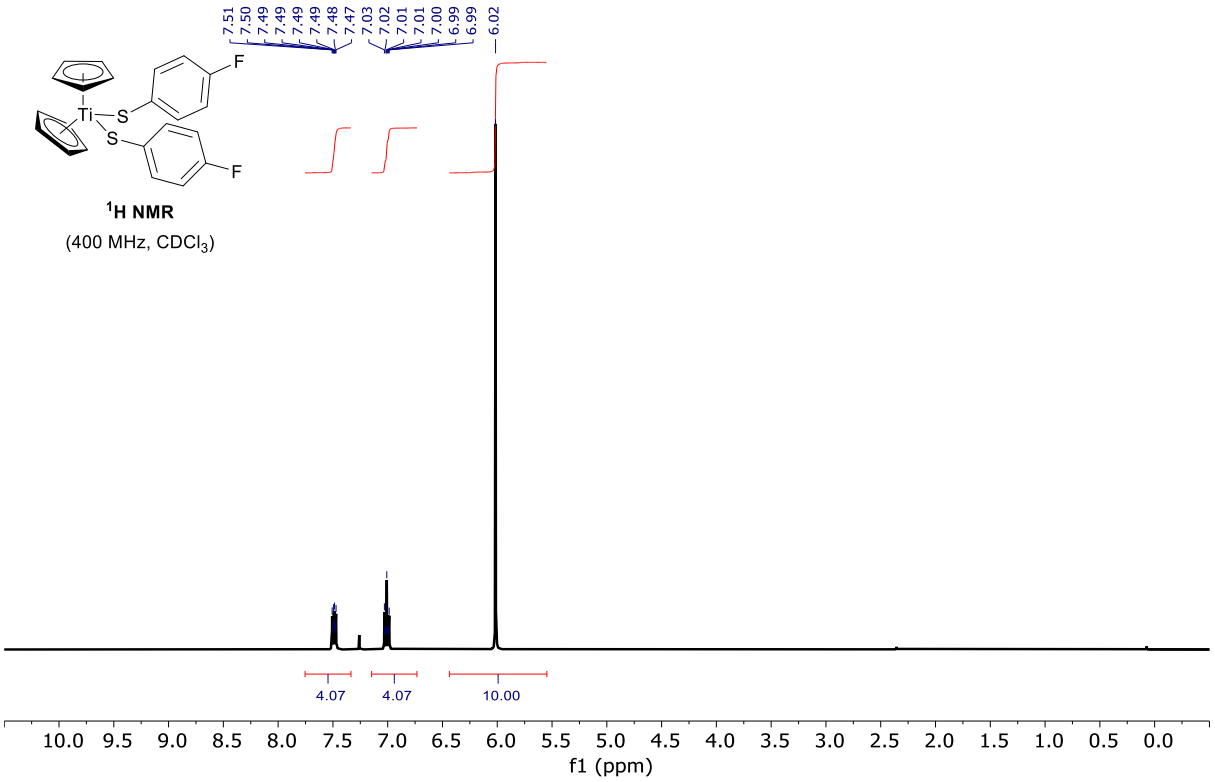

^{1}H NMR

(400 MHz, $CDCl_3$)

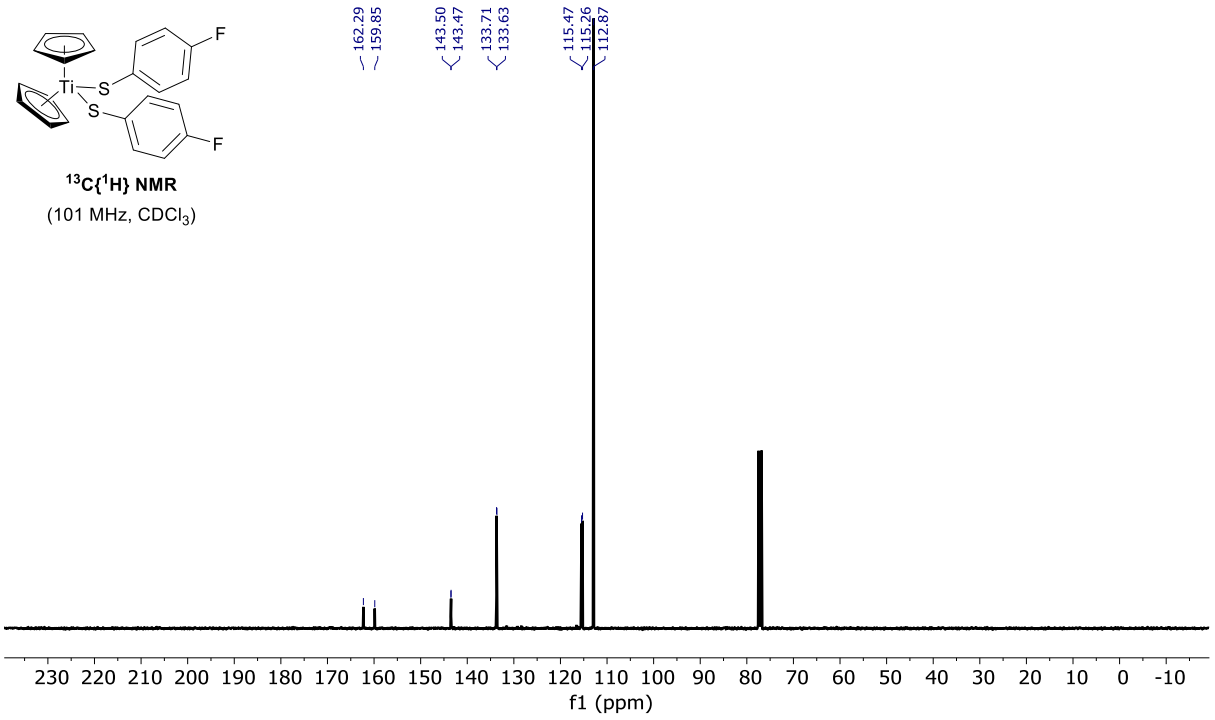

^{13}C{^{1}H} NMR

(101 MHz, $CDCl_3$)

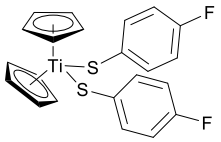

^{19}F NMR

(377 MHz, $CDCl_3$)

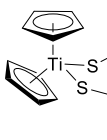

^{1}H NMR

(400 MHz, $CDCl_3$)

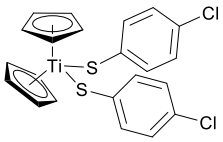

$^{13}C\{^{1}H\}$ NMR

(101 MHz, $CDCl_3$)

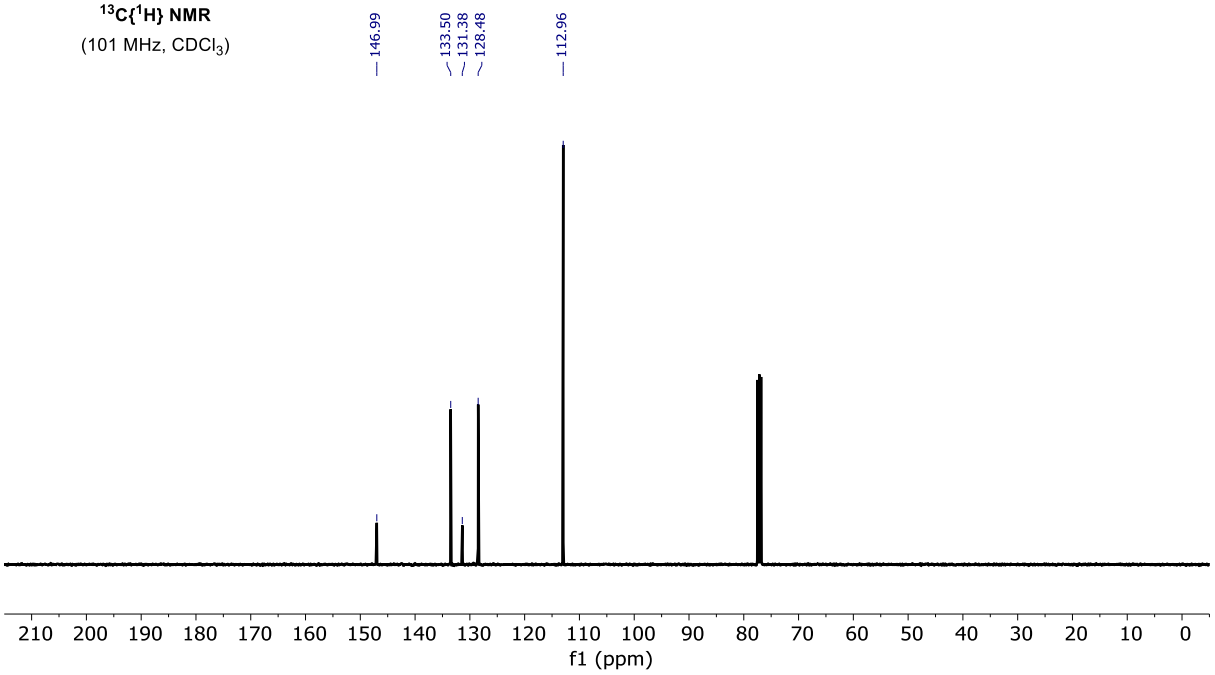

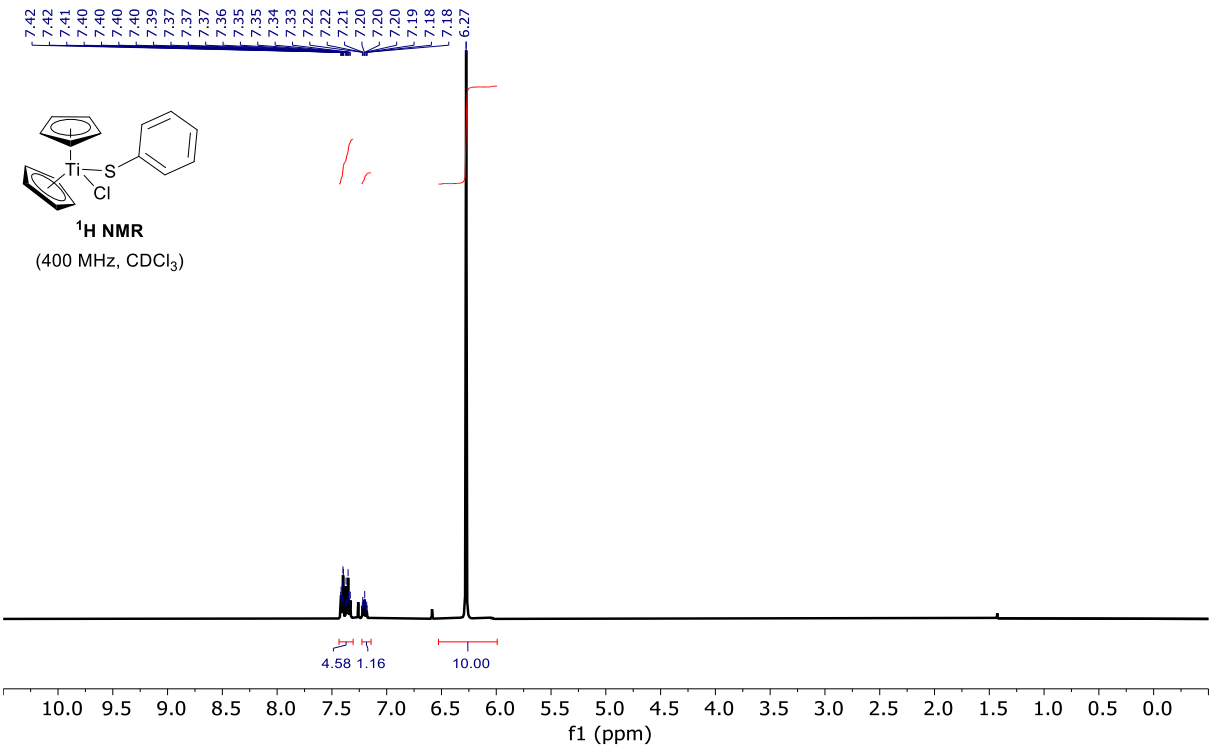

^{1}H NMR

(400 MHz, $CDCl_3$)

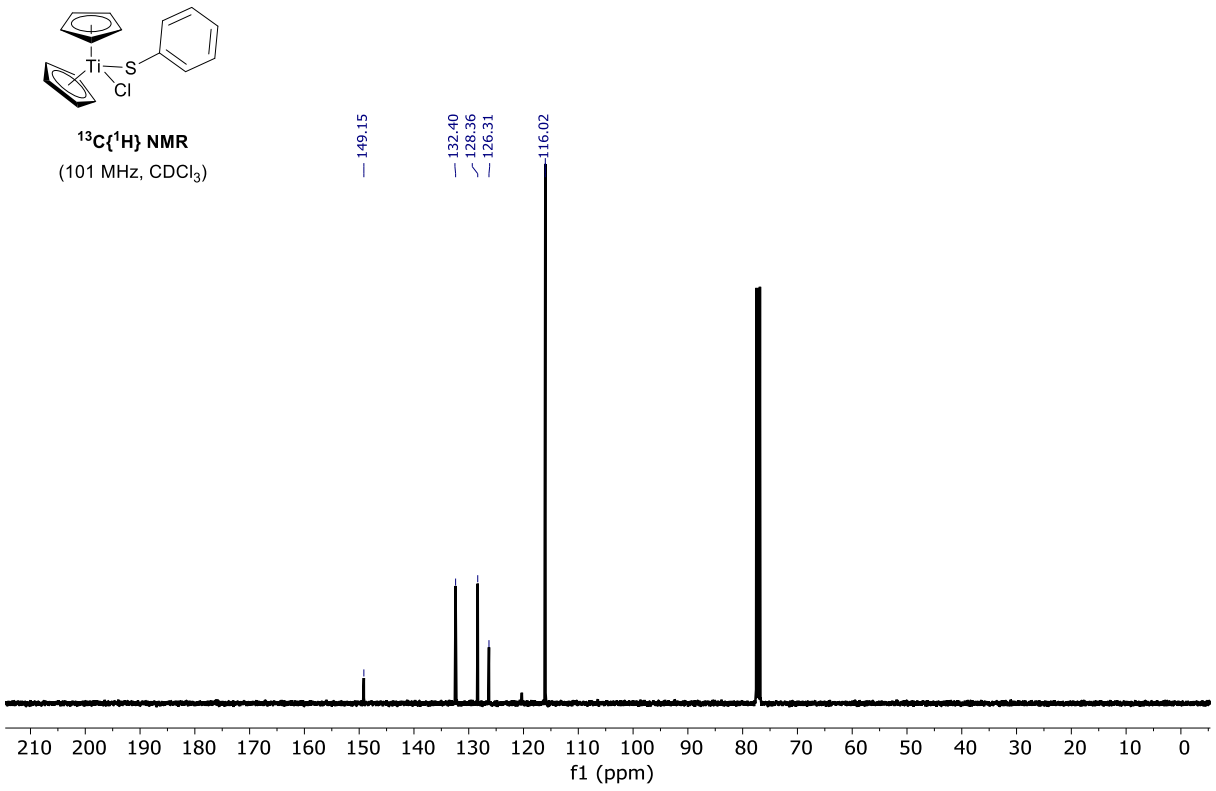
Ti
S
Cl
$^{13}C\{^{1}H\}$ NMR
(101 MHz, $CDCl_3$)
149.15
132.40
128.36
126.31
116.02
210 200 190 180 170 160 150 140 130 120 110 100 90 80 70 60 50 40 30 20 10 0
f1 (ppm)

11. Computational Investigations

11.1 General Considerations

All calculations have been performed using Orca 5.0.2[S14] and xtb[S15] version 6.4.1. Unless otherwise stated, parameters for the respective calculations are the program default parameters. All Orca calculations employed the highest default integration grid setting ('DEFGRID3') and very tight SCF convergence criteria ('VERYTIGHTSCF'). All geometry optimizations were run at very tight optimization convergence criteria ('VERYTIGHTOPT'). A representative example of an Orca input file used in this work can be found in Section S11.5.

All stationary points were optimized and characterized with the r^{2}SCAN-3c[S16] composite method in the gas phase (See Section S11.2). Frequency calculations were performed to characterize stationary points as either minima (no imaginary frequencies) or transition states (one imaginary frequency). Transition states were located via the nudged elastic band method (NEB)[S17], and their final geometries further verified via intrinsic reaction coordinate (IRC)[S18] calculations along the negative vibrational mode. All stationary point geometries are provided in a separate .xyz file. All frequency calculations employed the qRRHO[S19] approximation of Grimme and coworkers with a cutoff frequency of 50 cm^{-1}. Statistical thermodynamic corrections have been calculated at T = 298.15 K and p = 1.0 atm. These values result in an ideal gas concentration of 0.0409 M. These free energy corrections were converted into a 1 M standard state by adding 0.003019 Hartree.

Geometries of minima were preoptimized with the xtb semiempirical method. The lowest energy conformers were located with crest[S20] version 2.11.2 and further refined with CENSO[S21] version 1.12. The r^{2}SCAN-3c composite method was used for the conformer sampling procedure. All conformer search calculations were performed in the gas phase.

All single-point calculations were carried out employing the r^{2}SCAN functional[S22] and D4 dispersion correction.[S23] The ma-def2-QZVPP basis set was employed for Ti and the ma-def2-TZVPP basis set for all other atoms.[S24] The auxiliary basis set def2/J was employed for all single-point calculations.[S25] The SMD continuum solvation model was employed with DCM as the solvent.[S26]

The chosen computational method used for calculations and comparison of results shown within this work is:

r^{2}SCAN-D4-SMD(DCM)/ma-def2-QZVPP(Ti), ma-def2-TZVPP(All)//r^{2}SCAN-3c.

11.2 Analysis of methods and benchmarking

For initial geometry optimization explorations, the methods B97-D3(BJ),[S27] BP86-D3(BJ),[S28] PBE-D3(BJ),[S29] revPBE-D3(BJ),[S30] BLYP-D3(BJ),[S31] OLYP-D3(BJ),[S32] SCAN-D3(BJ),[S33] r^{2}SCAN-3c, M06L-D3(0),[S34] TPSS-D3(BJ),[S35] TPSSh-D3(BJ),[S36] TPSS0-D3(BJ),[S37] PBE0-D3(BJ),[S38] B3LYP-D3(BJ),[S39] M06-D3(0),[S40] and PW6B95-D3(BJ)[S41] were explored using the def2-SVP basis set. The geometry of Cp_2TiS_5 was optimized using each of these functionals and compared to a crystal structure,[S42] a geometry optimized at the TPSS-D3(BJ)/def2-TZVP and a geometry optimized at the PBE0-D3(BJ)/def2-TZVP levels of theory. In all cases, geometries were shown to be practically invariant to the functional used. However, computational cost was markedly higher for hybrid functionals (Table S2).

Table S2. Summary of geometrical parameters of different functionals compared to a crystal structure of Cp_2TiS_5.

Entry	Functional[a]	RMSD[b] (Å)	RMSD TiS_5[c] (Å)	MAD / AMAX [d] Bond (Å)	MAD / AMAX [e] Angle (°)	N_{iter} / WT (min) [f]
1	r^{2}SCAN-3c[g]	0.337	0.036	0.026 / 0.046	0.8 / 2.0	13 / 7.7
2	B97-D3(BJ)	0.350	0.047	0.036 / 0.057	0.9 / 3.0	20 / 6.9
3	BP86-D3(BJ)	0.350	0.047	0.033 / 0.052	1.0 / 3.1	10 / 4.4
4	PBE-D3(BJ)	0.348	0.045	0.031 / 0.047	0.9 / 2.9	7 / 3.3
5	revPBE-D3(BJ)	0.348	0.045	0.033 / 0.051	0.9 / 2.8	7 / 3.1
6	BLYP-D3(BJ)	0.347	0.062	0.050 / 0.075	1.0 / 3.3	11 / 5.0
7	OLYP-D3(BJ)	0.343	0.033	0.021 / 0.044	0.9 / 2.6	14 / 7.1
8	SCAN-D3(BJ)	0.328	0.073	0.068 / 0.086	1.8 / 3.9	33 / 19.3
9	M06L-D3(0)	0.313	0.052	0.034 / 0.058	1.3 / 2.7	21 / 14.3
10	TPSS-D3(BJ)	0.316	0.043	0.032 / 0.048	1.0 / 2.8	12 / 8.4
11	TPSSh-D3(BJ)	0.314	0.035	0.026 / 0.035	0.9 / 2.5	7 / 15.6
12	TPSS0-D3(BJ)	0.313	0.028	0.020 / 0.046	0.9 / 2.2	8 / 17.7
13	B3LYP-D3(BJ)	0.317	0.040	0.031 / 0.043	0.9 / 2.7	11 / 22.4
14	PBE0-D3(BJ)	0.319	0.029	0.018 / 0.041	0.8 / 2.3	9 / 17.7
15	M06-D3(0)	0.380	0.045	0.030 / 0.045	0.8 / 2.4	22 / 44.2
16	PW6B95-D3(BJ)	0.376	0.032	0.019 / 0.044	0.9 / 2.5	7 / 15.6

[a] def2-SVP, def2/J
[b] Root Mean Square Deviation of geometry from crystal structure
[c] Root Mean Square Deviation of geometry from crystal structure excluding Cp Ligands
[d] Mean Absolute Deviation and Absolute Maximum Deviation of selected bond lengths from crystal structure between atoms: 1-2, 1-6, 1-9, 1-18, 2-3, 3-4, 4-5, 5-6 (for numbering, see .xyz file)
[e] Mean Absolute Deviation and Absolute Maximum Deviation of selected angles from crystal structure between atoms: 2-1-6, 2-1-9, 2-1-18, 1-2-3, 2-3-4, 3-4-5, 4-5-6, 5-6-1 (for numbering, see .xyz file)
[f] N_{iter} is the number of SCF iterations until Orca signaled convergence. WT = Wall Time in minutes for geometry optimization using six processors.
[g] The composite method uses a different basis set. For details, see ref. S16

r²SCAN-3c was the method of choice for geometry optimization in this study due to its implementation in the CENSO conformer search program and its balanced basis set, computational performance, and basis-set superposition corrections.

Single-point electronic energy calculations for benchmarking purposes were performed with the BP86-D4, PBE-D4, revPBE-D4, B97-D3(BJ), BLYP-D4, OLYP-D4, M06L-D3(0), r²SCAN-D4, TPSS-D4, TPSSh-D4, TPSS0-D4, PBE0-D4, B3LYP-D4, B97M-V,[S43,] and ωB97M-V[S44,] functionals, where D4, D3(0) and D3(BJ) indicate different versions of Grimme and coworkers' dispersion corrections,[S45] as well as the DLPNO-CCSD(T)[S46] method. All single-point calculations were carried out employing the ma-def2-QZVPP basis set for Ti and the ma-def2-TZVPP basis set for all other atoms. The auxiliary basis set def2/J was employed for all DFT calculations and the auxiliary basis set def2-TZVPP/C was employed for all DLPNO-CCSD(T) calculations.[S47] To find a suitable method, eight experimental reactions were evaluated (Table S3). Their corresponding experimental bimolecular rate constants, k_{rxn} ($M^{-1}s^{-1}$), were transformed into microkinetic reaction barriers for S-S bond formation at the experimental temperature, 295 K ($\Delta G^{‡}_{295K}$), using Eyring equation as described within Table S3.

Table S3. Reactions used in benchmarking studies, experimental bimolecular rate constants and microkinetic activation barriers for S-S bond formation at 295 K.

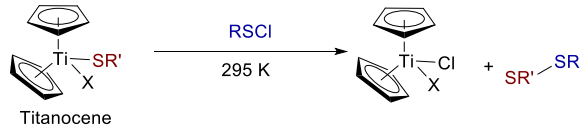

$$k_{rxn}\,(M^{-1}\cdot s^{-1}) = n\cdot k_{s\text{-}s} = n\left(\frac{\kappa k_b T}{h}\right) e^{\frac{-\Delta G^{‡}}{RT}}$$

$$\Delta G^{‡} = RT\ln\left(\frac{\kappa k_b T}{h k_{rxn}}\right) + RT\ln(n)$$

k_{rxn}	Empirical process rate constant ($M^{-1}s^{-1}$)
$k_{S\text{-}S}$	Microkinetic S-S bond formation rate constant
n	Number of equivalent microkinetic S-S bond formation events
κ	Transmission coefficient of each microkinetic S-S bond formation
k_b	Boltzmant constant
T	Temperature
h	Planck Constant
$\Delta G^{‡}$	Free enegy activation barrier of microkinetic S-S bond formation
R	Ideal gas constant

Rxn	Titanocene	RSCl	k_{rxn} ($M^{-1}s^{-1}$)	n	$\Delta G^{‡}_{295K}$ (kcal/mol)
A	$Cp_2TiS_4(CMe_2)$	S_2Cl_2	$3.4\cdot10^4$	4	12.0
B	Cp_2TiS_5	S_2Cl_2	$3.2\cdot10^2$	4	14.7
C	Cp_2TiS_5	MorphNSCl	$4.8\cdot10^1$	2	15.4
D	$Cp_2TiCl(S_6NMorph)$	MorphNSCl	$6.8\cdot10^1$	1	14.8
E	$Cp_2Ti(4\text{-}Cl\text{-}C_6H_4S)_2$	MorphNSCl	$2.9\cdot10^3$	2	13.0
F	$Cp_2Ti(SPh)_2$	MorphNSCl	$1.3\cdot10^4$	2	12.1
G	$Cp_2TiCl(4\text{-}Cl\text{-}C_6H_4S)$	MorphNSCl	$2.1\cdot10^3$	1	12.8
H	$Cp_2TiCl(SPh)$	MorphNSCl	$6.5\cdot10^3$	1	12.1

The calculations consider the number of equivalent microkinetic S-S bond forming reactions (n) contributing to the observed reaction process rate ($k_{rxn} = nk_{S\text{-}S}$). This number (n) corresponds to the equivalent reactive sites in the corresponding bimolecular process (i.e. number of combinations of the two species that lead to identical transition states), and thus depends on structure of starting reagent and electrophile (Table S3). Transmission coefficients for microkinetic S-S bond forming processes of unity were input in these calculations. The conversions allow comparisons with computational data, which consider only a single microkinetic S-S bond formation event. Computational barriers are given at 298.15 K. Comparison of experimental and computational data by various methods, using linear regression analysis is shown in Table S4. Figure S64-S66 show the different linear correlations in graphic form.

Table S4. Summary of regression parameters of computed microkinetic barriers ($\Delta G^{\ddagger}_{298K}$) with different functionals compared to measured experimental microkinetic barriers ($\Delta G^{\ddagger}_{295K}$).

		Microkinetic free energy barrier, $\Delta G^{\ddagger}_{298K}$ (kcal/mol)								**RSQ[a]**
Entry	**Functional**	**Rxn A**	**Rxn B**	**Rxn C**	**Rxn D**	**Rxn E**	**Rxn F**	**Rxn G**	**Rxn H**	**(-)**
1	Experiment[b]	12.0	14.7	15.4	14.8	13.0	12.1	12.8	12.1	-
2	BP86-D4	9.8	15.3	18.4	15.3	13.0	11.8	13.3	12.9	0.850
3	PBE-D4	12.3	17.6	20.5	17.6	15.5	14.3	15.6	15.2	0.855
4	revPBE-D4	11.9	16.7	20.0	17.6	15.2	14.0	15.4	15.0	0.831
5	B97-D3(BJ)	10.6	16.5	19.4	16.2	13.8	12.6	14.0	13.5	0.879
6	BLYP-D4	9.5	15.6	18.9	15.6	13.0	11.8	13.6	13.2	0.827
7	OLYP-D4	13.9	18.6	21.7	19.2	16.9	15.7	17.0	16.5	0.864
8	M06L-D3(0)	16.6	18.9	20.0	19.1	16.7	15.3	17.2	16.4	0.919
9[c]	r^{2}SCAN-D4	15.3	19.6	21.9	20.0	18.3	17.1	18.1	17.5	0.880
10	B97M-V	18.2	20.6	21.9	20.4	18.3	16.9	18.4	17.6	0.927
11	TPSS-D4	11.9	16.5	19.8	17.6	14.9	13.7	15.1	14.7	0.855
12	TPSSh-D4	15.2	18.0	20.9	18.9	16.5	15.2	16.5	15.9	0.922
13	TPSS0-D4	19.5	19.5	21.8	20.4	18.6	17.2	18.2	17.3	0.686
14	PBE0-D4	19.8	20.4	22.5	20.5	19.1	17.7	18.6	17.7	0.740
15	B3LYP-D4	16.3	18.6	21.0	18.4	16.5	15.1	16.4	15.7	0.886
16	ωB97M-V	25.5	21.5	22.5	21.7	20.7	19.1	19.9	18.7	0.040
17	DLPNO-CCSD(T)	21.7	20.5	22.4	21.0	19.2	17.9	19.3	18.4	0.392

[a] Square of the Pearson product moment correlation coefficient, R^2, when all values in entry are correlated to all experimental values.
[b] Experimental barriers measured at 295K. Computational barriers (entries 2 – 17) were calculated at 298.15 K.
[c] Functional chosen for computational analysis within this work.

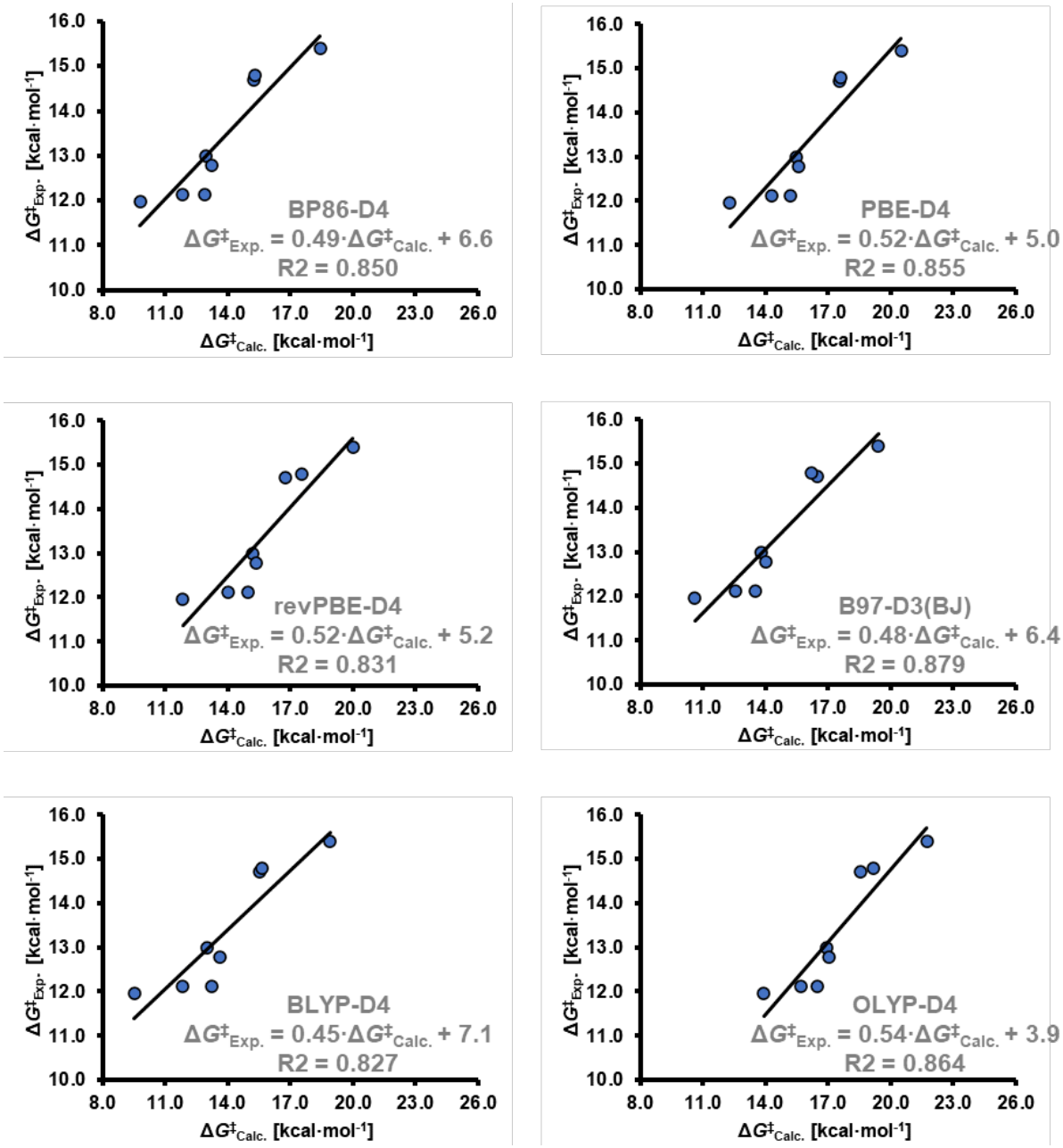

Figure S64. Correlations between experimental and computed microkinetic free energy reaction barriers for GGA density functionals (Table S4, Entries 2–7). Note that $\Delta G^{\ddagger}_{Exp}$ are at 295K and $\Delta G^{\ddagger}_{Calc}$ at 298.15 K.

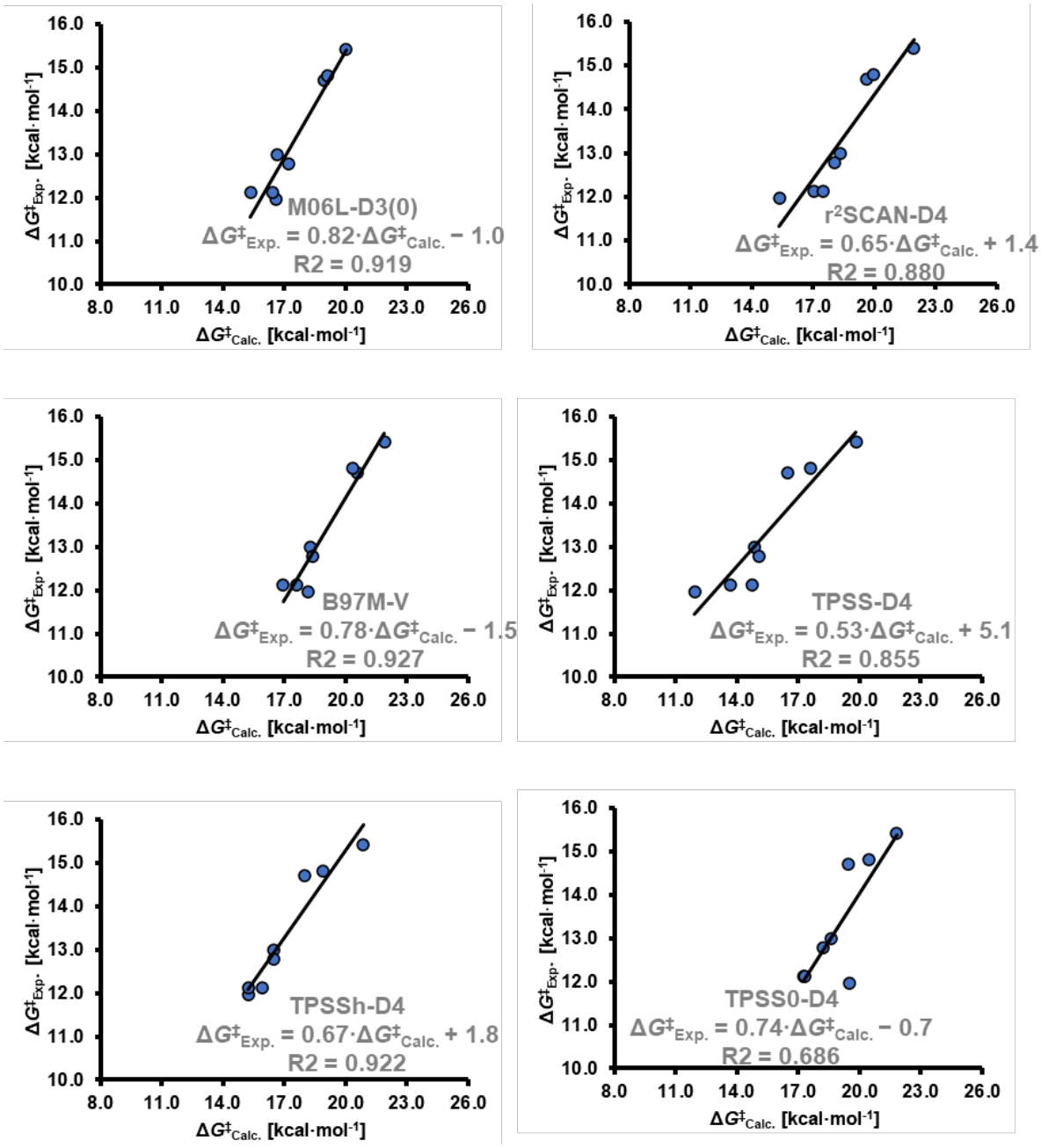

Figure S65. Correlations between experimental and computed microkinetic free energy reaction barriers for meta-GGA density functionals (Table S4, Entries 8–11) and for hybrid variants of the TPSS mGGA functional, TPSSh (xHF = 10%, Table S4, entry 12) and TPSS0 (xHF = 25%, Table S4Entry 13). Note that $\Delta G^{\ddagger}_{Exp}$ are at 295K and $\Delta G^{\ddagger}_{Calc}$ at 298.15 K.

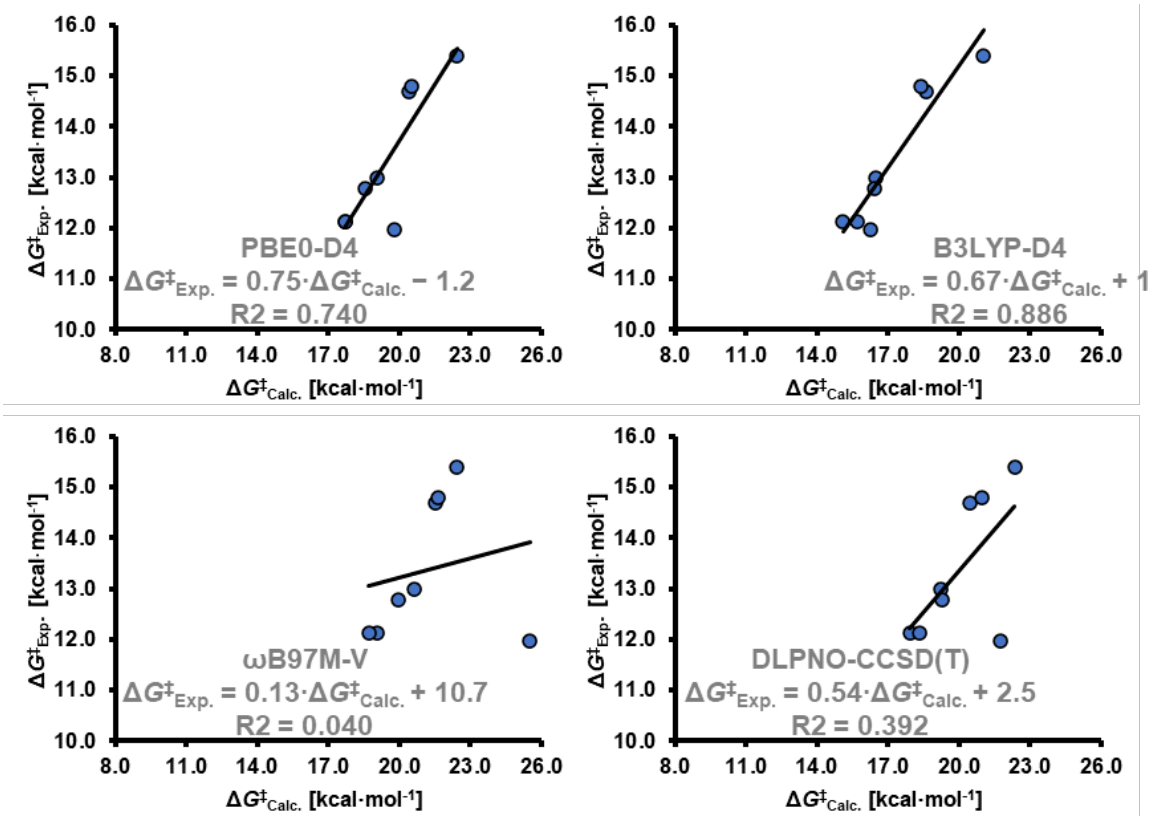

Figure S66. Correlations between experimental and computed microkinetic free energy reaction barriers for hybrid density functionals PBE0 (Table S4, Entry 14), B3LYP (Table S4, Entry 15), for the range-separated hybrid density functional ωB97M-V (Table S4, Entry 16) and for the wavefunction method DLPNO-CCSD(T) (Table S4, Entry 17). Note that $\Delta G^{\ddagger}_{Exp}$ are at 295 K and $\Delta G^{\ddagger}_{Calc}$ at 298.15 K.

The results in Table S4 indicate that all tested GGA functionals (Entries 2–7 in Table S4, Figure S64) perform qualitatively well to similar degrees. All tested mGGA functionals (Entries 8–11 in Table S4, Figure S65) perform better than GGA functionals. Addition of HF exchange (xHF) to functionals, as exemplified by the TPSS family of functionals (Entries 11–13 in Table S4, Figure S65), has a marked effect on the qualitative description of experimental trends. Compared to TPSS (Entry 11 Table S4, xHF = 0%), TPSSh (Entry 12, xHF = 10%) shows a slightly improved correlation, but further increase of xHF in TPSS0 (Entry 13 Table S4, xHF = 25%) results in a worse correlation. A similar decrease in quality of correlation is observed for PBE (Entry 3 Table S4, xHF = 0%) and PBE0 (Entry 14 Table S4, xHF = 25%, Figure S51). When xHF is introduced in the form of range-separation, as for ωB97M-V (Entry 16, xHF = 15–100%, Figure S66), it leads to significantly worse performance than its mGGA counterpart B97M-V (Entry 10 in Table S4, xHF = 0%). Notably, B3LYP (Entry 15 in Table S4, Figure S66, xHF = 20%) results in a better correlation than pure counterpart BYLP (Entry 6 in Table S4, xHF = 0%). However, inclusion of xHF exchange in B3LYP involves a more elaborate, 3 parameter model and a direct comparison is not as useful as in the cases of TPSS and PBE and their hybrid counterparts. The wavefunction method DLPNO-CCSD(T) (Entry 17 in Table S4, Figure S66, xHF =

100%) performed poorly despite the better general performance across various systems compared to all DFT functionals employed in this benchmark.

Reaction A (i.e., $Cp_2TiS_4(CMe_2)$ + S_2Cl_2) stands out as a clear outlier when methods with large values of xHF are employed. Its microkinetic free energy activation barrier is significantly overestimated by almost all functionals containing a non-zero fraction of xHF, with exception of B3LYP and TPSSh. These results prompted further examination. The trend of increasing xHF and increasing erratic predictions suggests that the electronic structure of some species involved in the study are not well described by a single electronic reference. That is, there may be significant multireference character in some species, and single-reference methods involving xHF such as hybrid DFT, MP2 and DLPNO-CCSD(T) are poorly suited to properly represent the electronic structure.[S48] In order to explore whether multireference character was present, the fractional occupation density (FOD) approach by Grimme and coworkers was employed to assess reaction A ($Cp_2TiS_4(CMe_2)$ + S_2Cl_2).[S48] FOD calculations were carried out employing the default settings in Orca (TPSS, T_{El} = 5000 K) and plots of reagents and were generated with a contour value of 0.002 e $Bohr^{-3}$. The resulting plots of the ground state of cylic complex and electrophile, $Cp_2TiS_4(CMe_2)$ and S_2Cl_2, and the transition state (Figure S67) indicate a complex electronic structure. If single reference methods are employed for this system, methods which utilize xHF should be avoided. Although removing Reaction A from the correlation set leads to a significant improvement in correlation for most hybrid functionals and for DLPNO-CCSD(T), the FOD results show that multireference character is present in at least one of the species in the benchmark set, and therefore methods employing exact exchange were not further applied in this work. A mGGA functional, r^2SCAN, was ultimately chosen based on two factors: its good correlation with the benchmark set and on its good computational performance.

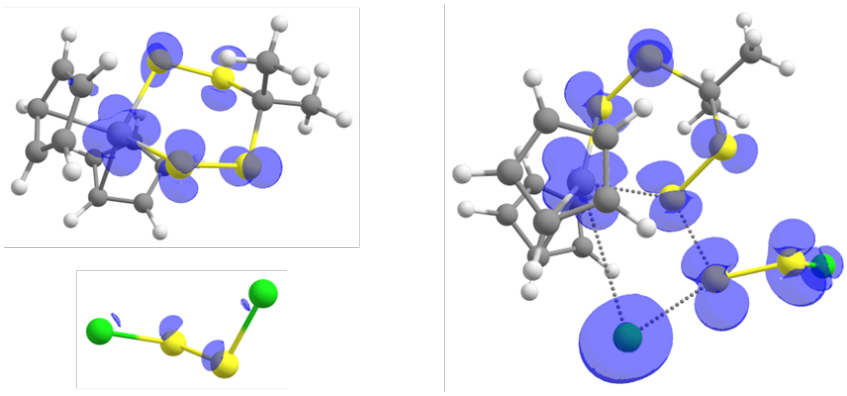

Figure S67. FOD plots (TPSS, T_{El} = 5000 K; contour value 0.002 e $Bohr^{-3}$) of the species involved in Reaction A ($Cp2TiS_4(CMe_2)$ + S_2Cl_2). Left: reactants calculated separately. Right: transition state.

11.3 Alternative pathways explored

Alternative reaction pathways for the reaction of Cp_2TiS_5 and S_2Cl_2 in addition to the *σ*-bond metathesis mechanism proposed in this work were explored (Figure S68). All energies are reported relative to a reference state of separate Cp_2TiS_5 and S_2Cl_2 molecules. Alternative pathways leading to the minimum energy structures shown in the arbitrary reaction coordinate depicted in Figure S68, are highly endergonic and inconsistent with a reaction proceeding in the ms-s scale at room temperature. At the level of theory used, the pathways discarded are:

- Heterolytic S-Cl pre-dissociation from S_2Cl_2 (ΔG = 244.9 kcal/mol or 66.1 kcal/mol)
- Homolytic S-Cl pre-dissociation from S_2Cl_2 (ΔG = 43.2 kcal/mol)
- Homolytic S-S pre-dissociation from S_2Cl_2 (ΔG = 56.4 kcal/mol)
- TiS_5 ring opening via chloride attack from S_2Cl_2 (ΔG = 77.6 kcal/mol). It was not possible to locate a minimum energy structure where S_2Cl_2 is coordinated via its chlorine atom to Cp_2TiS_5. Attempts to locate an analogue process leading to similar structure than Min-I without Ti-S bond dissociation were unsuccessful.
- Formation of TiS-S_2Cl bond via loss of atomic chlorine (ΔG = 54.3 kcal/mol)
- Reaction via chlorosulfonium intermediate (ΔG = 44.4 kcal/mol)
- Homolytic Ti-S pre-dissociation (ΔG = 35.6 kcal/mol). Calculation of heterolytic dissociation were unsuccessful to linear polysulfide were unsuccessful, because of pentasulfide chain "backbiting" on itself and divertion to other species.
- Reaction via thiosulfonium intermediate (ΔG = 24.2 kcal/mol).

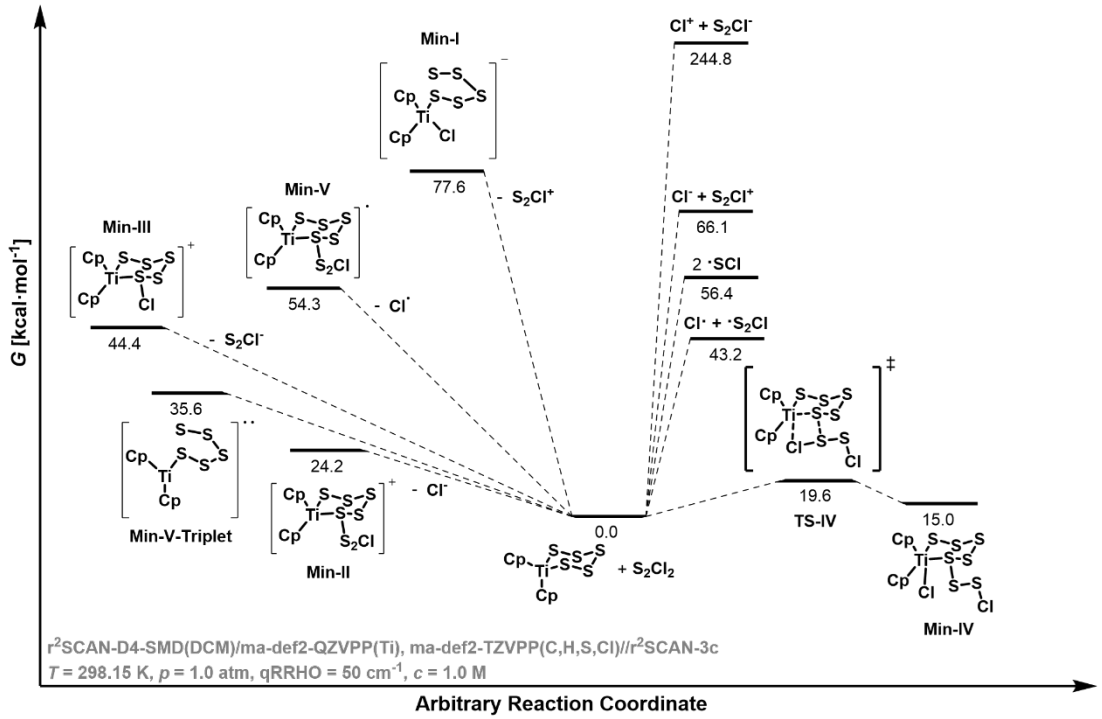

Figure S68. Arbitrary reaction coordinate of pathways explored within this work at the same level of theory. Note free energy axis is not scaled to height for illustration purposes.

11.4 Comparison of computed results to experiment

A correlation between the 32 experimental microkinetic free energies of activation with their computed analogues was established (Table S5). While individual calculations fail to directly predict quantitave reaction rates (See Section S11.2), the methodology described herein is useful to provide qualitative results across a range of structurally different nucleophiles and electrophiles (Figure S69). Overall, the calculated barriers ($\Delta G^{\ddagger}_{Calc}$) are overestimated relative to experiment ($\Delta G^{\ddagger}_{Exp}$), and so the experimental reaction rate is likely to be faster than what the $\Delta G^{\ddagger}_{Calc}$ directly predicts. The linear correlation between $\Delta G^{\ddagger}_{Calc}$ and $\Delta G^{\ddagger}_{Exp}$ was used as a predictive model, generating a linearly corrected calculated barrier, $\Delta G^{\ddagger}_{Pred}$, for each entry in Table S5. $\Delta G^{\ddagger}_{Pred}$ values predict all calculated reaction barriers within one order of magnitude of the experimentally measured barriers (mean absolute deviation = 0.6 kcal·mol^{-1}).

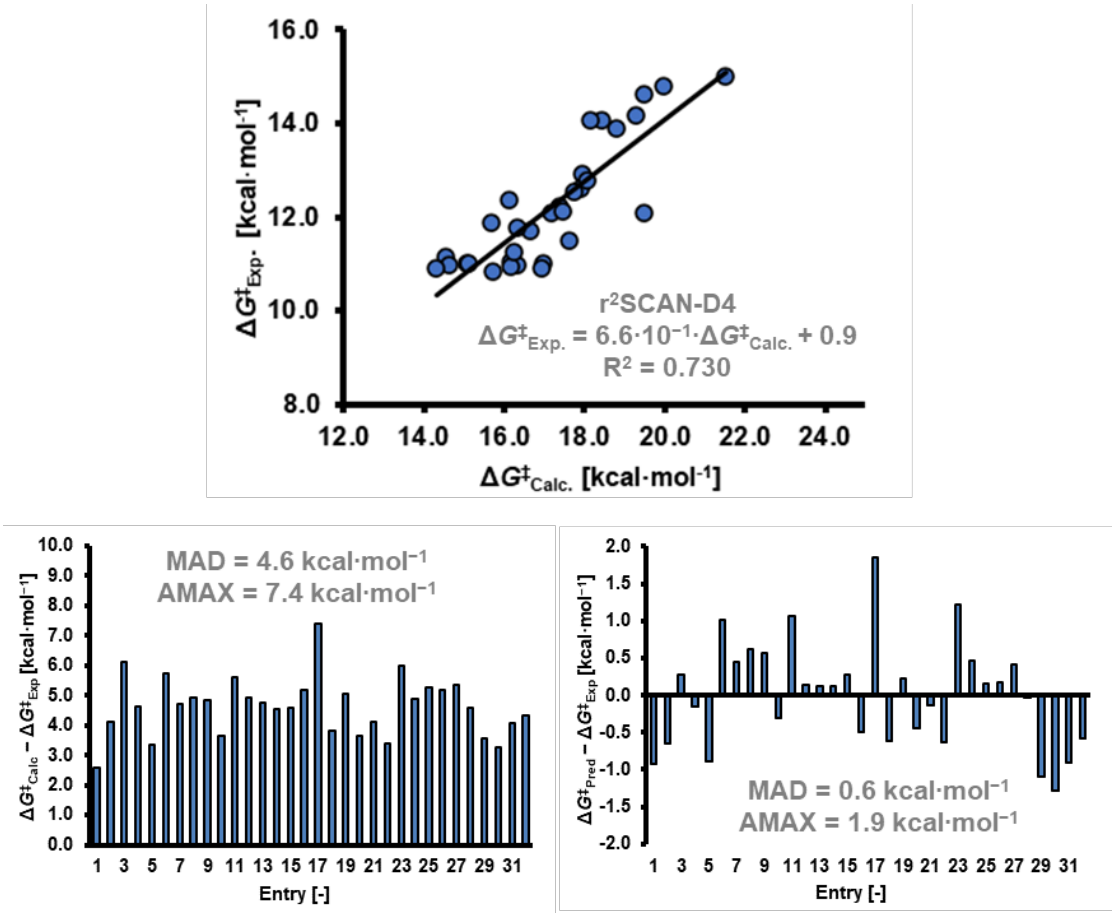

Figure S69. Top: correlation between all experimental microkinetic reaction barriers and calculated barriers. Left: Differences between experimental ($\Delta G^{\ddagger}_{Exp}$) and computational ($\Delta G^{\ddagger}_{Calc}$) values for each reaction entry in Table S5 (see below). Right: Differences between experimental and linearly corrected computational values as per correlation ($\Delta G^{\ddagger}_{Pred} = 6.6\cdot10^{-1}\cdot\{\Delta G^{\ddagger}_{Calc}\}+0.9$) for each reaction entry in Table S5 (see below). MAD = Mean absolute deviation; AMAX = absolute maximum deviation. Note that $\Delta G^{\ddagger}_{Exp}$ and $\Delta G^{\ddagger}_{Pred}$ are at 295K and $\Delta G^{\ddagger}_{Calc}$ at 298.15 K.

Table S5. Summary of experimental and computed microkinetic barriers of reactions of various titanocenes and electrophiles.

Rxn	Titanocene [a]	RSCl [a]	k_{rxn} ($M^{-1}s^{-1}$)	n	$\Delta G^{‡}_{Exp}$ [b] (kcal/mol)	$\Delta G^{‡}_{Calc}$ (kcal/mol)	$\Delta G^{‡}_{Pred}$ [c] (kcal/mol)
1	$Cp_2TiS_4(CMe_2)$	S_2Cl_2	$3.4\cdot10^4$	4	12.0	15.3	11.0
2	Cp_2TiS_5	S_2Cl_2	$3.2\cdot10^2$	4	14.7	19.6	14.1
3	Cp_2TiS_5	MorphNSCl	$4.8\cdot10^1$	2	15.4	21.9	15.7
4	Cp_2TiS_5	PhthNSCl	$1.7\cdot10^3$	2	13.3	18.4	13.2
5	Cp_2TiS_5	AcSSCl	$4.4\cdot10^3$	2	12.8	16.5	11.9
6	Cp_2TiS_5	$Ar^{NO2}SCl$	$1.9\cdot10^4$	2	11.9	18.0	12.9
7	Cp_2TiS_5	$Ar^{Cl}SCl$	$4.1\cdot10^4$	2	11.4	16.6	11.9
8	Cp_2TiS_5	$Ar^{Br}SCl$	$4.5\cdot10^4$	2	11.4	16.7	12.0
9	Cp_2TiS_5	$Ar^{F}SCl$	$4.9\cdot10^4$	2	11.3	16.6	11.9
10	Cp_2TiS_5	PhSCl	$4.2\cdot10^4$	2	11.4	15.5	11.1
11	Cp_2TiS_5	$Ar^{OMe}SCl$	$4.4\cdot10^4$	2	11.4	17.4	12.5
12	$Cp_2Ti(SAr^{Cl})_2$	MorphNSCl	$2.9\cdot10^3$	2	13.0	18.3	13.1
13	$Cp_2Ti(SAr^{F})_2$	MorphNSCl	$5.4\cdot10^3$	2	12.6	17.8	12.8
14	$Cp_2Ti(SPh)_2$	MorphNSCl	$1.3\cdot10^4$	2	12.1	17.1	12.2
15	$Cp_2Ti(SAr^{OMe})_2$	MorphNSCl	$2.8\cdot10^4$	2	11.7	16.6	11.9
16	$Cp_2TiCl(S_6NMorph)$	MorphNSCl	$6.8\cdot10^1$	1	14.8	20.0	14.3
17	$Cp_2TiCl(S_6NPhth)$	PhthNSCl	$6.9\cdot10^3$	1	12.1	19.5	13.9
18	$Cp_2TiCl(S_7Ac)$	AcSSCl	$9.8\cdot10^3$	1	11.9	15.7	11.3
19	$Cp_2TiCl(S_6Ar^{NO2})$	$Ar^{NO2}SCl$	$6.8\cdot10^3$	1	12.1	17.2	12.3
20	$Cp_2TiCl(S_6Ar^{Cl})$	$Ar^{Cl}SCl$	$4.6\cdot10^4$	1	11.0	14.6	10.5
21	$Cp_2TiCl(S_6Ar^{Br})$	$Ar^{Br}SCl$	$4.3\cdot10^4$	1	11.0	15.1	10.9
22	$Cp_2TiCl(S_6Ar^{F})$	$Ar^{F}SCl$	$5.0\cdot10^4$	1	10.9	14.3	10.3
23	$Cp_2TiCl(S_6Ph)$	PhSCl	$5.0\cdot10^4$	1	10.9	16.9	12.1
24	$Cp_2TiCl(S_6Ar^{OMe})$	$Ar^{OMe}SCl$	$5.7\cdot10^4$	1	10.8	15.7	11.3
25	$Cp_2TiCl(SAr^{Cl})$	MorphNSCl	$2.1\cdot10^3$	1	12.8	18.1	12.9
26	$Cp_2TiCl(SAr^{F})$	MorphNSCl	$3.2\cdot10^3$	1	12.5	17.7	12.7
27	$Cp_2TiCl(SPh)$	MorphNSCl	$6.5\cdot10^3$	1	12.1	17.5	12.5
28	$Cp_2TiCl(SAr^{OMe})$	MorphNSCl	$1.2\cdot10^4$	1	11.8	16.3	11.7
28	$(EtCp)_2TiS_5$	S_2Cl_2	$2.4\cdot10^2$	4	14.9	19.2	13.8
30	$(n\text{PrCp})_2TiS_5$	S_2Cl_2	$2.4\cdot10^2$	4	14.9	18.9	13.6
31	$(i\text{PrCp})_2TiS_5$	S_2Cl_2	$9.0\cdot10^1$	4	15.4	20.3	14.5
32	$(n\text{BuCp})_2TiS_5$	S_2Cl_2	$2.0\cdot10^2$	4	15.0	20.1	14.4

[a] Ar^X = (4-X-C_6H_4-); NMorph = *N*-morpholino; NPhth = *N*-phthalimido
[b] Applying Eyring equation as shown in procedure within Table S3
[c] Calculated from computational values via linear correlation: $\Delta G^{‡}_{Pred} = 6.6\cdot10^{-1}\{\Delta G^{‡}_{Calc}\} + 0.9$

A comparison of linear free energy relationships (LFER) between experiment and calculations for the reactions with titanocene thiophenolates are shown in Figure S70. Rate constant data extracted from computational microkinetic barriers represents the predicted process rate constant (i.e. k_{rxn} = $nk_{S\text{-}S}$; with n being the number of reagent combinations leading to identical transition states). Predicted rate constants have been calculated using the corresponding computational activation barrier as calculated ($\Delta G^{\ddagger}_{Calc}$, Table S5). The results show that curvature trend in experimental Hammett plot is also predicted with computation for the first reaction step.

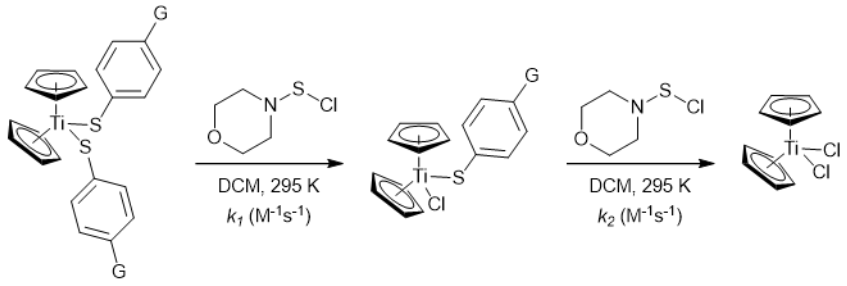

			Experimental Data		Computational Data	
G	σ_p	σ^0	k_1 ($M^{-1}s^{-1}$)	k_2 ($M^{-1}s^{-1}$)	k'_1 ($M^{-1}s^{-1}$)	k'_2 ($M^{-1}s^{-1}$)
OMe	- 0.27	- 0.1	$4.4 \cdot 10^{4}$	$5.7 \cdot 10^{4}$	$3.3 \cdot 10^{-1}$	$2.6 \cdot 10^{-1}$
H	0	0	$4.2 \cdot 10^{4}$	$5.0 \cdot 10^{4}$	$8.2 \cdot 10^{-1}$	$4.5 \cdot 10^{-1}$
F	0.15	0.2	$4.9 \cdot 10^{4}$	$5.0 \cdot 10^{4}$	$2.8 \cdot 10^{-1}$	$6.9 \cdot 10^{-1}$
Cl	0.23	0.28	$4.1 \cdot 10^{4}$	$4.6 \cdot 10^{4}$	5.8	4.8

$$k'_1\,(M^{-1}\cdot s^{-1}) = 2\cdot k_{s\text{-}s} = 2\left(\frac{\kappa k_b T}{h}\right) e^{\frac{-\Delta G_1^{\ddagger}{}_{calc}}{RT}}$$

$$k'_2\,(M^{-1}\cdot s^{-1}) = 1\cdot k_{s\text{-}s} = 1\left(\frac{\kappa k_b T}{h}\right) e^{\frac{-\Delta G_2^{\ddagger}{}_{calc}}{RT}}$$

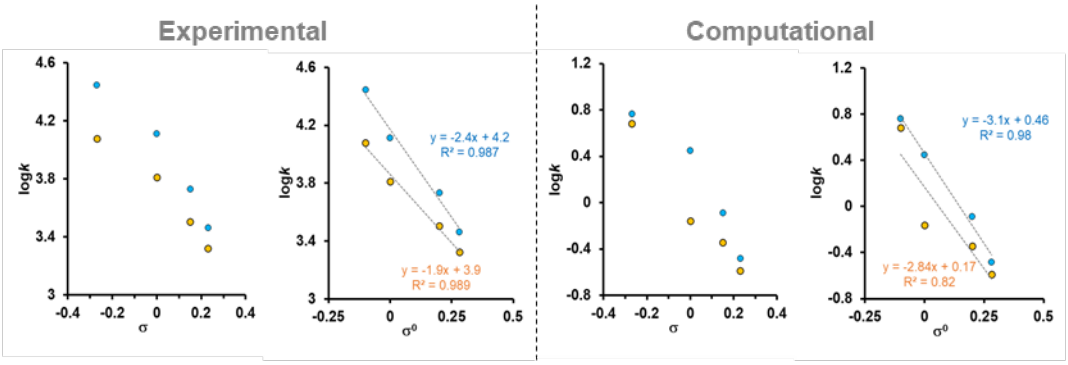

Figure S70. Comparison between experimental and computational LFER for reaction of titanocene thiophenolates with *N*-morpholinosulfenyl chloride (data in blue: step 1; orange: step 2).

11.5 Representative Orca Input File

A representative Orca input file (grey text) used for calculations in this work is shown with H_2 as a model. The input file has the input geometry (charge, multiplicity, atom identity and xyz coordinates) and calls for a geometry optimization, frequency calculation followed by a single-point calculation on the optimized geometry.

TEXT OF INPUT FILE BEGINS BELOW

```
* xyz 0 1
H       0.000000000     0.000000000     0.000000000
H       0.000000000     0.000000000     0.740000000
*
%pal nprocs 6 end
%maxcore 3000
%compound

Variable Concentration = 1.0;
Variable T;
Variable P;
Variable Opt_EEl ;
Variable Opt_ZPE ;
Variable Opt_H ;
Variable Opt_G ;
Variable Opt_Hcorr ;
Variable Opt_Gcorr ;
Variable Solvcorr ;
Variable G_1Mcorr ;

Variable r2SCAN_SCF ;
Variable r2SCAN_DISP ;
Variable r2SCAN_SPE ;
Variable r2SCAN_G_1M ;
Variable r2SCAN_G_1M_kJ ;
Variable r2SCAN_G_1M_kcal ;

   NEW_STEP
   ! r2SCAN-3c Opt Freq VERYTIGHTSCF VERYTIGHTOPT DEFGRID3
   %freq quasirrho true cutofffreq 50 end
   %geom maxstep 0.3 trust 0.3 maxiter 500 end
```

```
   STEP_END

Read T = THERMO_TEMPERATURE[1];
Read P = THERMO_PRESSURE[1];
Solvcorr = (8.314*T*ln((8.314*T*Concentration/(P*101325))*1000))/(2625500) ;
Read Opt_EEl = THERMO_ELEC_ENERGY[1];
Read Opt_ZPE = THERMO_ZPE[1];
Read Opt_H = THERMO_ENTHALPY_H[1];
Read Opt_G = THERMO_FREE_ENERGY_G[1];
Opt_Hcorr = Opt_H - Opt_EEl ;
Opt_Gcorr = Opt_G - Opt_EEl ;
G_1Mcorr = Opt_Gcorr + Solvcorr ;


   NEW_STEP
   ! r2SCAN D4 ma-def2-TZVPP def2/J CPCM VERYTIGHTSCF DEFGRID3
   %basis newgto Ti "ma-def2-QZVPP" end end
   %cpcm smd true smdsolvent "dichloromethane" end

   STEP_END

   Alias SP1
   Read r2SCAN_SCF = SCF_ENERGY[SP1] ;
   Read r2SCAN_DISP = VDW_CORRECTION[SP1] ;
   r2SCAN_SPE = r2SCAN_SCF + r2SCAN_DISP ;


r2SCAN_G_1M = r2SCAN_SPE + G_1Mcorr ;
r2SCAN_G_1M_kJ = r2SCAN_G_1M*2625.50  ;
r2SCAN_G_1M_kcal = r2SCAN_G_1M*627.5095  ;


end
TEXT OF INPUT FILE ENDED ABOVE
```

11.6 Summary of computational output data

Table S6-A. Summary of all titanocene species which are minima on the potential energy surface.

Entry	Species[a]	Chg/ Mult.	E_{el} Opt (Eh)	ZPE (Eh)	H_{corr} (Eh)	G_{corr} (Eh)	E_{El} SP (Eh)	G (Eh)[b]
1	Cp_2TiS_5	0/1	-3227.4746	0.1780	0.1948	0.1362	-3227.5838	-3227.4446
2	$Cp_2TiS_4(CMe)_2$	0/1	-2947.1809	0.2591	0.2784	0.2155	-2947.2913	-2947.0728
3	$(^{Et}Cp)_2TiS_5$	0/1	-3384.6894	0.2897	0.3116	0.2432	-3384.8114	-3384.5652
4	$(^{n\text{P}r}Cp)_2TiS_5$	0/1	-3463.2917	0.3463	0.3700	0.2981	-3463.4211	-3463.1200
5	$(^{i\text{P}r}Cp)_2TiS_5$	0/1	-3463.2916	0.3454	0.3699	0.2967	-3463.4196	-3463.1199
6	$(^{n\text{Bu}}Cp)_2TiS_5$	0/1	-3541.8929	0.4028	0.4283	0.3527	-3542.0302	-3541.6745
7	$Cp_2Ti(SAr^{Cl})_2$	0/1	-3541.8927	0.4023	0.4294	0.3511	-3542.0278	-3541.6737
8	$Cp_2Ti(SAr^{F})_2$	0/1	-3415.2713	0.3343	0.3571	0.2864	-3415.3966	-3415.1071
9	$Cp_2Ti(SPh)_2$	0/1	-2694.5955	0.3371	0.3590	0.2904	-2694.7093	-2694.4159
10	$Cp_2Ti(SAr^{OMe})_2$	0/1	-2496.1051	0.3537	0.3748	0.3079	-2496.2160	-2495.9051
11	$Cp_2TiS_7Cl_2$	0/1	-4944.2238	0.1828	0.2055	0.1340	-4944.3680	-4944.2310
12	$Cp_2TiS_4C(Me)_2S_2Cl_2$	0/1	-4663.9315	0.2640	0.2875	0.2152	-4664.0789	-4663.8607
13	$Cp_2Ti(SAr^{Cl})Cl$	0/1	-2786.1217	0.2532	0.2705	0.2107	-2786.2228	-2786.0091
14	$Cp_2Ti(SAr^{F})Cl$	0/1	-2425.7839	0.2546	0.2715	0.2128	-2425.8794	-2425.6636
15	$Cp_2Ti(SPh)Cl$	0/1	-2326.5387	0.2630	0.2799	0.2212	-2326.6327	-2326.4085
16	$Cp_2Ti(SAr^{OMe})Cl$	0/1	-2441.0443	0.2951	0.3137	0.2516	-2441.1487	-2440.8941
17	$Cp_2TiClS_6NMorph$	0/1	-4372.9929	0.3043	0.3286	0.2546	-4373.1528	-4372.8952
18	Cp_2TiClS_6NPhth	0/1	-4598.2616	0.2852	0.3114	0.2339	-4598.4292	-4598.1923
19	Cp_2TiClS_7Ac	0/1	-4637.2697	0.2284	0.2526	0.1784	-4637.4204	-4637.2390
20	$Cp_2TiClS_6Ar^{NO2}$	0/1	-4521.9555	0.2730	0.2990	0.2216	-4522.1155	-4521.8909
21	$Cp_2TiClS_6Ar^{Cl}$	0/1	-4777.0378	0.2607	0.2846	0.2113	-4777.1896	-4776.9753
22	$Cp_2TiClS_6Ar^{Br}$	0/1	-6890.9973	0.2602	0.2843	0.2102	-6891.1467	-6890.9335
23	$Cp_2TiClS_6Ar^{F}$	0/1	-4416.6987	0.2622	0.2857	0.2134	-4416.8463	-4416.6298
24	Cp_2TiClS_6Ph	0/1	-4317.4548	0.2706	0.2941	0.2217	-4317.6010	-4317.3762
25	$Cp_2TiClS_6Ar^{OMe}$	0/1	-4431.9617	0.3028	0.3281	0.2524	-4432.1183	-4431.8629
26	Cp_2TiCl_2	0/1	-2156.9709	0.1721	0.1848	0.1348	-2157.0480	-2156.9102
27	$Cp_2TiS_4(CMe)_2$_Adduct1	0/1	-4663.9005	0.2642	0.2884	0.2148	-4664.0463	-4663.8284
28	Cp_2TiS_5_Adduct1	0/1	-4944.1848	0.1828	0.2046	0.1350	-4944.3276	-4944.1895
29	$Cp_2TiS_4CF_2$	0/1	-3067.0560	0.1874	0.2054	0.1446	-3067.1652	-3067.0176
30	$Cp_2TiS_4CH_2$	0/1	-2868.5719	0.2037	0.2200	0.1625	-2868.6771	-2868.5116
31	Cp_2TiS_4CPh2	0/1	-3330.5663	0.3639	0.3873	0.3163	-3330.6995	-3330.3802
32	$Cp_2TiS_4C(CF_3)_2$_Twist	0/1	-3542.6597	0.2115	0.2343	0.1638	-3542.7847	-3542.6179
33	$Cp_2TiS_4C(CN)_2$	0/1	-3052.9969	0.1996	0.2190	0.1552	-3053.1099	-3052.9517
34	$Cp_2TiS_4C(HNO_2)$_ax	0/1	-3073.0593	0.2058	0.2247	0.1618	-3073.1816	-3073.0167
35	$Cp_2TiS_4CH(CHO)$_ax	0/1	-2981.8774	0.2124	0.2309	0.1688	-2981.9889	-2981.8171
36	$Cp_2TiS_4CH(CN)$_ax	0/1	-2960.7895	0.2020	0.2202	0.1589	-2960.9020	-2960.7401
37	Cp_2TiS_4CHF_ax	0/1	-2967.8087	0.1957	0.2129	0.1537	-2967.9180	-2967.7614
38	$Cp_2TiS_5Cl^-$	-1/1	-3687.7513	0.1774	0.1962	0.1328	-3687.9210	-3687.7852
39	$Cp_2TiS_5Cl^+$	1/1	-3687.3932	0.1795	0.1973	0.1363	-3687.5655	-3687.4262
40	$Cp_2TiS_5S_2Cl^+$	1/1	-4483.7650	0.1824	0.2028	0.1362	-4483.9552	-4483.8160
41	$Cp_2TiS_5S_2Cl$*	0/2	-4483.9975	0.1812	0.2014	0.1343	-4484.1315	-4483.9942
42	Cp_2TiS_5**	0/3	-3227.4126	0.1754	0.1909	0.1330	-3227.5239	-3227.3879
43	$Cp_2TiS_4C(OMe)_2$_Twist	0/1	-3097.5733	0.2671	0.2882	0.2213	-3097.6967	-3097.4724
44	$Cp_2TiS_4C(NMe_2)_2$_Twist	0/1	-3136.4058	0.3477	0.3724	0.2989	-3136.5419	-3136.2399
45	$Cp_2TiS_4C(COOMe)_2$_Twist	0/1	-3324.2533	0.2871	0.3121	0.2370	-3324.3891	-3324.1490

[a] Ar^X = (4-X-C_6H_4-); NMorph = *N*-morpholino; N-Phth = *N*-phthalimido
[b] G = Eel SP + Gcorr + 0.003019 Eh.

Table S6-B. Summary of all non-titanocene species which are minima on the potential energy surface.

Entry	Species[a]	Charge/ Multiplicity	E_{el} Opt (Eh)	ZPE (Eh)	H_{corr} (Eh)	G_{corr} (Eh)	E_{El} SP (Eh)	G (Eh)[b]
1	S_7	0/1	-2787.2668	0.0102	0.0208	-0.0259	-2787.3392	-2787.3621
2	S_6CMe_2	0/1	-2506.9801	0.0915	0.1036	0.0553	-2507.0580	-2506.9997
3	MorphNSSAr^{C}	0/1	-1774.6499	0.2067	0.2195	0.1686	-1774.7335	-1774.5619
4	MorphNSSAr^{F}	0/1	-1414.3123	0.2081	0.2205	0.1707	-1414.3904	-1414.2167
5	MorphNSSPh	0/1	-1315.0675	0.2165	0.2289	0.1792	-1315.1440	-1314.9618
6	MorphNSSAr^{OMe}	0/1	-1429.5731	0.2486	0.2627	0.2095	-1429.6603	-1429.4478
7	S_2Cl_2	0/1	-1716.7057	0.0044	0.0107	-0.0265	-1716.7454	-1716.7689
8	MorphNSCl	0/1	-1145.4760	0.1260	0.1351	0.0926	-1145.5338	-1145.4382
9	PhthNSCl	0/1	-1370.7363	0.1066	0.1176	0.0705	-1370.8005	-1370.7270
10	AcSSCl	0/1	-1409.7473	0.0499	0.0588	0.0167	-1409.7918	-1409.7721
11	Ar^{NO2}SCl	0/1	-1294.4274	0.0943	0.1041	0.0592	-1294.4840	-1294.4217
12	Ar^{Cl}SCl	0/1	-1549.5137	0.0824	0.0910	0.0488	-1549.5606	-1549.5088
13	Ar^{Br}SCl	0/1	-3663.4726	0.0818	0.0906	0.0471	-3663.5175	-3663.4674
14	Ar^{F}SCl	0/1	-1189.1771	0.0838	0.0920	0.0510	-1189.2186	-1189.1646
15	PhSCl	0/1	-1089.9315	0.0921	0.0995	0.0604	-1089.9715	-1089.9081
16	Ar^{OMe}SCl	0/1	-1204.4401	0.1244	0.1343	0.0897	-1204.4913	-1204.3986
17	Ar$^{Cl}S_3Cl$	0/1	-2345.8835	0.0855	0.0965	0.0484	-2345.9509	-2345.8995
18	Ar$^{F}S_3Cl$	0/1	-1985.5466	0.0869	0.0976	0.0506	-1985.6086	-1985.5550
19	PhS_3Cl	0/1	-1886.3015	0.0952	0.1050	0.0599	-1886.3619	-1886.2991
20	Ar$^{OMe}S_3Cl$	0/1	-2000.8088	0.1274	0.1398	0.0894	-2000.8800	-2000.7876
21	SCl*	0/2	-858.3016	0.0013	0.0048	-0.0218	-858.3207	-858.3395
22	S_2Cl^+	1/1	-1256.1748	0.0033	0.0080	-0.0242	-1256.2835	-1256.3047
23	Cl^-	-1/1	-460.2382	0.0000	0.0024	-0.0150	-460.3468	-460.3588
24	S_2Cl^-	-1/1	-1256.5929	0.0023	0.0073	-0.0260	-1256.6935	-1256.7166
25	Cl^+	1/1	-459.5444	0.0000	0.0024	-0.0150	-459.6502	-459.6622
26	S_2Cl*	0/2	-1256.5143	0.0029	0.0077	-0.0256	-1256.5447	-1256.5673
27	Cl*	0/2	-460.1141	0.0000	0.0024	-0.0157	-460.1201	-460.1328

[a] Ar^{X} = (4-X-C_6H_4-); NMorph = *N*-morpholino; N-Phth = *N*-phthalimido
[b] G = Eel SP + Gcorr + 0.003019 Eh.

Table S7. Summary of all computed transition states. All listed transition states are neutral singlets unless otherwise stated.

Entry	Species[a]	ν_{TS} (cm^{-1})	E_{el} Opt (Eh)	ZPE (Eh)	H_{corr} (Eh)	G_{corr} (Eh)	E_{El} SP (Eh)	G (Eh)[b]
1	$Cp_2TiS_5\_S_2Cl_2$	-35.7	-4944.1707	0.1828	0.2054	0.1341	-4944.3193	-4944.1822
2	$Cp_2TiS_4(CMe_2)\_S_2Cl_2$	-22.4	-4663.8825	0.2640	0.2892	0.2134	-4664.0337	-4663.8172
3	$(^{Et}Cp)_2TiS_5\_S_2Cl_2$	-12.3	-5101.3851	0.2946	0.3223	0.2415	-5101.5479	-5101.3034
4	$(^{Pr}Cp)_2TiS_5\_S_2Cl_2$	-21.4	-5179.9874	0.3511	0.3807	0.2961	-5180.1578	-5179.8587
5	$(^{iPr}Cp)_2TiS_5\_S_2Cl_2$	-57.2	-5179.9864	0.3502	0.3807	0.2949	-5180.1544	-5179.8564
6	$(^{Bu}Cp)_2TiS_5\_S_2Cl_2$	-26.2	-5258.5868	0.4074	0.4381	0.3515	-5258.7659	-5258.4114
7	$Cp_2Ti(SAr^{Cl})_2\_S_2Cl_2$	-34.9	-5131.9744	0.3393	0.3671	0.2860	-5132.1421	-5131.8530
8	$Cp_2Ti(Sar^{F})_2\_S_2Cl_2$	-35.6	-4411.2995	0.3421	0.3691	0.2899	-4411.4559	-4411.1630
9	$Cp_2Ti(SPh)_2\_S_2Cl_2$	-36.0	-4212.8108	0.3588	0.3849	0.3073	-4212.9637	-4212.6534
10	$Cp_2Ti(Sar^{OMe})_2\_S_2Cl_2$	-35.4	-4441.8235	0.4231	0.4536	0.3678	-4441.9974	-4441.6266
11	$Cp_2TiS_5\_MorphNSCl$	-22.6	-4372.9359	0.3041	0.3286	0.2542	-4373.1050	-4372.8478
12	$Cp_2TiS_5\_PhthNSCl$	-41.0	-4598.2046	0.2848	0.3111	0.2332	-4598.3786	-4598.1423
13	$Cp_2TiS_5\_AcSSCl$	-40.6	-4637.2163	0.2284	0.2535	0.1774	-4637.3707	-4637.1903
14	$Cp_2TiS_5\_Ar^{NO2}SCl$	-26.5	-4521.8895	0.2726	0.2988	0.2207	-4522.0613	-4521.8376
15	$Cp_2TiS_5\_Ar^{Cl}SCl$	-28.1	-4776.9758	0.2606	0.2846	0.2109	-4777.1409	-4776.9269
16	$Cp_2TiS_5\_Ar^{Br}SCl$	-27.5	-6890.9348	0.2600	0.2842	0.2096	-6891.0979	-6890.8853
17	$Cp_2TiS_5\_Ar^{F}SCl$	-27.6	-4416.6390	0.2620	0.2856	0.2129	-4416.7987	-4416.5828
18	$Cp_2TiS_5\_PhSCl$	-27.1	-4317.3939	0.2704	0.2940	0.2212	-4317.5522	-4317.3280
19	$Cp_2TiS_5\_Ar^{OMe}SCl$	-22.3	-4431.9004	0.3026	0.3279	0.2519	-4432.0703	-4431.8154
20	$Cp_2Ti(SAr^{Cl})_2\_MorphNSCl$	-26.8	-4560.7363	0.4608	0.4912	0.4056	-4560.9247	-4560.5161
21	$Cp_2Ti(SAr^{F})_2\_MorphNSCl$	-27.9	-3840.0610	0.4635	0.4932	0.4095	-3840.2382	-3839.8257
22	$Cp_2Ti(SPh)_2\_MorphNSCl$	-29.1	-3641.5717	0.4802	0.5090	0.4269	-3641.7459	-3641.3160
23	$Cp_2Ti(SAr^{OMe})_2\_MorphNSCl$	-29.3	-3870.5835	0.5444	0.5767	0.4881	-3870.7787	-3870.2876
24	$Cp_2TiS_7Cl_2\_Close$	-48.9	-4944.1992	0.1825	0.2044	0.1344	-4944.3497	-4944.2124
25	$Cp_2TiS_4(CMe_2)S_2Cl_2\_Close$	-50.3	-4663.9120	0.2640	0.2892	0.2136	-4664.0683	-4663.8516
26	$Cp_2TiS_6Cl\_MorphNSCl$	-23.3	-5518.4564	0.4303	0.4616	0.3742	-5518.6787	-5518.3015
27	$Cp_2TiS_6Cl\_PhthNSCl$	-43.4	-5968.9927	0.3918	0.4276	0.3318	-5969.2230	-5968.8882
28	$Cp_2TiS_6Cl\_AcSSCl$	-47.7	-6047.0141	0.2787	0.3095	0.2221	-6047.2112	-6046.9861
29	$Cp_2TiS_6Cl\_pNO2PhSCl$	-33.7	-5816.3703	0.3674	0.4018	0.3080	-5816.5963	-5816.2853
30	$Cp_2TiS_6Cl\_pClPhSCl$	-15.9	-6326.5406	0.3434	0.3737	0.2881	-6326.7519	-6326.4608
31	$Cp_2TiS_6Cl\_pBrPhSCl$	-17.7	-10554.4588	0.3421	0.3728	0.2857	-10554.6655	-10554.3767
32	$Cp_2TiS_6Cl\_pFPhSCl$	-13.1	-5605.8664	0.3463	0.3757	0.2921	-5606.0668	-5605.7717
33	$Cp_2TiS_6Cl\_pHPhSCl$	-30.4	-5407.3750	0.3631	0.3926	0.3086	-5407.5689	-5407.2573
34	$Cp_2TiS_6Cl\_pOMePhSCl$	-20.4	-5636.3926	0.4276	0.4603	0.3704	-5636.6098	-5636.2364
35	$Cp_2TiCl(SAr^{Cl})\_S_2Cl_2$	-42.8	-4502.8244	0.2584	0.2823	0.2084	-4502.9652	-4502.7537
36	$Cp_2TiCl(SAr^{F})\_S_2Cl_2$	-42.9	-4142.4872	0.2598	0.2833	0.2104	-4142.6224	-4142.4090
37	$Cp_2TiCl(SPh)\_S_2Cl_2$	-42.6	-4043.2428	0.2681	0.2908	0.2195	-4043.3765	-4043.1540
38	$Cp_2TiCl(SAr^{OMe})\_S_2Cl_2$	-42.6	-4157.7500	0.3003	0.3256	0.2493	-4157.8941	-4157.6418
39	$Cp_2TiCl(SAr^{Cl})\_MorphNSCl$	-31.4	-3931.5874	0.3797	0.4055	0.3287	-3931.7502	-3931.4185
40	$Cp_2TiCl(SAr^{F})\_MorphNSCl$	-31.9	-3571.2499	0.3811	0.4065	0.3307	-3571.4072	-3571.0735
41	$Cp_2TiCl(SPh)\_MorphNSCl$	-30.9	-3472.0052	0.3894	0.4139	0.3398	-3472.1616	-3471.8188
42	$Cp_2TiCl(SAr^{OMe})\_MorphNSCl$	-30.3	-3586.5115	0.4216	0.4487	0.3696	-3586.6787	-3586.3062
43	$Cp_2TiS_4(CMe_2)\_Adduct1\_TSInsertion$	-71.6	-4663.8979	0.2639	0.2874	0.2151	-4664.0448	-4663.8267
44	$Cp_2TiS_5\_Adduct1\_TSInsertion$	-67.3	-4944.1834	0.1827	0.2046	0.1347	-4944.3271	-4944.1893
45	$Cp_2TiS_4CF_2\_S_2Cl_2$	-36.6	-4783.7527	0.1923	0.2161	0.1425	-4783.8993	-4783.7538
46	$Cp_2TiS_4CH_2\_S_2Cl_2$	-20.2	-4585.2717	0.2086	0.2308	0.1604	-4585.4181	-4585.2546
47	$Cp_2TiS_4CPh_2\_S_2Cl_2$	-33.2	-5047.2703	0.3688	0.3972	0.3155	-5047.4422	-5047.1236
48	$Cp_2TiS_4C(CF_3)_2\_S_2Cl_2$	-32.1	-5259.3528	0.2164	0.2442	0.1632	-5259.5162	-5259.3499
49	$Cp_2TiS_4(CN)_2\_S_2Cl_2$	-46.9	-4769.6866	0.2042	0.2296	0.1530	-4769.8367	-4769.6807
50	$Cp_2TiS_4CHNO_2\_ax\_S_2Cl_2$	-45.1	-4789.7529	0.2105	0.2345	0.1605	-4789.9145	-4789.7509
51	$Cp_2TiS_4CH(CHO)\_ax\_S_2Cl_2$	-30	-4698.5730	0.2170	0.2407	0.1674	-4698.7248	-4698.5544
52	$Cp_2TiS_4CHCN\_ax\_S_2Cl_2$	-39.4	-4677.4835	0.2068	0.2309	0.1568	-4677.6358	-4677.4760
53	$Cp_2TiS_4CHF\_ax\_S_2Cl_2$	-37	-4684.5063	0.2006	0.2236	0.1515	-4684.6550	-4684.5004
54	$Cp_2TiS_4C(OMe)_2\_Twist\_S_2Cl_2$	-31.6	-4814.2768	0.2720	0.2990	0.2192	-4814.4392	-4814.2169
55	$Cp_2TiS_4C(NMe_2)_2\_Twist\_S_2Cl_2$	-29.3	-4853.1127	0.3520	0.3823	0.2968	-4853.2914	-4852.9916
56	$Cp_2TiS_4C(COOMe)_2\_Twist\_S_2Cl_2$	-23.7	-5040.9493	0.2920	0.3210	0.2370	-5041.1268	-5040.8864

[a] Ar^X = (4-X-C_6H_4-); NMorph = *N*-morpholino; N-Phth = *N*-phthalimido
[b] G = Eel SP + Gcorr + 0.003019 Eh.

12. References

[S1] See Experiment 11.18 in page 512 within, S Berger, S. Braun in *200 and More NMR Experiments: A Practical Course*, Wiley-VCH, Chichester, 2004.

[S2] a) C. P. Johnston, T. H. West, R. E. Dooley, M. Reid, A. B. Jones, E. J. King, A. G. Leach, and G. C. Lloyd-Jones, *J. Am. Chem. Soc.* 2018, **140**, 11112 – 11124; b) R. Wei, A.M.R. Hall, R. Behrens, M.S. Pritchard, E.J. King and G.C. Lloyd-Jones, *Eur. J. Org. Chem*, 2021, 2331–2342.

[S3] G. Lente, *J. Math. Chem.* 2017, ***55***, 832–848.

[S4] a) Dielectric constant and ET_{30} parameters were extracted from: J.-L. M. Abboud and R. Notario, *Pure Appl. Chem.,* 1999, **71**, 645 – 718; b) Catalán parameters were extracted from: J. Catalán, *J. Phys. Chem. B* 2009, **113***,* 5951–5960.

[S5] a) Taft steric parameters E_s were taken from Table 1 within M. Sigman and J. J. Miller, *J. Org. Chem*. 2009, **74**, 7633–7643; b) Charton parameters ($\nu = \nu_{eff}$) were extracted from Table 4 within: M Charton, in *Steric Effects in Drug Design*, Springer, Berlin, Heidelberg, 1983, vol. 114, pp. 57 – 91 c) For cone angle parameters, see: N. J. Coville, M. S. Loonat, D. White, and L. Carlton, *Organometallics*, 1992, **11**, 1082–1090.

[S6] a) C. Hansch, A. Leo and R. W. Taft, *Chem. Rev.* 1991, **91**, 165–195; b) For σ_p(F), see: A. T. Shulgin and A. W. Baker, *Nature* 1958, **182**, 1299.

[S7] Yukawa-Tsuno standard parameter σ^0 was extracted from Table 1 in: Y. Tsuno and M. Fujio, in *Advances in Physical Organic Chemistry,* Eds. D. Bethell, Academic Press, London, Vol. 32, 1999, pp 267 – 385.

[S8] A. Shaver, J. M. McCall, *Organometallics* 1984, **3**, 1823–1829.

[S9] D. M. Giolando, T. B. Rauchfuss, A. L. Rheingold and S. R. Wilson, *Organometallics* 1987, **6**, 667–675.

[S10] a) R. Huang, R. Duchateau, C. E. Koning and J. C. Chadwick, *Macromolecules* 2008, **41**, 579–590; b) S. M. Rehbein, M. J. Kania and S. R. Neufeldt, *Organometallics* 2023, **42**, 1179–1189.

[S11] G. Tainturier and B. Gautheron, *Phosphorus, Sulfur Relat. Elem.* 1988, **36**, 11–14.

[S12] K. Osakada, T. Hosoda and T. Yamamoto, *Bull. Chem. Soc. Jpn.* 2000, **73**, 923–930.

[S13] M. Y. Darensbourg, M. Pala, S. A. Houliston, K. P. Kidwell, D. Spencer, S. S. Chojnacki and J. H. Reibenspies, *Inorg. Chem.* 1992, **31**, 1487–1493.

[S14] F. Neese, *WIREs Comput. Mol. Sci.* 2022;**12**:e1606.

[S15] C. Bannwarth, E. Caldeweyher, S. Ehlert, A. Hansen, P. Pracht, J. Seibert, S. Spicher and S. Grimme, *WIREs Comput. Mol Sci* 2021;**11**:e1493.

[S16] S. Grimme, A. Hansen, S. Ehlert and J.-M. Mewes, *J. Chem. Phys.* 2021, **154,** 064103.

[S17] V. Ásgeirsson, B. O. Birgisson, R. Bjornsson, U. Becker, F. Neese, C. Riplinger and H. Jónsson, *J. Chem. Theory Comput.* 2021, **17**, 4929–4945.

[S18] K. Ishida, K. Morokuma and A. Komornicki, *J. Chem. Phys.* 1977, **66**, 2153–2156.

[S19] S. Grimme, *Chem. Eur. J.* 2012, **18**, 9955–9964.

[S20] P. Pracht, F. Bohle and S. Grimme, *Phys. Chem. Chem. Phys.* 2020, **22**, 7169–7192.

[S21] S. Grimme, F. Bohle, A. Hansen, P. Pracht, S. Spicher and M. Stahn, *J. Phys. Chem. A* 2021, **125**, 4039–4054.

[S22] J. W. Furness, A. D. Kaplan, J. Ning, J. P. Perdew and J. Sun, *J. Phys. Chem. Lett.*, 2020, **11**, 8208–8215.

[S23] E. Caldeweyher, S. Ehlert, A. Hansen, H. Neugebauer, S. Spicher, C. Bannwarth and S. Grimme, *J. Chem. Phys.* 2019*,* **150**, 154122.

[S24] a) F. Weigend and R. Ahlrichs, *Phys. Chem. Chem. Phys.* 2005, **7**, 3297. b) J. Zheng, X. Xu and D. G. Truhlar, *Theor. Chem. Acc.* 2011, **128**, 295–305.

[S25] F. Weigend, *Phys. Chem. Chem. Phys.* 2006, **8**, 1057–1065.

[S26] A. V. Marenich, C. J. Cramer and D. G. Truhlar, *J. Phys. Chem. B* 2009, **113**, 6378–6396.

[S27] S. Grimme, *J. Comput. Chem*. 2006, **27**, 1787–1799.

[S28] J. P. Perdew, *Phys. Rev. B* 1986, **33**, 8822–8824.

[S29] J. P. Perdew, K. Burke, M. Ernzerhof, *Phys. Rev. Lett.* 1996, **77**, 3865–3868.

[S30] Y. Zhang, W. Yang, *Phys. Rev. Lett.* 1998, **80**, 890.

[S31] A. D. Becke, *Phys. Rev. A* 1988, **38**, 3098–3100.

[S32] N. C. Handy, A. J. Cohen, *Molecular Physics* 2001, **99**, 403–412.

[S33] J. Sun, A. Ruzsinszky and J. P. Perdew, *Phys. Rev. Lett.* 2015, **115**, 036402.

[S34] Y. Zhao, D. G. Truhlar, *J. Chem. Phys.* 2006, **125**, 194101.

[S35] J. Tao, J. P. Perdew, V. N. Staroverov, G. E. Scuseria, *Phys. Rev. Lett.* 2003, **91**, 146401.

[S36] H. J. A. Dale, G. R. Hodges and G. C. Lloyd-Jones, *J. Am. Chem. Soc.* 2019, **141**, 7181–7193.

[S37] S. Grimme, *J. Phys. Chem. A* 2005, **109**, 3067–3077.

[S38] C. Adamo and V. Barone, *J. Chem. Phys.* 1999, **110**, 6158–6170.

[S39] P. J. Stephens, F. J. Devlin, C. F. Chabalowski and M. J. Frisch, *J. Phys. Chem.* 1994, **98**, 11623–11627.

[S39] Y. Zhao and D. G. Truhlar, *Theor. Chem. Acc.*, 2007, **120**, 215–241.

[S40] Y. Zhao and D. G. Truhlar, *J. Phys. Chem. A* 2005, **109**, 5656–5667.

[S41] E. F. Epstein, I. Bernal and H. Köpf, *J. Organomet. Chem.*, 1971, **26**, 229–245.

[S42] N. Mardirossian, M. Head-Gordon, *J. Chem. Phys.* 2015, **142**, 074111.

[S43] N. Mardirossian, M. Head-Gordon, *Phys. Chem. Chem. Phys.* 2014, **16**, 9904–9924.

[S44] a) S. Grimme, J. Antony, S. Ehrlich and H. Krieg, *J. Chem. Phys.* 2010, **132**, 154104. b) S. Grimme, S. Ehrlich and L. Goerigk, *J. Comput. Chem.* 2011, **32**, 1456–1465.

[S45] Y. Guo, C. Riplinger, U. Becker, D. G. Liakos, Y. Minenkov, L. Cavallo and F. Neese, *J. Chem. Phys.* 2018, **148**, 011101.

[S46] A. Hellweg, C. Hattig, S. Hofener and W. Klopper, *Theor. Chem. Acc*. 2007, **117**, 587–597.

[S47] S. Grimme and A. Hansen, *Angew. Chem. Int. Ed.* 2015, **54**, 12308–12313.